The Development and Applications of an Improved Model for Indoor Air Chemistry

Toby Jacob Carter

Doctor of Philosophy

University of York

Environment and Geography

May 2024

Abstract

The need for good indoor air quality is imperative for healthy living. In recent years, computational models have become an important tool to aid understanding of the chemical transformations which arise following emissions of pollutants from indoor sources. Models are particularly helpful where there are experimental or logistical challenges determining the concentrations of indoor species. The aims of this thesis are, therefore, to develop and improve a detailed indoor air chemical model focusing on three key elements: indoor surfaces, indoor-outdoor exchange, and air cleaning, so developing improved understanding their impacts on indoor air quality.

Modelling results showed that surface emissions were important indoors, both through formation of secondary pollutants following surface oxidation, and through influencing indoor air pollutant concentrations depending on the surface composition within a room. For instance, total secondary pollutant concentrations were found to be 6.7 ppb in a kitchen, 4.8 ppb in an office and 5.8 ppb in a bedroom.

Through investigation of the impact of indoor activities on outdoor air, ventilation rates and timing and frequency of cooking and cleaning controlled the emissions of volatile organic compounds from indoors to outdoors. Total emissions following these activities were estimated to be approximately 29% of those released from traffic in the UK.

Elevated ozone and radical concentrations followed simulated use of a far-UVC air cleaning device using light between 220 and 230 nm. Ozone and OH radical concentrations reached 30.3 ppb and 2.3×10^5 molecule cm^{-3} respectively, approximately 1200 and 500% above baseline values, perturbing the subsequent chemistry.

This thesis contributes to an improved understanding of indoor air chemistry through the development and use of a detailed chemical model. As outdoor air quality continues to improve in the future, indoor sources of pollution will play an increasing role in our exposure to air pollution both indoors and outdoors.

Contents

List of Tables

List of Figures

Acknowledgements

First and foremost I would like to profoundly thank my supervisor Professor Nicola Carslaw for giving me the initial opportunity to pursue a PhD and giving me the confidence and support to be able to thrive. I've thoroughly enjoyed my time learning from her and I have become a more experienced and established scientist as a result. She has provided outstanding guidance and kindness and helped me through my PhD adventure, it is something I will look back on with great fondness and something I will treasure for the rest of my life.

Secondly, I'd like to thank Dr. David Shaw, my second (unofficial) supervisor. Dave has been ever present throughout my PhD and has been a constant source of support and laughs over the last three and a half years. Dave has always been there to help and give advice from his past experiences and it has been brilliant to work and learn from him. Even though he does (often) tease me, he means well and I know that I can always rely on him as both a colleague and a friend.

I'd like to also thank Dr. Helen Davies, Ellen Harding-Smith and Dr. Georgia Beel for making my PhD experience so enjoyable. From group meetings on a Friday afternoon to conferences across Europe and the US, I've had the best time and it's thanks to an amazing research group. I've learnt so much not only as a scientist but as a person. I'm so lucky to have found such a friendly and kind group of people who have always supported me throughout my time at York. I now look forward to beginning my next chapter as a Research Associate under Helen's excellent leadership!

Without funding, I wouldn't have been able to complete my PhD and all of the amazing opportunities it has provided me. I'd therefore like to thank Dr. Paula Olsiewski and the Alfred P. Sloan Foundation for funding my PhD as part of the Chemistry of Indoor Environments program. The program has provided support and encouragement for not only myself but has been the driving force of indoor chemistry studies. I'm thankful I can be a

cog in the wider indoor environments team. I'd like to also thank the MOCCIE team and co-PI of the project Professor Manabu Shiraiwa for providing support and stimulating discussion and driving research of modelling indoor environments forward.

Thanks go to Professor Alistair Boxall and Dr. Colin McClean for their advice and guidance as my TAP and progression mentors respectively. I'd like to also thank collaborators Dr. Dustin Poppendieck and Professor David Carslaw for providing insight and invaluable help with comments in the journal articles we have published.

Thank you to my brother Noah, Grandie, Gran, Grandad, Pollyanna and I suppose Marble too who have all been there for me and helped me through my PhD with their love and support.

Of course, I would also like to thank my partner Annabelle who has been ever so supportive. I'm so appreciative of her and all of the inspiration she provides for me. Annabelle has helped me through this journey through her love, support and encouragement and I'm ever so grateful. I hope I make her just as happy as she continues to make me.

Finally, the greatest thanks go to to my parents, Amanda and Mark, who have been there for me not just throughout my PhD but for the last 26 years of my life. I would not be where I am today if it wasn't for them, I'm so thankful for all of their support, love and kindness. I've always wanted to do the best I could possibly do and they have enabled me to do just that by always believing in me and leading me down the right paths, I am eternally grateful. They deserve so much thanks and I hope I make and continue to make them proud.

Declaration

This thesis has not previously been accepted for any degree and is not being concurrently submitted in candidature for any degree other than Doctor of Philosophy of the University of York. This thesis is the result of my own investigations, except where otherwise stated. All other sources are acknowledged by explicit references.

Part of this thesis has been already been published and is explicitly referred to in the thesis where necessary:

Carter, TJ., Poppendieck, DG., Shaw, DR. and Carslaw, N. (2023), 'A Modelling Study of Indoor Air Chemistry: The Surface Interactions of Ozone and Hydrogen Peroxide', *Atmospheric Environment*, **297**, 119598.

Shaw, DR., **Carter, TJ.**, Davies, HL., Harding-Smith, E., Crocker, EC., Beel, G., Wang, Z. and Carslaw, N. (2023), 'INCHEM-Py v1.2: a community box model for indoor air chemistry', *Geoscientific Model Development*, **16**(24), 7411-7431.

Carter, TJ., Shaw, DR., Carslaw, DC. and Carslaw, N. (2024), 'Indoor Cooking and Cleaning as a Source of Outdoor Air Pollution in Urban Environments', *Environmental Science: Processes & Impacts*, **26**(6), 975-990.

Chapter 1

Introduction

1.1 What is air pollution and why is important?

According to the World Health Organisation, air pollution is the "contamination of the indoor or outdoor environment by any chemical, physical or biological agent that modifies the natural characteristics of the atmosphere" (World Health Organisation, 2021a) and affects 91% of the global population (World Health Organisation, 2023).

Environmentalists are becoming increasingly concerned about the impact air pollution has on climate change and physical health. Air pollution was estimated to contribute to nearly 7 million deaths a year in 2017, 9% of global deaths (World Health Organisation, 2023; Ritchie and Roser, 2017), with 3.4 million of these deaths considered premature (GBD 2017 Risk Factor Collaborators, 2018). Guidelines are implemented worldwide to prevent air pollution from impacting our health (World Health Organisation, 2021b); despite this, some countries globally still exceed the WHO fine particulate matter ($PM_{2.5}$) exposure limit of 10 μg m^{-3} (Ritchie and Roser, 2019), as shown in Figure 1.1. Other outdoor air pollutants include ozone (O_3), nitrogen dioxide (NO_2) and sulfur dioxide (SO_2) (World Health Organisation, 2021b).

Exposure to $PM_{2.5}$ (Buonanno et al., 2015) leads to respiratory and cardiovascular health effects (Guo et al., 2023). The Global Burden of Disease Study found that in 2017, ambient particulate matter caused 2.94 million early deaths globally (GBD 2017 Risk Factor

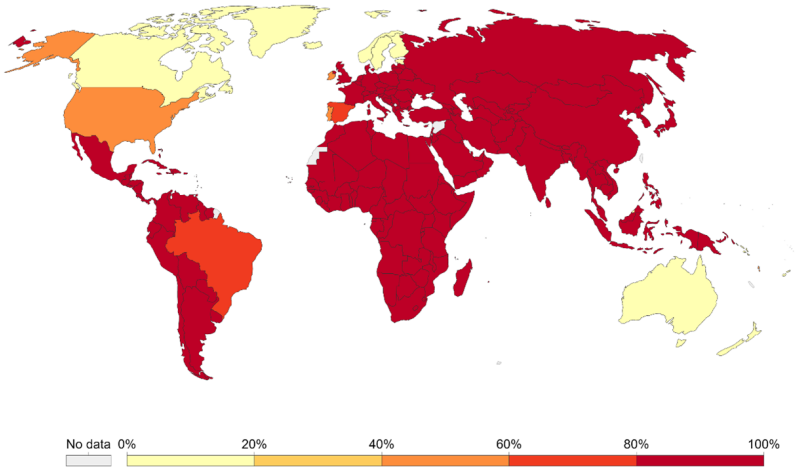

Figure 1.1: Percentage of the population of different countries exceeding the annual World Health Organisation (WHO) concentration limit for fine particulate matter ($PM_{2.5}$) of 10 μg m^{-3} (Source: (Ritchie and Roser, 2019).

Collaborators, 2018). It also showed that there were 83 million DALYs (disability adjusted life-years), with 73.6 million DALYs attributed to ambient particulate matter pollution. About 1.64 million deaths in 2017 were attributed to household air pollution, mainly as a result of solid fuel burning (GBD 2017 Risk Factor Collaborators, 2018). However, few epidemiological studies to date have reported the effect of indoor pollution (as distinct from outdoor air pollution) on health (Goldstein et al., 2021). Only in the last few years, has attention focused more on indoor air pollution, how that affects our health, and the importance of good indoor air quality in our homes.

Over the last century, much of the focus on air quality has been on the outdoor environment, owing to existing regulation. There has been little focus on indoor environments, even though people spend approximately 90% of their time indoors in developed countries (Klepeis et al., 2001), whether sleeping, working or partaking in recreational activity. A shift in working patterns over recent decades has also resulted in more office jobs (Felgueiras et al., 2023), shifting attention towards indoor air pollution (Van Tran et al., 2020).

Figure 1.2 gives an overview of indoor air pollutants and their respective health effects. Most of these pollutants are produced from common household activities as described in Section 1.2. The emitted pollutants can have health impacts, but also react in the indoor

environment with outdoor pollutants forming secondary products whose health implications are relatively unknown (Goldstein et al., 2021).

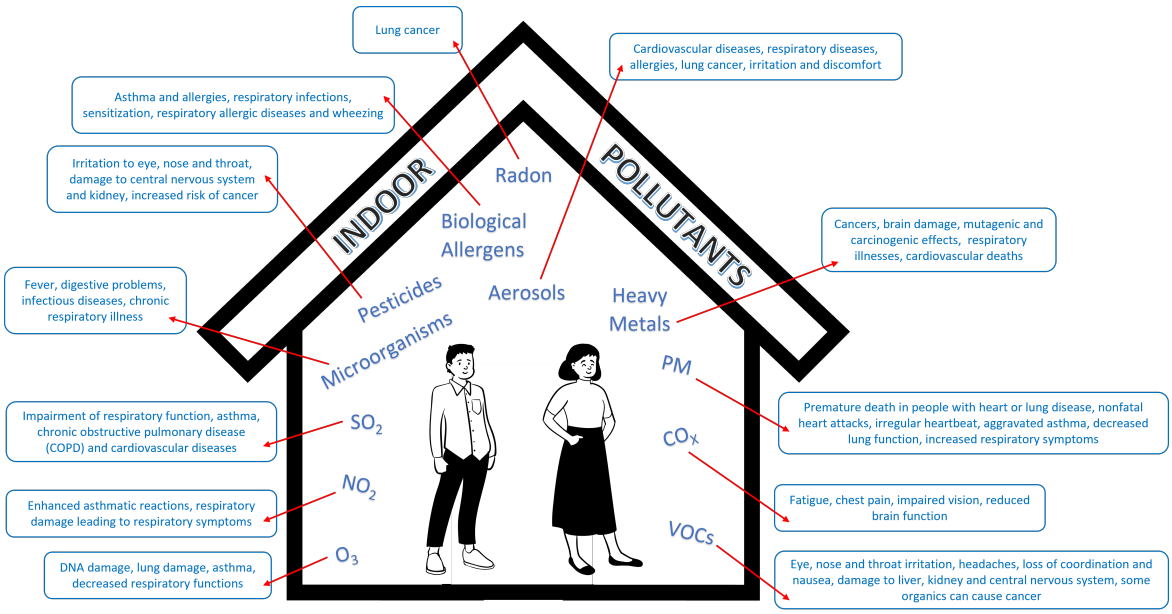

Figure 1.2: The common air pollutants present indoors along with their respective health impacts. Figure adapted from source: Van Tran et al. (2020).

Among the most common indoor pollutants, particulate matter can infiltrate the lungs, where the finer particulates can be transported into the alveoli (Cooper and Loxham, 2019). Particulate matter can also diffuse in the bloodstream, causing blood clots (Nelin et al., 2012). In some extreme cases, particulate matter has been found to be present in the brain (Peeples, 2020). Particulate matter has been strongly linked as a causation of lung cancer in non-smokers (Buonanno et al., 2015), chronic obstructive pulmonary disease (COPD) and risk of strokes (World Health Organisation, 2023).

Volatile organic compounds (VOCs) are ubiquitous indoors and some have recognised health impacts. For instance, formaldehyde (HCHO) causes irritation to the eyes and skin, and with prolonged exposure, can be carcinogenic (Swenberg et al., 2013). It is readily produced through common household actions including candle burning and cooking (Salthammer, 2019). Formaldehyde used to be directly added to cleaning and cosmetic products as a preservative, to prevent bacteria from growing (Malinauskiene et al., 2015; McDonnell and Russell, 1999), posing a potential health risk.

Ozone can also be detrimental to health via indoor exposure. Direct inhalation of 1 ppm of ozone for four hours has been found to cause DNA and lung damage in rats (Miller et al., 2018). It can also lower respiratory functionality (Huang et al., 2019). Ozone concentrations however, tend to be low indoors and is unlikely to cause direct harm to health but it can react with VOCs through ozonlysis reactions to form secondary pollutants, many of which have unknown toxicity, including epoxides, hydroperoxides and secondary ozonides (Goldstein et al., 2021). Epoxides can exhibit carcinogenic characteristics through reaction with DNA (Zhou et al., 2017). Some of the functional products resulting from ozonlysis reactions have been determined to cause endocrine disruption in the hormone system, and some have even been proposed to cause autism and dementia (Schrank et al., 2009; Birnbaum, 2013).

In summary, the health effects from indoor air pollution are understudied, but it is clear that good indoor air quality is vitally important to human health. Many chemicals formed indoors have unknown toxicities. There is a knowledge gap surrounding how detrimental these species are to physical health and how they are formed indoors. There needs to be more research into the health implications of different indoor pollutants, so that appropriate mitigation measures can be adopted.

1.2 Sources of Indoor Air Pollution

Many activities form pollutants indoors. These pollutants include an array of reactive chemicals, which are the driving force of indoor chemistry. Figure 1.3 shows the many different sources of indoor air pollution that could be present in a typical home. Recent studies have indicated multiple factors affect the level of indoor air pollution, including time of the day, amount of sunlight, ventilation, surface deposition, outdoor pollutant concentration, moisture and occupant activities (Weschler and Carslaw, 2018).

Indoor air pollution does not only occur in the home (Yang et al., 2020; Uchiyama et al., 2015; Li et al., 2019; Gilbert et al., 2006; Beldean-Galea et al., 2020; Walgraeve et al., 2011; Shinohara et al., 2013), but also in offices (Destaillats et al., 2008; Brickus et al., 1998;

Figure 1.3: A typical house with indoor air pollutant sources indicated.

Mandin et al., 2017; Nunes et al., 2019), schools (Bayati et al., 2021; Szabados et al., 2021), and public places, such as cinemas (Stönner et al., 2018). Table 1.1 shows common indoor pollutants found indoors and their respective emission sources.

Table 1.1: The major emission sources of indoor air pollutants (Sources: Van Tran et al. (2020); DeLuca et al. (2022); Tran et al. (2019)).

Pollutant	**Major Emission Sources**
Particulate Matter (PM)	Outdoor air, cooking, combustion, candle burning, stoves, fireplaces, cleaning and cigarette smoking
Volatile Organic Compounds (VOCs)	Paints, varnishes, solvents, adhesives, wood, wax, buidling materials, air fresheners, plastics cleaning materials, tobacco products, personal care products, furnishings, people
Nitrogen Oxides (NO_x)	Gas-fueled cooking and heating appliances
Ozone (O_3)	Outdoor sources, photocopiers, disinfectant devices
Sulfur Dioxide (SO_2)	Cooking stoves, fireplaces, outdoor air
Carbon Monoxide (CO) and Carbon Dioxide (CO_2)	Cooking stoves, tobacco smoking, fireplaces, outdoor air.
Heavy metals	Outdoor sources, fuel-consumption products, incense burning, building materials
Radon (Rn)	Soil, building materials, tap water
Pesticides	Disinfectants, herbicides, building materials, carpets
Biological Allergens	House dust, pets, mould, pollen, plants
Microorganisms	Bacteria, viruses, fungi
Per- and polyfluoroalkyl substances (PFAS)	Cleaning materials, dust, food and water and personal care products
Siloxanes	Personal care products, dust and indoor surfaces

Air pollution exposure in developed countries differs significantly to that in less developed countries. For example, less developed countries cook with solid fuels more often, leading to poorer indoor air quality and prolonged health effects. According to Kim et al. (2011) indoor living is considered to be a paradox, where there is a need to cook and clean to live, yet these activities can contribute to indoor air pollution and in some cases, be a detriment to our health.

Some pollutant concentrations indoors can be higher than outdoors (Lunderberg et al., 2021). For instance, McDonald et al. (2018) found that volatile chemical product (VCPs) concentrations were seven times higher indoors than outdoors. The health impact of air pollution indoors has also been shown to be 2 to 5 times higher on humans than the effect of outdoor air pollution (EPA, 2017).

1.2.1 Cooking

Cooking and heating appliances, such as stoves and ovens, produce large concentrations of pollutants including the hydroxyl radical (OH), nitric oxide (NO), nitrogen dioxide (NO_2), nitrous acid (HONO), VOCs and $PM_{2.5}$ (Wang et al., 2020a; Farmer et al., 2019; Reidy et al., 2023). These pollutants are often directly inhaled as a result of standing in the vicinity of the cooking source, and exposure can be accentuated if there is inadequate ventilation. A study on the frying of fish determined that the concentrations of propanal, butanal and benzene that were produced as a result was 0.23, 2.9 and 6.1 ppb respectively (Ahn et al., 2014). The study also identified traces of ketones and fatty acids.

Particulate matter is also emitted by cooking, both from the ingredients that are being charred or fried, and from the complete and incomplete combustion of the cooking fuel. Kang et al. (2019) investigated the concentration of particulate matter produced from different methods of cooking and found that the broiling of fish produced an average of approximately 5000 $\mu g\ m^{-3}$ for both $PM_{2.5}$ and PM_{10}. The WHO daily exposure limit for $PM_{2.5}$ and PM_{10} is 15 and 45 $\mu g\ m^{-3}$ respectively (World Health Organisation, 2021b).

Reidy et al. (2023) investigated the impact on radical chemistry during preparation and

cooking of a typical Thanksgiving meal as part of the HOMEChem campaign (Farmer et al., 2019). The study found OH concentrations reached over 6.0×10^6 molecule cm^{-3} during the Thanksgiving cooking, with maximum HONO concentrations attaining approximately 45 ppb. These species attained higher indoor concentrations than outdoors. Typical outdoor OH and HONO concentrations are 1.1×10^6 molecule cm^{-3} (Li et al., 2018) and 0.9 ppb respectively (Lee et al., 2002). Chapter 5 expands on the sources and impacts of indoor cooking.

1.2.2 Cleaning

Cleaning products produce an array of terpenes, bleach (sodium hypochlorite), and ammonia (Nazaroff and Weschler, 2004). Bleach cleaning in particular is commonly undertaken to disinfect homes, offices and other indoor settings. Hypochlorous acid (HOCl), nitryl chloride ($ClNO_2$) and chlorine (Cl_2) are produced in high quantities during periods of bleach cleaning. Mattila et al. (2020b) found that during a bleach cleaning experiment, maximum HOCl, Cl_2, and $ClNO_2$ concentrations rose to approximately 400, 130 and 20 ppbv respectively from low baseline concentrations (< 5 ppbv for each species). Chapter 5 expands on the sources and impacts of indoor bleach cleaning.

Monoterpene-based cleaning products are also used for indoor disinfection. Limonene and α-pinene are two commonly found monoterpenes in cleaning agents, giving citrus and pine smells respectively (Rosales et al., 2022). During cleaning episodes, limonene mixing ratios can increase significantly, increasing from 1 to 13 ppb in one study (Rossignol et al., 2013).

During the COVID-19 pandemic, the need for clean and healthy indoor living environments was accentuated, which resulted in the development of air cleaning devices. These air cleaning devices used a range of different methodologies including filtration, adsorption and UV light (Mata et al., 2022). One of the most popular was germicidal ultraviolet-C (UVC) light (at a wavelength of 222 or 254 nm) to remove airborne pathogens and germs. Many of these UVC air cleaning devices effectively removed COVID-19 (Nardell, 2021;

Buonanno et al., 2020; Truong et al., 2023), but often at the expense of indoor air quality. For instance, preliminary studies have identified a significant amount of ozone can be produced from these cleaning devices (Link et al., 2023b; Peng et al., 2023a). The effect of UVC photochemistry on indoor environments is explored further in Chapter 6.

1.2.3 Surfaces and Furnishings

Surfaces are an important source of indoor air pollution, with building and construction attributed as one of the main sources of VOCs indoors (Ruiz-Jimenez et al., 2022). Carpets and wood release primary emissions comprising of straight-chained aldehydes, including formaldehyde and hexanal (Yrieix et al., 2010; Katsoyiannis et al., 2008). Other materials including paint, paper and gypsum board can also release VOCs, primarily aldehydes but also some ketones, via oxidation reactions at the surface (Morrison and Nazaroff, 2002a; Mason and Ceragioli, 2011; Poppendieck et al., 2007b; Cheng et al., 2015).

The primary emissions from, and the degradation of plastics, are further sources of indoor air pollution, releasing VOCs (Beel et al., 2023). An increase in indoor temperature (to 28°C) caused concentrations of formaldehyde released by plastics to increase by 31.6%, which could further increase with climate change (Beel et al., 2023). Chapter 4 expands on the sources and impacts of indoor surfaces and furnishings.

1.2.4 Occupants, Personal Care Products and Household Objects

Humans are a source of indoor pollutants. We produce chemicals, such as squalene from skin oil, (Wisthaler and Weschler, 2010) which can soil surfaces leading to ozonolysis reactions (Liu et al., 2021). Other VOCs including acetone, isoprene and methanol were found be given off from human breath (Fenske and Paulson, 1999; Kruza and Carslaw, 2019; Wang et al., 2022a).

Not only are people sources of indoor pollutants, but the products brought into and used in the home can also contribute to indoor pollution. These can include deodorants, perfumes, air fresheners and even toothpaste (Steinemann, 2021). Personal care products

from bathing and showering produce VOCs (Yeoman et al., 2021). Yeoman et al. (2021) determined that limonene, benzyl alcohol and ethanol were emitted during a showering activity. The total amount of VOCs emitted from showering were 1.77 mg of limonene, 1.07 mg of benzyl alcohol and 0.33 mg of ethanol. Steinemann (2015) found a wide variety of VOCs in fragranced consumer products, with the most prevalent being ethanol, limonene, β-pinene and α-pinene.

A further common source of indoor air pollution is candle burning. Bekö et al. (2013) undertook a study which analysed 56 homes in Denmark to determine the occupants' exposure to particulate matter. In one of the homes, 97% of the occupants total daily exposure to particulate matter was found to derive from candle burning.

Appliances that use electricity such as inkjet printers and computers form ozone indoors (Weschler, 2006; Destaillats et al., 2008). Bakó-Biró et al. (2004) also showed that phenol and toluene were emitted from PCs at emission rates of 63.0 $\mu g\ h^{-1}$ and 47.0 $\mu g\ h^{-1}$ respectively per computer. The study also found traces of formaldehyde and long-chained alkanes including decane (11.6 $\mu g\ h^{-1}$) and undecane (7.6 $\mu g\ h^{-1}$).

1.2.5 Outdoor Air

There have been many studies which focus on how air pollution from outdoor sources affects outdoor air quality (Guenther, 1995; Veres et al., 2013; Lelieveld et al., 2015). These outdoor sources are also a source of indoor air pollutants. The main method through which outdoor pollutants affect indoor environments is through air exchange into buildings (Breen et al., 2014). Leaky and poorly insulated buildings will have a higher air exchange rate, over 2 h^{-1}, leading to outdoor pollutants infiltrating the home relatively quickly. However, modern buildings with a lower air exchange rate, less than 0.2 h^{-1}, are more tightly sealed (Nazaroff, 2021). Outdoor pollutants can enter buildings through open doors and windows (Abbatt and Wang, 2020).

In buildings with high ventilation rates, outdoor pollutants, such as ozone and particulate matter, can infiltrate the indoor environment and impact indoor air chemistry (Gold-

stein et al., 2021). Once inside, the outdoor pollutants can react with indoor generated pollutants. The reactions between outdoor and indoor pollutants form a myriad of secondary pollutants which are often detrimental to health (Weschler and Carslaw, 2018; Carslaw, 2019; Goldstein et al., 2021; Link et al., 2023a). In the absence of indoor sources, indoor concentrations of outdoor derived pollutants are often lower than outdoors, for instance, Farmer et al. (2019) found that ozone concentrations were 3.5 higher outdoors than indoors. The study also found that NO, NO_2 and CO concentrations were 29, 1.4 and 4 times lower indoors than outdoors respectively.

1.3 The Chemistry of Indoor Air

Short-lived radical species form from chemical processes both indoors and outdoors. These include the hydroxyl radical (OH), the hydroperoxy radical (HO_2), organic peroxy radicals (RO_2), the nitrate radical (NO_3) and Criegee intermediates (Weschler and Carslaw, 2018). It is considered that OH and O_3 are the most important oxidants in indoor chemistry (Young et al., 2019).

OH reacts with all hydrocarbons, whereas O_3 only reacts with double-bonded species such as terpenes, both resulting in the formation of secondary gas-phase multifunctional compounds. Monoterpenes, such as limonene, α-pinene and linalool dominate the unsaturated VOC mixture, driving O_3 reactions, forming secondary organic aerosols (SOAs), OH (which triggers further oxidation chemistry), HO_2 and RO_2. The ozone-terpene derived products have high molecular weights, meaning they have a lower volatility so can form particles. Nitrate radicals (NO_3) can also react with unsaturated organic compounds to form a variety of products. Figure 1.4 details how these different species can be formed from reactions of O_3, OH and NO_3.

Product	Product of reaction with:		
	O_3	OH	NO_3
Primary Ozonides			
Stabilised Criegee Biradicals			
Hydroxyl Radicals			
Alkyl Radicals			
Hydroxyalkyl Radicals			
Nitrooxyalkyl Radicals			
Hydroperoxy Radical			
Alkoxy Radical			
Unidentified Radical			
α-Hydroxyhydroperoxides			
Hydrogen Peroxide			
Hydroperoxides			
Peroxy-hemiacetals			
Secondary Ozonides			
Epoxides			
Hydroxy Carbonyls			
Dihydroxy Carbonyls			
Hydroxy Nitrates			
Carbonyl Nitrates			
Formaldehyde			
Other Aldehydes			
Acetone			
Other Ketones			
Formic Acid			
Other Carboxylic Acids			
Organic Nitrates			
Multifunctional oxidation products with carbonyl, carboxylate and/or hydroxyl groups			
Secondary organic aerosols via gas/particle partitioning of low Volatility products			

Figure 1.4: The reported products formed indoors from reactions of indoor oxidants (ozone (O_3), hydroxyl radicals (OH) and nitrate radicals (NO_3)) with unsaturated organic species. The green sections indicate the product can be formed from the respective oxidant reaction. The red sections indicate the product cannot be formed from the respective oxidant reaction. Figure adapted from source: Nazaroff and Weschler (2004).

The photolysis of O_3 initiates ambient air chemistry during daylight hours. Between wavelengths of 200 to 350 nm, the photolysis of O_3 produces excited oxygen atoms. The rate of this photochemical reaction indoors is slow compared to outdoors. Reaction 1.1 shows this photolysis reaction, where O^* denotes the excited oxygen atom in the singlet

D (^{1}D) state.

$$O_3 + h\nu \xrightarrow{200 < \lambda < 350\ \text{nm}} O^* + O_2 \tag{1.1}$$

The primary fate of the excited oxygen atom is reaction with ambient oxygen (O_2) or nitrogen (N_2), to form the ground state oxygen atom (O^3P) (Reaction 1.2). However, around 10% of the excited oxygen atoms (O^*) react with water (H_2O), forming OH radicals (Reaction 1.3).

$$O^* + O_2/N_2 \longrightarrow O + O_2/N_2 \tag{1.2}$$

$$O^* + H_2O \longrightarrow 2OH \tag{1.3}$$

The ground state oxygen atom formed in Reaction 1.2, can react with O_2 to form O_3. The process then repeats itself, enabling the production of more excited state oxygen atoms to initiate the chemical reaction sequence (Finlayson-Pitts and Pitts Jr, 1986, 2000).

In areas with high levels of NO_x, e.g. urban areas, OH reacts with the ingressed NO_2 to irreversibly form nitric acid (HNO_3) (Reaction 1.4). Reaction with NO forms nitrous acid (HONO) (Reaction 1.5), which can be photolysed (where $310 < \lambda < 400$ nm), to form OH and NO (Finlayson-Pitts and Pitts Jr, 2000) (Reaction 1.6).

$$OH + NO_2 \longrightarrow HNO_3 \tag{1.4}$$

$$OH + NO \longrightarrow HONO \tag{1.5}$$

$$HONO + h\nu \xrightarrow{300 < \lambda < 400\ \text{nm}} OH + NO \tag{1.6}$$

OH can also react with hydrocarbons to form a range of RO_2. For example, the simplest hydrocarbon, methane (CH_4), which is present in ambient air from natural gas,

will react with OH forming a methylperoxy radical (CH_3O_2) and H_2O (Reaction 1.7). The methylperoxy radical can subsequently react with NO to form an alkoxy radical, or in this case methoxide (CH_3O) (Reaction 1.8). The methylperoxy radical can also react with HO_2 to form methyl hydroperoxide (CH_3OOH) (Reaction 1.9) (Gaffney and Marley, 2003; Tyndall et al., 2001).

$$OH + CH_4 + O_2 \longrightarrow CH_3O_2 + H_2O \tag{1.7}$$

$$CH_3O_2 + NO \longrightarrow CH_3O + NO_2 \tag{1.8}$$

$$CH_3O_2 + HO_2 \longrightarrow CH_3OOH + O_2 \tag{1.9}$$

OH can react with carbon monoxide (CO), O_3 or hydrogen (H_2) to form HO_2. Given the HO_2 can subsequently react with O_3 and NO to form OH, these reactions are effectively reversible. HO_2 can also react with itself to form H_2O_2. Figure 1.5 summarises key routes for indoor chemistry. It shows how indoor and outdoor rates differ. Many indoor rates are much slower than outdoors, such as photolysis reactions. However, the reaction of biogenic VOCs with OH is 6 times higher indoors than outdoors, indicating how indoor reaction rates can be of a similar magnitude to those outdoors. Figure 1.5 also shows how the rates of reaction of ozone with monoterpenes are approximately two times higher indoors than outdoors.

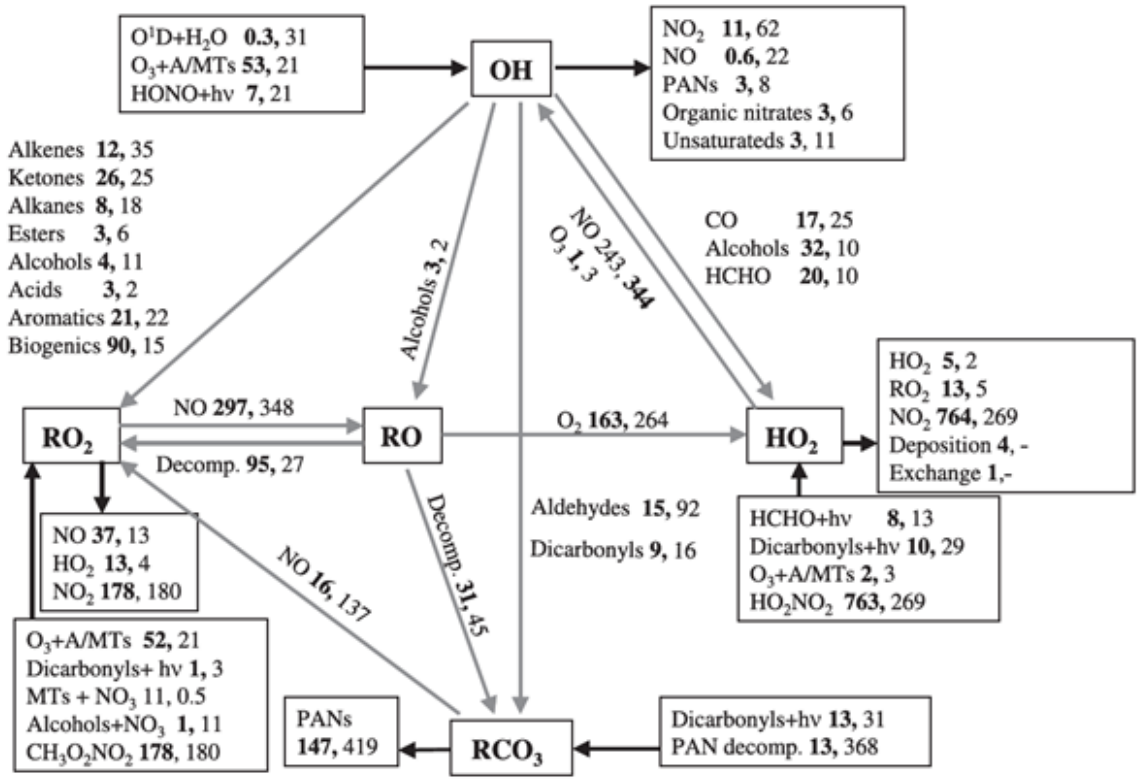

Figure 1.5: The key initiation (black arrows pointing into the radical), propagation (grey arrows) and termination (black arrows pointing out of the radical) routes for the radicals involved in indoor chemistry. The numbers in bold are rates of reaction for indoors, whereas, the normal font numbers are rates of reaction outdoors taken from Emmerson et al. (2007). In the figure, A/MTs refers to alkenes/monoterpenes, where PANs are peroxyacetylnitrates (Source: Carslaw (2007)).

Alkoxy radicals (RO) can also form aldehydes and HO_2 in the presence of O_2. For example, CH_3O can react to produce formaldehyde and HO_2. Formaldehyde can be photolysed, react with NO_3 or OH. These are described in Reactions 1.10, 1.11, 1.12, 1.13 and 1.14.

$$CH_3O + O_2 \longrightarrow HCHO + HO_2 \tag{1.10}$$

$$HCHO + h\nu + O_2 \longrightarrow CO + 2HO_2 \tag{1.11}$$

$$HCHO + h\nu + O_2 \longrightarrow H_2 + CO \tag{1.12}$$

$$HCHO + NO_3 \longrightarrow HNO_3 + CO + HO_2 \tag{1.13}$$

$$HCHO + OH + O_2 \longrightarrow HO_2 + CO \tag{1.14}$$

Different reactions and chemical transformations can take place indoors which can alter the air composition compared to outdoors (Weschler and Carslaw, 2018; Carslaw, 2019; Nazaroff and Weschler, 2020). For example, the biggest difference between indoor and outdoor O_3 is its ability to react with chemicals in the gas-phase. As shown in Table 1.2, 97% of O_3 outdoors reacts with NO to form NO_2 and O_2 (Tyndall et al., 2001), owing to the fast rate of reaction. Indoor O_3, however, can react with NO, deposit onto a surface, or be vented outdoors.

Table 1.2: The probability of the fate of ozone (O_3) in an indoor and an outdoor environment (Source: (Weschler and Carslaw, 2018)).

What does Ozone do?	**Outdoor (%)**	**Indoor (%)**
Reacts with NO	97	≈40
Reacts with unsaturated VOC	≈1	1
Deposition to a surface	≈1	≈40
Photolysed	≈1	0
Removed through air exchange	0	20

1.4 Knowledge Gap

Indoor air chemistry is a relatively new field of study in comparison to outdoor atmospheric chemistry. Consequently, there is still much to learn and discover about the chemical processes and transformations that take place in an indoor setting. Currently, there is a lack of understanding surrounding how oxidant deposition can affect radical chemistry in different indoor microenvironments. It is important to understand how rooms with varying surface area-to-volume ratios of materials will affect indoor pollutant concentrations and how our exposure to these pollutants change over the course of a typical day. Recently, there has been much focus on how outdoor air pollution can affect indoor air chemistry, however, there has been little attention on how indoor air pollution can affect outdoor urban environments. It is important to be able to categorise

which sources of indoor air pollution can affect outdoor air quality and which species can be attributed to each source. Furthermore, since the COVID-19 pandemic, indoor UVC air cleaning devices have become a popular choice to remove airborne pathogens. However, there is currently a lack of research determining how UVC light, emitted from these devices, can affect indoor air chemistry and the subsequent production of secondary pollutants. It is important to be able to understand how UVC photolysis affects indoor pollutant concentrations and determine whether it is safe for further and future worldwide distribution.

Modelling studies are an excellent way of exploring and detailing indoor chemistry, especially when experiments do not always provide the full picture. Experimental campaigns are sometimes limited by logistics and cost, therefore, models can be used as an alternative to provide detailed estimates. Models can also be effectively used alongside field campaigns, by incorporating experimental measurements to further provide a more accurate and deeper understanding of indoor chemistry. The INdoor CHEMical Model in Python, INCHEM-Py, is a detailed zero-dimensional indoor chemical box model which provides predicted concentrations of indoor pollutants over time. INCHEM-Py is a helpful tool to further elucidate indoor gas-phase chemistry and categorise which sources of indoor air pollution are key to the production of certain species and how they degrade indoors. INCHEM-Py is constrained by experimental data where possible (see Chapter 3), and is an excellent tool to provide an overall outlook of indoor air chemistry.

1.5 Thesis Aim

The primary aim of this thesis is to further develop INCHEM-Py to better represent indoor air chemistry and the myriad of gas-phase processes and transformations that take place. This improved model will be used to analyse how surface chemistry, indoor-outdoor exchange and UVC photochemistry can affect the production of both radicals and secondary pollutants in an indoor environment. These three aspects of indoor chemistry are key to further understanding the complex nature of air chemistry and results from this thesis can be used to find new methods of improving indoor air quality

both now and into the future.

1.6 Thesis Objectives

The main objectives of this thesis are:

• The improvement and development of the INdoor CHEmical Model in Python (INCHEM-Py) to include new chemical degradation mechanisms, and to update and expand outdoor VOC concentrations.

• Update and expand the representation of surface interactions in INCHEM-Py and investigate how this affects different indoor microenvironments.

• Use INCHEM-Py to evaluate how indoor activities (specifically cooking and cleaning) affect indoor and outdoor air quality and explore the interplay of pollutants at the indoor/outdoor interface.

• Develop INCHEM-Py to include photolysis between 200-300 nm and determine how light in this wavelength range affects indoor gas-phase chemistry.

1.7 Thesis Structure

The chapters which make up the thesis are structured accordingly:

Chapter 2: This chapter provides a detailed literature review of how indoor air quality modelling has changed over time. It also describes how current models are being used and developed to further broaden our knowledge of indoor chemistry.

Chapter 3: This chapter describes the methodology of INCHEM-Py and the development and updates for this thesis. The enhancements to the model include an improved representation of outdoor VOCs, and the addition of new chemical mechanisms. The impact of these new additions is also quantified.

Chapter 4: This chapter examines the impact of surface deposition of ozone and hydrogen peroxide onto different indoor materials and the subsequent chemical interactions. It also quantifies the impacts of surface interactions on indoor air pollutant concentrations.

Chapter 5: This chapter describes the impact that indoor cooking and cleaning have on the indoor and outdoor environment for a typical house and along an urban street.

Chapter 6: This chapter examines the effect of UVC photochemistry on the indoor environment, through incorporation of photolysis in the 200-300 nm wavelength region into INCHEM-Py.

Chapter 7: This chapter summarises the results of the thesis, explores how they have impacted indoor air chemistry research and provides proposals for future study.

Chapter 2

Literature Review

2.1 Introduction

There is a good understanding of outdoor air pollution and its health effects, but much less understanding of indoor air chemistry, where, use of everyday chemical products, the infiltration of outdoor pollutants and the resulting transformations, can result in high levels of indoor air pollution. Over time, indoor air pollution has become an increasingly important topic. The chemistry of indoor environments is complex and our understanding of the field has been aided by the development of models to help process and analyse experimental data. This chapter describes the development of indoor air chemistry models and how, over time, models have been updated and improved based on breakthroughs in the field.

2.2 The Evolution of Modelling Indoor Air Chemistry

Modelling has rapidly progressed our understanding of indoor air chemistry over the last 40 years. It is a useful addition to understand indoor chemistry, particularly when experimentation is limited by accuracy, sensitivity, logistics and cost. Models enable an exploration of the impact of building and environmental variables, such as air exchange rate, temperature and humidity, on indoor air chemistry (Shiraiwa et al., 2019). This often means that more, insightful data is produced that would be challenging to extract

using measurements alone. Models have to be developed and evaluated if they are to yield useful information. Working in tandem with experimentalists often yields the most robust modelling systems. Experiments often identify what data and aspects are missing in models, and provide guidance for future inputs.

The first indoor air mathematical model was created by Nazaroff and Cass in 1986. This model simulated pollutants which were chemically reactive in an indoor environment (Nazaroff and Cass, 1986). The model predicted the concentrations of important indoor species, including NO, NO_2, O_3, HNO_3, peroxyacetylnitrates (PAN), NO_3 and HCHO among others, in a simulated indoor gallery in California. Nazaroff and Cass used differential equations to simulate the change of concentration of a chemical species over time (Equation 2.1).

$$\frac{dC}{dt} = S - LC \tag{2.1}$$

In Equation 2.1, $\frac{dC}{dt}$ represents the change of concentration of a chemical species over time or the rate of change of a species' concentration, where C is the concentration of a chemical species indoors. S represents the sum of all source terms, including emissions and ingress from outdoors. L represents the total value of all sink terms, including loss to surfaces and chemical reactions. The model considered ventilation, chemical kinetics, photolysis rates, heterogeneous reactions, direct emissions and outdoor concentrations (Nazaroff and Cass, 1986).

The model was used to analyse pollutant concentrations for the Virginia Steele Scott Gallery, USA (Nazaroff and Cass, 1986). This was to ensure the concentrations of certain species, such as SO_2, NO_x and O_3 were being sufficiently controlled, in order to preserve rare books and archives from degrading and deteriorating. The rotting of antiques can occur with high levels of pollutants and elevated humidity (Güneş et al., 2022). The building had a surface area of 3060 m^2 and a total volume of 2530 m^3 (Nazaroff and Cass, 1986).

The model included a variety of source inputs for different species. For example, an in-

door hydrocarbon source and an indoor NO_x source was added, representing a preservation laboratory and cooking in a cafeteria respectively. Model sensitivity was also tested, such as through an assumption of 'low NO_2 wall loss', where the deposition velocity for NO_2 was set to zero. This allowed Nazaroff and Cass to explore gas-phase NO_2 chemistry assuming no loss to surfaces. Other scenarios included; excluding chemistry and switching all internal surfaces to glass. The different scenarios enabled Nazaroff and Cass (1986) to determine the average modelled concentrations of indoor pollutants which would otherwise be difficult to determine experimentally. The modelled concentrations for a variety of pollutants in the Scott Gallery are given in Figure 2.1.

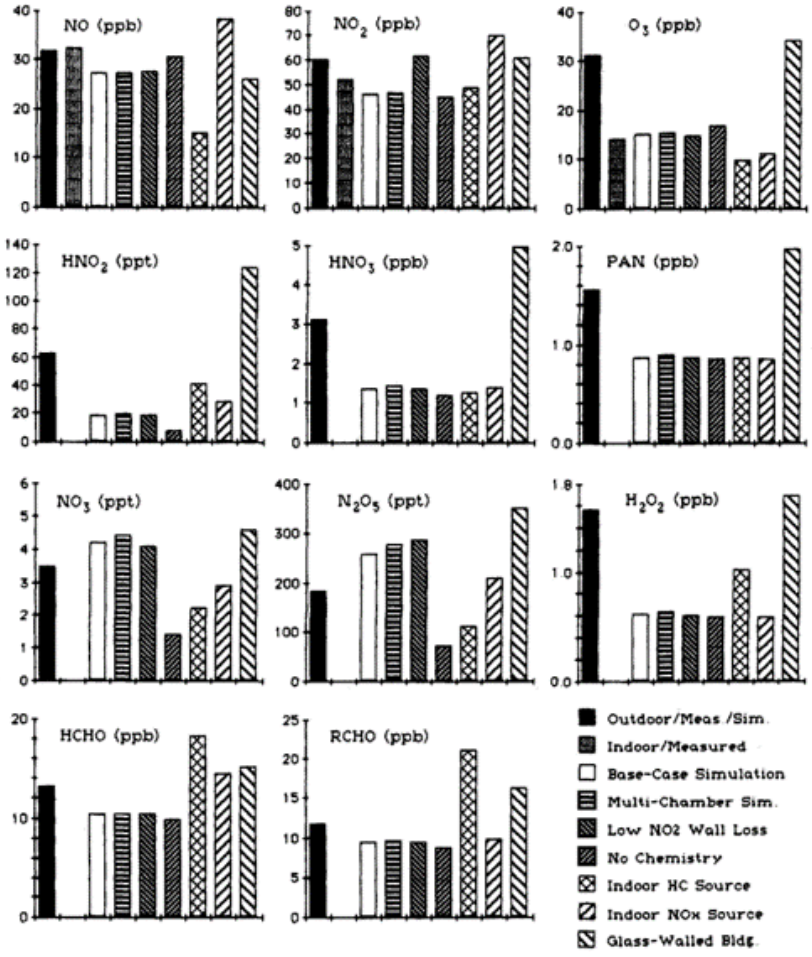

Figure 2.1: The average concentrations of modelled pollutant concentrations in the Scott Gallery under a variety of scenarios. The measured indoor and outdoor concentrations are given as a comparison. Some of the outdoor concentrations have been simulated due to a lack of data. In the figure, HC refers to hydrocarbon (Source: Nazaroff and Cass (1986)).

The modelled pollutant concentrations in the base case simulation compared well to the measured indoor concentrations for O_3, NO and NO_2 in the gallery. The results also provided a good comparison between indoor and outdoor pollutant concentrations. The results in Figure 2.1 showed how we may be able to modify indoor environments to provide more controlled pollutant concentrations without the need for measurements. This model and study revolutionised indoor air chemistry and there has been a rapid advancement in indoor chemistry modelling since it was developed by Nazaroff and Cass (1986). New parameters and ways of thinking had to be developed, particularly around exchange with outdoors and indoor sources.

The model reported by Tichenor and Mason (1988), predicted indoor air pollutant concentrations by incorporating known emissions from building and construction materials, including silicone caulk. The model considered ventilation, temperature and source emissions. Tichenor and Mason (1988) found that after the addition of 227 g of silicone caulk into a 14.5 m^3 bathroom, the concentrations of ketones, alcohols and esters all increased (Figure 2.2). The concentrations of these functional groups reached concentrations of above 700, 500 and 300 µg m^{-3} respectively. After 10 hours, the concentrations of ketone and ester had almost dissipated (<0.1 µg m^{-3}), with the elevated alcohol concentrations sustained for around 100 h (<0.1 µg m^{-3}).

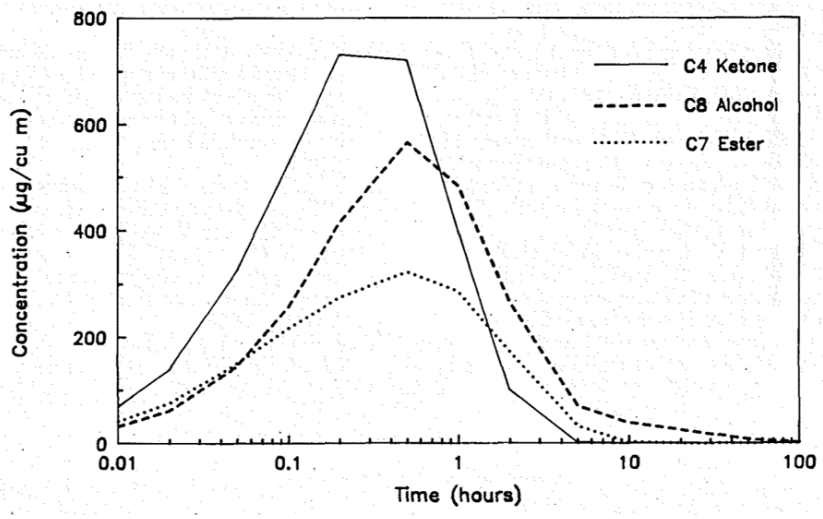

Figure 2.2: The modelled concentrations of a ketone, alcohol and an ester upon the addition of 227 g of silicone caulk in a bathroom (Source: Tichenor and Mason (1988)).

Nazaroff and Cass (1989) further developed their model through integration of an indoor aerosol dynamics component, which considered particle deposition velocities, particle collision frequency and sectional mean coagulation coefficients (Nazaroff and Cass, 1989). The model was tested by evaluating how indoor cigarette smoke interacted as an indoor aerosol. It was difficult to measure the success of the model as at this point, there were few experimental studies which detailed how cigarette aerosols behaved indoors (Nazaroff and Cass, 1989). It did show however, that despite the lack of experimental evidence, these simulations can be used alongside, and in place of, experiments to understand the indoor environment.

Cano-Ruiz et al. (1993) predicted indoor deposition velocities, through a model that examined the kinetics of the interactions at a gas-surface interface, and conceptualised reaction probability values for common indoor surfaces such as glass, concrete and paint for their respective reactions with ozone. Previously, Nazaroff and Cass (1989) incorporated the deposition velocities of particles and gas-phase species onto indoor surfaces. However, they assumed the surface uptake was fast and limited by mass transport. Cano-Ruiz et al. (1993) went a step further and integrated surface kinetics into their model by incorporating reaction probability (γ). This described the surface-pollutant interactions in the model, as defined by Equation 2.2.

$$\gamma = \frac{\text{pollutant removal rate}}{\text{pollutant collision rate}} \tag{2.2}$$

The reaction probability determines how much of a pollutant is removed from a surface. For example, if γ is zero there is no removal of a pollutant onto a surface, but if γ equals one, the pollutant is completely removed by a surface (Cano-Ruiz et al., 1993). This enabled their model to utilise how different surfaces affect pollutant uptake in an indoor environment.

Morrison and Nazaroff (2002b) went a step further and incorporated ozone deposition onto specific surfaces, developing a module which predicted reaction probabilities of ozone onto carpets, both the fibers and the backing material. Carpets have large surface

areas and are common in many homes: they have a complex surface due to the contrasting thickness and fibres used. Ozone can react with the fibres in the carpet forming secondary products (Morrison and Nazaroff, 2002a). The model succeeded in simulating ozone uptake on a carpet using mass transport and diffusion equations. The schematic used in the Morrison and Nazaroff (2002b) model for the uptake of ozone onto a carpet is shown in Figure 2.3.

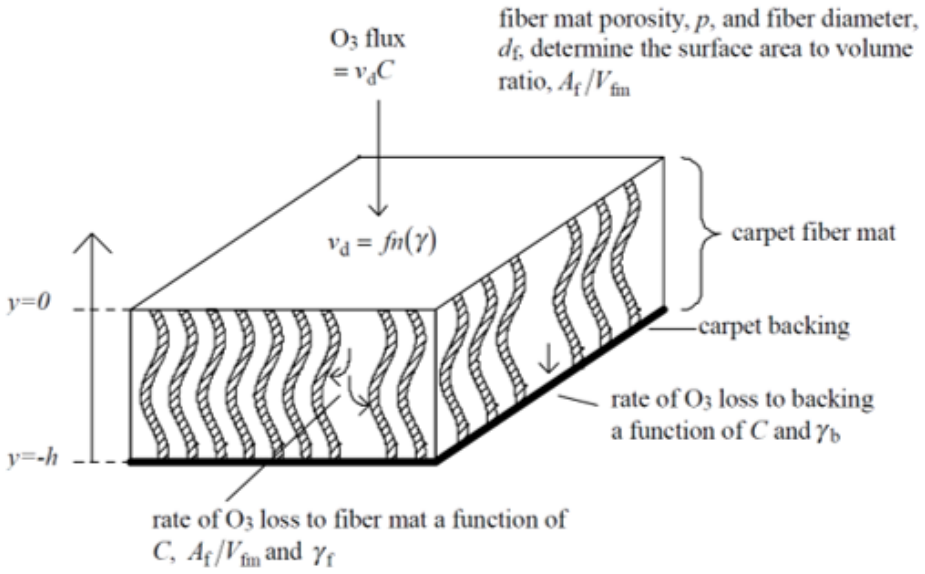

Figure 2.3: The schematic for the uptake of ozone onto a carpeted surface in the Morrison and Nazaroff (2002b) model. ν_d is the deposition velocity of ozone, h is the carpet depth, γ, γ_f and γ_b are the reaction probabilities of ozone for the overall carpet, the carpet fibre and the carpet backing respectively, C is the ozone concentration, A_f/V_{fm} is the surface area-to-volume ratio of the carpet fibres (Source: Morrison and Nazaroff (2002b)).

The deposition velocity of ozone onto a carpet was determined be between 0.016 and 0.064 cm s^{-1}, consistent with experimentally measured values (Morrison and Nazaroff, 2002b). The study also found that carpet backing can uptake the same amount of ozone as the fibres, even given the higher surface area-to-volume ratio of the fibres. For the first time, deposition velocities of ozone were able to be predicted for carpeted surfaces. This led to further studies identifying the uptake of ozone (Poppendieck et al., 2007a) and other oxidants onto different types of surfaces (Poppendieck et al., 2021).

Liu et al. (2014) incorporated semi-volatile organic compounds (SVOCs) and their partitioning between airborne particles and the gas-phase into their model, to determine the

environmental fate of SVOCs in the indoor and outdoor environments and how they affected human health. The partitioning between SVOCs and particles were incorporated into this model for both outdoor and indoor scenarios. The model simulated the size and distribution of indoor and outdoor particles, including polycyclic aromatic hydrocarbons (PAHs) from SVOCs (Liu et al., 2014). The simulations provided understanding into how indoor particulate matter forms and the expected size distribution in an indoor and outdoor environment.

The first model to consider detailed indoor chemistry was that developed by Carslaw (2007), using a 'near-explicit' chemical mechanism. The 'Indoor Detailed Chemical Model' (INDCM) was based on the Master Chemical Mechanism (MCM), which provided degradation reactions for VOCs following oxidation (Jenkin et al., 1997). The MCM is regularly updated to include information for new species as they become available. For example, Jenkin et al. (2015) describes the degradation of isoprene which consisted of 602 closed shell and free radical species and 1926 reactions. Isoprene plays a key role in indoor air chemistry given it is emitted from breathing and is considered one of the most abundantly released non-methane VOC in the atmosphere (Jenkin et al., 2015). The MCM also includes photolysis reactions for species which dissociate in the presence of light.

The INDCM did not use any lumping of reactions or surrogate species, a 'representative' species assumed to be a proxy for a certain class or functional group of chemicals (Carslaw, 2007). The purpose of the INDCM was to simulate indoor air pollutant concentrations in urban homes, schools and offices throughout the UK. The model included approximately 15,400 reactions, whilst utilising around 4,700 species (Carslaw, 2007). The initial model included deposition onto surfaces, basic surface emissions, chemical and photolysis reactions, and exchange with outdoor air.

Carslaw et al. (2012) upgraded the INDCM to include 41 gas- to particle-phase partitioning for limonene oxidation products. Limonene, a cyclic monoterpene, is the most dominant terpene in indoor chemistry and drives secondary organic aerosol (SOA) formation indoors. Figure 2.4 shows the major gas- and particle-phase products and the oxidation pathways of limonene following cleaning with a limonene-based product. The volatility

of each of these products determines whether it exists predominantly in the gas-phase or particle-phase. This model was used to simulate cleaning, through the addition of 200 ppb of limonene in a typical home setting for 30 minutes, based on observations by Singer et al. (2006). The surface area-to-volume ratio of the room was 3 m^{-1} and the air change rate was 0.76 air changes per hour (Carslaw, 2013). The concentrations of pollutants were averaged between the hours of 10 am and 2 pm and ranked accordingly by the difference in concentration between periods with and without cleaning. The concentration of ozone in the model in this study was approximately 5 ppb (Carslaw, 2013). LIMKET (4-acetyl-1-methyl-1-cyclohexene) and C729CHO (structure given in Figure 2.4) had differential concentrations of 1,744 and 898 ppt, whilst PAN, glyoxal and formaldehyde had differential concentrations of 567, 479 and 426 ppt respectively. Limonene cleaning can therefore efficiently produce secondary products in a home environment (Carslaw, 2013).

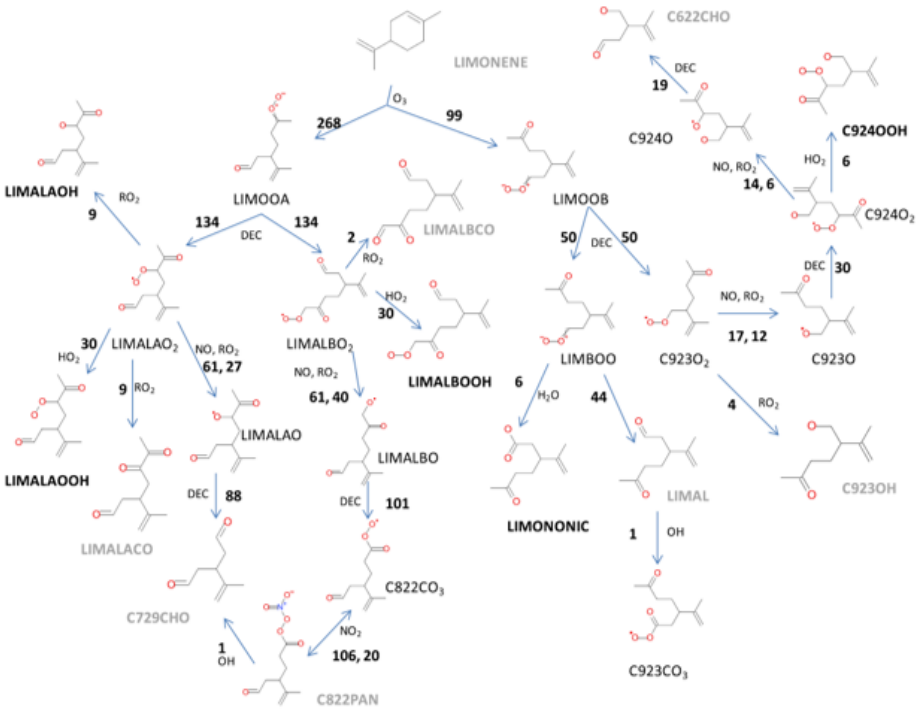

Figure 2.4: The oxidation of limonene by ozone following cleaning. The numbers on the schematic represent the rates of reaction (units of 1 × 10^5 molecule cm^{-3} s^{-1}). The bold numbers represent the key particle-phase species, whereas the species in grey denote key species that are predominantly in the gas-phase. The reactant and product names in the figure refer to species names from the Master Chemical Mechanism (Source: Carslaw (2013)).

Kruza et al. (2020) implemented gas-to-particle partitioning for α-pinene. 136 gas-phase oxidation products were identified following α-pinene oxidation which were thought likely to partition to the particle-phase. These were non-radical species and contained more than 5 carbon atoms, and were assumed to undergo gas-to-particle partitioning according to Pankow (1994). Gas-to-particle partitioning was also added to the INDCM for β-pinene. The INDCM model was recently refactored to an open-source model using Python (Shaw and Carslaw, 2021; Shaw et al., 2023), named INCHEM-Py. INCHEM-Py is the model used in this thesis and it is described in detail in Chapter 3.

2.3 The Modelling Consortium for Chemistry of Indoor Environments

The Modelling Consortium for Chemistry in Indoor Environments (MOCCIE) involves a number of research groups working on the progression and development of models for indoor air chemistry. The consortium was initiated from the Chemistry of Indoor Environments program funded by the Alfred P. Sloan Foundation in 2017, initially for two years. Due to the success of the first MOCCIE program (MOCCIE 1), two further MOCCIE programs (MOCCIE 2 and MOCCIE 3) were funded by the Alfred P. Sloan Foundation, with the MOCCIE projects finishing in 2024.

The MOCCIE groups use models that incorporate computational fluid dynamics (CFD), molecular dynamics, kinetic processes, gas-phase chemistry, and organic aerosol chemistry across varying temporal and spatial scales (Shiraiwa et al., 2019). These temporal scales range from nanoseconds to days, with the spatial scale ranging from nanometres to tens of metres (Shiraiwa et al., 2019) (Figure 2.5).

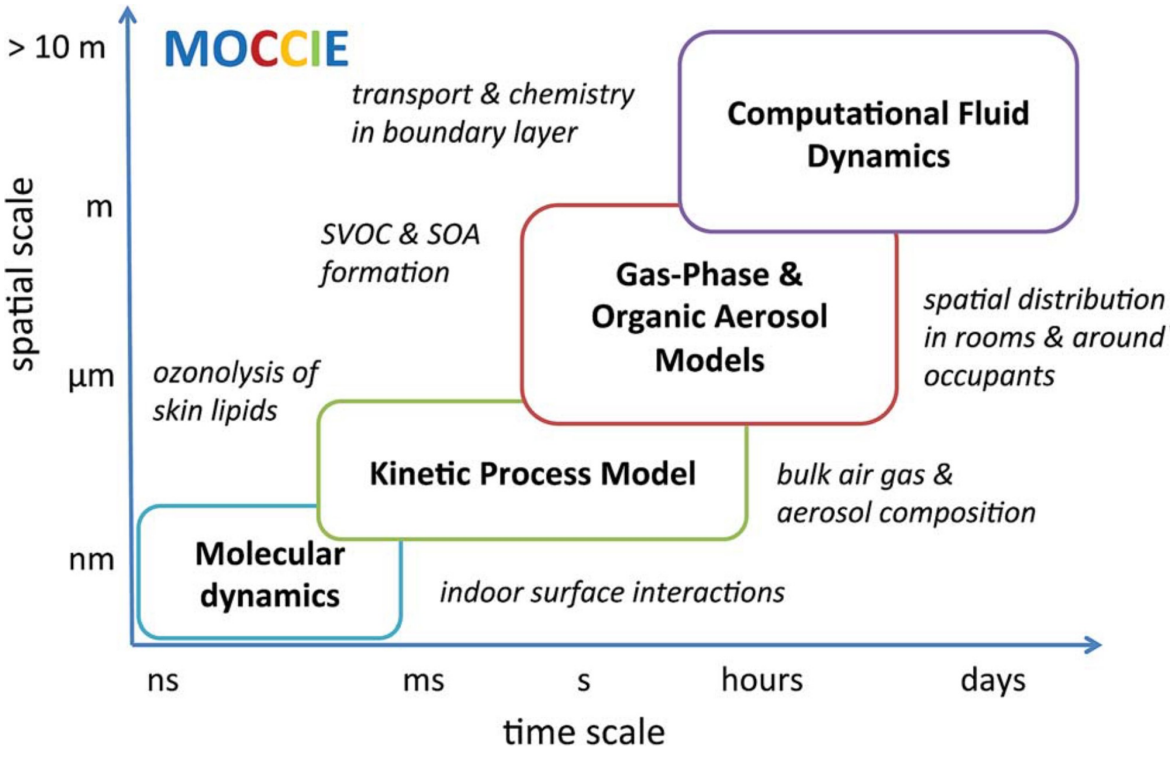

Figure 2.5: The spatial and temporal scales of different models used to study indoor chemistry in the Modelling Consortium for Chemistry in Indoor Environments (MOCCIE). In the figure, SVOC and SOA are referred to as semi-volatile organic compound and secondary organic aerosol respectively (Source: Shiraiwa et al. (2019)).

The aims and objectives of MOCCIE were (Shiraiwa et al., 2019):

• To determine gaps in our knowledge of the processes and transformations of indoor chemistry.

• To guide the design of field campaigns and experimental studies by providing predicted measurements of indoor species, also helping to identify the parameters driving model uncertainty.

• To use models to assist with the analysis of experimental field campaigns and underpin species or measurements that would have been difficult to determine experimentally.

MOCCIE provides a framework for indoor air models to be developed, whilst utilising experimental data from various studies, including the work from HOMEChem (Farmer et al., 2019). Its goal was to develop physical-chemical models which considered surface,

particle-phase, and gas-phase chemistry in indoor microenvironments. The models also needed to consider the impact of building properties, people and occupants and regular indoor activities such as cooking or cleaning.

The aim of MOCCIE was never to provide a unified model, rather to exploit links between the models, using them to inform and develop each other, whilst encapsulating the complex nature of indoor air chemistry. Figure 2.6 provides an overview of the different models in the consortium, and how each is being used and developed to contribute to indoor chemistry research. It also shows how the different models and modelling areas have been interconnected to further yield insightful information about a particular topic or area of focus (Shiraiwa et al., 2019).

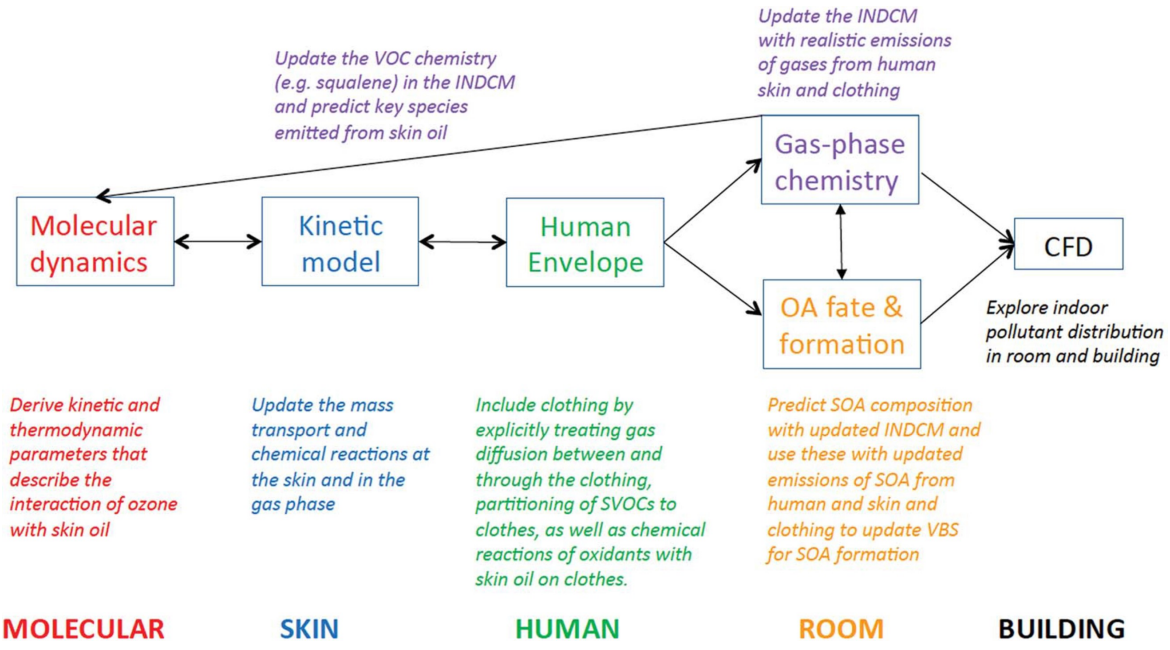

Figure 2.6: The different modelling areas in the Modelling Consortium for Chemistry in Indoor Environments (MOCCIE) and connections between them. In the figure, INDCM is referred to as the indoor detailed chemical model (see Section 2.2). CFD is referred to as computational fluid dynamics (Source: Shiraiwa et al. (2019)).

The following sections provide an overview of the different models and research areas that are currently used to categorise indoor chemistry through the MOCCIE project.

2.3.1 Molecular Dynamics Modelling

Molecular dynamics modelling represents the smallest temporal and spatial scale in the MOCCIE schematic (Figure 2.5) dealing with time scales of nanoseconds and spatial scales of nanometres. This type of modelling is used to understand the molecular dynamics of electron and proton transfer, as well as photolysis reactions in liquid-surface interfaces and in the gaseous phase (Gerber and Sebek, 2009; Gerber et al., 2015). The molecular dynamics area of MOCCIE is led by Doug Tobias of the University of California, Irvine, USA and has been applied to analysis of molecules moving across the skin-air interface, as well as molecular interactions on surfaces.

Fang et al. (2019) investigated the interactions of limonene, benzene, cyclohexene and cyclohexane with hydroxylated silicon dioxide (SiO_2) using ab initio molecular dynamics (AIMD). The SiO_2 is hydrophilic and is the main component of glass, a surface which is commonly found indoors. Fang et al. (2019) found that benzene and cyclohexene showed π-hydrogen bonding with OH groups that were present on the glass surface. Cyclohexane however showed interaction with the same OH groups through forces of dispersion. This observation demonstrated that the interaction between limonene and glass was stronger than the interactions of glass with the other species, with the cyclohexane interaction the weakest (Fang et al., 2019).

Following on from the work by Fang et al. (2019), Frank et al. (2020) investigated the interaction of water which had adsorbed onto a glass surface (SiO_2) with adsorbed limonene. The aim of the study was to understand how this interaction changed as relative humidity varied indoors. This study also utilised ab initio molecular dynamics (AIMD) and force field-based molecular dynamics. It found that as the relative humidity increased, limonene was still attached to the SiO_2 surface and was not completely displaced by the increase in adsorbed water (Figure 2.7). Even when the relative humidity was approximately 80%, over half of the limonene was still attached to the surface (Frank et al., 2020). These simulations are key to understanding how these types of species interact with surfaces indoors at the molecular level. It can provide a base to understand how other or-

ganic species interact with surfaces, potentially leading to the creation of indoor sensors (Frank et al., 2020).

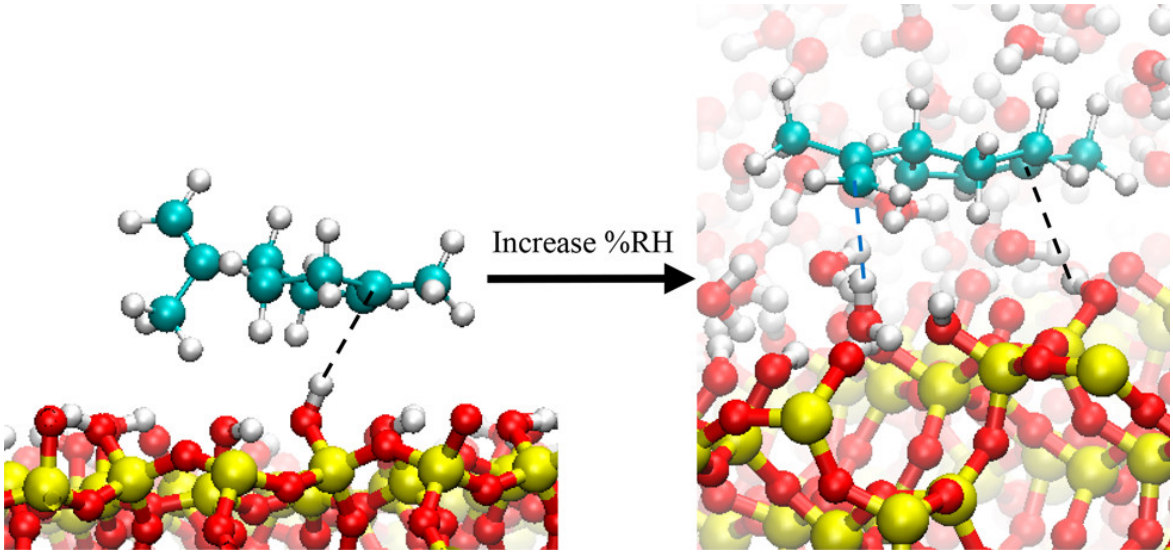

Figure 2.7: An output from ab initio molecular dynamics (AIMD) simulations detailing the effect of limonene interactions with silicon dioxide (SiO_2) with an increase in indoor relative humidity (RH). The yellow molecules represent silicon, the red molecules represent oxygen, the white molecules represent hydrogen and the light blue molecules represent carbon (Source: Frank et al. (2020)).

Other molecular dynamic simulation studies performed through MOCCIE, investigated the interaction between other species on SiO_2 including oxygenated organic compounds (Huang et al., 2021b), cyclic monoterpenes (Huang et al., 2021a), carvone (Fan et al., 2022) and 6-methyl-5-hepten-2-one (6-MHO) which is a key product of skin oil ozonolysis (Frank et al., 2023). The Tobias group also investigated the molecular dynamics of skin oils, including the orientation of squalene, commonly found in human skin oils (Wisthaler and Weschler, 2010; Weschler, 2016), at the skin-air interface (Von Domaros et al., 2021). The study identified a preferred orientation for squalene, which helped to understand its reactivity indoors, especially through ozonolysis reactions (Von Domaros et al., 2020). Studies like these help to identify the interactions of indoor pollutants with indoor surfaces and their subsequent impact on the indoor chemistry.

2.3.2 Kinetic Process Modelling

The kinetic process modelling activities within MOCCIE are led by Manabu Shiraiwa at the University of California, Irvine, USA and Glenn Morrison at the University of North Carolina, Chapel Hill, USA. These activities have mainly involved consideration of the kinetics and mass transport at the skin-air-clothing interface.

Lakey et al. (2017) developed a model to predict chemical reactions at the gas-skin interface called the KM-SUB-Skin model. The model was able to accurately predict concentrations of squalene (found in skin oil) ozonlysis products over time (Lakey et al., 2017). The study used a development of the KM-SUB model (Shiraiwa et al., 2010), which was previously used to determine the impact of bulk diffusion on the rate of uptake of oleic acid ozonolysis particles onto surfaces (Shiraiwa et al., 2010). Lakey et al. (2017) found that when exposed to approximately 30 ppb of ozone indoors, the concentration of products which are formed from skin oil ozonolysis can reach several ppb.

Lakey et al. (2019) also investigated the impact of clothing on skin oil ozonolysis products and ozone. The addition of skin and clothing bulk chemistry and a new boundary and clothing layer, allowed the production of a new model called the KM-SUB-Skin-Clothing model (Lakey et al., 2019), which is a further extension of the KM-SUB-Skin model (Lakey et al., 2017). The model structure is shown in Figure 2.8 (Lakey et al., 2019). This enabled Lakey et al. (2019) to predict the lifetime of squalene on clothing surfaces and the concentration under various indoor conditions, such as with high and low ambient ozone concentrations present.

The parameters of three experimental datasets were inputted into the KM-SUB-Skin-Clothing model (Lakey et al., 2019). The first experimental dataset consisted of soiled t-shirts exposed to ozone in a 28.5 m^3 chamber with an air change rate of 3 hr^{-1} (Wisthaler et al., 2005). The second dataset consisted of a worn 250 cm^2 cotton shirt in a 10.5 L chamber where the air change rate was 23 hr^{-1} (Coleman et al., 2008). The third dataset was based on Rai et al. (2014), who exposed worn 0.9 m^2 cotton shirts to ozone in a 5.1 m^3 chamber, with air change rates of 2.7 hr^{-1} and 0.5 hr^{-1} (Lakey et al., 2019). The concentrations of squalene ozonlysis products were identified and predicted by the model.

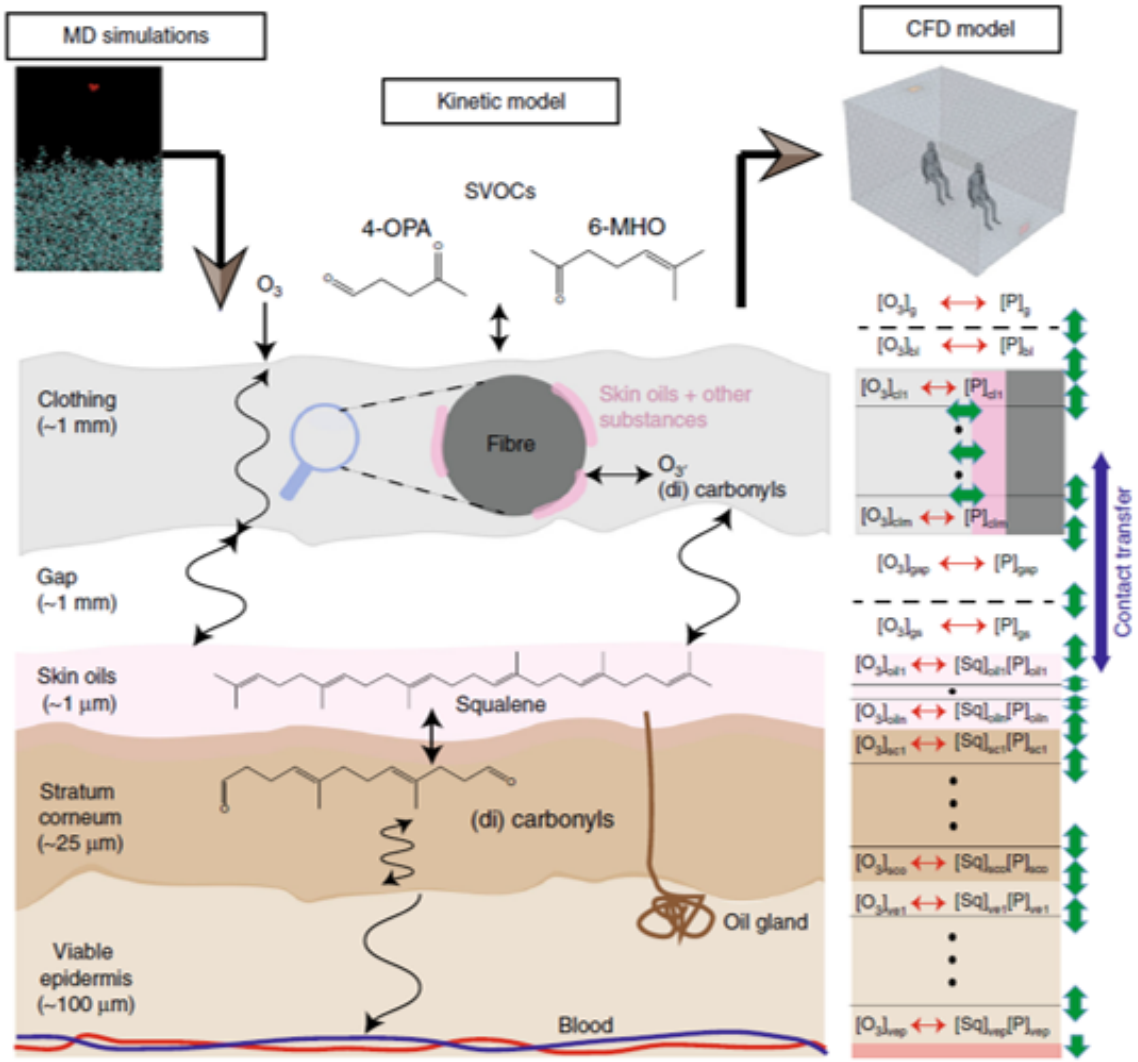

Figure 2.8: The structure of the KM-SUB-Skin-Clothing model, showing how ozone interacts with skin, skin oils and clothing and how different species can diffuse between these contrasting layers. (Source: Lakey et al. (2019)).

Figure 2.9 shows the concentrations of three key squalene-ozonolysis reaction products, acetone, 4-OPA and 6-MHO, as well as the concentration of ozone.

Figure 2.9 shows that the model predictions are in excellent agreement with experimental data. In the Wisthaler et al. (2005) comparison (Figure 2.9a), the model followed the steady increase of ozone as it was added into the chamber, reaching approximately 110 ppb after 6 hours in the non-clothing simulation and approximately 80 ppb in the clothed simulation (Lakey et al., 2019). The model also compared well in predicting the concentrations of squalene oxidation including acetone, 4-OPA and 6-MHO, which all increased

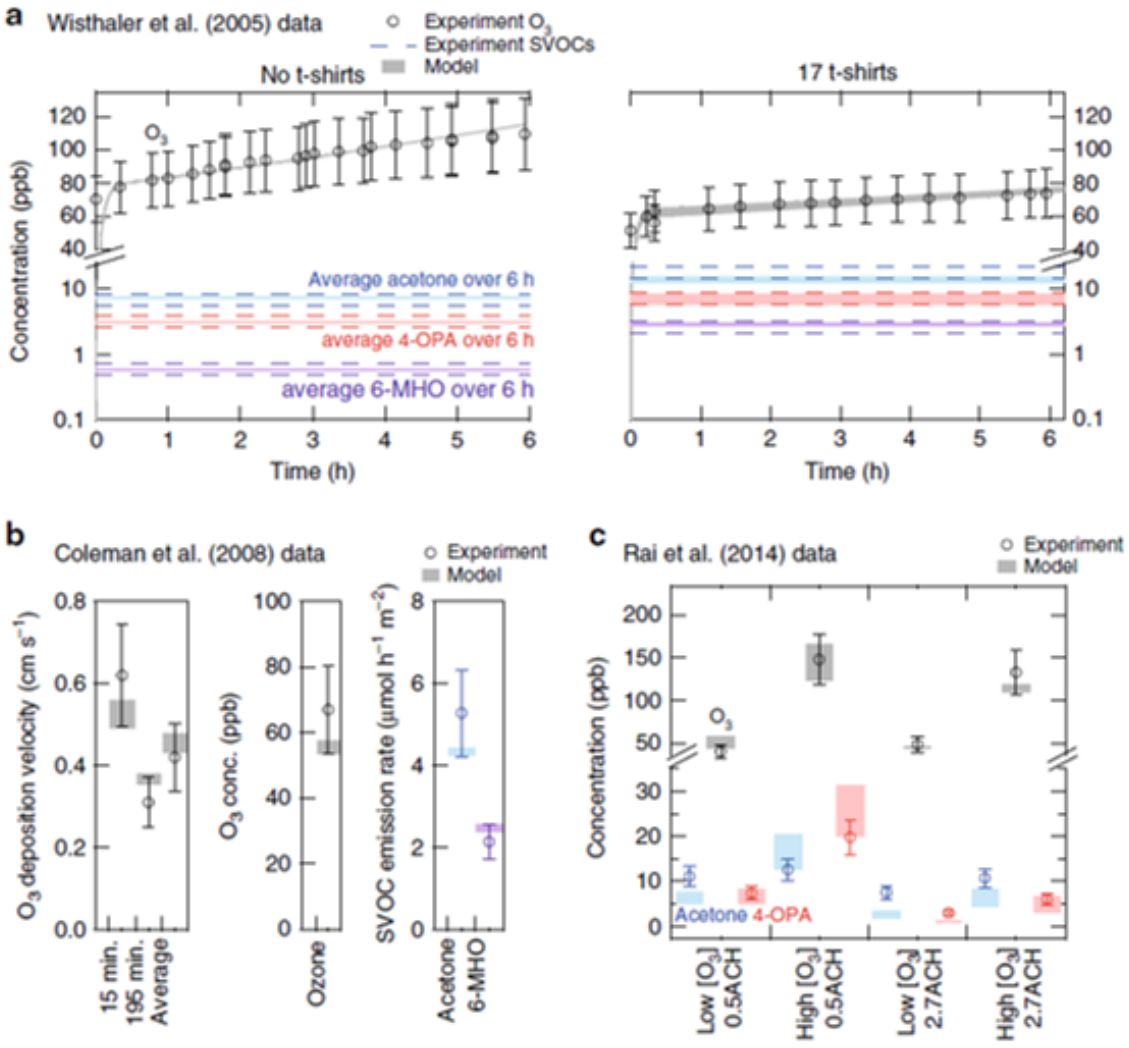

Figure 2.9: The outputs from the KM-SUB-Skin-Clothing model for the three experimental datasets. The top graphs (labelled 'a') show the modelled and experimental (from Wisthaler et al. (2005)) concentrations of ozone, acetone, 4-OPA and 6-MHO with no t-shirts present (left) and 17 t-shirts present (right) over 6 hours. The bottom left graphs (labelled 'b') shows the modelled and experimental (from Coleman et al. (2008)) deposition velocity of ozone onto soiled clothing after 15 minutes, 195 minutes and an overall average. It also shows the ozone concentration and the emission rates of acetone and 6-MHO during exposure of ozone onto soiled clothing. The bottom right graph (labelled 'c') shows the average modelled and experimental (from Rai et al. (2014)) concentrations of ozone, acetone and 4-OPA under various air changes per hour (ACH). (Source: Lakey et al. (2019)).

by a few ppb upon the addition of soiled clothing. The model also predicted the deposition velocity of ozone from the Coleman et al. (2008) experiment (Figure 2.9b) and was within the range of uncertainty for the deposition velocity of ozone at different time points. Similarly, the model showed good agreement with the formation of squalene-

ozonlysis products in Rai et al. (2014) under a range of ozone concentrations and air change rates (Figure 2.9c). Overall, the study provides confidence in the predicted concentrations for ozone, acetone, 4-OPA and 6-MHO.

Further developments of the kinetic multi-layer model have been the implementation of boundary layer processes, bulk diffusion and multi-layer adsorption, denoted as the KM-FILM model (Lakey et al., 2021). KM-FILM (Kinetic Multi-Layer Model of Film Formation, Growth and Chemistry) has been used to simulate film formation on surfaces by considering gas-phase diffusion and turbulence on a particular surface (Lakey et al., 2021). It also showed that the rate of film growth was enhanced by approximately a factor of two through heterogeneous reactions (Lakey et al., 2021). The KM-FILM model was also used to simulate organic film formation on indoor surfaces (Lakey et al., 2023).

Multiphase ozonlysis for oleic acid-based lipids, such as triolein, was also identified utilising the KM-GAP (Kinetic Multi-Layer Model for Gas and Particles) model which simulates gas-particle interactions in clouds and aerosols (Shiraiwa et al., 2012). Zhou et al. (2022) found that "crust" accumulation on surfaces as a result of ozone-lipid chemistry can affect indoor air quality via the re-emission of VOCs. Other kinetic process modelling as part of the MOCCIE consortium has led to the development of a model which accounts for ozone deposition chemistry at a surface. For example, Morrison et al. (2019) identified that reactive intermediates which have shorter lifetimes have higher concentrations closer to surfaces indoors than in the bulk air, which leads to higher deposition velocities than those with longer lifetimes.

2.3.3 Gas-Phase Chemistry Modelling

The gas-phase chemistry modelling part of MOCCIE3 includes the work in this thesis, where, the INdoor CHEmical Model in Python (Shaw and Carslaw, 2021; Shaw et al., 2023) has been developed to simulate gas-phase chemistry to account for surfaces (Chapter 4), indoor-outdoor chemistry (Chapter 5) and UVC photochemistry (Chapter 6). The Methodology of INCHEM-Py is discussed in Chapter 3. The gas-phase chemistry modelling area of MOCCIE is led by Nicola Carslaw at the University of York, UK.

During MOCCIE 1 and MOCCIE 2, the INDCM was developed to include surface ozone interactions (Kruza et al., 2017), breath and skin emissions (Kruza and Carslaw, 2019), and improved representation of the formation of secondary organic aerosols (Kruza et al., 2020). Kruza et al. (2017) found that deposition onto surfaces accounts for 80% of ozone loss indoors and found that nonanal (5-7 ppb) was the most important aldehyde to be formed indoors as a result of ozone deposition onto painted walls. Kruza and Carslaw (2019) found that modelled concentrations of skin oil oxidation products including formic acid, acetic acid and 4-OPA reached a maximum of 0.5, 0.1 and 0.8 ppb respectively in a school classroom. Similarly, concentrations of 6.6, 21.5 and 22.3 ppb were measured for methanol, ethanol and acetone (Kruza and Carslaw, 2019). These species were attributed to be mostly emissions as a result of breath. Kruza et al. (2020) showed that highly oxygenated molecules (HOMs) needed to be included in the INDCM to better reproduce measured secondary organic aerosol mass.

Using these new developments, a Monte Carlo analysis was performed on the INDCM to determine model sensitivity to the input parameters (Kruza et al., 2021). Over 1,000 model runs, key input parameters were stochastically varied based on literature data, including air change rates, deposition velocities, temperature and UV light transmission. Kruza et al. (2021) found that transmission of UV light led to the largest Spearman's rank positive correlation with concentrations of OH (+0.92) and organic nitrates (+0.95). The study also identified that more accurate measurements of ozone deposition velocities onto surfaces and UV light transmission indoors reduced model uncertainty of ozone and OH concentrations by 70-80% (Kruza et al., 2021). The INDCM (Kruza et al., 2017; Kruza and Carslaw, 2019; Kruza et al., 2020, 2021) formed the basis of INCHEM-Py, which will be the focus of this thesis.

2.3.4 Aerosol Composition and Thermodynamic Modelling

Aerosol composition and thermodynamic modelling has been used to describe the character and behaviour of organic aerosols, including SOA formation (Shiraiwa et al., 2019). The package used to characterise organic aerosol behaviour is called IMAGES (Indoor

Model of Aerosols, Gases, Emissions and Surfaces) (Waring, 2014; Cummings and Waring, 2019; Cummings et al., 2024) which uses the 2D volatility basis set (2D-VBS) (Jimenez et al., 2009; Donahue et al., 2011). The IMAGES model describes the thermodynamic characteristics of aerosols and gas-phase kinetic chemistry and accounts for emissions from standard building materials and people (Shiraiwa et al., 2019). Aerosol viscosity modelling has also been considered to provide further insight into aerosol behaviour indoors (Lilek and Zuend, 2022). The aerosol composition and thermodynamic modelling area of MOCCIE is led by Michael Waring at Drexel University, Philadelphia, USA and Andreas Zuend at McGill University, Montreal, Canada.

Cummings et al. (2020) investigated the impact of water content and relative humidity on the phase state of organic and inorganic aerosols in residences in the United States. Using the IMAGES model, the concentrations of organic aerosols were simulated, based on the thermodynamics associated with US buildings (Cummings and Waring, 2019). The model was expanded to incorporate speciated inorganic aerosol concentrations, aerosol water uptake and organic aerosol phase states (Cummings et al., 2020). The aerosol water mass was approximately 10 to 100 times smaller than dry particulate matter mass in the residences, whilst the the aerosol water mass outdoors was 10 times larger than indoors (Cummings et al., 2020). This finding helps to understand aerosol mass and composition indoors, and differences with those found outdoors.

Another study by this group (Cummings et al., 2021) investigated the effect of mass-transport and temperature gradients on indoor aerosol partitioning. Figure 2.10 shows the model conceptually and how changes in temperature when moving between indoors and outdoors, can affect thermodynamic equilibrium and hence indoor concentrations of aerosols (Cummings et al., 2021). The study found that in 16 climate zones across the United States, not including this repartitioning process resulted in errors of between 40 to 60% of the total organic aerosol concentration, indicating how important repartitioning is when considering indoor aerosol concentrations (Cummings et al., 2021).

Further studies from the MOCCIE campaign have explored the impact of phase states on organic aerosol repartitioning (Cummings et al., 2022), as well as relative humidity

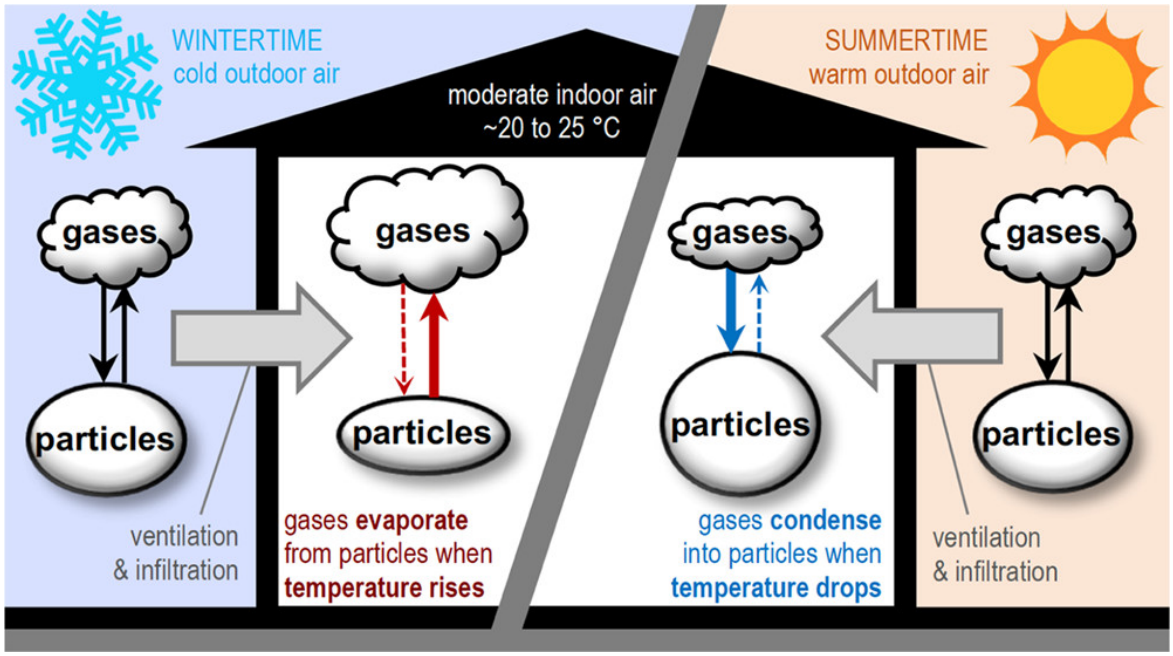

Figure 2.10: Conceptualisation of the transport and thermodynamics of gases and aerosols as they transition from indoors to outdoors and vice versa (Source: Cummings et al. (2021)).

(Serrano Damha et al., 2024). The HOMEChem experimental dataset (Farmer et al., 2019) has also been used to predict semi-volatile organic compound emissions, where cooking was found to increase particle concentrations and emission rates by one to two orders of magnitude (Cummings et al., 2023).

2.3.5 Computational Fluid Dynamics Modelling

Computational fluid dynamics (CFD) models provide predicted concentrations of species by solving spatially and temporally using parameters including temperature, mass balance and momentum in a specific indoor environment (Rim et al., 2018; Sorensen and Weschler, 2002). Outputs from the CFD model quantify the movement and concentration of species indoors and respective air flow distribution under various ventilation rates and environmental conditions (Nielsen, 2015). The computational fluid dynamics modelling area of MOCCIE is led by Donghyun Rim at Penn State University, Pennsylvania, USA.

Rim et al. (2018) investigated the impact of human surfaces indoors, particularly on

ozone uptake and deposition. Rim et al. (2018) used CFD modelling to investigate various air flows and ventilation rates to analyse the reaction dynamics of ozone in the vicinity of people. For indoor settings with an air change rate of less than 5 air changes per hour and a room volume of 58.1 m^3, Rim et al. (2018) found that ozone deposition onto oil from human skin had a deposition velocity of between 8 and 10 m h^{-1}, compared to between 2 and 3 m h^{-1} onto unsoiled clothing. From these deposition rates, the formation of major products from ozone surface chemistry were predicted. In a simulation with 90 ppb of indoor ozone in a room, emission rates of 6-MHO, nonanal, decanal and acetone were 0.1, 0.1, 0.2 and 0.3 mg hr^{-1} $person^{-1}$ respectively (Rim et al., 2018). This indicates how important CFD models are for determining how ozone interacts with skin both spatially and temporally.

Won et al. (2020) predicted spatial distributions and concentrations of ozone, geranyl acetone, 6-MHO and 4-OPA from a CFD simulation which analysed the effects of soiled and unsoiled clothing (Figure 2.11). The air change rate in these simulations was 1 hr^{-1} and the area of the room was 28.5 m^3. Figure 2.11 shows how ozone concentrations are highest in the laundered clothing simulation, indicating that ozone is depositing more readily onto soiled clothing, reducing its indoor concentration. Consequently, the concentrations of geranyl acetone, 6-MHO and 4-OPA are higher in the soiled clothing scenario compared to laundered clothing (Won et al., 2020). The enhanced concentration of the species directly above the human in Figure 2.11 for all of the eight graphs is the result of the human thermal plume.

Won et al. (2020) also developed the CFD model to include breathing zones from humans, which can be simulated to predict the concentrations of species during normal exhalation (6 L min^{-1}) compared to breathing during exercise (12 L min^{-1}) (Won et al., 2020). It was found that the average concentration of isoprene in a 28.5 m^3 room was 8 ppb during exercise, compared to 4 ppb with a normal breathing rate (Won et al., 2020).

Further studies of CFD modelling during the MOCCIE campaign include simulating the photolysis of HONO indoors and the subsequent reactions involving HO_2 and OH radicals (Won et al., 2019). The study found that production of OH and HO_2 were limited

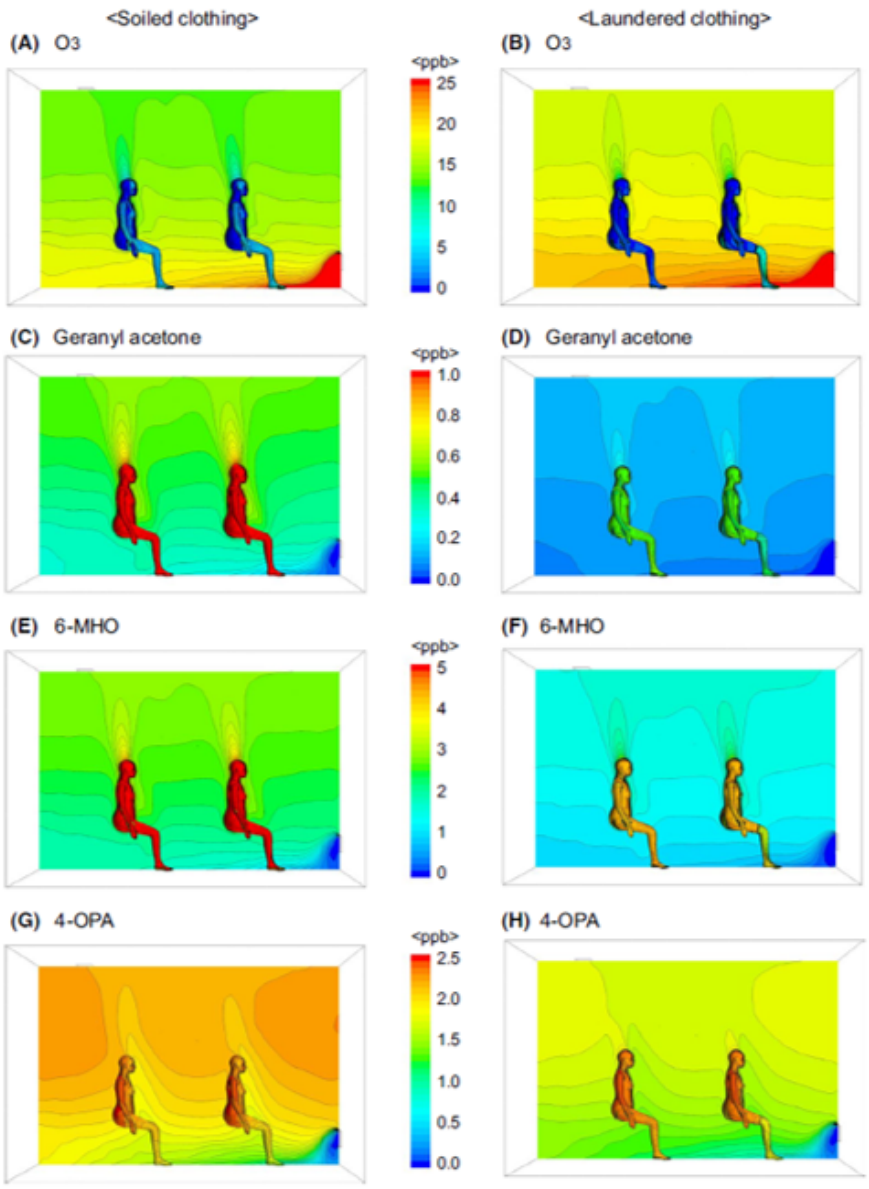

Figure 2.11: The spatial concentrations of ozone, geranyl acetone, 6-MHO and 4-OPA from CFD modelling comparing soiled clothing (left) with clean clothing (right). The air change rate was assumed to be 1 air change per hour (Source: Won et al. (2020)).

to the volume of room within the photolysing light (near the window). However, as the illuminated volume of the room increased, OH concentrations also increased resulting in higher concentrations of oxidation products (Won et al., 2019). CFD models can also be used to evaluate ozone-skin reactions and hence determine ozone transport and deposition within surface boundary layers indoors (Pei and Rim, 2021; Pei et al., 2022).

2.4 Summary

This review of the literature has documented the history of modelling indoor chemistry and has detailed how new computational models are continuously being developed to improve our understanding of the field. Modelling chemistry in indoor environments has been developed comprehensively since the pioneers released their model in 1986 (Nazaroff and Cass, 1986). From the implementation and development of surface chemistry (Cano-Ruiz et al., 1993; Morrison and Nazaroff, 2002b), to the development of oxidation pathways with monoterpenes (Carslaw, 2013), indoor air modelling is continuing to help us to understand the complex nature of indoor environments.

The Modelling Consortium of Indoor Environments (MOCCIE) was funded in order to maintain and secure the development of indoor chemistry models for many years to come. Molecular dynamics provide understanding of electron and proton transfer, with kinetic processes detailing reaction rates and mass transport. Thermodynamic modelling enables the characteristics and composition of aerosols to be determined, where computational fluid dynamics provides spatial and temporal concentrations using air flow and mass balance. Despite the rapid advancement of modelling indoor chemistry, there are still gaps in our understanding. Each varying model type strives to fill certain research gaps. INCHEM-Py, a gas-phase chemistry model, attempts to fill one of these research gaps, in a way CFD and other model types cannot. INCHEM-Py has a complex mechanism, which contains over 20,000 reactions to help solve indoor chemistry. For other model types, this level of complexity would be would be computationally difficult. It is important however, that computational models are used harmoniously to progress the understanding of indoor chemistry.

This thesis, therefore, contributes to the upkeep and evolution of indoor chemistry models via the development and application of the gas-phase indoor air chemistry model, INCHEM-Py (Shaw and Carslaw, 2021; Shaw et al., 2023).

Chapter 3

Methodology

Section 3.3.4 details the review and implementation of new outdoor VOC concentrations in the model, carried out by me as part of my PhD studies, and subsequently included in Shaw et al. (2023).

3.1 Introduction

This research thesis was conducted using an indoor gas-phase chemistry model, the INdoor CHEMical model in Python, INCHEM-Py (Shaw and Carslaw, 2021; Shaw et al., 2023). This model is a zero-dimensional, detailed chemical box model, which provides predicted concentrations of indoor gas-phase chemical species over time. The model creates a scheme of coupled ordinary differential equations (ODEs), which calculate the change in the species concentration with time. INCHEM-Py is a refactored and updated version of a previous indoor air chemistry model, the Indoor Detailed Chemical Model (Carslaw, 2007). INCHEM-Py assumes a single, well-mixed environment, and the processes and operations that the model uses are described in Shaw et al. (2023).

INCHEM-Py utilises the Master Chemical Mechanism (MCM) v3.3.1 (Master Chemical Mechanism, 2024), which describes the main atmospheric reactions and rate coefficients. The model also includes modules that describe indoor photolysis, surface deposition, particle formation and some additional customised chemical mechanisms. Alongside species' concentrations, the model can output; rates of production, species reac-

tivity and summations of organic nitrates, peroxyacetylnitrates and peroxy radical (RO_2) concentrations. Common application of the model is typically simulating experimental measurements, to provide insight into the chemical processes and transformations that occur. It also predicts species' concentrations that may otherwise be unknown owing to challenges in measurement technology. However, it is important for model development to utilise experimental data where possible, to evaluate the model results.

3.2 The Master Chemical Mechanism

The Master Chemical Mechanism, MCM, is a near-explicit kinetic and mechanistic description of outdoor atmospheric chemistry. It contains over 20,000 chemical reactions and details the degradation of 143 volatile organic compounds (VOCs), with over 6,000 incorporated species (Jenkin et al., 1997). The MCM does not utilise any surrogate species or contain any lumping. Since its launch, the MCM has been developed to include degradation schemes for monoterpenoid species including α- and β-pinene, aromatics (Bloss et al., 2005; Jenkin et al., 2003), non-aromatic VOCs (Saunders et al., 2003), β-caryophyllene (Jenkin et al., 2012) and isoprene (Jenkin et al., 2015). The MCM was built with a focus on outdoor atmospheric models, however, it has been modified for use in indoor gas-phase models, such as INCHEM-Py.

The MCM is constructed based on kinetic information around the oxidation of VOCs. Where kinetic literature is not readily available, the rate coefficients and products are assigned by a detailed protocol described in Jenkin et al. (1997) and Jenkin et al. (2003). Figure 3.1 demonstrates the major degradation reactions involved in atmospheric chemistry which are present in the MCM.

The oxidation chemistry is initiated via the reaction of a volatile organic compound (VOC) with OH (Jenkin et al., 2018), NO_3 (Jenkin et al., 2019) or O_3 (Jenkin et al., 2020). Individual VOCs can also be broken down through photolysis. These reactions produce reactive intermediates, such as oxy radicals (RO), peroxy radicals (RO_2), excited Criegee (RC(OO)R')* and stabilised Criegee (RC(OO)R') species. These reactive species further

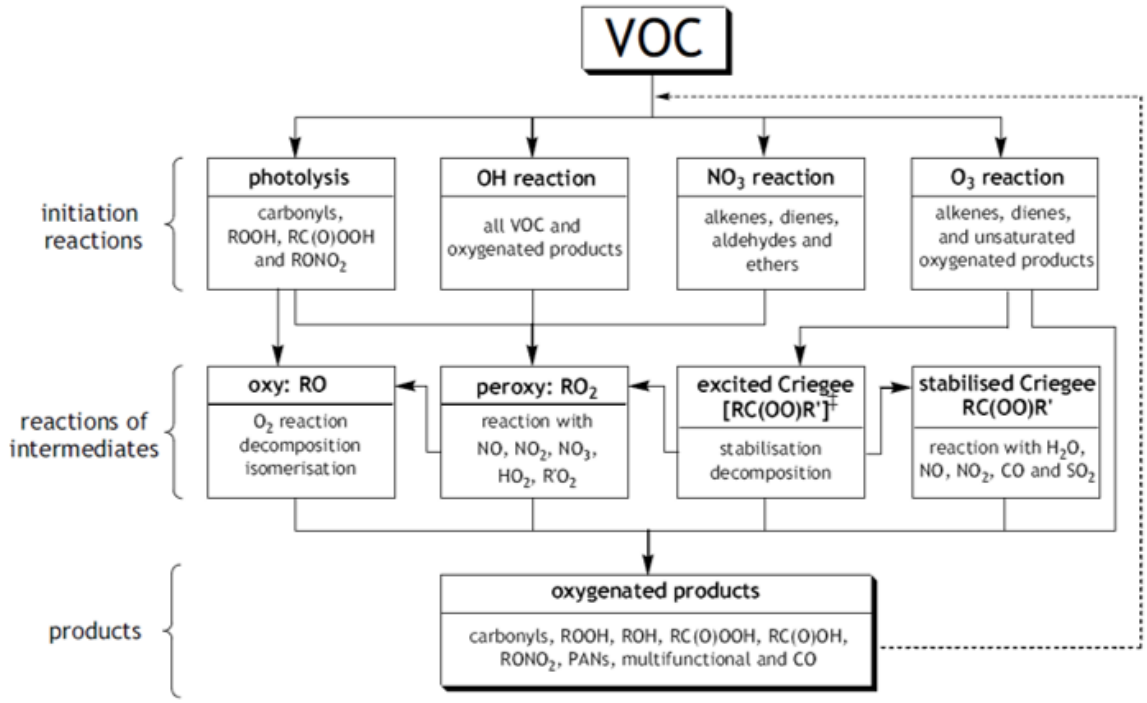

Figure 3.1: The schematic for the MCM degradation protocol which follows the major reaction pathway of VOCs (Source: Saunders et al. (2003)).

react forming a range of products, including carbonyls, carboxylic acids and other multi-functional oxygen containing species, in a series of termination reactions. These oxygenated species participate in further chemical reactions until the ultimate products of water (H_2O) and carbon dioxide (CO_2) are formed (Jenkin et al., 1997).

Through the initiation step, all VOCs can react with OH to form RO_2. An example of an alkane (propane), alkene (ethene) and aromatic species (toluene) reacting with OH is shown in Reactions 3.1, 3.2 and 3.3 respectively to form an RO_2 radical.

$$C_3H_8 + OH + O_2 \longrightarrow C_3H_7O_2 \tag{3.1}$$

$$C_2H_4 + OH + O_2 \longrightarrow HOCH_2CH_2O_2 \tag{3.2}$$

$$C_6H_5CH_3 + OH + O_2 \longrightarrow C_6H_5CH_2O_2 \tag{3.3}$$

Abstraction of the hydrogen atom (H) from the carbon chain occurs in alkanes (Reaction 3.1), whereas alkenes undergo an addition reaction to the C=C forming RO_2 (Reaction 3.2). Aromatics undergo an addition reaction on the benzene ring (Reaction 3.3). The carbon-carbon triple bond in alkynes also undergoes addition (Jenkin et al., 1997).

The RO_2 treatment is complex. There are around 1000 different RO_2 radicals in the MCM and each can theoretically react with every single other RO_2 radical present. To avoid chemical and computational complexity, a pool of RO_2 is assumed. This 'pool' sums the concentration of each individual RO_2 radical to give a total concentration, and then each individual RO_2 radical reacts once with the pool, rather than with 1000 other individual species (Jenkin et al., 1997).

The RO_2 radicals then react with each other, other radical species, NO and NO_3 (Reactions 3.4 to 3.10), forming oxygenated species, including carbonyls (Reaction 3.5), alcohols (Reaction 3.6) and nitrated species (Reaction 3.8). Reactions 3.4 to 3.10 show these initial reactions with an RO_2 derivative ($C_3H_7O_2$) of propane (Reaction 3.1).

$$C_3H_7O_2 + RO_2 \longrightarrow C_3H_7O \tag{3.4}$$

$$C_3H_7O_2 + RO_2 \longrightarrow C_2H_5CHO \tag{3.5}$$

$$C_3H_7O_2 + RO_2 \longrightarrow C_3H_7OH \tag{3.6}$$

$$C_3H_7O_2 + NO \longrightarrow C_3H_7O + NO_2 \tag{3.7}$$

$$C_3H_7O_2 + NO \longrightarrow C_3H_7ONO_2 \tag{3.8}$$

$$C_3H_7O_2 + HO_2 \longrightarrow C_3H_7OOH \tag{3.9}$$

$$C_3H_7O_2 + NO_3 \longrightarrow C_3H_7O + NO_2 \tag{3.10}$$

3.3 The Model

3.3.1 Software & Integration

INCHEM-Py was run using the Spyder integrated developer environment (Python 3.9), part of the Anaconda suite of software. Anaconda provided the Conda command line tool, including the installation of Python and management of Python libraries. The prominent ODE created and solved by INCHEM-Py for each chemical species is shown as Equation 3.11:

$$\frac{dC_i}{dt} = \sum R_{ij} + (\lambda_r C_{i,out} - \lambda_r C_i) - v_d \left(\frac{A}{V}\right) C_i \pm k_{t_i} \tag{3.11}$$

where the term on the left hand side of the equation represents the change in indoor concentration of species i (C_i) over time (t). The first term on the right hand side of the equation determines the rate of reaction between species i and species j, where the rate of each individual reaction is dictated by the rate constant and the concentrations of the respective reactant species. The second term refers to the indoor-outdoor exchange of species i, where λ_r is the air change rate (ACR) and $C_{i,out}$ is the outdoor concentration of species i. This term and its development will be the focus of Chapter 5. The third term in the equation refers to the irreversible surface deposition of species i, where v_d is the surface deposition velocity, A is the internal surface area and V is the total internal volume. This term and its development will be the focus of Chapter 4. The final term in the equation refers to emissions of species i, where k_{t_i} represents the emission rate of species i over time. Figure 3.2 details how the model orders operations and the processes and factors considered when calculating the concentrations of indoor species at each time step.

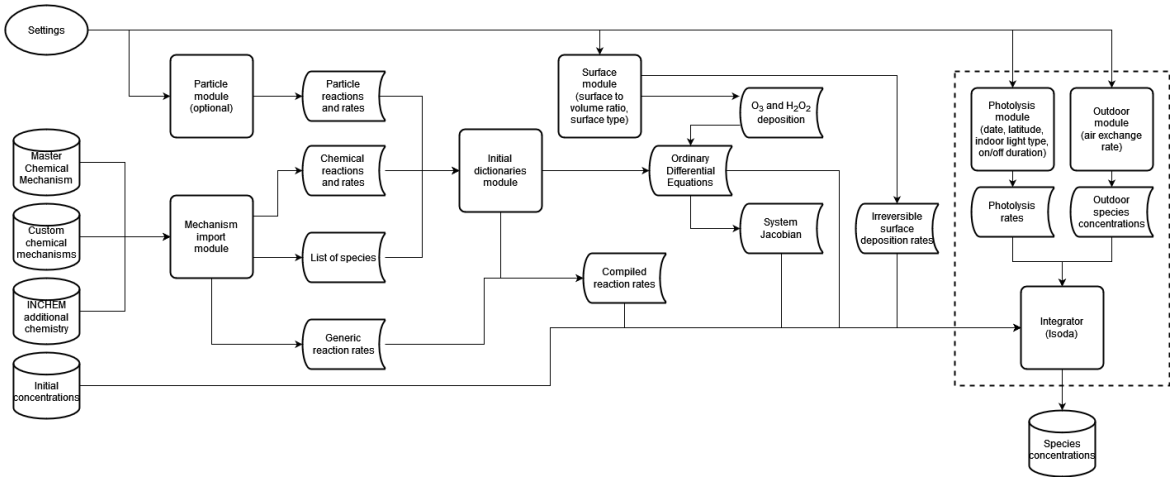

Figure 3.2: A schematic for the operational working of INCHEM-Py (Source: Shaw et al. (2023)).

The model uses the scipy.integrate.ode package to solve each equation, returning corresponding change in concentrations for all species present in the model. The model constructs the master array, which is a dictionary of species and their respective ordinary differential equations. At each time step, the ODEs are computed by the parsing of each reaction.

Timed emissions can be included in simulations, with emissions (in molecule cm^{-3} s^{-1}) added for any species and over a specific time period. This feature is utilised in Chapter 5 and Chapter 6 of the thesis with the addition of cooking and cleaning emissions. The model also considers the indoor temperature (K) and relative humidity (%). Additional degradation schemes for some species not currently in the MCM have been designed based on previous literature. These include chlorine chemistry (Wong et al., 2017; Xue et al., 2015; Wang et al., 2020b), and degradation schemes for linalool, Δ3-carene, camphene, (Carslaw, 2007), octanal, nonanal and decanal (Kruza et al., 2017).

3.3.2 Surfaces and Deposition

INCHEM-Py assumes irreversible deposition of 3371 indoor gas-phase species onto surfaces, depending on the surface area-to-volume ratio and the deposition velocity. The rate of deposition (R_{dep} in s^{-1}) is denoted by Equation 3.12:

$$R_{dep} = v_d \times \left(\frac{A}{V}\right) \tag{3.12}$$

where v_d is the deposition velocity (cm s^{-1}), A is the surface area (cm^2) and V (cm^3) represents the volume of an indoor surface.

The deposition velocities are allocated to gas-phase species as outlined in Carslaw (2007) and shown in Table 3.1. For species where no measurements are available, deposition velocities are allocated based on functional group and as described by Carslaw (2007) (Table 3.2).

Table 3.1: The deposition velocities of individual species included in INCHEM-Py (Source: Sarwar et al. (2002) and Carslaw (2007)).

Species	**Deposition Velocity (cm s^{-1})**
O_3	0.0345
HNO_3	0.176
SO_2	0.029
NO_2	0.0261
H_2O_2	0.045
CH_3OH	0.0307
C_2H_5OH	0.0264
HCHO	0.035
CH_3CHO	0.0123
MGLYOX	0.0153
MACR	0.0109
HONO	0.065
NO_3	0.07
N_2O_5	0.07
HO_2	0.07

continued on next page

Species	Deposition Velocity (cm s^{-1})
OH	0.07
HO_2NO_2	0.113
$CH_3O_2NO_2$	0.113
HCOOH	0.0438
MVK	0.0160
PAN	0.0197
CH_3COCH_3	0.005

Table 3.2: Deposition velocities used for species not in Table 3.1 and based on functional groups (Source: Carslaw et al. (2012)).

Species	Deposition Velocity (cm s^{-1})
Organic Nitrate	0.0164
Alcohol	0.0162
Peroxy	0.0292
Peroxyacetylnitrate	0.0182
Aldehyde	0.0103
Carboxylic Acid	0.0359
Ketone	0.016

3.3.3 Air Exchange with Outdoors

Air exchange with outdoors removes pollutants from indoor air to the outdoor environment whilst moving outdoor pollutants indoors (Nazaroff, 2021). Important factors which affect air change rates include external elements such as the weather, wind speed, and temperature change. Internal factors also affect air change rates, which can vary based on occupancy (opening and closing of windows and doors) and characteristics of the building envelope (Nazaroff, 2021).

The rate at which outdoor concentrations ingress indoors depends on the air change rate which can vary from building to building. A high air change rate denotes a leakier building, where indoor air is quickly replenished by outdoor air (for example 2.0 air changes per hour), whereas a low air change rate suggests a more efficiently built building where it takes longer for outdoor air to ingress indoors (for example 0.1 air changes per hour) (Nazaroff, 2021). This thesis traditionally uses an air change rate of 0.5 air changes per hour (unless specified) as an appropriate median value. This was determined by a comprehensive literature review of air change rates in residential properties (Nazaroff, 2021).

3.3.4 Outdoor Concentrations

Outdoor concentrations drive indoor concentrations in the absence of indoor sources, and are necessary for the accurate prediction of indoor pollutant concentrations (Kruza et al., 2021). INCHEM-Py assumes that the concentrations of VOCs outdoors remain constant. The outdoor concentrations of O_3, NO, NO_2 and $PM_{2.5}$ are assumed to vary diurnally, based on outdoor measurements in suburban London (UK), urban London (UK), urban Bergen (Norway) and urban Milan (Italy) (Shaw et al., 2023); EEA (2018); Terry et al. (2014)). These outdoor measurements represent clean (Bergen), semi-polluted (London) and heavily polluted (Milan) scenarios. These profiles can be chosen based on user requirements.

Outdoor VOCs play an important role for indoor air chemistry, contributing to indoor VOC concentrations, particularly those with few or no indoor sources. Once indoors, they can react with key indoor species, including ozone (O_3) and the hydroxyl radical (OH). In the initial release of INCHEM-Py (v1.1) the static outdoor concentrations were based on limited literature values (Sarwar et al., 2002; Terry et al., 2014; Zhu et al., 2013). A literature search was therefore carried out to find more up-to-date outdoor VOC concentrations based on measurements from around the world. The most useful studies were those that measured VOC concentrations over a long-period of time and also in representative suburban locations where most people live.

The literature search identified 131 VOCs with representative outdoor concentrations,

and 103 of these VOCs had degradation mechanisms in INCHEM-Py. The experimental studies were from various global locations. The location, length and time of year of each study is given in Table 3.3.

Table 3.3: The locations, time of year and length of study for literature used to update outdoor concentrations in INCHEM-Py v1.2.

Reference	Location	Time of Year	Length of Study
Uchiyama et al. (2015)	Japan	Winter (January - March) and Summer (July to September)	3 years
Baudic et al. (2016)	France	All Year	11 months
Lü et al. (2006)	China	Winter (January - March)	2.5 months
Mentese and Bas (2020)	Turkey	All Year	1 year
Bari and Kindzierski (2018)	Canada (Calgary)	All Year	5 years
Sturaro et al. (2010)	Italy	February - November	10 months
Bari et al. (2016)	Canada (Fort McKay)	All Year	12 years
Gallego et al. (2016)	Spain	July - November	5 months
Hellén et al. (2018)	Finland	All Year	2 years
Hakola et al. (2009)	Finland	All Year	8 years
He et al. (2010)	China	July - September	2 months
Dlugokencky (2022)	Global	All Year	1 year
Vichi et al. (2016)	Switzerland and Czech Republic	Spring, Summer and Winter	4 years
Li et al. (2018)	Global	All Year	8 years
Liu et al. (2018)	China	November - July	9 months

The new outdoor VOC concentrations have been implemented in INCHEM-Py (v1.2) and are shown in Table 3.4, ordered by functional group.

Table 3.4: The outdoor concentrations of VOCs incorporated in the updated version of INCHEM-Py (v1.2). The values used in the previous version of the model (v1.1) are also included as a comparison.

Species	v1.1 Value (ppb)	v1.2 Value (ppb)	Ref. (v1.2)
Formaldehyde	3.7	2.5	Uchiyama et al. (2015)
Acetaldehyde	2.9	1.6	Uchiyama et al. (2015)
Propanal	0.82	0.38	Uchiyama et al. (2015)
3-Methylbutanal	-	0.04	Uchiyama et al. (2015)
Acrolein	2.0	0.11	Uchiyama et al. (2015)
Methacrolein	-	0.11	Baudic et al. (2016)
Crotonaldehyde	-	0.07	Uchiyama et al. (2015)
Pentanal	-	0.10	Uchiyama et al. (2015)
Hexanal	0.38	0.11	Uchiyama et al. (2015)
Heptanal	0.15	0.08	Uchiyama et al. (2015)
Octanal	0.29	0.10	Uchiyama et al. (2015)
Nonanal	1.0	0.60	Uchiyama et al. (2015)
Decanal	0.11	0.16	Uchiyama et al. (2015)
2-Nonenal	-	0.05	Uchiyama et al. (2015)
Acetone	0.53	2.0	Uchiyama et al. (2015)
2-Butanone (MEK)	0.10	0.22	Uchiyama et al. (2015)
3-Buten-2-one (MVK)	0.72	0.11	Baudic et al. (2016)
Cyclohexanone	0.04	0.69	Lü et al. (2006)
Benzaldehyde	2.5	0.06	Uchiyama et al. (2015)
o-Tolualdehyde	-	0.05	Uchiyama et al. (2015)

continued on next page

Species	v1.1 Value (ppb)	v1.2 Value (ppb)	Ref. (v1.2)
m-Tolualdehyde	-	0.08	Uchiyama et al. (2015)
p-Tolualdehyde	-	0.08	Uchiyama et al. (2015)
2,5-Dimethylbenzaldehyde	-	0.32	Uchiyama et al. (2015)
Benzene	0.24	0.39	Uchiyama et al. (2015)
Toluene	0.81	1.7	Uchiyama et al. (2015)
p-Xylene	0.26	0.25	Uchiyama et al. (2015)
m-Xylene	0.26	0.25	Uchiyama et al. (2015)
o-Xylene	0.53	0.17	Uchiyama et al. (2015)
Ethylbenzene	0.14	0.36	Uchiyama et al. (2015)
Propylbenzene	-	0.16	Mentese and Bas (2020)
2-Ethyltoluene	-	0.01	Bari and Kindzierski (2018)
3-Ethyltoluene	-	0.02	Bari and Kindzierski (2018)
4-Ethyltoluene	-	0.01	Bari and Kindzierski (2018)
1,3,5-Trimethylbenzene	0.89	0.07	Uchiyama et al. (2015)
1,2,4-Trimethylbenzene	0.09	0.22	Uchiyama et al. (2015)
1,2,3-Trimethylbenzene	0.33	0.05	Uchiyama et al. (2015)
p-Dichlorobenzene	-	0.50	Uchiyama et al. (2015)
Styrene	0.23	0.09	Mentese and Bas (2020)
Cumene	0.01	0.12	Mentese and Bas (2020)
Phenol	2.0	0.71	Sturaro et al. (2010)
Ethane	0.85	3.7	Baudic et al. (2016)
Propane	0.51	1.5	Baudic et al. (2016)
Butane	1.4	1.4	Baudic et al. (2016)
Isobutane	-	0.83	Baudic et al. (2016)
2,2-Dimethylbutane	-	0.08	Bari et al. (2016)

continued on next page

Species	v1.1 Value (ppb)	v1.2 Value (ppb)	Ref. (v1.2)
2,3-Dimethylbutane	-	0.11	Bari et al. (2016)
Pentane	0.37	0.35	Baudic et al. (2016)
2-Methylpentane	-	0.16	Bari et al. (2016)
3-Methylpentane	-	0.10	Bari et al. (2016)
Isopentane	-	0.60	Bari and Kindzierski (2018)
Hexane	0.37	0.45	Uchiyama et al. (2015)
2-Methylhexane	-	0.10	Bari et al. (2016)
3-Methylhexane	-	0.13	Bari et al. (2016)
Heptane	0.10	0.02	Uchiyama et al. (2015)
Octane	0.30	0.02	Uchiyama et al. (2015)
Nonane	0.41	0.12	Uchiyama et al. (2015)
Decane	0.08	0.40	Uchiyama et al. (2015)
Undecane	0.08	0.59	Uchiyama et al. (2015)
Dodecane	0.02	0.04	Mentese and Bas (2020)
Cyclohexane	0.05	0.03	Bari and Kindzierski (2018)
Ethene	0.51	1.4	Baudic et al. (2016)
Propene	0.17	0.37	Baudic et al. (2016)
1-Butene	-	0.16	Bari et al. (2016)
cis-2-Butene	0.14	0.02	Bari and Kindzierski (2018)
trans-2-Butene	0.16	0.02	Bari and Kindzierski (2018)
2-Methyl-1-butene	-	0.02	Bari and Kindzierski (2018)
2-Methyl-2-butene	0.28	0.02	Bari and Kindzierski (2018)
Isoprene	0.41	0.09	Baudic et al. (2016)
1,3-Butadiene	0.10	0.02	Bari and Kindzierski (2018)
trans-2-Pentene	-	0.02	Bari and Kindzierski (2018)

continued on next page

Species	v1.1 Value (ppb)	v1.2 Value (ppb)	Ref. (v1.2)
cis-2-Pentene	-	0.01	Bari and Kindzierski (2018)
Ethyne	-	0.64	Baudic et al. (2016)
Methanol	5.3	4.5	Baudic et al. (2016)
Ethanol	48.8	6.6	Gallego et al. (2016)
Isopropanol	0.81	3.8	Gallego et al. (2016)
1-Propanol	0.05	0.51	Gallego et al. (2016)
1-Butanol	0.53	1.0	Gallego et al. (2016)
1-Pentanol	-	0.002	Hellén et al. (2018)
1-Hexanol	-	0.001	Hellén et al. (2018)
2-Butoxyethanol	0.21	1.0	Gallego et al. (2016)
Linalool	-	0.001	Hellén et al. (2018)
Chloroform	0.01	0.03	Uchiyama et al. (2015)
Methylchloroform	3.4	0.31	Brickus et al. (1998)
Dichloromethane	0.04	0.10	Bari and Kindzierski (2018)
Trichloroethylene	0.001	0.37	Gallego et al. (2016)
Tetrachloroethylene	0.01	0.02	Bari and Kindzierski (2018)
1,2-Dichloroethane	-	0.02	Bari and Kindzierski (2018)
Chloromethane	-	0.57	Bari and Kindzierski (2018)
Hydrogen Chloride	-	1.5	Uchiyama et al. (2015)
Ethyl Acetate	-	0.10	Uchiyama et al. (2015)
Butyl Acetate	-	0.05	Uchiyama et al. (2015)
α-Pinene	0.06	0.13	Uchiyama et al. (2015)
β-Pinene	0.001	0.05	Gallego et al. (2016)
Limonene	0.04	0.10	Uchiyama et al. (2015)
Δ3-Carene	0.04	0.11	Hakola et al. (2009)

continued on next page

Species	v1.1 Value (ppb)	v1.2 Value (ppb)	Ref. (v1.2)
Camphene	0.02	0.02	Hakola et al. (2009)
β-Caryophyllene	0.001	0.004	Hellén et al. (2018)
Formic Acid	-	7.5	Uchiyama et al. (2015)
Acetic Acid	-	15.7	Uchiyama et al. (2015)
Propanoic Acid	-	0.08	Hellén et al. (2018)
Butanoic Acid	-	0.06	Hellén et al. (2018)
Pentanoic Acid	-	0.03	Hellén et al. (2018)
Heptanoic Acid	-	0.004	Hellén et al. (2018)

The outdoor concentrations of eight non-VOC species have also been updated and input into INCHEM-Py. These concentrations are given in Table 3.5, along with the appropriate reference.

Table 3.5: The outdoor concentrations of other species incorporated in the updated version of INCHEM-Py (v1.2). The values used in the previous version of the model (v1.1) are also included as a comparison. The concentration of OH is given in molecule cm^{-3} and that of all other species in ppb.

Species	v1.1 Value (ppb)	v1.2 Value (ppb)	Ref. (v1.2)
Hydrogen Peroxide	2.0	1.3	He et al. (2010)
Methane (CH_4)	1882	1891	Dlugokencky (2022)
Carbon Monoxide (CO)	102	195	EEA (2018)
Sulfur Dioxide (SO_2)	-	0.70	EEA (2018)
Nitric Acid (HNO_3)	2.0	0.39	Vichi et al. (2016)
Nitrous Acid (HONO)	0.07	0.65	Vichi et al. (2016)
Hydroxyl Radical (OH)	1×10^{06}	1.09×10^{06}	Li et al. (2018)

Species	v1.1 Value (ppb)	v1.2 Value (ppb)	Ref. (v1.2)
Peroxyacetyl Nitrate (PAN)	0.61	2.2	Liu et al. (2018)

A comparison was undertaken to quantify the changes to the model output, by using the new VOC outdoor concentrations compared to the old VOC concentrations. All of the other model inputs were kept constant for each run. The concentrations of major indoor species including OH, O_3, HO_2, RO_2, NO, NO_2, formaldehyde and HONO are shown in Figures 3.3 to 3.10. The percentage difference in concentrations of key indoor species for different outdoor VOC concentrations are shown in Table 3.6. The updated outdoor VOC concentrations increased the concentrations of key indoor oxidants, including, RO_2 (5.8%) and NO_2 (3.3%). O_3 has a minimal concentration increase (2.2%) with the new outdoor VOCs. HO_2 concentrations fluctuate throughout the day, but have an overall average percentage decrease of 2.9%. HONO concentrations increase indoors using the new VOC concentrations (6.0%). Average NO concentrations decrease but the change is small (approximately 0.1 ppb, 1.7%). Average formaldehyde concentrations decrease by approximately 0.2 ppb (29%) over the course of a day.

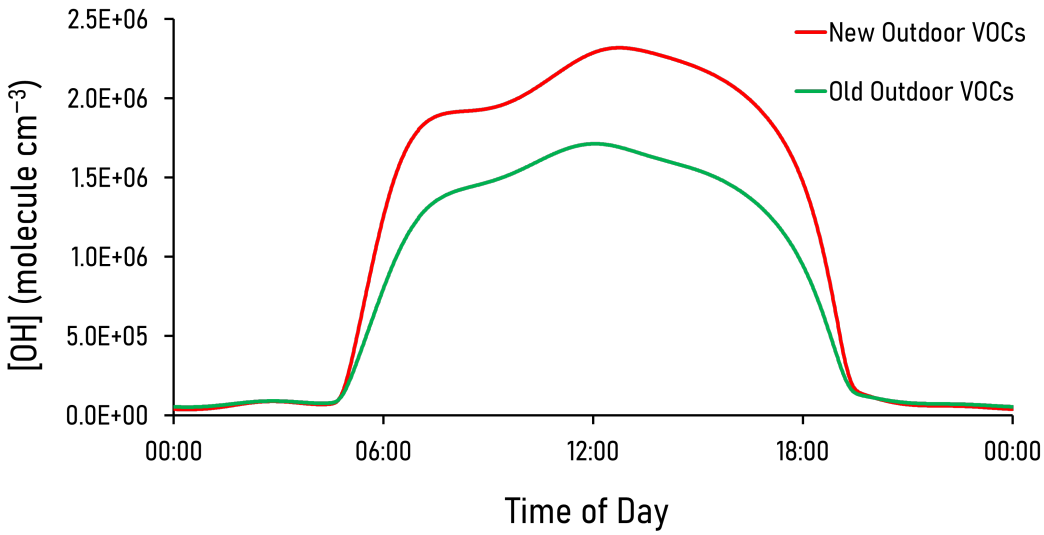

Figure 3.3: The indoor concentration of OH over one day, using old and new outdoor VOC concentrations.

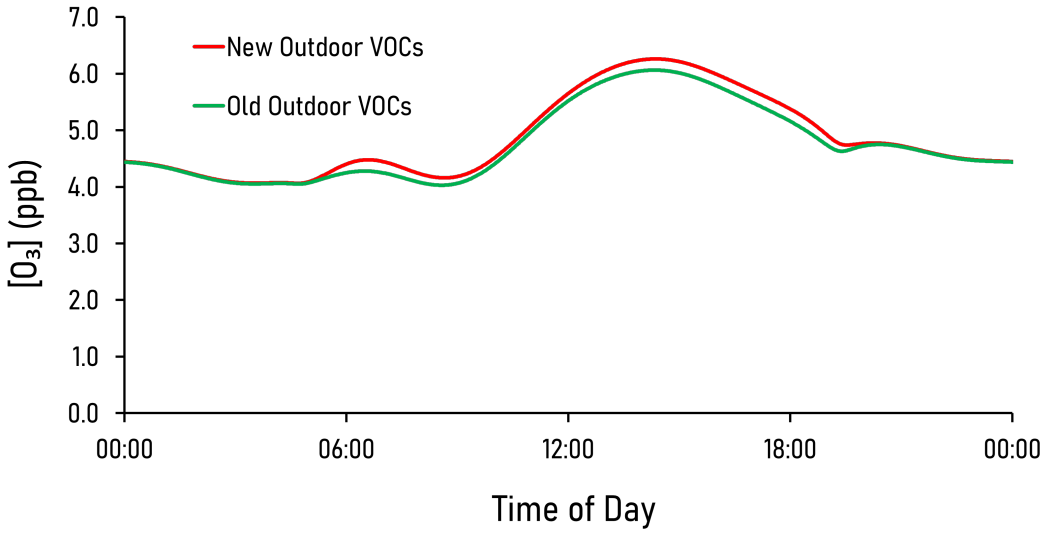

Figure 3.4: The indoor concentration of O_3 over one day, using old and new outdoor VOC concentrations.

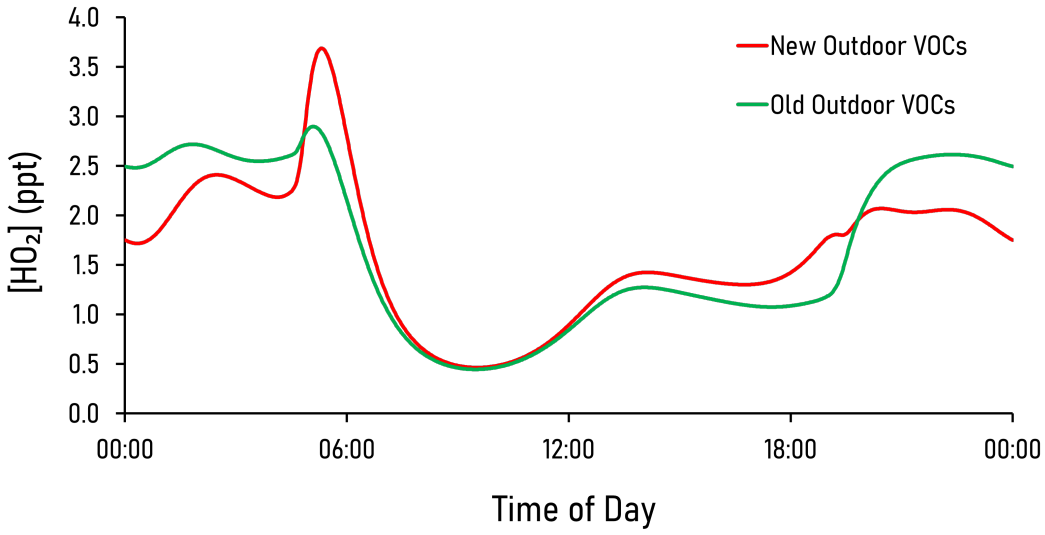

Figure 3.5: The indoor concentration of HO_2 over one day, using old and new outdoor VOC concentrations.

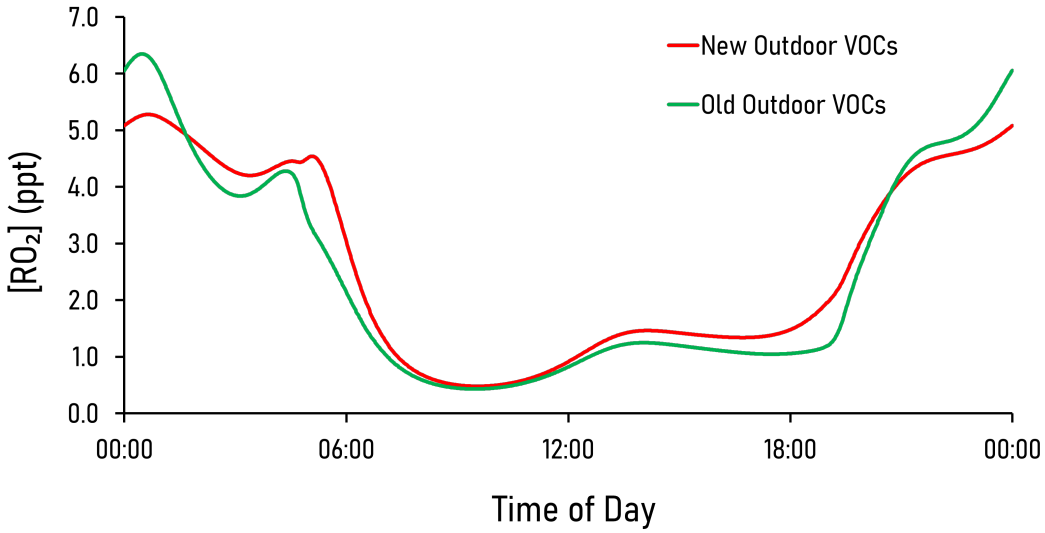

Figure 3.6: The indoor concentration of RO_2 over one day, using old and new outdoor VOC concentrations.

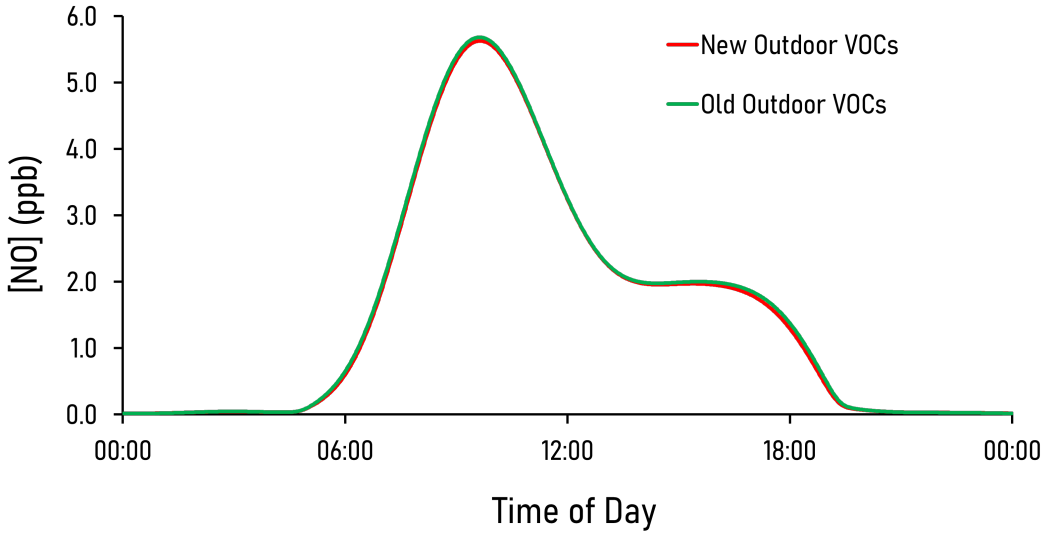

Figure 3.7: The indoor concentration of NO over one day, using old and new outdoor VOC concentrations.

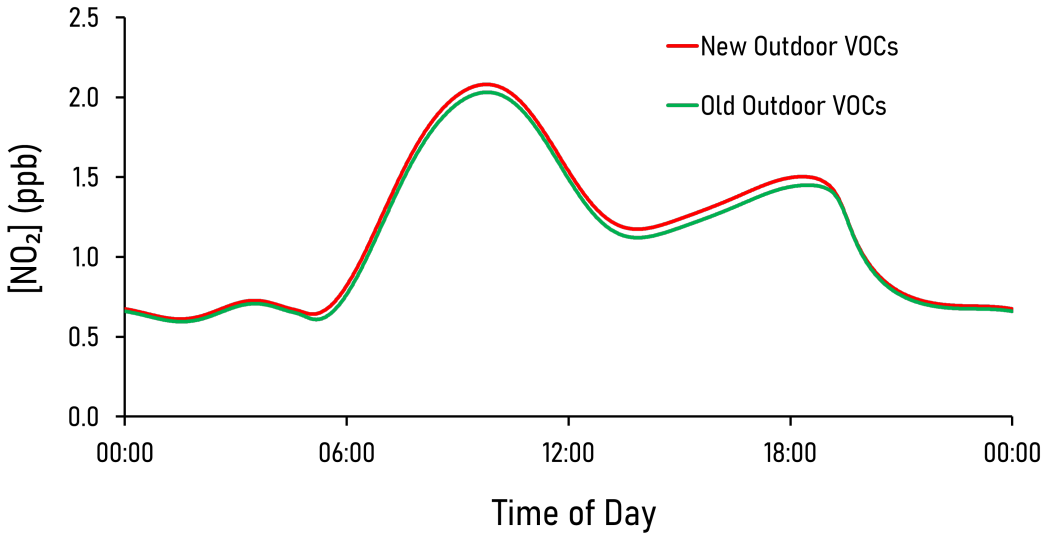

Figure 3.8: The indoor concentration of NO_2 over one day, using old and new outdoor VOC concentrations.

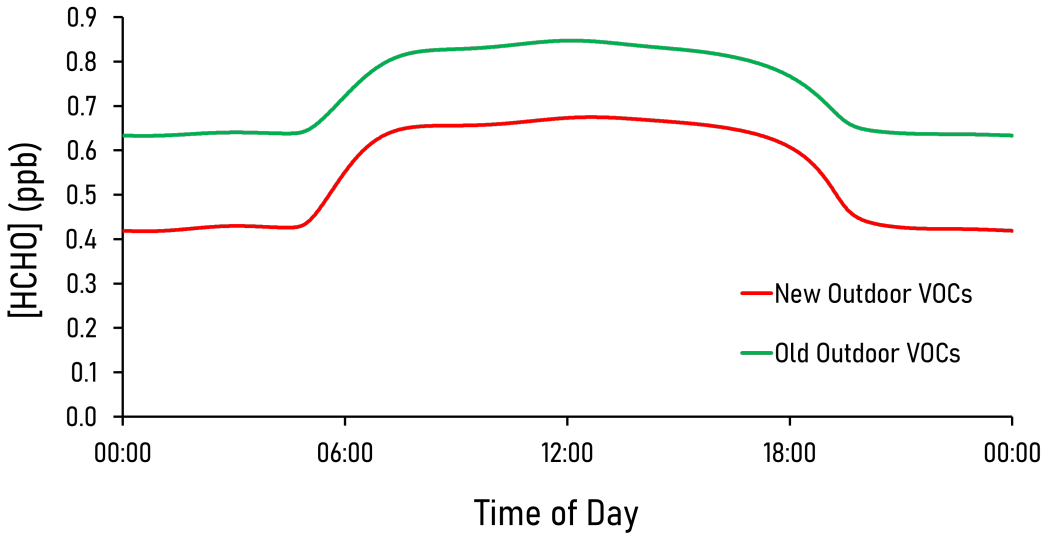

Figure 3.9: The indoor concentration of formaldehyde (HCHO) over one day, using old and new outdoor VOC concentrations.

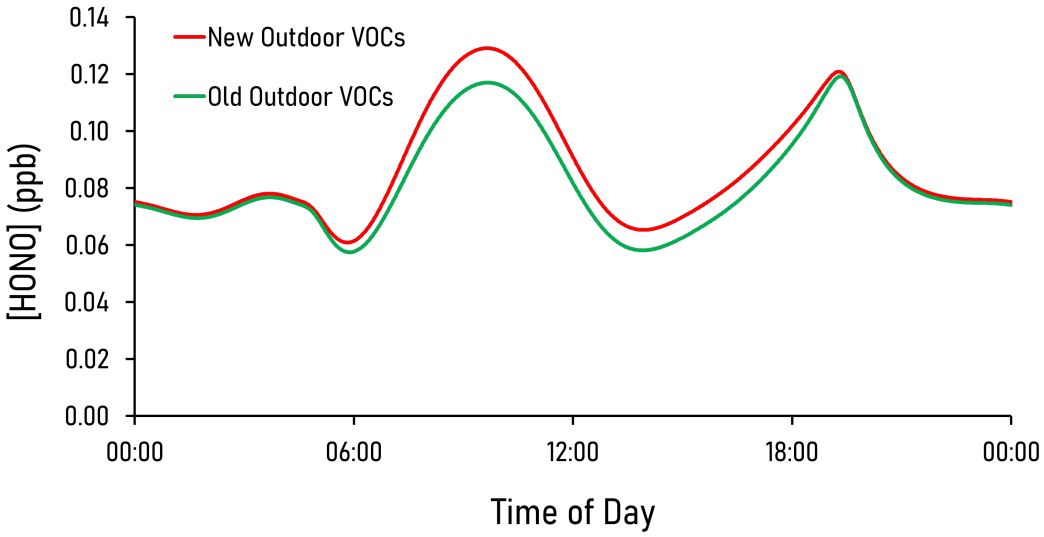

Figure 3.10: The indoor concentration of HONO over one day, using old and new outdoor VOC concentrations.

Table 3.6: The average concentration of key indoor species over 24-hours for simulations with the new and old outdoor VOCs. The percentage difference from the old outdoor VOCs to the new outdoor VOCs is also given in the table.

	Concentration		
Species	**New VOCs**	**Old VOCs**	**% difference**
OH (molecule cm^{-3})	1.12 x 10^6	8.15 x 10^5	31.8
O_3 (ppb)	4.9	4.8	2.2
HO_2 (ppt)	1.6	1.7	-2.9
RO_2 (ppt)	2.6	2.5	5.8
NO (ppb)	1.5	1.6	-1.7
NO_2 (ppb)	1.2	1.1	3.3
HONO (ppb)	0.09	0.08	6.0
HCHO (ppb)	0.55	0.74	-29.0

The change in outdoor VOC and non-VOC concentrations only really affects indoor concentrations of OH and HCHO under these conditions.

3.3.5 Photolysis

Photolysis also plays a key role in indoor air chemistry and has been integrated into INCHEM-Py. The model calculates photolysis rates based on both external sunlight fil-

tering in from outdoors and internal lighting sources. The model sums these values and calculates a total photolysis rate for each relevant species (Wang et al., 2022b; Shaw et al., 2023). Equation 3.13 calculates the outdoor photolysis rate coefficient for each species (Shaw et al., 2023).

$$J_{out} = l\cos(\theta)^m \exp(-n\sec(\theta)) \tag{3.13}$$

where J_{out} is the outdoor photolysis rate (s^{-1}), l, m and n are parameters which are optimised as discussed by Jenkin et al. (1997) and θ is the solar zenith angle (°).

Outdoor solar photolysis is calculated via the solar zenith angle in the model. INCHEM-Py uses local solar time to determine the solar declination angle (Equation 3.14).

$$Dec = -23.45 \times cos\left(\frac{360}{365.25}\right) \times (d + 10) \tag{3.14}$$

where d represents the number of days which have past since the 1st of January in that particular year, 360 is the completed angle, 365.25 represents the total number of days in a year, –23.45 represents the solar declination angle at the winter solstice (°), where 10 stands for the approximate difference in the number of days between the 1st of January and the winter solstice (Shaw et al., 2023).

An attenuation factor can be applied to J_{out} depending on which glass type has been selected (glass C, low emissivity or low emissivity with film), using a tailored transmission factor, ψ (Wang et al., 2022b). If a simulation with no sunlight is required, the transmission factor is set to 0.

The indoor photolysis rate (ϕ) for six unique light types (light emitting diode (LED), incandescent, halogen, covered fluorescent tube (CFT), uncovered fluorescent tube (UFT), fluorescent tube (FT) and compact fluorescent lamp (CFL) is based on the methodology developed by Wang et al. (2022b). Lights can also be turned off indoors, allowing the sole source of photolysis to be from attenuated outdoor sunlight. The overall photolysis rate (J in s^{-1}) is then the sum of the attenuated outdoor sunlight and any indoor lighting selected.

In total, there are 44 photolysis rate coefficients in the model, which are described in Table 3.7, along with the wavelength range over which the respective photolysis reactions can take place.

Table 3.7: The photolysis rate coefficients present in INCHEM-Py and the corresponding reactions.

J Value	**Reaction**	**Wavelength(s) Range (nm)**
J1	$O_3 \rightarrow O(^1D) + O_2$	300 - 349
J2	$O_3 \rightarrow O(^3P) + O_2$	300 - 349, 400 - 700
J3	$H_2O_2 \rightarrow OH + OH$	300 - 350
J4	$NO_2 \rightarrow NO + O(^3P)$	300 - 425
J5	$NO_3 \rightarrow NO + O_2$	586 - 640
J6	$NO_3 \rightarrow NO + O(^3P)$	585 - 640
J7	$HONO \rightarrow NO + OH$	300 - 399
J8	$HNO_3 \rightarrow NO_2 + OH$	300 - 350
J11	$HCHO \rightarrow H + HCO$	300 - 355
J12	$HCHO \rightarrow H_2 + CO$	300 - 360
J13	$CH_3CHO \rightarrow CH_3 + HCO$	300 - 330
J14	$C_2H_5CHO \rightarrow C_2H_5 + HCO$	300 - 330
J15	$C_3H_7CHO \rightarrow C_3H_7 + HCO$	300 - 364
J16	$C_3H_7CHO \rightarrow C_2H_4 + CH_3CHO$	300 - 364
J17	2-Methylpropanal (IPRCHO) $\rightarrow C_2H_4 + CH_3CHO$	300 - 330
J18	Methacrolein (MACR) $\rightarrow CH_2 = CCH_3 + HCO$	300 - 395
J19	Methacrolein (MACR) $\rightarrow CH_2 = C(CH_3)CO + H$	300 - 395
J20	$C_5H_8O_3 \rightarrow CH_3C(CHO) = CHCH_2O + OH$	300 - 395
J21	$CH_3C(O)CH_3 \rightarrow CH_3CO + CH_3$	300 - 327
J22	Methyl Ethyl Ketone (MEK) $\rightarrow CH_3CO + C_2H_5$	300 - 352

continued on next page

J Value	Reaction	Wavelength(s) Range (nm)
J23	Methyl Vinyl Ketone (MVK) → $CH_3CH = CH_2 + CO$	300 - 395
J24	Methyl Vinyl Ketone (MVK) → $CH_3CO + CH_2 = CH$	300 - 395
J31	Glyoxal (GLYOX) → $CO + CO + H_2$	300 - 355
J32	Glyoxal (GLYOX) → $HCHO + CO$	300 - 415
J33	Glyoxal (GLYOX) → $HCO + HCO$	300 - 445
J34	Methylglyoxal (MGLYOX) → $CH_3CO + HCO$	300 - 440
J35	2,3-Butanedione (BIACET) → $CH_3CO + CH_3CO$	300 - 460
J41	$CH_3OOH \rightarrow CH_3O + OH$	300 - 365
J51	$CH_3ONO_2 \rightarrow CH_3O + NO_2$	300 - 340
J52	$C_2H_5ONO_2 \rightarrow C_2H_5O + NO_2$	300 - 340
J53	$n\text{-}C_3H_7ONO_2 \rightarrow n\text{-}C_3H_7O + NO_2$	300 - 340
J54	$i\text{-}C_3H_7ONO_2 \rightarrow CH_3C(O)CH_3 + NO_2$	300 - 360
J55	$t\text{-}C_4H_9ONO_3 \rightarrow t\text{-}C_4H_9O + NO_2$	300 - 330
J56	2-Oxopropyl Nitrate (NOA) → $CH_3C(O)CH_2(O) + NO_2$	300 - 340
J57	2-Oxopropyl Nitrate (NOA) → $CH_3CO + HCHO + NO_2$	300 - 340
J70	$Cl_2 \rightarrow Cl + Cl$	300 - 550
J71	$ClNO_2 \rightarrow NO_2 + Cl$	300 - 470
J72	$ClONO_2 \rightarrow NO_3 + Cl$	300 - 430
J73	$ClONO_2 \rightarrow NO_2 + Cl$	300 - 430
J74	$HOCl \rightarrow OH + Cl$	300 - 420
J75	$OClO \rightarrow O + ClO$	300 - 475
J76	$ClO \rightarrow O + Cl$	300 - 475
J77	$ClOOCl \rightarrow ClOO + Cl$	300 - 400
J78	$ClOOCl \rightarrow ClO + ClO$	300 - 400

3.3.6 Particles

3.3.6.1 Particle Formation

Particles are represented in INCHEM-Py using gas-to-particle partitioning of three monoterpene species; α-pinene, β-pinene and limonene. This is based on the absorptive partitioning theory proposed by Pankow (1994). Pankow defines the thermodynamic equilibrium between the condensed-organic and gas-phases of certain species (Jenkin, 2004; Leungsakul et al., 2005). This process yields the respective phase-partitioning coefficient, which is given in Equation 3.15 (Shaw et al., 2023; Carslaw et al., 2012).

$$K_p = \frac{7.501RT}{W_{om}10^9\gamma_{om}\rho_L^o} \tag{3.15}$$

where K_p represents the partitioning coefficient in m^3 μg^{-1}, R represents the ideal gas constant (8.314 J K^{-1} mol^{-1}), T is the temperature in Kelvin (K), W_{om} represents the absorbing particles mean molecular weight (g mol^{-1}), γ_{om} is the species' activity coefficient (no units) in the condensed phase and ${\rho_L}^o$ is the species' liquid vapour pressure (Torr).

Note that W_{om} is set at 120 g mol^{-1} at the start of each model run (Sarwar and Corsi, 2007), however this value is re-calculated at each timestep (integration) in the model depending on particle composition. γ_{om} is presumed to be equal to 1 (Johnson et al., 2006; Jenkin, 2004).

Calculating the gas-particle partitioning using Equation 3.15 enables calculation of both the rate of absorption onto particles (k_{on}) and the rate of desorption back off the particles (k_{off}) by a particular species (Equation 3.16) (Leungsakul et al., 2005). The partitioning effectively acts as a dynamic balance between the two processes (Johnson et al., 2006; Jenkin, 2004).

$$K_p = \frac{k_{on}}{k_{off}} \tag{3.16}$$

where the rate of absorption (k_{on}) is set at a constant value of 6.2 x 10^{-3} m^3 μg^{-1} s^{-1}, which is independent of both temperature and species (Jenkin, 2004).

Outdoor particles are assumed to ingress indoors at a rate dependent on air change, with concentrations based on the measured data from one of four cities (Shaw et al., 2023). It is assumed that 30% of these outdoor particles are organic in nature (see Section 3.3.6.2).

3.3.6.2 Model Representation of Organic Particulate Matter

INCHEM-Py v1.1 assumed that 30% of the $PM_{2.5}$ that ingressed from outdoors was organic in nature. This proportion affects the simulated concentration of indoor $PM_{2.5}$ given it provides a seed on which indoor particles can grow. The literature was therefore reviewed to assess whether this assumption was still valid.

Organic component of particulate matter can be made up of many diverse organic species, for example, Mikuška et al. (2015), discovered, monosaccharide anhydrides, methoxyphenols, resin acids, PAHs and alkanes made up the organic proportion in the Czech city of Ostrava. These compounds are released through biomass combustion, wood combustion, incomplete combustion from transport and industry respectively. They also found saccharides, which originate from natural sources, such as sea spray, abrasion of leaves and from the soil. An industrialised or busy transport network location would have larger proportions of organic compounds in fine particulate matter than a location with fewer anthropogenic sources (Zhong et al., 2020; Murillo et al., 2013). However, there has been recent debate as to the size of the organic proportion of $PM_{2.5}$.

The DEFRA report on fine particulate matter in the United Kingdom prepared by the Air Quality Expert Group (Air Quality Expert Group, 2012) reported the results from a two-year sampling experiment in Birmingham where $PM_{2.5}$ was collected and speciated. The percentage of organics in this study was 26%, where generally these ambient organics were produced naturally in the environment and from combustion (Figure 3.11). Overall however, there has been little data on the source apportionment of $PM_{2.5}$.

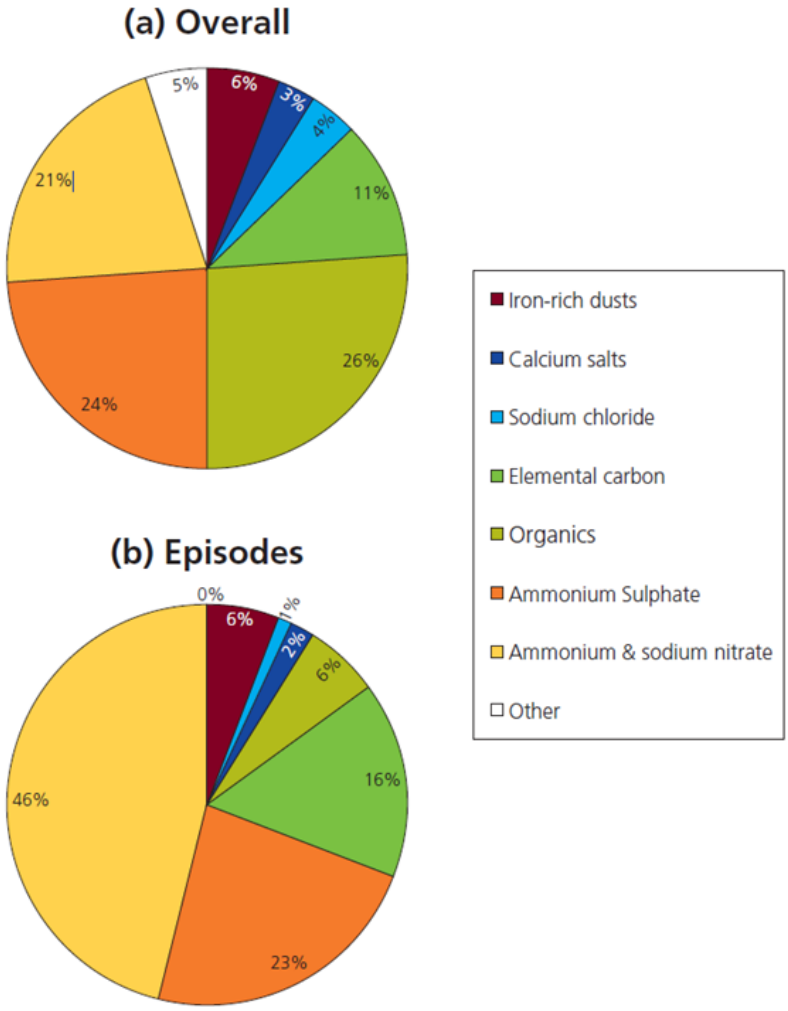

Figure 3.11: The composition of outdoor $PM_{2.5}$ in the United Kingdom (Source: Air Quality Expert Group (2012)).

Polidori et al. (2006) suggested that between 10% to 70% of $PM_{2.5}$ in an ambient environment was organic. However, there are limitations to identifying the composition of $PM_{2.5}$, as only 10% to 30% is actually properly identified and accounted for at the molecular level (Turpin et al., 2000). Polidori et al. (2006) also suggested that between 71% to 76% of indoor organic $PM_{2.5}$ was produced indoors, rather than the outdoor organic matter infiltrating the indoor setting. Figure 3.12 demonstrates $PM_{2.5}$ composition in the indoor and outdoor environment in America.

In a more recent study, Zhong et al. (2020) characterised and apportioned $PM_{2.5}$ during the winter of 2013 and 2018 in Beijing, China, where it was demonstrated that organic

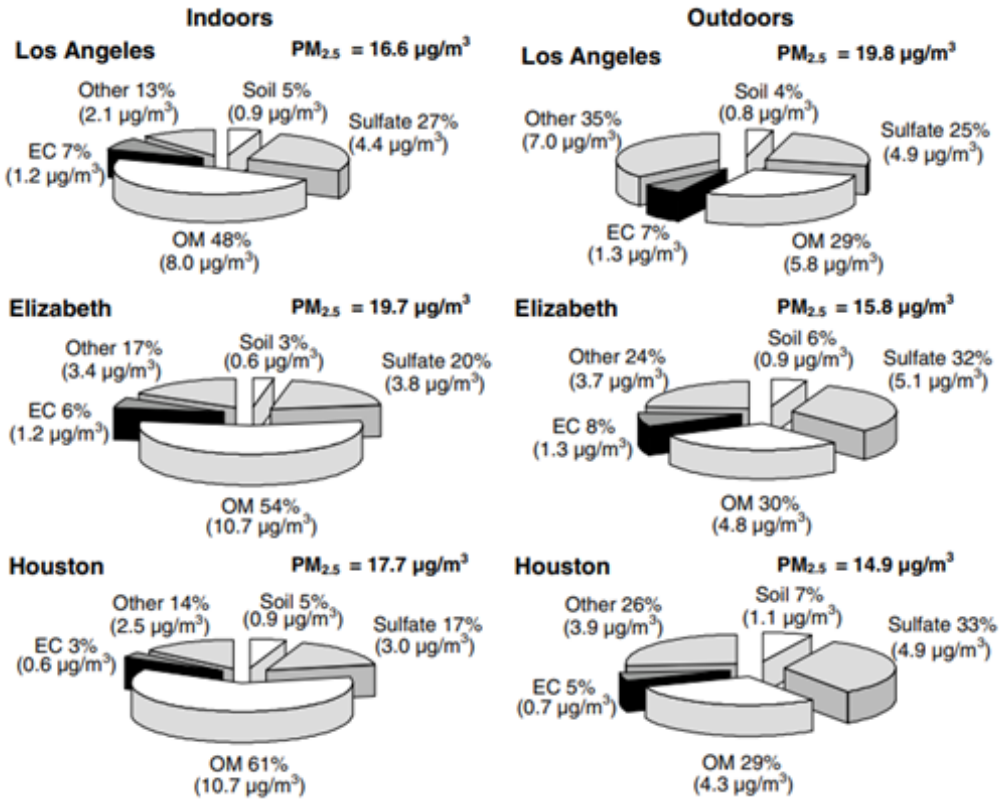

Figure 3.12: The mean contribution of species to indoor and outdoor particulate matter ($PM_{2.5}$) composition in suburban America. In the figure, EC and OM refer to elemental carbon and organic matter respectively (Source: Polidori et al. (2006)).

matter made up 31.7% and 31.4% of $PM_{2.5}$ in these two years respectively.

Table 3.8 shows the organic proportion (%) of $PM_{2.5}$ in a variety of suburban areas. The % organic proportion of $PM_{2.5}$ in Table 3.8 excludes elemental carbon. This is because elemental carbon would unlikely react with other materials or aerosols in the air, and is also considered photochemically inert (Karanasiou et al., 2015). Note that the measurements taken in Barcelona were taken in subway stations located across the city. The higher measurement recorded in Thessaloniki, Greece (27.1%) was taken near local traffic, whereas the lower recorded measurement (24.3%) was taken in a residential area.

In summary, Table 3.8 supports the assumption in INCHEM-Py that approximately 30% of the $PM_{2.5}$ that ingresses indoors from outdoors is organic in nature. This model assumption is therefore retained for the rest of the thesis.

Table 3.8: The organic % present in $PM_{2.5}$ in various locations across the world. The locations in red denote a warmer period in Joanic (25.9 °C), Santa Coloma (30.3 °C), Tetuan (21.8 °C) and Llefia (25.9 °C), whereas, the blue locations denote a colder period in Joanic (21.9 °C), Santa Coloma (19.6 °C), Tetuan (19.6 °C) and Llefia (21.0 °C).

Location	Organic % of $PM_{2.5}$	Reference
LA County, California (USA)	29 %	Polidori et al. (2006)
Elizabeth City, North Carolina (USA)	30 %	Polidori et al. (2006)
Houston, Texas (USA)	29 %	Polidori et al. (2006)
Beijing (China)	31.7 %	Zhong et al. (2020)
Beijing (China)	31.4 %	Zhong et al. (2020)
Joanic, Barcelona (Spain)	33.7 %	Martins et al. (2016)
Santa Coloma, Barcelona (Spain)	25.8 %	Martins et al. (2016)
Tetuan, Barcelona (Spain)	23.6 %	Martins et al. (2016)
Llefia, Barcelona (Spain)	21.7 %	Martins et al. (2016)
Joanic, Barcelona (Spain)	20.5 %	Martins et al. (2016)
Santa Coloma, Barcelona (Spain)	36.6 %	Martins et al. (2016)
Tetuan, Barcelona (Spain)	24.7 %	Martins et al. (2016)
Llefia, Barcelona (Spain)	30.0 %	Martins et al. (2016)
San Jose (Costa Rica)	25.9 %	Murillo et al. (2013)
Heredia (Costa Rica)	24.7 %	Murillo et al. (2013)
Belen (Costa Rica)	37.5 %	Murillo et al. (2013)
Moravia (Costa Rica)	34.9 %	Murillo et al. (2013)
Thessaloniki (Greece)	27.1 %	Samara et al. (2014)
Thessaloniki (Greece)	24.3 %	Samara et al. (2014)

3.3.7 New Degradation Schemes

Uchiyama et al. (2015) found that, 2,5-dimethylbenzaldehyde and 2-nonenal had a significant presence indoors, but neither of these species were represented in the MCM, or consequently, INCHEM-Py v1.1. 2,5-DMBA (2,5-dimethylbenzaldehyde) appears to be from industrial processes, but can be found in high concentrations indoors primarily from cigarette smoke (Pang and Lewis, 2011). According to Haze et al. (2001), 2-nonenal is often categorised as the 'old-person smell': it is a skin oil which all humans can emit, but it is more prominent in older people. New degradation mechanisms were constructed based on the MCM protocol (Jenkin et al., 1997) and other literature for these two species. The impacts of these new mechanisms on the model output was then explored.

2,5-Dimethylbenzaldehyde is assumed to follow the same degradation pathway as its iso-

mer 2,3-dimethylbenzaldehyde (2,3-DMBA), which is in the MCM. The chemistry can sometimes differ due to the location of the methyl groups attached to the benzene ring, given that stereochemistry often dictates kinetics and pathways of reactions involving aromatic species. Clifford and Wenger (2006) however, found that the initial rate coefficients for the reactions of the DMBA stereoisomers with the OH radical did not alter significantly depending on the location of the methyl group on the benzene ring. It can therefore be assumed that the reaction scheme for 2,5-DMBA follows a similar route to its stereoisomers for reactions with OH. 2,5-DMBA uses the same reaction mechanism as used for the degradation of 2,3-DMBA. The reaction scheme for the initial degradation steps for 2,5-DMBA are shown in Figure 3.13. The new degradation mechanism included in INCHEM-Py for 2,5-DMBA consists of 17 new, unique reactions. The full reaction scheme for the degradation of 2,5-DMBA is given in Appendix A.1.

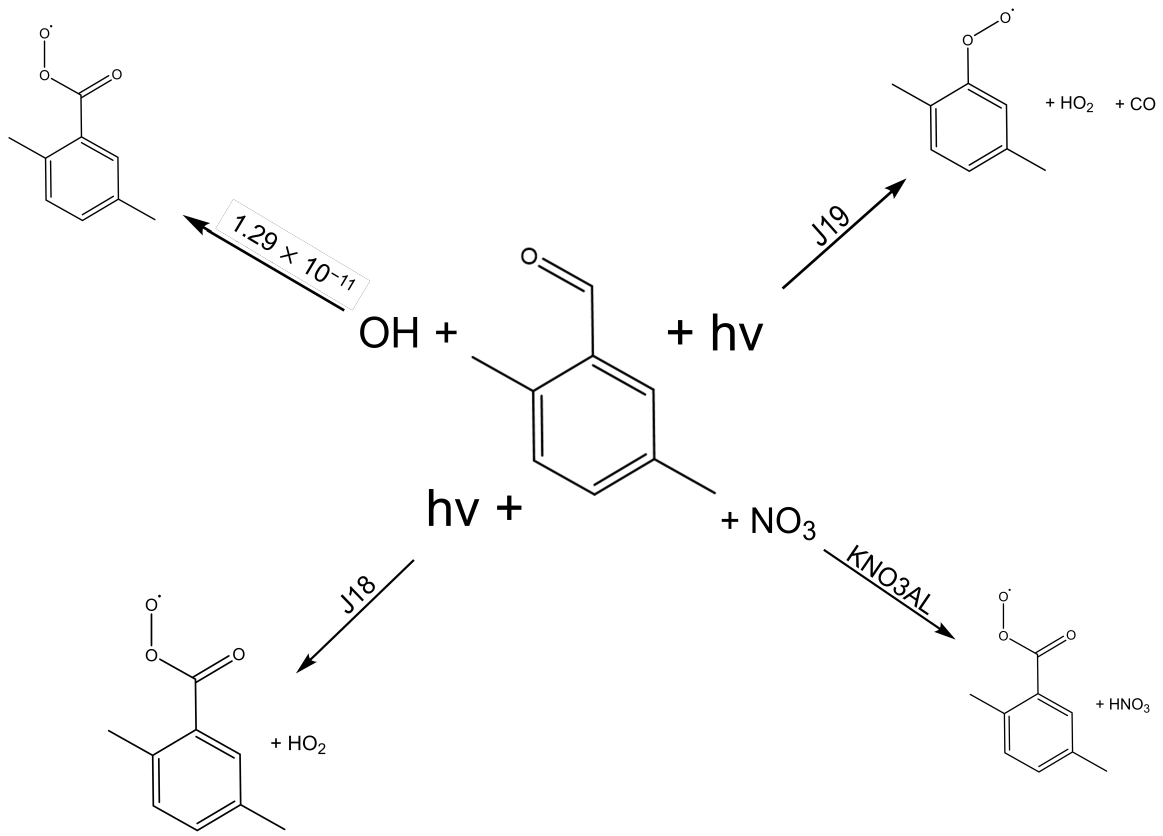

Figure 3.13: The initial reactions for the degradation of 2,5-dimethylbenzaldehyde (2,5-DMBA). The reaction rates are given in cm^3 $molecule^{-1}$ s^{-1}. hν represents the absorption of a photon. The J values (J18 and J19) and KNO3AL represent photolysis reactions and a rate coefficient respectively, both originating from the Master Chemical Mechanism.

The initial degradation of 2-nonenal is assumed to follow that of crotonaldehyde which is present in the MCM. Crotonaldehyde (2-butenal) is a four-carbon chained aldehyde with a double-bond situated in the 2 position. Although 2-nonenal has five more carbons than butenal, it is assumed that the two compounds will follow a similar degradation pathway, due to the unsaturation of both species.

2-Nonenal forms a single product from degradation via photolysis, three products via reaction with OH, two products via reaction with O_3 and a further three products via reaction with NO_3. The probability and subsequent distribution of these pathways were based on the crotonaldehyde degradation. The rate constants were obtained from numerous experimental studies, including the reactions of 2-nonenal with OH (Gao et al., 2009), O_3 (Gaona Colmán et al., 2017) and NO_3 (Kerdouci et al., 2012).

The reaction scheme for the inital degradation steps of 2-nonenal are shown in Figure 3.14. The new degradation mechanism included in INCHEM-Py for 2-nonenal consists of 138 new, unique reactions. The full reaction scheme for the degradation of 2-nonenal is given in Appendix A.2.

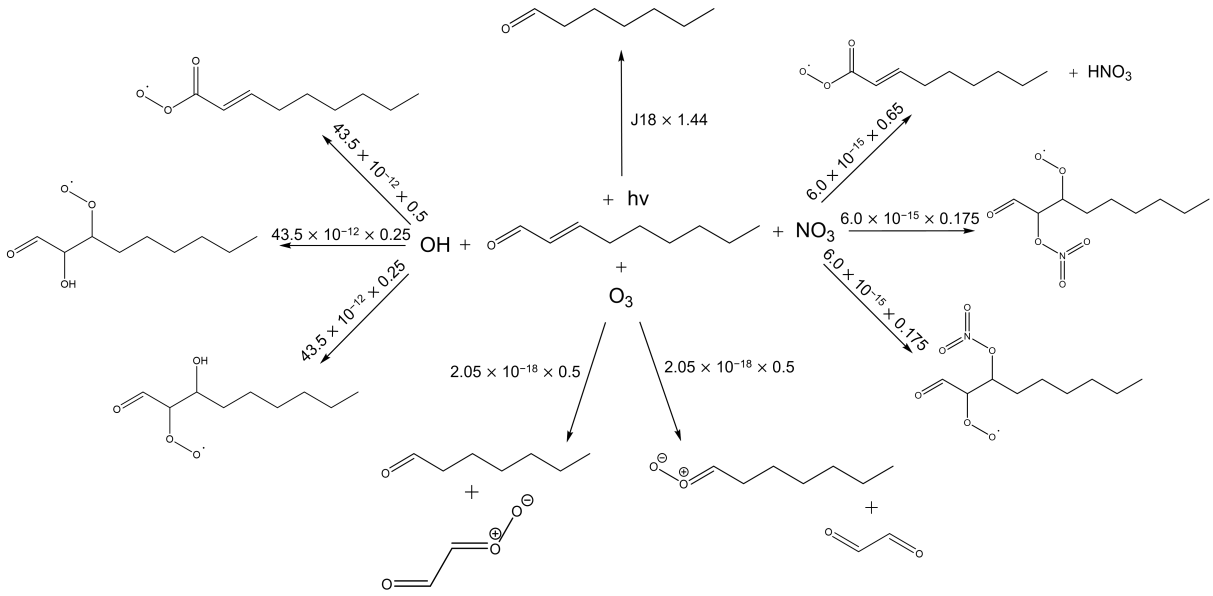

Figure 3.14: The initial reactions for the degradation of 2-nonenal. The rate coefficients have units of cm^3 $molecule^{-1}$ s^{-1}. hν represents the absorption of a photon.

The degradation of 2,5-dimethylbenzaldehyde, 2-nonenal and their subsequent impacts

on indoor air chemistry are not well known. INCHEM-Py has been used to provide insights on these aspects. A timed emission at 1 pm of 0.02 ppb s^{-1} of 2,5-DMBA or 2-nonenal was simulated and compared to a baseline (with no timed emission) to determine, firstly, whether the reaction schemes work, and secondly, what impact 2,5-DMBA and 2-nonenal have at higher concentrations. Figures 3.15 to 3.19 show the key indoor species' concentrations during degradation of these newly added species.

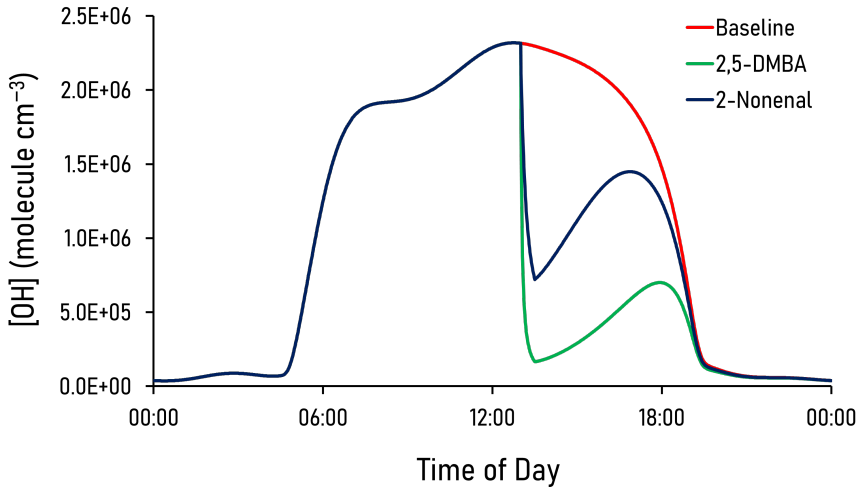

Figure 3.15: The indoor concentration of OH over 24 h, showing the impact of a timed emission of 0.02 ppb s^{-1} of 2,5-DMBA or 2-nonenal for 30 mins at 1pm and compared to the baseline (no timed emission).

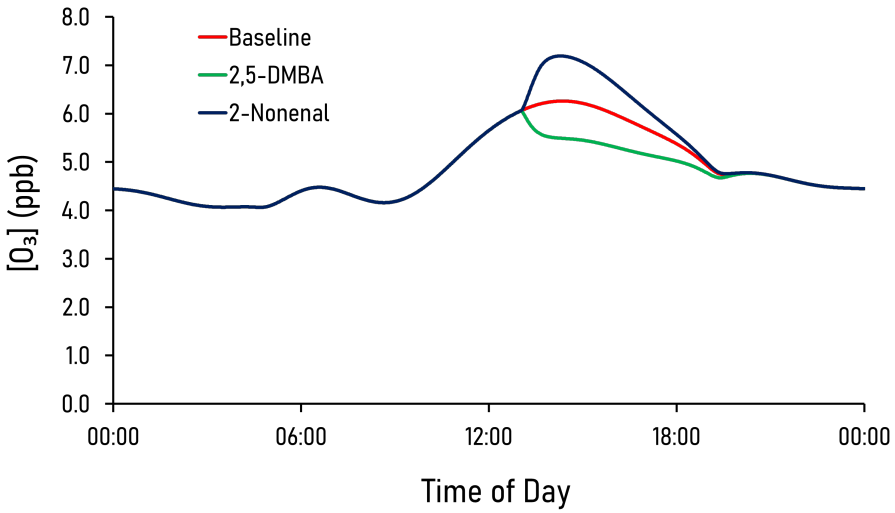

Figure 3.16: The indoor concentration of O_3 over 24 h, showing the impact of a timed emission of 0.02 ppb s^{-1} of 2,5-DMBA or 2-nonenal for 30 mins at 1pm and compared to the baseline (no timed emission).

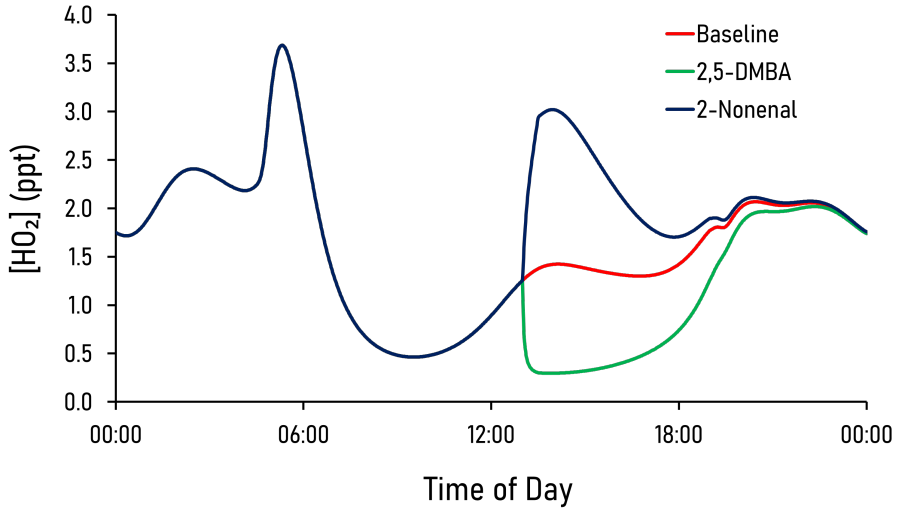

Figure 3.17: The indoor concentration of HO_2 over 24 h, showing the impact of a timed emission of 0.02 ppb s^{-1} of 2,5-DMBA or 2-nonenal for 30 mins at 1pm and compared to the baseline (no timed emission).

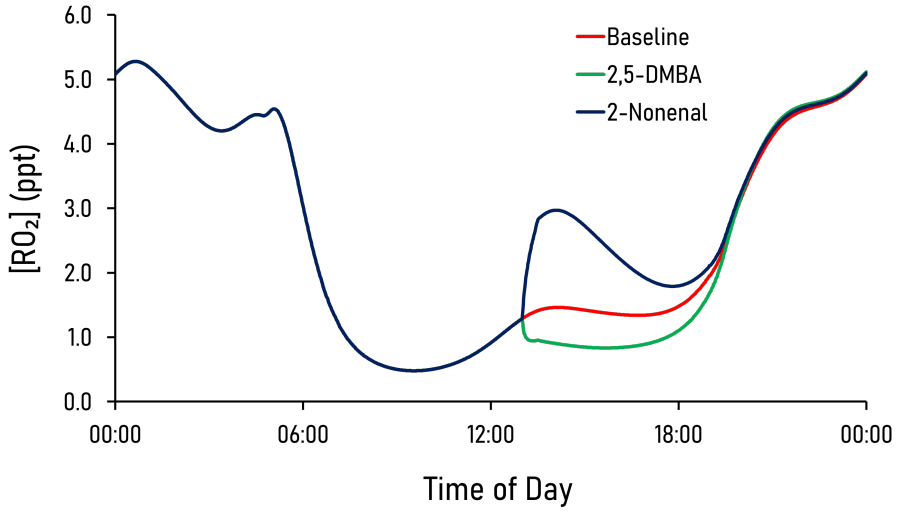

Figure 3.18: The indoor concentration of RO_2 over 24 h, showing the impact of a timed emission of 0.02 ppb s^{-1} of 2,5-DMBA or 2-nonenal for 30 mins at 1pm and compared to the baseline (no timed emission).

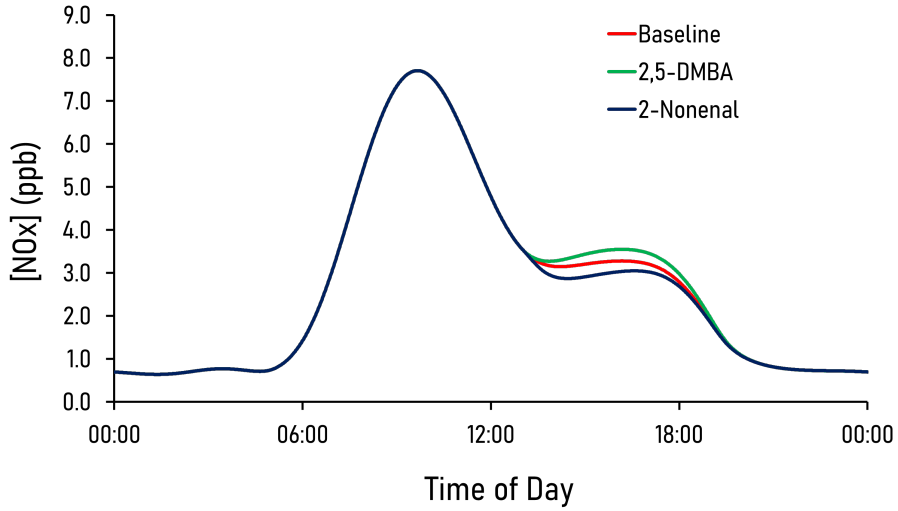

Figure 3.19: The indoor concentration of NO_x over 24 h, showing the impact of a timed emission of 0.02 ppb s^{-1} of 2,5-DMBA or 2-nonenal for 30 mins at 1pm and compared to the baseline (no timed emission).

In these simulations, with the 2,5-DMBA emission, the OH concentration decreased from 2.3×10^6 to 1.7×10^5 molecule cm^{-3}. For the 2-nonenal emission, the OH concentration decreased to 7.2×10^5 molecule cm^{-3}. O_3 increases from 6.1 to 7.2 ppb with 2-nonenal emission, but decreases from 6.1 to 5.5 ppb with 2,5-DMBA emission. These species also affect HO_2 and RO_2 concentrations. HO_2 decreases from 1.3 to 0.3 ppt with 2,5-DMBA emission but increases to 3.0 ppt with 2-nonenal emission. RO_2 decreases from 1.3 to 1.0 ppt with 2,5-DMBA emission but increases to 2.9 ppt with 2-nonenal emission. There is little change (<1 ppb increase) in NO_x concentrations with emission of either species. These simulations indicate that these species could affect key indoor radical concentrations and impact indoor air chemistry.

3.4 Summary

This chapter has described the operational workings of the detailed indoor chemical model for Python (INCHEM-Py) and its respective updates. The rest of the thesis describes the further development of the model for surfaces, indoor-outdoor exchange and far-ultraviolet light and uses the new developments to understand the respective implications on indoor air quality.

Chapter 4

The Role of Surfaces in Indoor Air Chemistry

The methodology in this chapter has been included in Shaw et al. (2023) and the chapter itself published as Carter et al. (2023). The hydrogen peroxide deposition and emission data were provided by Dr. Dustin Poppendieck, but analysed and utilised accordingly by myself.

4.1 Introduction

Indoor air pollution is a fairly modern area of study. There has been relatively little study into indoor air quality as opposed to the extensive research conducted for outdoor air pollution. The recent COVID-19 pandemic has highlighted the need for healthy indoor environments and the public is now much more aware of the benefits of good indoor air quality. This is important as people spend approximately 90% of their time indoors (Klepeis et al., 2001), whether at home, at work, or commuting between the two.

Sources of indoor pollutants originate from a variety of household activities, including cooking (Kang et al., 2019) and cleaning (Carslaw et al., 2017; Carslaw and Shaw, 2022). Other notable sources include candle burning (Bekö et al., 2013) and emissions from indoor surfaces (Poppendieck et al., 2007b), which are the focus of this chapter. These indoor pollutant sources release volatile organic compounds (VOCs), which can react with

oxidants in the gas-phase to form secondary pollutants, some of which are harmful to human health (Nørgaard et al., 2014).

The impact of internal surfaces on indoor gas-phase chemistry is an increasingly important area of focus (Ault et al., 2020). There are a wide range of surfaces indoors, such as carpets, wooden flooring, painted walls, and also the human surface (skin), which can act as both sinks and sources of indoor air pollutants (Fischer et al., 2013; Hodgson et al., 1993; Cheng et al., 2015; Katsoyiannis et al., 2008).

Indoor materials can emit pollutants either as primary emissions released directly from the surface, or as gas-phase transformation products that are formed following a surface interaction. Primary emissions released directly from indoor surfaces and building materials include a wide array of chemical species, including carboxylic acids, aldehydes and alcohols (Chin et al., 2019; Ruiz-Jimenez et al., 2022). Emission rates of species emitted directly from surfaces are highest for new materials, but can continue to produce pollutants as they get older (Morrison and Nazaroff, 2002a). In 30 newly constructed Korean apartment buildings, approximately 60% of total indoor VOCs arose from flooring and paint materials (Shin and Jo, 2013).

Secondary pollutants can also be formed following gas-phase surface interactions, whereby a chemical reaction (often oxidation) with the surface instigates the release of secondary species. The emission rates of these secondary pollutants are important to quantify indoors, as they can be harmful to human health (Nazaroff and Weschler, 2004) and include aldehydes and ketones (Wang and Morrison, 2006; Cheng et al., 2015; Poppendieck et al., 2007b; Katsoyiannis et al., 2008; Salthammer, 2019; Destaillats et al., 2008), alkanes and alkenes (Hodgson et al., 1993), aromatics and esters (Xiong et al., 2019), and secondary organic aerosols (SOA) (Waring and Siegel, 2013). Wang and Morrison (2006) found that indoor surfaces continue to produce secondary pollutants over a long period of time, with 14-year old surfaces in a house still a source of secondary pollution. Indoor surfaces can therefore modify indoor air composition.

The composition of secondary emitted species are surface dependent. Short and long-chain aldehydes are produced following ozone deposition onto soft fabrics (Cros et al.,

2012; Lamble et al., 2011), whereas concrete surfaces emit short, straight-chain and aromatic aldehydes and ketones following ozone deposition (Poppendieck et al., 2007b). Concrete surfaces likely emit other chemicals, but this study was limited by the instrumentation and quantification methods (Poppendieck et al., 2007b). Figure 4.1 shows the surface interactions taking place in a standard home setting.

Figure 4.1: The chemical processes and transformations following deposition of oxidants on internal surfaces in the indoor environment.

Skin can be an important contributor to indoor gas-phase chemistry, particularly in crowded spaces. Wang et al. (2022a) undertook a study of VOC emission rates from human skin, measuring a total VOC emission rate of 1150 µg hr^{-1} per person. This experiment was performed on young adults with an average age of 25 years under ozone free

conditions (< 1 ppb of ozone). Acetone and acetic acid had the largest emission rates from skin, contributing 16% and 19% of the total VOC emission respectively. The total VOC emission rate increased to 4450 μg hr^{-1} per person when ozone increased in concentration (to 36.3 ppb), suggesting that skin oxidation reactions were occurring and contributing to the VOC emissions from the skin surface (Wang et al., 2022a). Furthermore, Liu et al. (2021) discovered that products of ozone-skin lipid chemistry continued to contribute to measured VOC concentrations even in a home that had been empty for five days. This indicates that surfaces act as sources and reservoirs of VOCs indoors and can have a considerable effect on indoor chemistry.

Ozone can deposit onto a range of materials and surfaces indoors, where there are higher surface area-to-volume ratios compared to outdoor environments. The respective rate of deposition of an oxidant indoors, such as ozone, depends on the type of surface and how that affects the transportation and uptake of the oxidant (Reiss et al., 1994). For example, fleecy surfaces, such as carpets, have a higher oxidant deposition velocity (Morrison and Nazaroff, 2000; Abbass et al., 2017) than smoother surfaces, such as wood or concrete (Schripp et al., 2012; Poppendieck et al., 2007a; Lin and Hsu, 2015). Deposition velocities of ozone onto indoor materials have been previously reviewed (Kruza et al., 2017; Shen and Gao, 2018). There is often a wide variation in these values, where the age, nature of the material surface, oxidant concentrations and the measurement technique can all affect the deposition velocities that are determined through experiments (Lamble et al., 2011; Wang and Morrison, 2006).

Hydrogen peroxide (H_2O_2) can also participate in indoor surface deposition, though it has been much less studied than ozone in this respect (Zhou et al., 2020; Poppendieck et al., 2021). Often used as a cleaning agent, hydrogen peroxide can photolyse to form hydroxyl radicals (OH) (Kahan et al., 2012; Zhou et al., 2020), which initiate indoor gas-phase chemistry. OH chemistry often dominates the gas-phase chemistry of indoor environments due to its high reactivity (Waring and Wells, 2015; Carslaw et al., 2017).

Poppendieck et al. (2021) determined the surface deposition velocities of hydrogen peroxide onto a range of common indoor surfaces, including carpets and concrete and the

consequent emission rates of surface-formed species. Over a 6-hour period of indoor surface exposure to hydrogen peroxide, less than 2 mg m^{-2} of secondary pollutants were emitted. For exposure of flooring and wall coverings to ozone, between 1 and 20 mg m^{-2} of pollutants were emitted over 36 hours (Poppendieck et al., 2021, 2007b).

There has, to date, been little focus on how surface deposition of hydrogen peroxide and subsequent surface interactions affect the indoor air chemistry. In fact, there is currently little experimental data evaluating the impact of surface deposition on indoor air chemistry other than ozone. Therefore, this chapter uses experimental data on surface deposition of ozone and hydrogen peroxide, as well as information relating to the extent and composition of indoor surfaces in three different indoor micro-environments, to improve an existing model for indoor air chemistry. We use the model to investigate the interaction of these two oxidants with internal surfaces and in so doing, gain a better understanding of the consequent impacts on indoor air chemistry. The surface to volume ratios of materials found indoors have been updated to incorporate recent literature. This update includes expanding the range of surfaces and emissions considered for ozone interactions at the surface, but also defining completely new parameterisation for hydrogen peroxide. The updated model has then been used to investigate the following objectives:

• Explore the impact of indoor oxidation processes following ozone and hydrogen peroxide deposition onto indoor surfaces on indoor pollutant concentrations.

• Analyse the influence of a variety of surfaces on indoor gas-phase oxidant concentrations.

• Determine whether different rooms in a building have unique oxidant uptake and hence indoor air composition.

• Discover how our exposure to air pollution varies over the course of a typical working day.

4.2 Methods

4.2.1 The Model

This chapter focuses on the final term in the INCHEM-Py equation (Equation 3.11), and in particular, incorporates deposition of ozone and hydrogen peroxide onto internal surfaces and the resulting emissions of secondary pollutants from those surfaces. Whilst the ozone deposition and resulting emissions are an extension of the work by Kruza et al. (2017), the hydrogen peroxide treatment is a new addition to INCHEM-Py.

4.2.2 Development of the Model

The first order loss rate of ozone ($F_{s_{O_3}}$) and hydrogen peroxide ($F_{s_{H_2O_2}}$) to a surface (in s^{-1}) can be calculated using Equation 4.1 and Equation 4.2 respectively (Kruza et al., 2017). These equations are surface-specific.

$$F_{s_{O_3}} = \nu_{d_{O_3}} \frac{A}{V} \tag{4.1}$$

$$F_{s_{H_2O_2}} = \nu_{d_{H_2O_2}} \frac{A}{V} \tag{4.2}$$

ν_{dO_3} and $\nu_{dH_2O_2}$ represent the surface deposition velocities of ozone and hydrogen peroxide onto a material respectively (cm s^{-1}). Following an interaction at the surface, the emission rate, E_i (molecule cm^{-3} s^{-1}), of a secondary pollutant (species i), can be calculated using Equation 4.3 and Equation 4.4 for ozone and hydrogen peroxide deposition respectively (Morrison and Nazaroff, 2002a; Kruza et al., 2017).

$$E_i = \frac{A\nu_{d_{O_3}} Y_i C_{O_3}}{V} \tag{4.3}$$

$$E_i = \frac{A\nu_{d_{H_2O_2}} Y_i C_{H_2O_2}}{V} \tag{4.4}$$

In Equations 4.3 and 4.4, Y_i is the production yield of species i emitted from a given surface (dimensionless) and will arise from a combination of reactions with, or displace-

ment from, the surface. C_{O_3} and $C_{H_2O_2}$ are the concentrations of indoor ozone and hydrogen peroxide respectively (molecule cm^{-3}).

4.2.3 Oxidant Deposition

For this work, ozone deposition onto nine surfaces and hydrogen peroxide deposition onto six surfaces was considered, based on available literature. The range of deposition velocities of ozone (Sabersky et al., 1973; Lin and Hsu, 2015; Klenø et al., 2001; Grøntoft, 2002; Abbass et al., 2017; Gall et al., 2013; Tamás et al., 2006; Cros et al., 2012; Coleman et al., 2008; Ye et al., 2020; Lamble et al., 2011; Rim et al., 2016; Poppendieck et al., 2007a; Wang and Morrison, 2010, 2006; Nicolas et al., 2007; Morrison and Nazaroff, 2000; Fadeyi et al., 2013; Yao et al., 2020; Di et al., 2017; Rai et al., 2014; Fischer et al., 2013; Wisthaler and Weschler, 2010; Schripp et al., 2012; Mueller et al., 1973; Cox and Penkett, 1972; Grøntoft and Raychaudhuri, 2004; Simmons and Colbeck, 1990; Cano-Ruiz et al., 1993) and hydrogen peroxide (Poppendieck et al., 2021) are shown in Figure 4.2 and Figure 4.3 respectively. For the model simulations, the median deposition velocity was utilised.

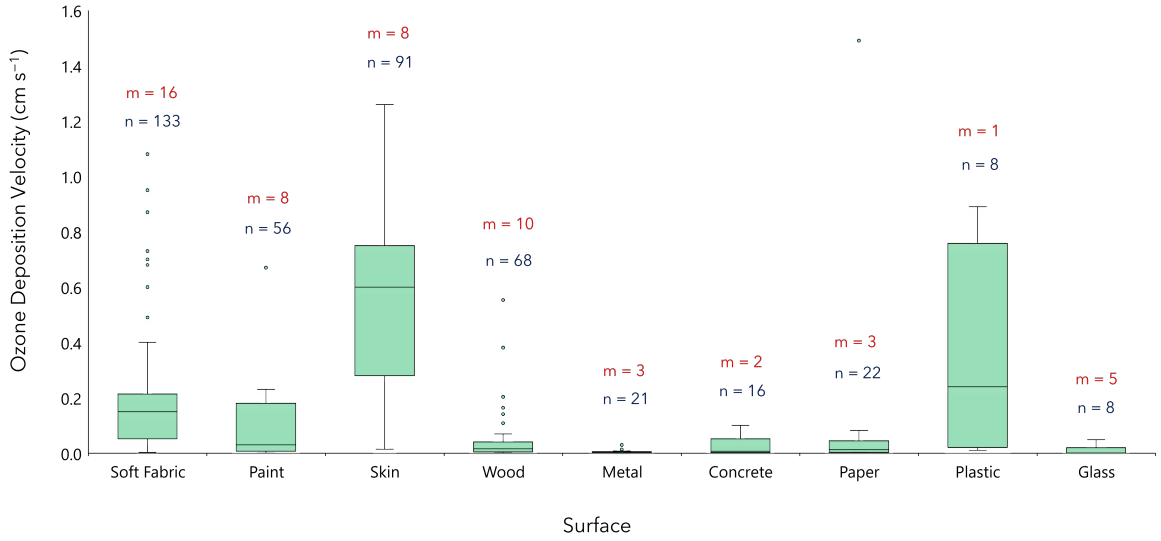

Figure 4.2: The distribution of reported ozone deposition velocities onto a range of indoor surfaces, including the median, the upper (75% percentile) and lower (25% percentile) quartiles, the upper whisker (Q3 + 1.5*IQR) and the lower whisker (Q1 −1.5*IQR) in cm s^{-1}. Values which fell outside the range of the upper and lower whiskers are also included in the plot as small circles. n denotes the total number of measurements per surface. m denotes the total number of studies consulted.

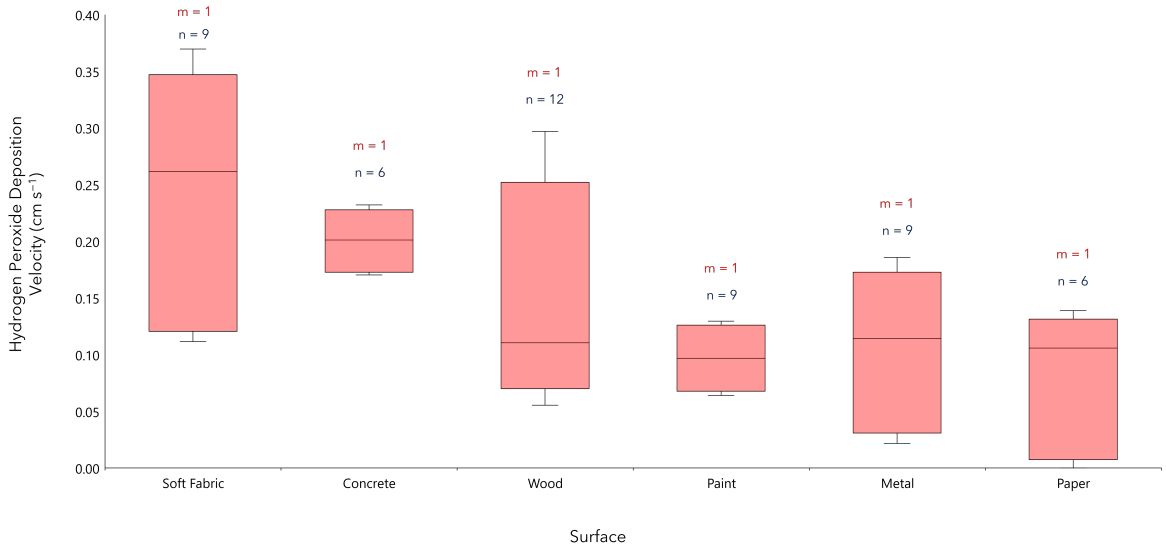

Figure 4.3: The distribution of reported hydrogen peroxide deposition velocities onto a range of indoor surfaces, including the median, the upper (75% percentile) and lower (25% percentile) quartiles, the upper whisker (Q3 + 1.5*IQR) and the lower whisker (Q1 −1.5*IQR) in cm s^{-1}. n denotes the total number of measurements per surface. m denotes the total number of studies consulted.

Figure 4.2 shows that skin has the highest median ozone deposition velocity (0.60 cm s^{-1}) out of the nine indoor materials evaluated. Plastic and soft fabric surfaces also have higher median ozone deposition velocities compared to the other surfaces (0.24 and 0.15 cm s^{-1} respectively). Figure 4.3 shows that soft fabric materials were found to have the highest median hydrogen peroxide deposition velocity (0.26 cm s^{-1}), which was higher than the median ozone deposition velocity.

4.2.4 Production Yields of Species from Surfaces

The production yields of species emitted from a range of surfaces as a result of ozone and hydrogen peroxide deposition have been collated from a range of literature sources (Wang and Morrison, 2010; Weschler et al., 2007; Kruza and Carslaw, 2019; Cheng et al., 2015; Poppendieck et al., 2007b, 2021; Coleman et al., 2008), and incorporated into the model (Table 4.1 and Table 4.2).

Table 4.1: Production yields following ozone deposition onto soft fabric, painted (Wang and Morrison, 2010), skin (Weschler et al., 2007; Kruza and Carslaw, 2019), wooden (Cheng et al., 2015), metallic, concrete, paper (Poppendieck et al., 2007b), and plastic (Coleman et al., 2008) surfaces. Absence of a yield indicates it was below the limit of detection (LOD) or the species wasn't measured for that surface. The units are dimensionless.

	Production Yield (dimensionless)								
Species	**Soft Fabrics**	**Paint**	**Skin**	**Wood**	**Metal**	**Concrete**	**Paper**	**Plastic**	**Glass**
Formaldehyde	$3.4x10^{-2}$	-	-	$7.2x10^{-1}$	$6.9x10^{-4}$	$4.2x10^{-4}$	$4.5x10^{-4}$	$1.9x10^{-2}$	-
Acetaldehyde	$4.0x10^{-3}$	-	-	$3.9x10^{-1}$	$6.6x10^{-4}$	$4.7x10^{-4}$	$1.9x10^{-3}$	$1.3x10^{-2}$	-
Propanal	$5.0x10^{-3}$	-	-	$1.9x10^{-1}$	$2.4x10^{-4}$	$2.9x10^{-4}$	$2.2x10^{-4}$	-	-
Butanal	$3.5x10^{-3}$	-	-	$1.9x10^{-1}$	$1.1x10^{-4}$	$1.2x10^{-4}$	$1.9x10^{-4}$	$5.1x10^{-3}$	-
Pentanal	$5.8x10^{-3}$	-	-	$1.4x10^{-1}$	$9.1x10^{-5}$	$6.3x10^{-5}$	$2.9x10^{-4}$	$5.1x10^{-3}$	-
Hexanal	$2.0x10^{-2}$	-	-	$1.0x10^{-1}$	$1.7x10^{-4}$	$1.1x10^{-4}$	$1.0x10^{-3}$	$5.1x10^{-3}$	-
Heptanal	$6.4x10^{-3}$	-	-	-	-	-	$2.5x10^{-5}$	$5.1x10^{-3}$	-
Octanal	$6.1x10^{-3}$	$1.0x10^{-2}$	-	-	$1.7x10^{-6}$	-	$1.9x10^{-5}$	$5.1x10^{-3}$	-
Nonanal	$4.8x10^{-2}$	$1.3x10^{-1}$	$1.8x10^{-2}$	-	-	-	$1.3x10^{-5}$	$3.3x10^{-2}$	-
Decanal	$1.4x10^{-2}$	$4.3x10^{-2}$	$2.6x10^{-2}$	-	-	-	-	$2.6x10^{-2}$	-
2-Nonenal	$1.9x10^{-3}$	-	-	-	-	-	-	-	-
Acrolein	-	-	-	$2.3x10^{-1}$	-	-	-	-	-
Methacrolein	-	-	-	$4.0x10^{-2}$	-	-	-	-	-
Crotonaldehyde	-	-	-	$1.2x10^{-1}$	$5.8x10^{-5}$	$1.1x10^{-5}$	-	-	-
Benzaldehyde	-	-	-	$1.4x10^{-1}$	-	$3.0x10^{-5}$	$1.0x10^{-4}$	-	-
m-Tolualdehyde	-	-	-	$1.0x10^{-1}$	$5.9x10^{-6}$	-	$1.1x10^{-5}$	-	-
4-OPA	-	-	$2.6x10^{-2}$	-	-	-	-	-	-
Acetone	-	-	$4.9x10^{-3}$	-	-	$4.6x10^{-4}$	$1.3x10^{-3}$	$2.4x10^{-2}$	-
Formic Acid	-	-	$8.5x10^{-3}$	-	-	-	-	-	-
Acetic Acid	-	-	$6.5x10^{-3}$	-	-	-	-	-	-
Isopentanal	-	-	-	-	$3.2x10^{-5}$	$1.4x10^{-5}$	$1.7x10^{-4}$	-	-
2,5-DMBA	-	-	-	-	-	$2.6x10^{-6}$	-	-	-

Table 4.2: Production yields for species as a result of hydrogen peroxide deposition onto indoor surfaces (Poppendieck et al., 2021). Absence of a yield indicates it was below the limit of detection (LOD). The units are dimensionless.

	Production Yield (dimensionless)								
Species	**Soft Fabrics**	**Paint**	**Skin**	**Wood**	**Metal**	**Concrete**	**Paper**	**Plastic**	**Glass**
Formaldehyde	$8.8x10^{-6}$	-	-	$2.0x10^{-5}$	$2.8x10^{-5}$	$2.1x10^{-5}$	-	-	-
Acetaldehyde	$6.5x10^{-6}$	-	-	$3.9x10^{-5}$	$3.4x10^{-6}$	$3.2x10^{-6}$	-	-	-
Propanal	$1.1x10^{-7}$	-	-	$4.4x10^{-7}$	-	$1.7x10^{-6}$	$1.0x10^{-6}$	-	-
Butanal	$5.4x10^{-6}$	-	-	$4.5x10^{-6}$	-	$1.7x10^{-6}$	-	-	-
Isopentanal	-	-	-	$2.1x10^{-6}$	-	$4.8x10^{-7}$	-	-	-
Pentanal	-	-	-	$1.8x10^{-7}$	-	$1.2x10^{-6}$	-	-	-
Hexanal	$8.0x10^{-8}$	-	-	$3.8x10^{-6}$	$2.8x10^{-7}$	$2.1x10^{-7}$	-	-	-
Heptanal	-	-	-	$1.0x10^{-6}$	-	$2.4x10^{-7}$	-	-	-
Octanal	-	-	-	$2.2x10^{-7}$	-	$2.2x10^{-7}$	-	-	-
Nonanal	-	-	-	$2.4x10^{-7}$	-	-	-	-	-
Crotonaldehyde	$2.6x10^{-7}$	-	-	$3.0x10^{-6}$	$3.8x10^{-6}$	$7.2x10^{-7}$	$1.2x10^{-5}$	-	-
Benzaldehyde	-	-	-	-	$3.4x10^{-6}$	$1.4x10^{-7}$	-	-	-
m-Tolualdehyde	-	-	-	$6.5x10^{-7}$	$1.9x10^{-7}$	-	-	-	-

4.2.5 Indoor Spatial Representation

It is important to consider the surface area of a material in the indoor environment, to better understand how oxidant sorption onto materials, and the transformations that subsequently occur, impact indoor air quality (Manuja et al., 2019; Ye et al., 2020). Recent studies (Manuja et al., 2019; Hodgson et al., 2004; Morgan and Cruickshank, 2014) have provided typical room sizes and surface area compositions. These studies provide the basis for predicting how replacing an indoor surface, for example a wooden floor, with an 'emission-free' or 'VOC friendly' alternative, will affect deposition, emissions and subsequently the impact on indoor air chemistry (Cheng et al., 2015).

Surfaces have been included in INCHEM-Py, and are categorised by material. For example, fleecy carpets and cushioned sofas are represented under the 'Soft Fabric' category, whereas wooden door frames and floors are assumed to be wooden surfaces. Most household items can then be considered in the model when analysing indoor surface deposition. The total surface area of each specific surface is divided by the total volume of the indoor space to yield a surface-specific surface area-to-volume ratio. Using a comprehensive study which measured the total surface area of common indoor materials in bedrooms, kitchens and work offices (Manuja et al., 2019), surface areas of each material have been averaged for each type of room and the surface-specific surface area-to-volume ratios calculated (Table 4.3, Table 4.4 and Table 4.5).

The average volumes of the bedroom, kitchen and office with their specific contents were 29, 25 and 35 m^3 respectively based on Manuja et al. (2019). For the model simulations, it was assumed that two adults would be present in the bedroom, one adult would be present in the kitchen and three adults present in the office. Adults are assumed to have $\approx$ 2 m^2 of skin surface (Fischer et al., 2013). Clothing is assumed to contribute to the 'skin' surface, as fabrics soiled with secreted skin oils and flakes have a similar ozone deposition velocity and respective secondary pollutant emission yields to bare skin (Rai et al., 2014; Lakey et al., 2017; Kruza and Carslaw, 2019).

Table 4.3: The surface areas and surface-to-volume ratios of materials found in a representative bedroom, based on an assumed volume of 29 m^3 and based on Manuja et al. (2019).

Material	Surface Area (m^2) ±Standard Deviation	Surface-to-Volume Ratio (m^{-1}) ±Standard Deviation
Soft Fabric	18.72 ±6.3	0.646 ±0.22
Paint	41.79 ±12.1	1.44 ±0.42
Skin	4.00 ±0.50	0.138 ±0.02
Wood	16.20 ±10.7	0.559 ±0.37
Metal	1.10 ±0.96	0.038 ±0.03
Concrete	0.003 ±0.01	0.0001 ±0.0003
Paper	2.10 ±5.8	0.073 ±0.20
Plastic	2.48 ±1.5	0.086 ±0.05
Glass	1.29 ±0.9	0.045 ±0.03
Total	**87.68 ±6.1**	**3.02 ±1.0**

Table 4.4: The surface areas and surface-to-volume ratios of materials found in a representative kitchen, based on an assumed volume of 25 m^3 and based on Manuja et al. (2019).

Material	Surface Area (m^2) ±Standard Deviation	Surface-to-Volume Ratio (m^{-1}) ±Standard Deviation
Soft Fabric	2.02 ±4.8	0.081 ±0.19
Paint	24.80 ±9.1	0.992 ±0.37
Skin	2.00 ±1.5	0.080 ±0.06
Wood	16.63 ±7.7	0.665 ±0.31
Metal	7.77 ±4.6	0.311 ±0.18
Concrete	1.17 ±1.5	0.048 ±0.06
Paper	0.204 ±0.27	0.008 ±0.01
Plastic	7.24 ±9.2	0.290 ±0.37
Glass	1.49 ±1.6	0.058 ±0.06
Total	**63.27 ±5.6**	**2.53 ±0.9**

Table 4.5: The surface areas and surface-to-volume ratios of materials found in a representative office, based on an assumed volume of 35 m^3 and based on Manuja et al. (2019).

Material	Surface Area (m^2) ±Standard Deviation	Surface-to-Volume Ratio (m^{-1}) ±Standard Deviation
Soft Fabric	10.51 ±6.3	0.300 ±0.18
Paint	34.68 ±4.6	0.991 ±0.13
Skin	6.00 ±0.50	0.171 ±0.01
Wood	21.86 ±9.3	0.625 ±0.26
Metal	13.36 ±8.2	0.382 ±0.23
Concrete	0.000 ±0.00	0.000 ±0.00
Paper	3.36 ±1.5	0.096 ±0.04
Plastic	32.85 ±8.3	0.939 ±0.24
Glass	5.05 ±6.5	0.144 ±0.19
Total	**127.69 ±6.0**	**3.65 ±1.0**

4.2.6 Model Parameterisation

The model was initialised to simulate a typical apartment located in suburban London. The temperature of the apartment was assumed to be 19.9 °C and the relative humidity 53.8 %, based on the mean values from extensive monitoring of air quality in homes across the United Kingdom (Ministry of Housing & Communities & Local Government (UK Government), 2019). Nazaroff (2021) undertook a comprehensive literature review of air change rates (ACR) in residential properties in Europe, North America and central Asia, and concluded that an appropriate median value of air change rates in homes is 0.5 hr^{-1}, with 95% of residential air change rates existing within a 0.125 and 2.0 hr^{-1} range. These findings were used to bound the ACR values in the model simulations.

Indoor photolysis rates are incorporated into the model and include the impact of indoor artificial light plus attenuated sunlight (Shaw and Carslaw, 2021; Wang et al., 2022b; Shaw et al., 2023). For these simulations, incandescent lighting is used and the windows assumed to admit sunlight with a wavelength down to 308 nm ('Glass C' in (Wang et al., 2022b)). The indoor lights were turned on at 07:00 GMT and switched off at 19:00 GMT. The date was assumed to be the 21st June and the latitude is set to that of central London, 51.5 °N.

The outdoor concentrations of key atmospheric species including OH, HO_2 and the methylperoxy radical (CH_3O_2), are defined in the model by diurnal profiles determined by the solar zenith angle (Carslaw, 2007). The outdoor concentrations of O_3, NO (nitric oxide) and NO_2 (nitrogen dioxide) were based on measurements in suburban London over the course of three summer months and follow a diurnal profile (Shaw and Carslaw, 2021; EEA, 2018). The average outdoor concentrations for these species for all of the subsequent model runs are provided in Table 4.6. The outdoor VOC and non-VOC concentrations used in this chapter are given in Tables 3.4 and 3.5 in Chapter 3. The outdoor hydrogen peroxide concentration in the model is assumed to be 1.3 ppb, based on He et al. (2010).

For the inclusion of people in the model, breath emissions have also been added (Table

Table 4.6: The average outdoor concentration of outdoor atmospheric species in suburban London.

Species	Average Outdoor Concentration
OH	1.4 x 10^6 molecule cm^{-3}
HO_2	2.5 ppt
CH_3O_2	0.54 ppt
O_3	24.9 ppb
NO	2.8 ppb
NO_2	3.4 ppb

4.7), using data from Kruza and Carslaw (2019), tailored according to how many adults are assumed to be present in each indoor space (Shaw et al., 2023).

Table 4.7: The emission rates of VOCs in breath for adults and children (in molecule cm^{-3} s^{-1}).

Species	Adult Emission Rate	Child Emission Rate
Acetone	2.5 x 10^7	4.8 x 10^6
Ethanol	2.0 x 10^7	3.0 x 10^6
Methanol	8.5 x 10^6	3.1 x 10^6
Isopropanol	3.9 x 10^6	6.6 x 10^5
Isoprene	5.4 x 10^6	6.0 x 10^5

4.3 Results and Discussion

4.3.1 The Uptake of Ozone and Hydrogen Peroxide on Indoor Surfaces

Kruza et al. (2017) found that 85% of the ozone present indoors was deposited onto indoor surfaces in their simulated apartment, conducted with an air change rate of 0.76 hr^{-1}. Similarly to this study, Kruza et al. (2017) also included surface specific deposition rates. This study has yielded comparable results, with 94, 91 and 94% of ozone deposited onto indoor surfaces in the bedroom, kitchen and office respectively. In addition, 96, 94 and 95% of indoor hydrogen peroxide is deposited onto indoor surfaces in the bedroom, kitchen and office respectively, with these model simulations using an air change rate of 0.5 hr^{-1}. These values reinforce the idea that indoor surfaces provide a key role in the

removal of ozone and hydrogen peroxide in the indoor environment.

For an air change rate of 2.0 hr^{-1}, the total deposition of indoor ozone and hydrogen peroxide onto surfaces was 78 and 87% in the bedroom, 78 and 81% in the kitchen, and 86 and 84% in the office respectively. Under these higher air change rate conditions, more of the oxidant migrates to the outdoor environment before reacting with an indoor surface. Figure 4.4 provides a breakdown of the percentage of the total deposition of ozone and hydrogen peroxide onto different indoor surfaces in the different study locations. The surface area of each material as a percentage of the total in each room is also given in Figure 4.4.

The importance of individual surfaces varies between rooms. For instance, soft fabric materials are responsible for 38% of the total ozone deposition in the bedroom, yet represent only 21% of the total surface area in the bedroom. Meanwhile, painted surfaces, which represent >45% of the bedroom surface area are only responsible for 17% of the total ozone deposition. In the kitchen and the office, soft fabrics represent approximately 3% and 8% of the total surface area respectively, but account for 7% and 11% of the total ozone deposition in these individual rooms. Plastic surfaces in the kitchen and the office are the most important ozone sink in these spaces, whilst metal, concrete, paper and glass surfaces are responsible for <1% of ozone deposition, owing to small surface areas and low ozone deposition velocities. Despite a low overall surface area, deposition of ozone onto skin was the second biggest deposition sink in all three rooms, highlighting the importance of occupants on ozone deposition indoors.

The rate of ozone deposition onto indoor surfaces changes with room type and surface area of a material (Weschler, 2000). For example, the rate of deposition of ozone onto soft fabrics decreases by a factor of approximately 6 when moving from the bedroom to the kitchen, as there are fewer soft surfaces in the latter. For plastic surfaces, the rate of ozone deposition in an office is approximately 14 times more than the deposition rate in the bedroom. Painted surfaces have a more comparable impact in different rooms, where the total ozone deposition only fluctuates by approximately 10% between the office, bedroom and kitchen.

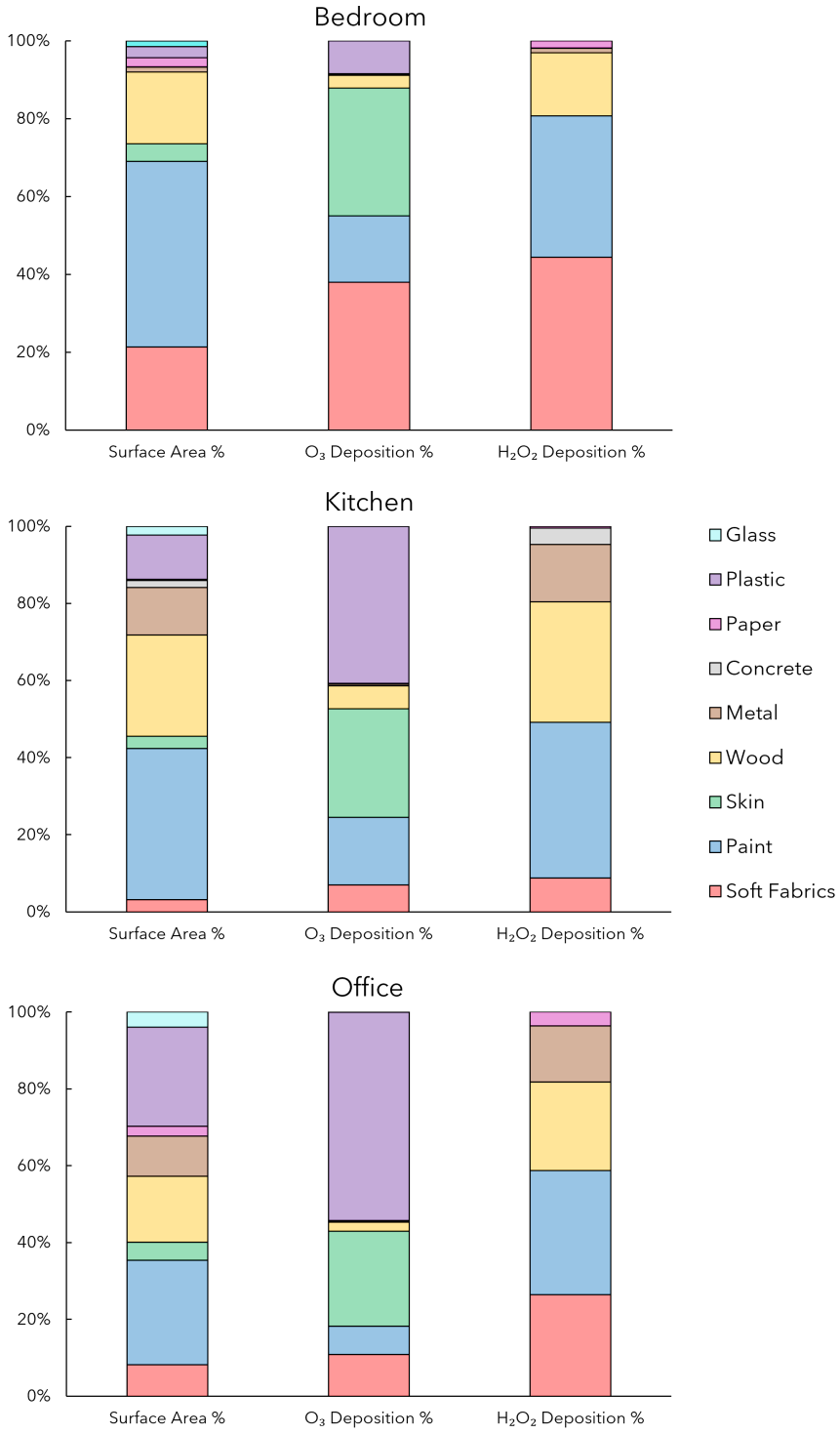

Figure 4.4: The percentage distribution of ozone and hydrogen peroxide deposition by surface for the studied rooms. The surface area of each material as a percentage of the total in each room are also included.

Figure 4.4 shows that indoor hydrogen peroxide deposition shows some similarities to ozone deposition. Soft fabrics are the most important material in the bedroom, accounting for 44% of the hydrogen peroxide deposition. However, unlike with ozone, hydrogen peroxide deposits predominantly onto painted surfaces in the kitchen (40%) and the office (32%). There are no data for hydrogen peroxide deposition onto plastic, glass and skin surfaces. Metallic surfaces have a larger proportion of hydrogen peroxide uptake than ozone in the kitchen and office, contributing to 15% of hydrogen peroxide uptake in both rooms. In absolute terms, the rates at which hydrogen peroxide deposits onto indoor surfaces are lower than for ozone, primarily due to the low indoor hydrogen peroxide concentration (averaged at 0.06 ppb over the three rooms). For hydrogen peroxide, the deposition rates are more closely aligned to the individual surface areas than ozone, given the deposition velocities vary over a smaller range than for ozone.

The average concentrations of key indoor species during the day (7am - 7pm) are reported in Table 4.8, for scenarios with no deposition (baseline) and then also assuming empty or occupied (two people in the bedroom, one in the kitchen, three in the office) rooms. The occupied and unoccupied simulations include deposition for both ozone and hydrogen peroxide.

These modelled concentrations can be compared to experimental studies which measured indoor aldehyde species. Uchiyama et al. (2015) reported concentrations of 0.16 ppb, 0.25 ppb, 1.4 ppb and 0.40 ppb for heptanal, octanal, nonanal and decanal respectively in Japanese homes. These measurement studies were carried out in various homes, each containing different materials and hence surface properties. The results (see Table 4.8) are comparable to these measured values, although the simulated heptanal concentrations are slightly lower than measured.

Indoor formaldehyde (19.2 ppb) and acetaldehyde (10.8 ppb) measurements from Uchiyama et al. (2015) however, were much higher than our results (factor of >24 and >11 higher respectively), although these are more likely to be influenced by human activities (such as cooking, cleaning and smoking) that we don't consider here. Indoor concentrations of these species have also likely decreased over time, as there is now more

Table 4.8: The average indoor concentration for a range of species in a bedroom, kitchen and office during the day, whilst the lights are on (7am to 7pm). The units for the concentration of OH are molecule cm^{-3}, the units for the concentration of HO_2 and RO_2 are ppt and the units for the rest of the species are given in ppb.

	Baseline			**Unoccupied**			**Occupied**		
Species	**Bedroom**	**Kitchen**	**Office**	**Bedroom**	**Kitchen**	**Office**	**Bedroom**	**Kitchen**	**Office**
OH	$1.1x10^6$	$1.2x10^6$	$9.9x10^5$	$8.9x10^5$	$9.7x10^5$	$8.6x10^5$	$7.4x10^5$	$9.0x10^5$	$6.1x10^5$
HO_2	3.6	3.7	3.5	1.0	1.2	0.80	1.3	1.3	1.2
RO_2	5.8	5.7	5.9	1.6	1.9	1.2	1.7	1.9	1.5
O_3	26.6	27.0	26.1	2.5	3.5	1.5	1.8	2.7	1.2
NO	0.40	0.44	0.36	2.1	1.9	2.5	2.2	2.1	2.4
NO_2	0.76	0.88	0.65	0.59	0.70	0.45	0.55	0.66	0.44
Formaldehyde	0.38	0.45	0.31	0.62	0.79	0.47	0.63	0.77	0.53
Acetaldehyde	0.47	0.54	0.41	0.68	0.92	0.58	0.61	0.82	0.53
Propanal	0.13	0.15	0.12	0.25	0.33	0.18	0.21	0.28	0.16
Butanal	< 0.01	< 0.01	< 0.01	0.11	0.19	0.09	0.08	0.15	0.07
Pentanal	0.03	0.03	0.03	0.13	0.18	0.10	0.10	0.14	0.08
Hexanal	0.03	0.04	0.03	0.19	0.17	0.11	0.14	0.14	0.09
Heptanal	0.02	0.03	0.02	0.07	0.06	0.06	0.05	0.05	0.05
Octanal	0.08	0.08	0.08	0.24	0.21	0.22	0.20	0.18	0.20
Nonanal	0.47	0.46	0.48	2.0	1.7	1.6	1.8	1.6	1.5
Decanal	0.13	0.13	0.13	0.66	0.73	0.73	0.75	0.77	0.82
4-OPA	< 0.01	< 0.01	< 0.01	< 0.01	< 0.01	< 0.01	0.08	0.08	0.06

awareness of the potential harm related to formaldehyde emissions from materials and furnishings (Ruiz-Jimenez et al., 2022).

4.3.2 Secondary Pollutants from Surface Interactions

Following oxidant deposition onto indoor surfaces in an occupied office, there was an increase in secondary pollutants, particularly in straight-chained aldehyde species compared to simulations with no deposition (Figure 4.5). Following ozone deposition, nonanal had the highest concentration (1.52 ppb), where emissions from plastic surfaces contributed the most. The concentration of decanal increased by ≈500% following ozone deposition onto surfaces. However, the percentage change in most aldehyde concentrations following hydrogen peroxide deposition was negligible and some concentrations even decreased slightly (≈–0.5% change from the baseline).

Surface deposition gives rise to numerous secondary pollutants, some of which are harmful to health. Carslaw and Shaw (2019) defined a metric for comparing the potential health impacts of the secondary pollutants that arose under different indoor conditions,

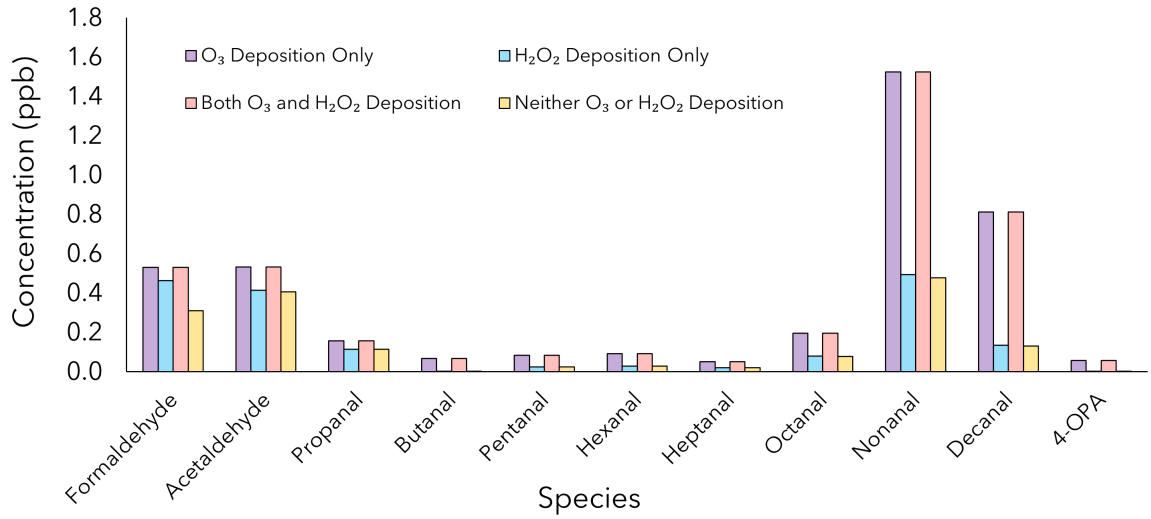

Figure 4.5: The concentrations of straight-chained aldehyde species and 4-oxopentanal (4-OPA) in an office with and without oxidant deposition onto surfaces.

using the so-called 'Secondary Product Creation Potential (SPCP)'. This metric has been adapted to consider the different model simulations here and is defined in Equation 4.5 as:

$$SPCP_{\text{mod}} = \Sigma \left(\begin{array}{l} [Total\ Organic\ Nitrates] + [PANs] + [O_3] + \\ [Glyoxal] + [Formaldehyde] + [Acetaldehyde] + \\ [Propanal] + [Butanal] + [Pentanal] + [Hexanal] + \\ [Heptanal] + [Octanal] + [Nonanal] + [Decanal] \end{array} \right) \tag{4.5}$$

SPCP_{mod} therefore provides the sum of the concentrations of potentially harmful pollutants that are formed under different model scenarios with units of ppb. This metric is a guideline value only, as we currently lack information on the health effects of some of these species and they are unlikely to exert an equal influence on human health. However, it does provide a guide to the harmful concentrations that could be attained indoors under different conditions.

For the three modelled rooms (with both ozone and hydrogen peroxide deposition included), the SPCP_{mod} values were 5.8, 6.7 and 4.8 ppb for the bedroom, kitchen and the office respectively, averaged over a full day. The concentrations of hexanal, octanal and nonanal were found to be highest in the bedroom (0.12 ppb, 0.19 ppb and 1.72 ppb),

whereas the concentration of decanal was found to be highest in the office (0.77 ppb). There were assumed to be three people present in the office, giving skin a higher surface to volume ratio (Weschler et al., 2007) than the other rooms, resulting in a higher decanal concentration. The rest of the species present in Equation 4.5 were found to have the highest concentrations in the kitchen.

4.3.3 Monitoring Individual Exposure to Indoor Air Pollution

Using our results, we have considered a typical day spent indoors, to determine the exposure to specific indoor air pollutants that might be experienced (Figure 4.6). We assumed that, on a typical day, a person will spend from: 00:00 - 07:00 h in the bedroom, 07:00 - 08:00 in the kitchen, 08:00 - 08:30 h outdoors (walking to the office), 08:30 - 12:00 h in the office, 12:00 - 13:00 h outdoors (lunch break outside), 13:00 - 17:00 h in the office, 17:00 - 17:30 h walking home outdoors, 17:30 - 19:00 h in the kitchen, 19:00 - 22:00 h in the living room, then the rest of the day in the bedroom. It was assumed there were no high concentration activities such as cooking and cleaning. We assumed that the bedroom was a proxy for the living area given we did not study this particular micro-environment, but it is likely to be dominated by similar soft furnishings.

The concentrations of key indoor radical species varied throughout the day, depending on time and location. The highest concentrations for pollutants tend to correspond with time spent outdoors, given that many of them are predominantly generated outdoors under our simulated conditions (no cooking or cleaning). The highest indoor concentration of OH was 1.1 x 10^6 molecule cm^{-3} at 7:58 am in the kitchen. The OH concentration is driven by the reaction of NO with HO_2. NO concentrations are higher in the morning as it is generated by rush-hour traffic from outdoors, which will ingress inside.

Our results show that of our total pollutant exposure over the course of the day, 60% of OH, 81% of HO_2, 32% of O_3 and 77% of NO_x exposure happens indoors. The highest exposure to OH (32%) and NO_x (43%) is found in the office, whereas the highest exposure to HO_2 (53%) is found in the bedroom and living room, primarily due to the duration of time spent in these rooms over the course of a day. The total pollutant exposure (%)

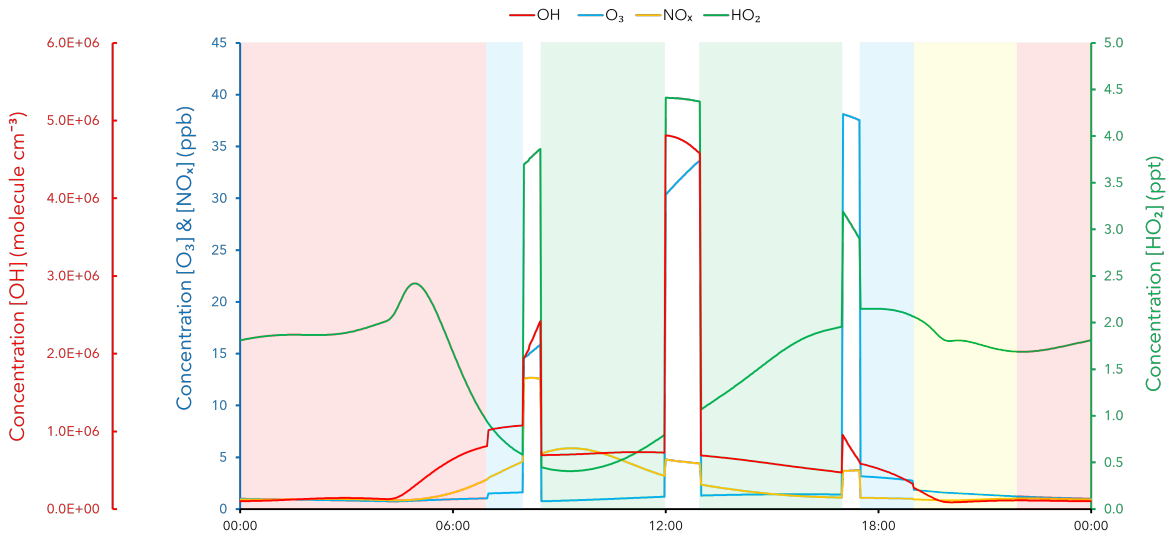

Figure 4.6: The concentrations of OH (molecule cm^{-3}), HO_2 (ppt), O_3 and NO_x (ppb) a person may be exposed to throughout the course of a typical day. The red shading on the graph indicates time spent in the bedroom, blue indicates time spent in the kitchen, green indicates time spent in the office, white indicates time spent outdoors and yellow indicates time spent in the living room.

experienced in each micro-environment over the course of the day is given in Table 4.9.

Table 4.9: The total pollutant exposure (%) experienced in different micro-environments over the course of a day. This is assuming a person spends 9 hours in the bedroom, 2.5 hours in the kitchen, 7.5 hours in the office, 2 hours outdoors and 3 hours in the living room.

	Pollutant Exposure (%)			
Location	**OH**	**HO_2**	**O_3**	**NO_x**
Bedroom/Living Room	16	53	15	23
Kitchen	12	9	7	10
Office	32	19	10	43
Outdoors	40	19	68	23

4.3.4 Surfaces for the Future

INCHEM-Py has been used to explore whether replacing individual surfaces can improve the indoor air quality. This is important as we consider more eco-friendly and sustainable materials to replace older, less environmentally beneficial surfaces in the future. In the bedroom and kitchen in this study, wooden surfaces drive emission rates of shorter-chained aldehyde species (C_1-C_5) following oxidant deposition, with soft fabric and plastic surfaces accounting for increased concentrations of longer-chained aldehyde species

(C_6-C_{10}). Concrete surfaces had the lowest rate of production for the majority of the straight-chain aldehydes, primarily due to their low surface-to-volume ratio. Occupants produced increases in the concentrations of decanal and 4-oxopentanal (4-OPA), both products of skin lipid ozonolysis (Weschler, 2016), which could be important for spaces which contain large groups of people.

We ran model simulations, replacing wooden surfaces in the bedroom and the kitchen with concrete surfaces to determine the impact on indoor air chemistry. In addition, the plastic surfaces in the office were replaced with concrete surfaces. The percentage difference of the concentration of straight-chained aldehydes and key indoor species were then calculated. When wooden materials are replaced by concrete equivalents in the bedroom and the kitchen respectively, most concentrations decreased: formaldehyde (by –14% and –24%), acetaldehyde (–19% and –28%), propanal (–30% and –45%), butanal (–76% and –81%), pentanal (–45% and –59%) and hexanal (–22% and –46%). Heptanal, octanal, nonanal and decanal concentrations all increased, but by minimal amounts (≈1%). This material replacement produced little change in radical concentrations in the bedroom and the kitchen.

In the office, where plastic was replaced by concrete, the concentration of short-chained aldehydes formaldehyde and propanal increased by 6% and 28% respectively, whereas octanal and decanal concentrations decreased by 19% and 10% respectively. However, the concentrations of HO_2 and RO_2 both increased by ≈37%, indicating a wider perturbation to the indoor chemistry. The concentration of ozone nearly doubled under these conditions, owing to the lower ozone deposition velocity of concrete, therefore, ozone will have a higher ambient indoor concentration if plastic is replaced by concrete. Although it may not be the most visually appealing, concrete surfaces contribute less to indoor air pollution than plastic or wooden surfaces and could improve indoor air quality.

4.4 Conclusions

This chapter evaluates how indoor surfaces react with oxidants to impact indoor air quality in a kitchen and bedroom in a home environment and an office in a work environment. The model results demonstrated that the importance of individual surfaces varied between different rooms. The dominant surfaces were those with the largest deposition velocities and/or surface areas. Large unreactive surfaces and small reactive surfaces had minimal impact on modelled concentrations. Further experiments focussing on surface deposition of a wider range of oxidants and the respective production yields for emitted species and for a range of surfaces, would be highly beneficial.

This chapter has evaluated the exposure of indoor air pollution for a person over the course of a day and the formation of potentially harmful pollutants. It was determined that whilst indoors, OH concentration during the day was highest in the kitchen, whereas the HO_2 concentration was highest early in the morning, in the bedroom. A modified value of the Secondary Product Creation Potential ($SPCP_{mod}$) was highest in the kitchen and lowest in the office, indicating greater total exposure to potentially harmful air pollutants in the kitchen than the bedroom and the office. However, in order to make these assessments more accurate, there needs to be more detailed information on the relative health impacts of the different species that have been studied. This would help us to better understand how changing surfaces impact on health, as changing a surface will inevitably increase some concentrations, but reduce others.

Chapter 5

The Role of Indoor Activities in Urban Environments

Material from this chapter has been published in Carter et al. (2024). The ADMS data was provided by Professor David Carslaw, but analysed and utilised accordingly by myself. Figure 5.1 was designed by me and invited to be the inside front cover for the June 2024 edition of the journal Environmental Science: Processes and Impacts.

Figure 5.1: A graphic which shows the possible release of cooking and cleaning pollution from homes in an urban community.

5.1 Introduction

Air pollution exposure is classified as the fourth most important global risk factor for human health (Juginović et al., 2021; Rafaj et al., 2018), with the World Health Organisation (WHO) attributing 6.7 million deaths per year to poor outdoor and indoor air quality (World Health Organisation, 2023). The WHO noted that household air pollution caused approximately 3.2 million of these annual deaths (World Health Organisation, 2023), with most of these occurring in lower income countries.

The public are becoming more aware of the health effects of air pollution, especially since the COVID-19 pandemic, which has also increased media interest in the topic. Consequently, there is heightened awareness that healthy indoor environments are important, particularly given we spend approximately 90% of our time indoors in high income countries like the UK (Klepeis et al., 2001), and where we receive most of our exposure to air pollution (Goldstein et al., 2021).

Household activities such as cooking and cleaning contribute to indoor air pollution. Cooking can emit primary pollutants including particulate matter (ultrafine and fine), nitrogen oxides and a variety of volatile organic compounds (VOCs) (Sankhyan et al., 2022; Tang and Pfrang, 2023; Kang et al., 2019; Seaman et al., 2009; Klein et al., 2019; Bekö et al., 2013; Wang et al., 2020a). The inhalation of particulate matter (PM) especially, has been found to affect our cardiovascular system: the risks can be accentuated through prolonged exposure (Nelin et al., 2012), such as might be the case when in close proximity during the preparation of a meal, or for those working in a commercial kitchen.

Secondary pollutants can be formed indoors mainly from the gas-phase reaction of VOCs with indoor oxidants, including ozone (O_3) and hydroxyl (OH) and nitrate radicals (NO_3) (Weschler and Carslaw, 2018; Waring and Wells, 2015; Carslaw, 2013; Rosales et al., 2022; Carslaw and Shaw, 2022; Chen et al., 2021; Kruza et al., 2021). These secondary chemicals can be more harmful to human health than the primary species themselves (Wolkoff et al., 2000; Wolkoff, 2020).

Different cooking methods including roasting, frying and grilling, all with varying chemi-

cal signatures: heating methods (e.g. gas versus electric) and food types also affect emissions (Arata et al., 2021; Ahn et al., 2014; Abdullahi et al., 2013). Cooking oils and spices have chemical fingerprints which can often pinpoint what type of meal is being prepared (Zhang et al., 2019; Abdullahi et al., 2013; Chen et al., 2018; Kim et al., 2011). For example, Davies et al. (2023) attributed garlic, ginger and chilli preparation to emissions of monoterpene species, whereas increases in concentrations of eucalyptol and sesquiterpenes were observed when these spices were cooked. The same study found that alcohol mixing ratios (mostly methanol) exceeded 1500 ppb, alkane mixing ratios (mostly nonane) were approximately 170 ppb and acetaldehyde mixing ratios exceeded 70 ppb during the cooking of a chicken stir fry (Davies et al., 2023). These experiments were conducted in a $\approx 4.3 \times 2.2 \times 2.3$ m space in a shipping container, where the air change rate was 0.77 h^{-1}.

Long, straight-chain alkanes are often produced from heating oils, including octane and nonane, which are produced from rapeseed oil (Davies et al., 2023). The corresponding aldehydes, octanal and nonanal, are also frequently produced from cooking fats and oils (Schauer et al., 1999; Klein et al., 2016). These long-chained aldehydes are currently relatively understudied in both indoor and outdoor air. Wernis et al. (2022) reported that nonanal had a mean concentration (from hourly measurements taken over the course of a month) of 150 ppt in suburban Livermore (California, USA). Indoor cooking from a commercial restaurant was identified as the likely source.

Cleaning is also a major contributor to indoor air pollution. Semi-volatile organic compounds (SVOCs) and VOCs, including aromatics, alkanes and monoterpenoids are emitted from cleaning products (Calderon et al., 2022; Nazaroff and Weschler, 2004; Zhou et al., 2020; Odabasi, 2008; Harding-Smith et al., 2024), some of which are known to be detrimental to human health (Dodson et al., 2012; Alford and Kumar, 2021; Shuai et al., 2018). Chlorinated species are also produced from cleaning, potentially increasing the risk of an asthma attack (Medina-Ramón et al., 2005; Archangelidi et al., 2021) and other adverse health-effects (Hoyle and Svendsen, 2016; Weill et al., 1969). Calderon et al. (2022) discovered that gas-phase concentrations of chloroform were 1131% higher

in indoor breathing zones than ambient indoor concentrations when bleach cleaning products were used. Chloroform is a suspected carcinogen and can affect the central nervous system (Health Protection Agency, 2007). During an occupational study, office workers were exposed to mixing ratios of between 14 and 400 ppm of chloroform. The health effects were reported to be jaundice, nausea, vomiting and toxic hepatitis (Health Protection Agency, 2007; Bingham et al., 2001; Agency for Toxic Substances and Disease Registry (ATSDR), 1997).

One of the most prominent sources of indoor pollution is from the outdoor environment (Leung, 2015; Shrestha et al., 2019). Outdoor air pollution can ingress into indoor spaces including homes and offices via windows and doors, but also through mechanical ventilation, which is now increasingly employed in the modern construction of new buildings (Link et al., 2023a). In more leaky buildings, this pollutant transport is accentuated (Vu et al., 2022). However, indoor air pollutants can also move outdoors. The impact of indoor air pollutants on outdoor air quality has started to receive attention only recently, with a number of studies identifying enhancements of outdoor species concentrations from emissions that had originated from indoor environments (McDonald et al., 2018; Borbon et al., 2023; Gkatzelis et al., 2021). However, the details of how these indoor emissions impact the outdoor ambient atmosphere remains largely unexplored. These household emissions could have a significant impact in urban areas, particularly those with densely packed housing and at times when many homes are emitting pollutants, for example, when cooking.

One example of indoor activities having an impact on outdoor air quality is wood stove use, particularly when numerous stoves are burning in a relatively small area, or in a valley during temperature inversions. This type of situation may lead to high local concentrations of $PM_{2.5}$. For instance, $PM_{2.5}$ concentrations up to 48.0 ±27.7 μg m^{-3} were recorded in a mountainous hollow in Slovenia (Glojek et al., 2022), similar to $PM_{2.5}$ concentrations found in more densely populated urban locations across Europe (Glojek et al., 2022). During wood stove use, emissions are transported to the outdoor environment through distinct plumes with high concentration gradients, compared to cooking

and cleaning emissions which will diffuse through indoor-outdoor exchange at various points in a building.

McDonald et al. (2018) found that volatile chemical products (VCPs) used indoors, were responsible for 39-62% of measured outdoor petrochemical VOCs, compared to only 15 to 42% from transportation. Cleaning materials are one of the six main VCP categories, however cooking pollutants could potentially have a similar effect (Sheu et al., 2021; Mattila et al., 2022; Eftekhari et al., 2021), as they are released outdoors via windows and cooking hoods. This chapter aims to identify the VOCs that are emitted when cooking and cleaning activities occur indoors, and to evaluate the potential impact of these indicator species on outdoor air quality. In this way, we can start to understand how indoor activities may impact the ambient atmosphere. The developed model has then been used to investigate the following objectives:

• Evaluate indoor air pollutant concentrations following cooking and cleaning.

• Determine the near-field concentrations of atmospheric species and rate of transport between the indoor and outdoor environments.

• Analyse the potential impact on the outdoor air quality of a suburban community as a result of indoor cooking and cleaning emissions.

• Consider how these findings contribute to total VOC emissions in the United Kingdom.

5.2 Methods

5.2.1 Addition of Primary Surface Emissions

The initial development to INCHEM-Py (v1.2 (Shaw et al., 2023)) was the addition of primary emissions from common indoor materials. Wood and paint are commonly found in homes, and are known to emit indoor air pollutants, primarily short and long-chained aldehydes (Alapieti et al., 2021; Gallon et al., 2020; Missia et al., 2010; Plaisance et al., 2017; Yrieix et al., 2010; Cheng et al., 2015; Harb et al., 2018; Simon et al., 2020; Kim, 2010;

Lin et al., 2009; Nicolle et al., 2009). New furniture often produces higher emissions of these species, which tend to decrease as it ages (Plaisance et al., 2017; Alapieti et al., 2021). Published emission rates from wood and paint for formaldehyde, acetaldehyde, propanal, butanal, pentanal, hexanal, heptanal, octanal, nonanal and decanal (Plaisance et al., 2017; Alapieti et al., 2021; Cheng et al., 2015) have been averaged and added into the model informed by the surface-area to volume ratio of wooden and painted materials in a typical kitchen (Manuja et al., 2019; Carter et al., 2023; Davies et al., 2023), and are provided in Table 5.1.

Table 5.1: The background primary emission rates of species from indoor wooden and painted surfaces in a kitchen (Plaisance et al., 2017; Alapieti et al., 2021; Cheng et al., 2015).

Species	**Emission Rate (molecule cm^{-3} s^{-1})**
Formaldehyde	1.7×10^8
Acetaldehyde	9.6×10^7
Propanal	4.1×10^7
Butanal	5.0×10^7
Pentanal	4.1×10^7
Hexanal	1.1×10^8
Heptanal	5.2×10^6
Octanal	4.8×10^6
Nonanal	8.5×10^6
Decanal	4.5×10^6

These aldehyde emission rates are assumed to remain constant throughout the simulation. Surface-specific oxidant deposition initiated emissions are also present in the model for ozone and hydrogen peroxide, as outlined in Carter et al. (2023) and Shaw et al. (2023).

5.2.2 Near-Field Concentration Development

For this work, we have added a near-field gas-phase concentration, ($C_{\mathrm{i,nf}}$) (molecule cm^{-3}), for 107 species (Table A.3 in the Appendix) to INCHEM-Py, which represents the concentration of a species, i, as it moves from indoors to outdoors. This enables the

concentration of an indoor air pollutant to be tracked as it leaves a building. $C_{\mathrm{i,nf}}$ is determined by the balance between formation and loss mechanisms, as shown in Equation 5.1. The formation of the near-field species is effectively determined by the exit rate of a species from indoors, the product of its indoor concentration (C_{i}), and the air change rate (λ_r). The loss rate is dependent on both chemical and physical losses. Chemical losses happen via photolysis and also by reactions with the hydroxyl radical (OH) and ozone (O_3), whilst we assume physical loss is driven by the rates of dispersion (k_{disp}) and outdoor deposition ($d_{i,out}$).

$$\frac{dC_{i,nf}}{dt} = \lambda_r C_i - k_{chem} C_{i,nf} - k_{disp} C_{i,nf} - d_{i,out} \tag{5.1}$$

The chemical loss rate for the near-field species as they move outdoors is calculated offline, based on the rate coefficients in the MCM (Jenkin et al., 1997) and assuming realistic outdoor concentrations of the oxidants (Table 3.4). For loss via photolysis once the species pass outdoors, the outdoor photolysis rates are calculated in INCHEM-Py, but without applying an attenuation factor as we would to calculate indoor photolysis rates. Note that we are only interested in the near-field concentration changes, not the impact on outdoor air pollutant concentrations.

The dilution rate due to dispersion was calculated using the Advanced Dispersion Modelling System (ADMS) (McHugh et al., 1997). ADMS is used to simulate the dispersion of air pollutant emissions from sources such as roads, chimney stacks and buildings (CERC, 2023). The ADMS simulation assumed a typical house-sized building (10m x 10m x 5m, represented as a volume source) and used meteorological conditions based on hourly data from London Heathrow in 2019. ADMS predicts the concentration of an air pollutant as a function of distance from the building, hence providing a rate of dispersion (McHugh et al., 1997). In this case, the unit emission of a non-reactive tracer was used, which provides the basis of dispersion for the other VOCs in the model. The fall-off in concentration was calculated from the eastern edge of the building extending in a west-east direction out to 200 m from the building facade i.e. approximately downwind of the prevailing wind direction (Table 5.2). The chosen distance from the ADMS output was 95

m because we explored street lengths varying between 100 and 140 m.

Table 5.2: The resultant grid from the ADMS output. The relative concentration and time columns have been added to the grid. The chosen distance was 95 m from which the loss rate was calculated in Equations 5.2 and 5.3 below.

X (m)	Y (m)	Z (m)	Dist. from House (m)	Dist. (cm)	SO_2 ($\mu g\, m^{-3}$) Concentration	Relative Concentration	Time (s)
6	0	2	1	100	160.98	1.000	0.5
10	0	2	5	500	126.49	0.786	2.5
15	0	2	10	1000	110.50	0.686	5
20	0	2	15	1500	102.73	0.638	7.5
30	0	2	25	2500	94.82	0.589	12.5
50	0	2	45	4500	88.25	0.548	22.5
100	0	2	95	9500	83.49	0.519	47.5
200	0	2	195	19500	81.55	0.507	97.5

A loss rate of 1.09 x 10^{-2} s^{-1} was calculated and used in the near-field framework (Equations 5.2 and 5.3). This value was used as a dilution factor for the near-field concentration. The time point of 47.5 s was used to calculate the dilution factor because this was the time taken to travel a distance of 95 m with a specific wind speed of 2 ms^{-1}. This was closest to our chosen street length (100-140 m) and represented a reasonable average loss rate for our ten-house analysis.

$$k = \frac{C_r}{t} \tag{5.2}$$

where k is the loss rate (s^{-1}), C_r is the relative concentration (no units) and t is time (s).

$$\frac{0.519}{47.5\ s} = 1.09 \times 10^{-2}\ s^{-1} \tag{5.3}$$

Physical loss owing to irreversible deposition is driven by the outdoor surface deposition velocities calculated for an average urban surface as described in Carslaw (2007) and assuming a constant boundary layer height (BLH) of 1000 m. The outdoor surface deposition velocities vary by species and the non-oxygenated VOCs are assumed not to undergo deposition (Shaw et al., 2023). The boundary layer height is assumed to be constant in our simulations and used only for the calculation of outdoor deposition rates. Emission

from the houses is the major controlling factor for the near-field concentrations under our simulated conditions.

5.2.3 Cooking & Cleaning Emission Rates

For typical cooking and cleaning emissions, the model has been informed by the HOME-Chem (The House Observations of Microbial and Environmental Chemistry) experimental field campaign performed in the University of Texas at Austin test-house facility in June 2018 (Farmer et al., 2019). The campaign focused on the impacts that human activities had on chemical transformations in the indoor environment, including the quantification of indoor air pollutant concentrations following various cooking (Reidy et al., 2023; Pothier et al., 2022), cleaning (Wang et al., 2022b; Mattila et al., 2020a; Ampollini et al., 2019), ventilation and human occupancy experiments (Aksenov et al., 2023; Arata et al., 2021; Zhou and Kahan, 2022).

For this work, we focused on the 25th June, which was considered a 'layered day'. A layered day attempts to replicate a standard day in the home, with three cooked meals and a solitary cleaning experiment (Farmer et al., 2019). During these experiments, the VOCs were measured using PTR-TOF-MS (Liu et al., 2021; Tang et al., 2016) and Iodide-CIMS (Brophy and Farmer, 2015) instruments. The emission rates for the detected VOCs emitted from the separate cooking and cleaning events were implemented into INCHEM-Py as timed emissions as provided in Table 5.3. These emission rates were back-calculated from concentration measurements.

Table 5.3: The emission rates (calculated from HOMEChem (Farmer et al., 2019)), in molecule cm^{-3} s^{-1}, inputted into INCHEM-Py for the breakfast, lunch, dinner and cleaning activities. The time over which these activites are applied is detailed in Section 5.2.4.

Species	**Breakfast**	**Lunch**	**Dinner**	**Cleaning**
Methane	-	6.9×10^{8}	2.0×10^{8}	-
Carbon Monoxide	1.9×10^{10}	2.8×10^{10}	1.6×10^{10}	-
Acetaldehyde	9.8×10^{6}	1.9×10^{7}	3.6×10^{7}	1.8×10^{8}
Acetone	-	-	-	1.8×10^{7}
α-Pinene	2.9×10^{6}	-	-	2.2×10^{5}
Benzene	7.2×10^{5}	5.8×10^{5}	3.8×10^{5}	1.8×10^{6}
β-Pinene	2.6×10^{6}	-	2.0×10^{6}	1.3×10^{7}
Chloroform	-	-	-	3.0×10^{6}
cis-But-2-ene	6.6×10^{4}	7.2×10^{4}	1.8×10^{4}	9.5×10^{4}
cis-Pent-2-ene	2.2×10^{4}	2.5×10^{4}	3.1×10^{4}	-
Ethane	2.9×10^{7}	4.6×10^{7}	2.4×10^{8}	-
Ethene	6.2×10^{7}	4.1×10^{7}	2.9×10^{7}	1.6×10^{8}
Ethylbenzene	1.2×10^{6}	-	-	1.3×10^{5}
Ethyne	3.3×10^{7}	3.9×10^{7}	7.8×10^{7}	3.8×10^{8}
Isoprene	1.5×10^{6}	1.6×10^{6}	3.8×10^{6}	1.8×10^{7}
Isobutane	2.0×10^{7}	2.4×10^{7}	4.1×10^{8}	-
Isopentane	9.8×10^{5}	-	-	-
Limonene	8.3×10^{6}	-	2.9×10^{6}	1.5×10^{7}
Methyl Ethyl Ketone (MEK)	1.2×10^{6}	8.2×10^{5}	-	-
m-Xylene	5.2×10^{4}	-	8.8×10^{4}	6.7×10^{5}
p-Xylene	5.2×10^{4}	-	8.8×10^{4}	6.7×10^{5}
Butane	1.4×10^{7}	9.0×10^{6}	-	-
Decane	1.1×10^{5}	-	9.9×10^{4}	4.5×10^{5}
Heptane	1.8×10^{5}	-	1.4×10^{5}	6.8×10^{5}

continued on next page

Species	Breakfast	Lunch	Dinner	Cleaning
Hexane	1.4×10^{6}	1.9×10^{6}	-	-
Nonane	1.7×10^{6}	3.7×10^{4}	1.4×10^{5}	-
Octane	1.4×10^{5}	1.8×10^{5}	1.8×10^{4}	1.3×10^{5}
Pentane	1.1×10^{6}	1.1×10^{6}	2.1×10^{6}	1.0×10^{7}
Propane	3.4×10^{9}	3.7×10^{9}	-	-
Propene	5.9×10^{7}	3.9×10^{7}	2.9×10^{7}	1.4×10^{8}
Styrene	1.6×10^{5}	2.8×10^{5}	-	5.3×10^{5}
o-Xylene	1.6×10^{5}	2.8×10^{5}	-	5.3×10^{5}
trans-But-2-ene	5.3×10^{4}	6.6×10^{4}	1.9×10^{4}	1.1×10^{5}
But-1-ene	4.8×10^{5}	7.8×10^{5}	1.3×10^{6}	-
o-Ethyltoluene	2.8×10^{6}	-	1.5×10^{5}	7.5×10^{5}
2-Methylbut-1-ene	3.4×10^{4}	-	4.9×10^{3}	2.7×10^{4}
m-Ethyltoluene	5.6×10^{6}	-	-	-
p-Ethyltoluene	5.6×10^{6}	-	-	-
1,2,3-Trimethylbenzaldehyde	1.9×10^{6}	-	2.8×10^{6}	1.5×10^{7}
1,3,5-Trimethylbenzaldehyde	1.4×10^{5}	2.4×10^{6}	9.9×10^{4}	4.7×10^{5}
Chloroformic Acid	-	-	-	3.0×10^{6}
Nitryl Chloride	-	-	-	1.8×10^{8}
Chlorine (Cl_2)	-	-	-	6.7×10^{8}
Hypochlorous Acid	-	-	-	5.7×10^{8}

5.2.4 Model Simulations and Assumptions

5.2.4.1 Layered Day Analysis Simulation

The model was parameterised to replicate a house situated in suburban London (latitude of 51.45 °N) in the United Kingdom. The temperature, relative humidity and air change rate of the property was assumed to be 19.9 °C, 53.8 % (Ministry of Housing & Communities & Local Government (UK Government), 2019) and 0.5 hr^{-1} (Nazaroff, 2021), as outlined in Carter et al. (2023). The date of the simulation was the 21st June 2023, the most

photochemically active day. The date and latitude used in the model determine the solar zenith angle used to calculate outdoor photolysis rates, which are then attenuated depending on glass type to calculate indoor photolysis rates (Shaw et al., 2023; Wang et al., 2022b).

The window panel was assumed to consist of glass with a transmission range of between 315 to 800 nm (Glass C in Blocquet et al. (2018)). The outdoor concentrations for O_3, nitric oxide (NO) and nitrogen dioxide (NO_2) are based on measurements made at a monitoring station ('GB0586A, suburban London, 0.070766 51.45258') in suburban London (EEA, 2018), and follow a diurnal profile in the model. The OH outdoor mixing ratios are also diurnal. Outdoor OH has negligible impact on indoor concentrations due to the short lifetime of the OH radical. Full diurnal profiles of these species are described in Shaw et al. (2023). Diurnal profiles for outdoor O_3, NO and NO_2 are also given in Figure 5.3. The outdoor VOC concentrations are set as described in Shaw et al. (2023) and the outdoor concentration of carbon monoxide is assumed to be 195 ppb (EEA, 2018). The outdoor VOC concentrations are averages based on available literature and are given in Table 3.4.

Based on the HOMEChem emission rates (Table 5.3), a standard day spent in the home has been simulated. A full-English breakfast (fried sausages, eggs and tomatoes) is cooked at 7:30am (till 7:46am), a vegetable stir-fry lunch at 12 noon (till 12:29pm) and a chilli con-carne dinner at 6pm (till 7:02pm). A chlorine-based cleaning activity occurred after lunch at 2:00pm (till 2:13pm). It should be noted that a pilot light on the stove emitted high levels of propane during the cooking periods in the HOMEChem study (Farmer et al., 2019), from a possible fuel leak.

The simulations take place in a kitchen, with a total surface area of 63.3 m^2 and an internal volume of 25.0 m^3. The overall surface area to volume ratio (SA/V) in the kitchen is 2.53 m^{-1} based on the measurements from Manuja et al. (2019) and calculations from Carter et al. (2023). The surface area to volume ratios for soft fabric, paint, skin, wood, metal, concrete, paper, plastic and glass are defined in Carter et al. (2023) for the simulated kitchen. It is assumed that one adult (2 m^2 of skin) is present in the kitchen. We

have included emission rates from breath according to Kruza and Carslaw (2019) and Weschler et al. (2007).

5.2.4.2 Ten-House Analysis Simulations

The ten-houses analysis assumes ten houses, 5 m apart, to replicate a typical detached row of houses. These ten houses were randomly assigned different air change rates, numbers of inhabitants and cooking and cleaning times. These parameters were varied to understand how different aspects of daily life affected key pollutant concentrations. Each house had a unique parameter set in order to compare and contrast pollutant variation between houses. A ten-house ensemble provides a reasonable representation of the variation in day-to-day lifestyles and routines, providing an opportunity to vary air exchange rates, surfaces, meal times and occupancy to cover a range of scenarios, balanced against model complexity and runtime. The street length was 140 m and each house was assumed to be 10m x 10m x 5m. The conditions and input parameters for each house are described in Table 5.4. The temperature, relative humidity, latitude, date, surface-specific surface area-to-volume ratios (except for human surfaces) (Manuja et al., 2019) and glass type are the same as for the layered day simulation (described in Section 5.2.4.1). The surface-specific surface area-to-volume ratios for the simulated kitchen is based on measurements by Manuja et al. (2019) who measured nine representative kitchens in the United States. The air change rate distributions are based on Nazaroff (2021). Where indoor artificial lighting is present (lights on), LED lighting was used (Wang et al., 2022b). A wind speed of 2 ms^{-1} along the street is assumed, with the pollution assumed to be emitted from the centre of each house. The wind is assumed to blow along the length of the row of houses, as demonstrated by the schematic in Figure 5.2.

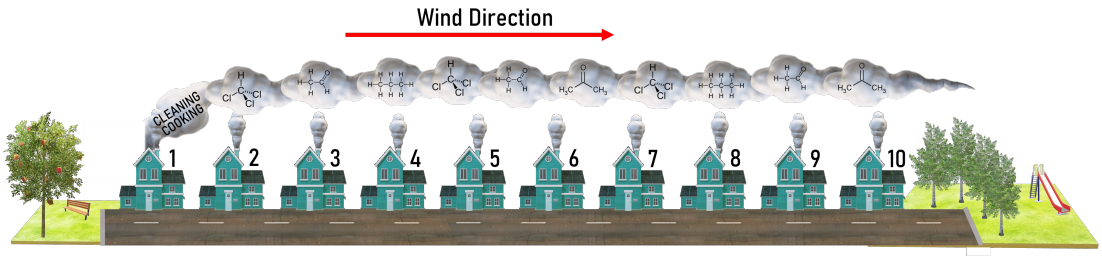

Figure 5.2: A schematic of the ten-house analysis replicating a typical row of detached houses. The airflow is assumed to be along the length of the street.

Table 5.4: The simulation conditions for the ten-house analysis.

Parameter	House 1	House 2	House 3	House 4	House 5
ACR (hr^{-1})	0.5	0.2	2.0	1.5	0.2
Lights On	7am	7am	7am	7am	No Lights
Lights Off	7pm	7pm	7pm	7pm	No Lights
AV (cm^{-1})	0.0269	0.0253	0.0253	0.0253	0.0245
Human AV (cm^{-1})	0.0024	0.0008	0.0008	0.0008	0
Adults	2	1	1	1	0
Children	2	0	0	0	0
Breakfast (Time of Day)	7:30-7:46	No	7:30-7:46	7:30-7:46	No
Lunch (Time of Day)	12:00-12:29	12:00-12:29	No	12:00-12:29	No
Dinner (Time of Day)	18:00-19:02	18:00-19:02	18:00-19:02	No	No
Cleaning (Time of Day)	14:00-14:13	14:00-14:13	14:00-14:13	14:00-14:13	No
Parameter	House 6	House 7	House 8	House 9	House 10
ACR (hr^{-1})	0.5	1.2	0.7	0.5	1.0
Lights On	7am	7am	7am	7am	7am
Lights Off	7pm	7pm	7pm	7pm	7pm
AV (cm^{-1})	0.0253	0.0253	0.0269	0.0257	0.0245
Human AV (cm^{-1})	0.0008	0.0008	0.0024	0.0012	0.0008
Adults	1	1	2	1	1
Children	0	0	2	1	0
Breakfast (Time of Day)	7:30-7:46	9:30-9:46	7:30-7:46	7:30-7:46	7:30-7:46
Lunch (Time of Day)	12:00-12:29	14:00-14:29	12:00-12:29	12:00-12:29	12:00-12:29
Dinner (Time of Day)	18:00-19:02	18:00-19:02	20:00-21:02	18:00-19:02	18:00-19:02
Cleaning 1 (Time of Day)	8:00-8:13	15:00-15:13	14:00-14:13	14:00-14:13	No
Cleaning 2 (Time of Day)	14:00-14:13	-	-	-	-
Cleaning 3 (Time of Day)	20:00-20:13	-	-	-	-

5.3 Results & Discussion

5.3.1 Simulated Indoor Air Pollutant Concentrations following Cooking & Cleaning

The diurnal profiles of key indoor species (OH, O_3, NO, NO_2, HO_2, RO_2 and CH_3CHO) following cooking and cleaning are shown in Figure 5.3. Cooking had a minimal effect on the OH concentration. The indoor OH concentration an hour before cleaning (1:00pm) was 2.8 x 10^5 molecule cm^{-3}. During the cleaning event however, OH reached a maximum concentration of 3.4 x 10^6 molecule cm^{-3} at 2:01pm, caused by photolytic degradation of hypochlorous acid (HOCl), producing both OH and chlorine radicals as shown in Reaction 5.4 (Remucal and Manley, 2016). One minute after cleaning ended (2:14 pm), the indoor concentration of the OH radical was 6.8 x 10^5 molecule cm^{-3}.

$$HOCl + h\nu \xrightarrow{\lambda < 400\ \text{nm}} OH + Cl \tag{5.4}$$

Figure 5.4 gives an expanded view of the concentrations during the cleaning event. Cleaning caused a ≈1200% increase in OH radical concentrations. OH then quickly returns to a background level, through consumption by indoor VOCs.

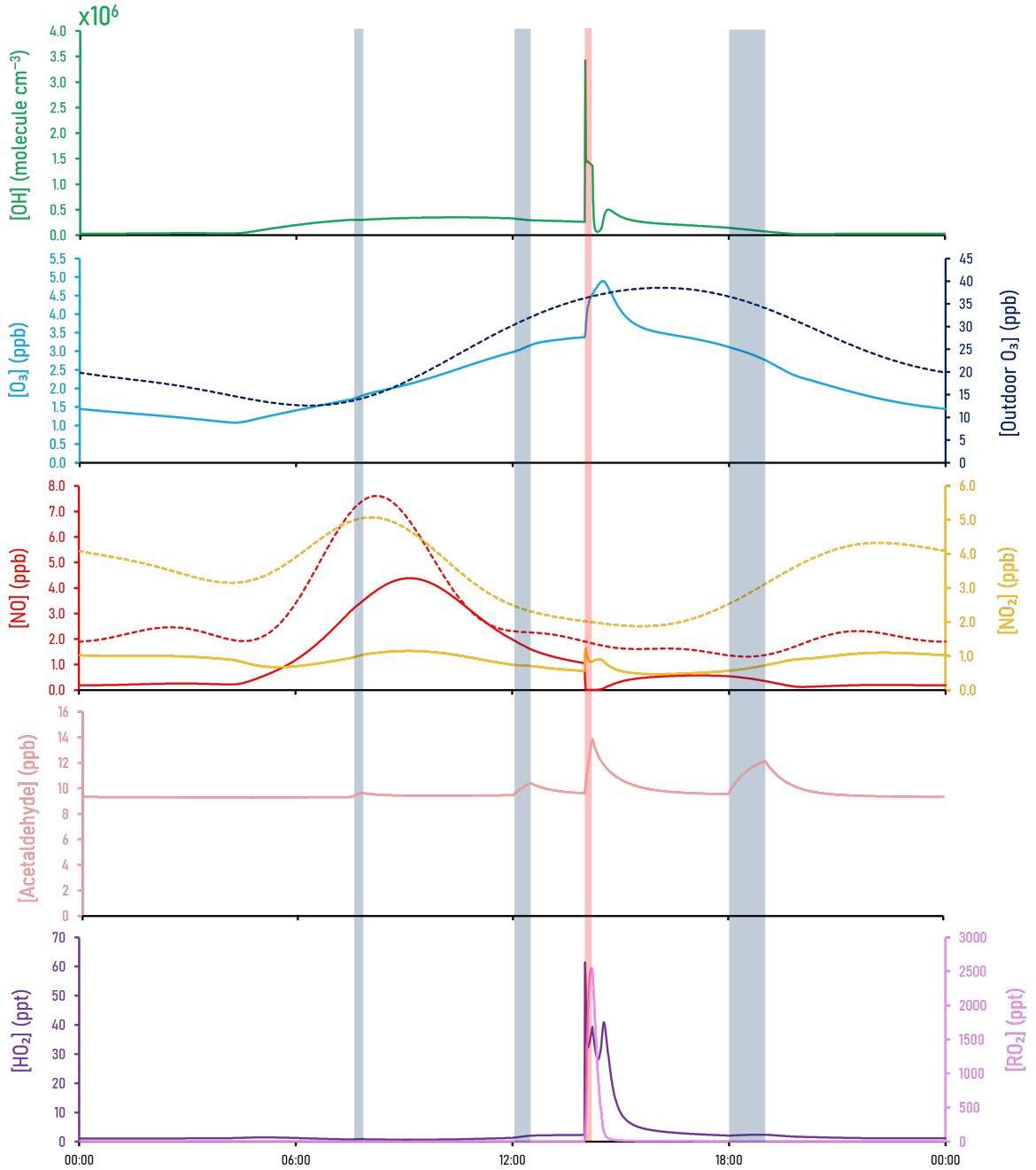

Figure 5.3: The concentrations of key indoor species in the kitchen over the duration of a typical day spent in the home. The grey shaded areas indicate periods of cooking, and the red shaded area indicates a chlorine cleaning period. The outdoor concentrations of NO (red), NO_2 (orange) and O_3 (dark blue) are shown as dashed lines on the graphs.

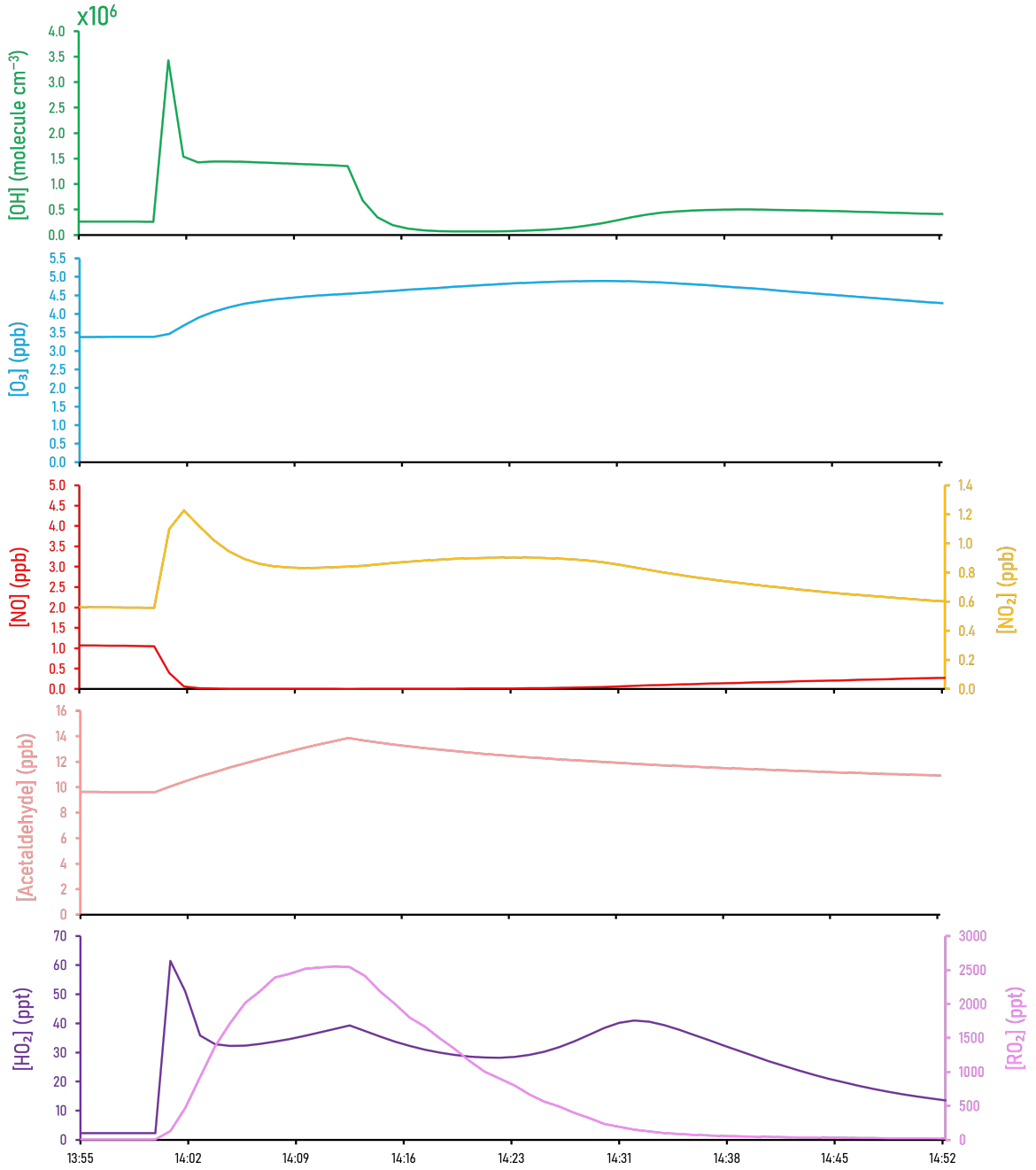

Figure 5.4: An expanded view of the concentrations of key indoor species during the 13-minute cleaning event (starting at 2pm).

Acetaldehyde concentrations were enhanced by approximately 1.02, 1.1 and 1.3 times during breakfast, lunch and dinner respectively, where the maximum acetaldehyde mixing ratios during these periods were 9.5, 10.4 and 12.1 ppb respectively, driven primarily by emissions from hot cooking oils. The background value was 9.3 ppb. Our cooking sim-

ulations didn't produce the acetaldehyde concentrations of 70 ppb reported by Davies et al. (2023) during a chicken stir-fry, indicating possible emission of acetaldehyde from the cooking of chicken. Acetaldehyde reaches a maximum mixing ratio of 13.9 ppb during the cleaning event, which is an enhancement of 1.5 times from the background value.

O_3 acts as a strong oxidant in the indoor environment, reacting with unsaturated VOCs produced by cooking and cleaning via ozonolysis reactions. The indoor diurnal profile of O_3 is also dictated by ingress from outdoors. During cleaning, the O_3 mixing ratio increased by 45% and reached a maximum mixing ratio of 4.9 ppb at 2:30pm.

At 9:10am, NO and NO_2 increase to 4.4 ppb and 1.1 ppb respectively (from 1.2 ppb and 0.7 ppb at 6am). These early morning peaks are caused by cooking but also from increased NO_x concentrations outdoors during rush-hour, creating an accumulation of NO_x indoors. Cleaning causes a change in the form of NO_x, where during the first two minutes, NO decreases (by 94%), as NO_2 concentration increases (by 120%). This change is partially caused by enhanced concentrations of HO_2 available to react with NO, to form OH and NO_2 (Reaction 5.5). Peroxy radical (RO_2) concentrations are also enhanced, reacting with NO to form alkoxy radicals (RO) and NO_2 (Reaction 5.6), the latter of which is then photolysed to make O_3 (Reactions 5.7 and 5.8). Since NO readily depletes O_3, the reduced levels of NO allows O_3 to accumulate.

$$HO_2 + NO \longrightarrow OH + NO_2 \tag{5.5}$$

$$RO_2 + NO \longrightarrow RO + NO_2 \tag{5.6}$$

$$NO_2 + h\nu \xrightarrow{\lambda < 420\ \text{nm}} NO + O \tag{5.7}$$

$$O + O_2 \longrightarrow O_3 \tag{5.8}$$

HO_2 and RO_2 significantly increase with chlorine-based cleaning; HO_2 increased from a

background mixing ratio of 2.3 ppt to 61.4 ppt over one minute, with RO_2 increasing from a background mixing ratio of 3.2 ppt to 2548 ppt over 12 minutes. The sudden rise in HO_2 stems from the alkoxy radicals (RO) reacting with oxygen (O_2), through a hydrogen-migration reaction to form a carbonyl (RCHO) and HO_2 (Reaction 5.9) (Setokuchi and Sato, 2002; Davis and Francisco, 2011).

$$RO + O_2 \longrightarrow RCHO + HO_2 \tag{5.9}$$

HO_2 is also produced from the reaction of OH with formaldehyde (Reaction 5.10).

$$HCHO + OH \longrightarrow CO + HO_2 \tag{5.10}$$

The increase in RO_2 is due to the reaction of VOCs with OH (Reaction 5.11)

$$OH + VOC + O_2 \longrightarrow RO_2 + H_2O \tag{5.11}$$

The chlorine-based cleaning has a much greater effect on the indoor species in Figure 5.3 compared to cooking under our simulated conditions. The high concentrations of OH, HO_2 and RO_2 produced from the resultant chlorine chemistry can continue to drive indoor gas-phase reactions post-cleaning. The high OH concentrations resulted in further reactions with VOCs to form HO_2 and RO_2 for some time after cleaning had ceased. HO_2 and RO_2 did not return to baseline levels until approximately 3.5 and 5 hours respectively after the cleaning had finished.

5.3.2 Temporal Variability of Indoor Concentrations

Indoor air pollutant concentrations vary depending on a range of factors, such as time of day, location, and indoor activities. This section considers ten different houses with varying lifestyle routines (as described in Section 5.2.4.2). The range of concentrations from these ten houses at different points during the day are shown in Figure 5.5, to better understand how concentrations might vary in physically identical houses and at different times of day, according to different routines and conditions.

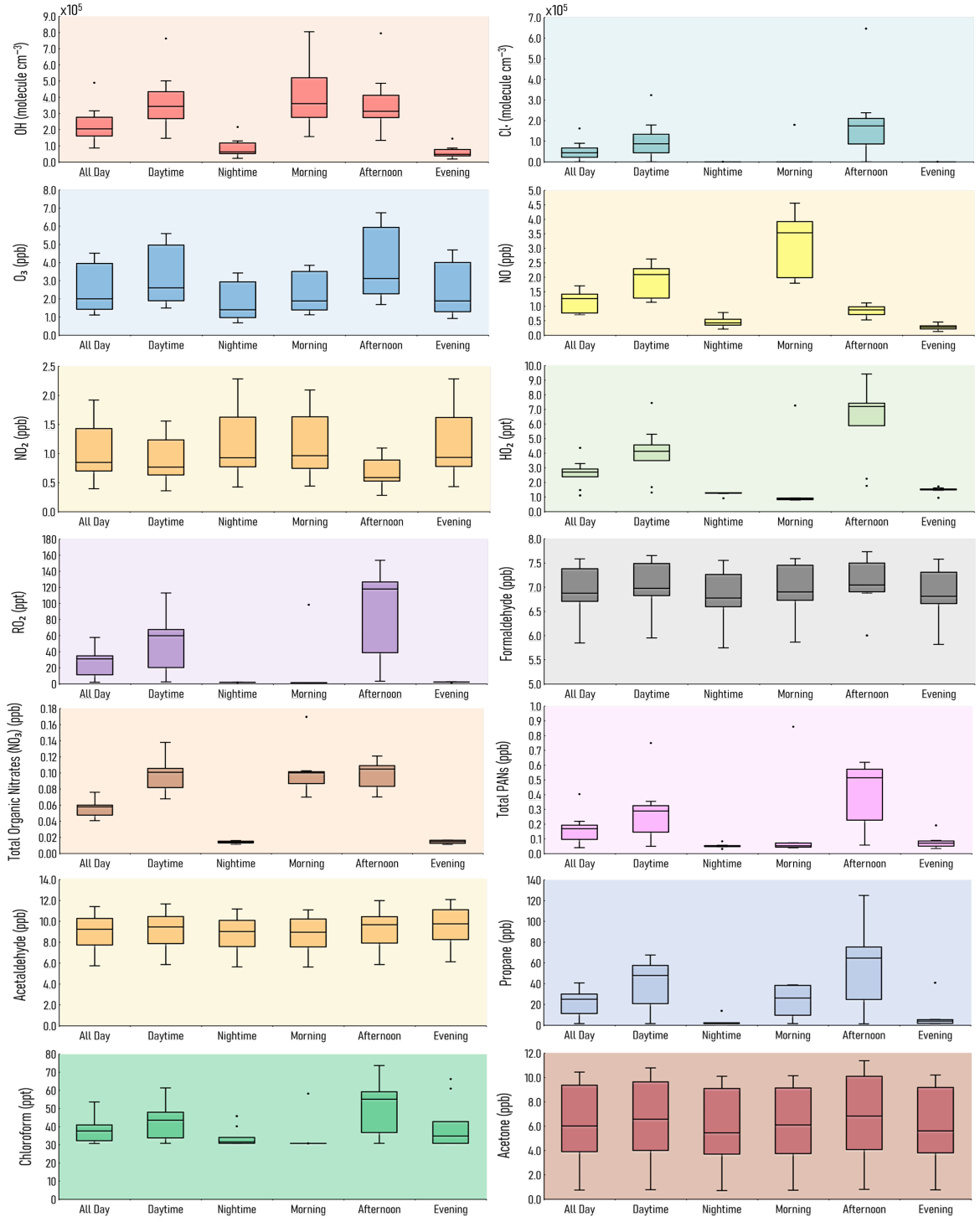

Figure 5.5: Concentrations of key indoor species from ten different houses, showing the median, the upper (75%) and lower (25%) percentiles and the upper (Q3 + 1.5*IQR) and lower whiskers (Q1 –1.5*IQR). The small circles represent values which lie outside of the upper and lower whisker range. The denoted time periods are: all day (12am to 12am), daytime (7am to 7pm), nighttime (7pm to 7am), morning (6am to 12pm), afternoon (12pm to 6pm) and evening (6pm to 10pm).

The OH concentrations are lowest during nighttime and the evening. OH and NO are highest during daytime, indicating a role for photochemistry. For instance, NO and OH can be formed via the photolysis of HONO (Reaction 5.12).

$$HONO + h\nu \xrightarrow{300\text{ nm} < \lambda < 400\text{ nm}} NO + OH \tag{5.12}$$

The median OH concentration for the full day (24-hour average) is 2.0 x 10^5 molecule cm^{-3}. However, House 3 is an outlier, with an all day concentration of 4.9 x 10^5 molecule cm^{-3}, which is more than two times higher than the median. It is assumed that the House 3 occupants do not cook lunch, and there is a relatively high air change rate (2 hr^{-1}).

RO_2 and chlorine radical concentrations are highest in the afternoon, since this is when cleaning occurs in our simulations. Average afternoon chlorine radical concentration in House 3 reaches 6.5 x 10^5 molecule cm^{-3}, which is higher than House 6 who clean three times a day. The occupants of House 3 do not cook lunch.

Formaldehyde shows little diurnal variation. House 5 has the highest average formaldehyde mixing ratio over the course of a day (7.6 ppb), but in the absence of cooking or cleaning since this house is presumed empty. However, it is also assumed to have a low air change rate (0.2 hr^{-1}), allowing emissions from building materials to accumulate. House 3 has the lowest average formaldehyde mixing ratio over the course of a day (5.9 ppb), as it is lost outdoors owing to a relatively high air change rate.

HO_2 mixing ratios are highest during the day, with a median value of 2.7 ppt. Outliers which are lower than the median result are for House 10 (1.5 ppt) and House 5 (1.1 ppt). There is no cleaning in House 5 as it is empty. There is no cleaning in House 10, but the occupants still cook breakfast, lunch and dinnertime meals. House 6 has the highest all day concentration of 4.4 ppt, due to three cleaning sessions post cooking.

The main precursor for organic nitrate (RNO_3) formation is primarily from reaction of OH with VOCs to form RO_2 radicals, which then react with NO to form organic nitrates (RNO_3) (Reaction 5.13b). This route however, is the minor pathway (≤ 20%), with formation of an alkoxy radical (RO) more likely (≥ 80%) (Reaction 5.13a).

$$RO_2 + NO \xrightarrow{\geq 80\%} RO + NO_2 \tag{5.13a}$$

$$RO_2 + NO \xrightarrow{\leq 20\%} RNO_3 \tag{5.13b}$$

Organic nitrates can also form from the reaction of chlorine radicals with alkanes and the subsequent reaction of RO_2 with NO, following the same reaction scheme as outlined above in Reactions 5.13a and 5.13b.

Total organic nitrate (NO_3) levels are highest during the day, as they are primarily formed by the chlorine cleaning. House 6 has a higher mixing ratio compared to the other houses (0.2 ppb), where cleaning happens after every meal, resulting in elevated total organic nitrate levels during and shortly after these cleaning periods. Since cleaning generally occurs during daylight hours, total organic nitrate mixing ratios are higher during the day (0.1 ppb) than they are at nighttime (0.01 ppb).

Peroxyacetylnitrate (PAN) is formed by the reaction of the acetylperoxy radical (CH_3CO_3) with NO_2 (Reaction 5.14). Acetyl peroxy radicals are formed via photochemical degradation of aldehyde species, with each acetyl peroxy radical forming a distinct PAN species, which we then sum to find the total PAN concentration.

$$CH_3CO_3 + NO_2 \longrightarrow CH_3C(O)OONO_2 \tag{5.14}$$

Total PANs follow a similar trend to total organic nitrate concentrations, where the median mixing ratio during the day is 0.3 ppb compared to 0.1 ppb at night. House 6 has the highest total PANs mixing ratio during the daytime (0.8 ppb) due to the extra cleaning that takes place in this house. Davies et al. (2023) reported total PANs and total organic nitrate mixing ratios of approximately 50 and 60 ppt respectively during a simulated stir fry activity. Harding-Smith et al. (2024), reported the total PANs mixing ratio from a scented surface cleaning product was, on average, 25 ppt over 3 hours. Total PAN concentrations

increased as a result of any cleaning activity, whilst, total organic nitrate concentrations varied depending on which cleaning product was used.

Acetaldehyde mixing ratios stay fairly constant throughout the day, and show little fluctuation. Average acetaldehyde levels in the evening reach 12.1 ppb in House 2, which is the highest of the chosen time periods. Acetone follows a similar trend to acetaldehyde, where there is little diurnal variation. However, the range of acetone mixing ratios is higher than for acetaldehyde. For example, acetone levels in the afternoon in House 4 reach 11.4 ppb, but are only 0.8 ppb in House 5. Propane levels are highest in the afternoon, predominantly from lunchtime cooking, where the mixing ratio in House 2 reaches a maximum of 125 ppb in the afternoon.

Chloroform mixing ratios are dictated by cleaning activities. House 5 has the lowest average all-day chloroform mixing ratio (due the lack of cleaning in this house) at 30.7 ppt. This increases to 53.5 ppt in House 6, which has three cleaning events over the course of that day. Cleaning activities are therefore one of the major driving factors for high indoor air pollution concentrations.

5.3.3 How Indoor Sources Contribute to Outdoor Air Pollution

Figure 5.6 shows the enhancement of emission rates from indoors to outdoors of a selection of VOCs during cooking (the three meals are averaged to one emission rate) and cleaning, over background conditions (with no cooking and cleaning activities). These emission rates are taken from the one house layered day simulation (Section 5.2.4.1), with the cooking and cleaning considered in separate model runs. This separation was enforced to identify which VOCs were associated with the different activities. When cooking and cleaning activities are simulated in the same model day, there is some crossover between the two activities.

The increase in emission rate of propane is the highest relative to the other VOCs, and it was highest during the cooking (approximately 56.3 mg hr^{-1}). Isobutane showed a similar pattern and is another good indicator for cooking with gas. Relatively high increases in

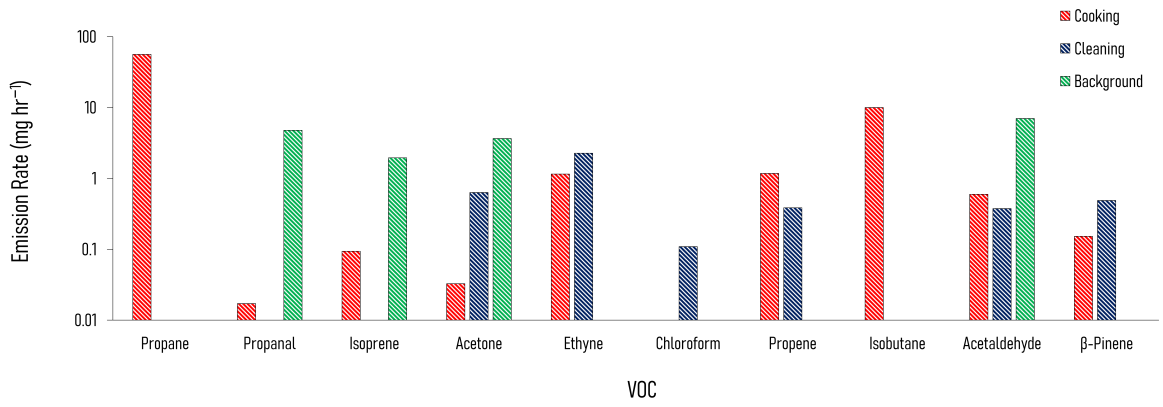

Figure 5.6: The enhancement in emission rates from indoors to outdoors over background values for a variety of VOCs (mg hr^{-1}) during cooking and cleaning, from the house described in Section 5.2.4.1. The background emission rates are shown for comparison, and comprise of emissions from building and furnishing materials and from people.

emission rates follow cleaning for acetone (0.6 mg hr^{-1}), ethyne (2.3 mg hr^{-1}), and chloroform (0.1 mg hr^{-1}). The emission rate of propene is also enhanced following cleaning (0.4 mg hr^{-1}), but there is a larger enhancement following cooking (1.2 mg hr^{-1}). Some of the VOCs, such as acetone and acetaldehyde are emitted outdoors from cooking, cleaning and background activities. Therefore, emission rates from the different species, or the ratio of these, can potentially be used to distinguish indoor activities from outdoor sources in the ambient environment.

In an urban environment, there are often densely-packed houses. These houses all have the potential to emit pollutants, primarily from cooking and cleaning activities, which can potentially affect other homes in the nearby vicinity depending on conditions. Figure 5.7 shows the simulated maximum downwind concentrations of 4 VOCs (acetaldehyde, propane, chloroform and acetone), at different times of the day along the idealised ten house street (as described in Section 5.2.4.2). Average near-field background mixing ratios without cooking or cleaning for acetaldehyde, propane, chloroform and acetone were 0.1 ppb, 0.02 ppb, 0.4 ppt and 0.4 ppb respectively.

Acetaldehyde has the highest maximum downwind concentration at 7pm, from the chilli con carne cooking, whereas propane is highest at 8am due to stove use for the full-English breakfast cooking. Chloroform and acetone are highest at 3pm, as a result of

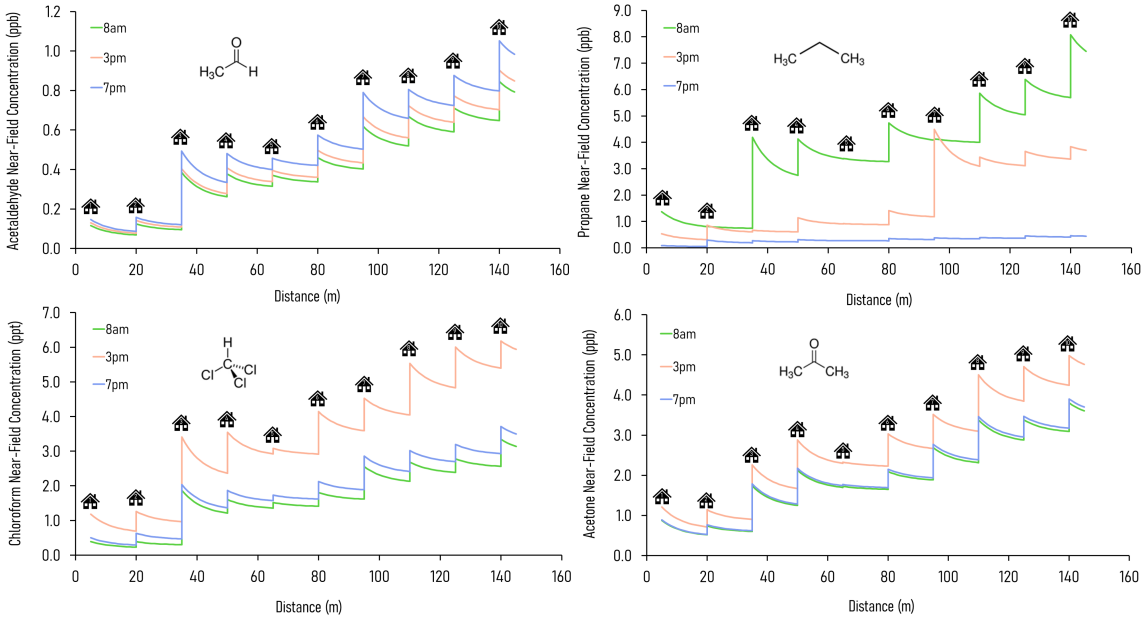

Figure 5.7: The cumulative near-field concentrations of acetaldehyde (ppb), propane (ppb), chloroform (ppt) and acetone (ppb) along a street of ten houses at 8am, 3pm and 7pm. The concentration at the 10th house is the maximum downwind concentration.

cleaning. Along the 140 m street, the maximum downwind acetaldehyde concentration increases by 629, 592 and 618 % at 8am, 3pm and 7pm respectively between the first and last houses. The highest increase in near-field acetaldehyde concentration occurs at 7pm from House 3 (increase of 0.4 ppb), which is assumed to have a higher air change rate in the simulations. House 10 also has a notable increase in near-field concentration (0.3 ppb) at 7pm: the occupants of this house cook all three meals but do not clean, therefore cooking without cleaning leads to higher acetaldehyde concentrations.

The maximum downwind propane concentration increases by 488, 619 and 417% at 8am, 3pm and 7pm respectively between the first and last houses in the street. The highest increase (3.4 ppb) in near-field propane concentration occurs at 8am from House 3, again due to the higher air change rate. House 7 also provides a notable increase in near-field propane concentration (3.3 ppb) at 3pm, owing to a later lunch (at 2pm).

The maximum downwind chloroform concentration increases by 754, 422, 644 % at 8am, 3pm and 7pm respectively, primarily from the chlorine cleaning. The highest increase in near-field chloroform concentration occurs at 3pm from House 3 (increase of 2.4 ppt).

There are smaller increases in near-field chloroform at 8am and 7pm as cleaning occurs mostly in the afternoon in the ten-house analysis. House 8 also has a notable increase in near-field chloroform (1.5 ppt) at 3pm. House 8 is cleaned at the same time as most other houses (2pm), but dinner is not prepared until 8pm. This indicates that there is a smaller increase in near-field chloroform when food, in this case a chilli con carne, is being cooked and prepared.

Finally, the maximum downwind acetone concentration increases by 334, 311, 338% at 8am, 3pm and 7pm respectively, with a smaller variation over time than for the other species. The lower variation is due to a constant source of indoor acetone from the occupants (skin and breath). The highest increase in near-field acetone concentration occurs at 3pm from House 3 (increase of 1.4 ppb), owing to a higher air change rate. House 5 shows little increase in near-field acetone concentration during the day (0.02 - 0.03 ppb) as it is empty.

A comparative analysis simulated a more densely-packed street, where houses are terraced with no gap between them. This analysis uses the same ten-house conditions as described in Section 5.2.4.2, but the length of the street was assumed to be 100 m. The increase in maximum downwind acetaldehyde concentration from House 1 to House 10 at 8am was 648% which is slightly higher than the 629% increase in the detached house street. The percentage increase in maximum downwind concentration of acetone at 7pm on the terraced street was 351%. The percentage increase of maximum downwind propane and chloroform across the terraced street was highest at 3pm and 8am (639 and 776% respectively). The overall increase over the ten houses for the detached and the terraced streets at 8am, 3pm and 7pm for maximum downwind acetaldehyde, propane, chloroform and acetone are given in Table 5.5.

This indicates that due to the closer proximity of the houses, there is a higher maximum downwind concentration of the emitted VOCs for terraced housing than detached housing, however this increase is minimal. Alternative arrangements of our houses, or different activities within them, will lead to different levels of air pollution.

Table 5.5: The maximum downwind concentration increases of acetaldehyde (ppb), propane (ppb), chloroform (ppt) and acetone (ppb) on a detached (D) (140 m) and terraced (T) street (100 m) from the ten-house analysis.

Time of Day	Acetaldehyde	Propane	Chloroform	Acetone
8am (D)	0.7	6.7	3.0	2.9
3pm (D)	0.8	3.3	5.0	3.8
7pm (D)	0.9	0.4	3.2	3.0
8am (T)	0.8	6.9	3.0	3.0
3pm (T)	0.8	3.4	5.2	3.9
7pm (T)	0.9	0.4	3.3	3.1

5.3.4 The Contribution of Cooking and Cleaning Activities to Overall UK VOC Emissions

VOC emissions from households and their relative contribution to the total VOC emissions produced annually in the United Kingdom have not been studied in great detail, compared to the impact from large-scale industrial processes. The UK National Atmospheric Emissions Inventory (NAEI) categorises industrial processes, transport and agricultural emissions of non-methane volatile organic compounds (NMVOCs) (Air Quality Expert Group, 2020). In the UK in 2021, 0.78 million tonnes of NMVOCs were emitted in total, primarily from solvent use, industrial processes and transport. Domestic solvent use and food and drink manufacture contributed 0.19 (24%) and 0.12 (15%) million tonnes of NMVOCs to the total respectively (Department for Environment & Food & Rural Affairs, 2023).

From our layered day simulation (as described in Section 5.2.4.1), the total emission rates of NMVOCs from one house following cooking and cleaning activities are 0.56 and 0.13 grams per day respectively. This equates to approximately 205 and 47 grams per year emitted from one house as a result of cooking and cleaning activities respectively. This has been calculated using Equation 5.15 detailed below:

$$E_i = \frac{C_i \times ACR \times 10^6 \times M_r \times V_{house}}{N_A} \tag{5.15}$$

where: C_i is the indoor VOC concentration (molecule cm^{-3}), ACR is the air change rate (12 day^{-1}), M_r represents the molecular weight (g mol^{-1}), V_{house} is the volume of a house

(500 m^3), N_A is Avogadro's Constant (6.022×10^{23} molecule mol^{-1}) and E_i is the VOC emission rate (g day^{-1}). The emission rates from the individual NMVOCs are then summed to produce a total VOC emission rate ($E_{i,tot}$).

The cooking emission derives partially from combustion of the gas and partially from the food itself. We assume that the ethane and propane emissions account for the former and the rest of the emissions are from the food (the contribution of propane and ethane to emissions from cooking was approximately 9% of the total measured VOCs for our conditions). Therefore, out of the 204.7 g/year from cooking, we assume that 19.2 g are from burning the gas and 185.5 g are from cooking the food. Note that we are ignoring background emissions of ethane and propane from the pilot light and just focusing on cooking activities.

According to the Office for National Statistics, there are 26.4 million houses in the UK (Office for National Statistics, 2023). Therefore, the propane and ethane emissions would equate to 508 tonnes per year from burning gas for cooking (469 and 39 tonnes per year respectively). According to the Air Quality Expert Group in the UK (Air Quality Expert Group, 2022), 4.01 ktonnes of propane was emitted indoors from residential buildings in 2019. The estimated propane emissions from cooking with gas in this chapter, are around 13% of the total propane estimated to be emitted from homes in the UK.

Approximately 61.5% of these homes use gas hobs whereas the other 38.5% use electric (Department of Energy & Climate Change, 2013). We can therefore predict that 61.5% of homes emit 204.7 g/year and the other 38.5% emit 185.8 g/year, giving a total annual emission of 5403 tonnes of NMVOCs emitted outdoors from cooking in UK homes. Similarly, 1229 tonnes are emitted outdoors from cleaning in homes in the UK each year. Based on these assumptions and for the species we have studied, cooking constitutes approximately 0.69% of the total yearly NMVOCs emitted in the UK and cleaning approximately 0.16%. Note that, UK inventory emissions are significantly impacted by sources outside of urban areas, so our values likely underplay the impacts of cooking and cleaning where most of these activities occur.

We can also put these estimated emission rates into context with other sectors. In 2021, road transport in the UK released 23,000 tonnes of NMVOCs (Department for Environment & Food & Rural Affairs, 2023). Our household emissions from cooking and cleaning equate to approximately 29% of those released from traffic. Given that vehicle emissions are likely to continue to decline, e.g. as the vehicle fleet is electrified, household emissions will become proportionally more important in the future.

5.3.5 Limitations of the Study

Although this chapter aims to understand how indoor sources affect outdoor air pollution, there are some limitations in our methods. The model doesn't account for buoyancy of species once they are released outdoors, especially those emitted from cooking. This should be negligible (even for wood stoves which are much hotter) because the mass of air involved is low. The model also assumes outdoor concentrations of VOCs remain constant, whereas the indoor emissions will enhance them in reality, which will feedback as these pollutants enter other houses. The outdoor VOCs are compiled from a literature search of comprehensive studies performed worldwide, though relatively few exist (Shaw et al., 2023). Depending on the outdoor VOC concentrations at a location of interest, our findings may have larger or smaller local impacts. The model also uses a one-dimensional airflow scheme, so pollution only travels in one direction along the street. Cooking and cleaning emissions will vary between homes, depending on the meal which is being prepared, the cooking process and fuel used and the type of cleaning product. HOMEChem is still one of the most detailed indoor studies to date, but the cooking emission rates compare reasonably well with more recent, smaller-scale UK studies (Davies et al., 2023). In the future, indoor emissions inventories would permit a more detailed exploration of the range of likely emissions indoors from cooking and cleaning activities. Finally, the propane emissions in the HOMEChem study were high owing to emissions from the pilot light (Farmer et al., 2019). Our results are more representative of gas cooking than electric or induction.

5.4 Conclusions

The aim of this chapter was to provide a deeper understanding of how cooking and cleaning contribute to indoor air pollution and the subsequent influence they have on the surrounding urban environment. The INCHEM-Py model has demonstrated the impact that both cooking and cleaning have on secondary indoor chemistry. Chlorine cleaning was much more important for radical chemistry than cooking. The concentrations of OH, HO_2 and RO_2 all increased markedly upon the initiation of cleaning.

We identified some VOCs associated with indoor cooking and cleaning, based on data from the HOMEChem study. Propane and isobutane were good indicators for cooking, and chloroform was a good indicator for bleach cleaning activities. For a row of detached houses, the emissions from each house depend crucially on the activities within those houses and physical parameters such as the air change rate. Emissions can also change depending on the order of activities. For instance, cleaning after cooking suppresses the emission of acetaldehyde.

Our estimated total VOCs from cooking and cleaning indoors is a small proportion of total UK emissions, but that does not mean the impact is negligible because of direct indoor exposures. Even in close proximity to a house(s), near-field VOC concentrations tend to be generally lower than outdoor concentrations, although there is uncertainty in outdoor concentrations of many VOC species. There are generally only limited spatial and temporal measurements of VOCs available. More representative outdoor VOC concentrations would be highly beneficial to better understand the impact of emissions from indoors.

Chapter 6

The Role of UVC Photolysis in Indoor Air Chemistry

6.1 Introduction

Since the COVID-19 pandemic emerged in late 2019, widespread lockdowns resulted in large numbers of people having to remain indoors in order to prevent spread of the virus. These enforced lockdown periods meant that our exposure to indoor air pollution increased and the importance of healthy indoor environments was highlighted during this time. This realisation led to the development of a variety of air cleaning devices, which focused on how to remove airborne and surface pathogens to prevent disease transmission. These treatment technologies have also been proposed for controlling indoor air pollutant concentrations. However, the impact on indoor gas-phase phase chemistry from air cleaning devices is relatively unexplored.

There are numerous types of indoor air cleaning devices which use a range of different technologies including media filtration, sorbents, UVC, plasma, photocatalytic oxidation, plants and ozone (Siegel, 2016). Each cleaning type has associated positive and negatives, both with implications on chemistry and health (SAGE EMG, 2020). Mechanical filtration is the most commonly used air cleaning method. It mainly filters out particulate matter, through fibres or coarse materials. Filtration cleaners are more effective

indoors with higher clean air circulation rates (Mata et al., 2022). However, mechanical filtration devices can be expensive to maintain, are ineffective against pollutants other than particulate matter and are often noisy (Liu et al., 2017). Electronic filtration is another filter-based cleaning method. These devices charge particles and attract them to an oppositely charged plate (Mata et al., 2022). The efficacy of particle (0.3-6 μm) removal for these type of devices is over 90% (Bliss, 2005; Mata et al., 2022). However, these filters can produce other pollutants including ozone and ionised VOC compounds (Waring and Siegel, 2011). Adsorption cleaning is sometimes used to remove VOCs from the air using an adsorbent surface. However, adsorption cleaning doesn't destroy pollutants, it just deposits them onto a surface which then requires further treatment and disposal (Luengas et al., 2015). Other cleaning devices can include ionisation and plant-based purification systems (Mata et al., 2022).

This chapter focuses on UVC light disinfection technology in air cleaning devices, and its impact on indoor air chemistry. Cleaning devices which emit ultraviolet light in the UVC region (200-280 nm) have become increasing popular for household and office cleaning following the COVID-19 pandemic. The UV air purifier market currently has a global size of $1.78 B and the pace of market growth is accelerating (Grand View Research, 2023). It expected that the UV air purifier market will increase in growth by 10.7% over the next six years (Grand View Research, 2023). UV cleaners adopt the wavelengths of 222 nm or 254 nm to inactivate airborne viruses, including COVID-19 (Truong et al., 2023; Eadie et al., 2022; Kitagawa et al., 2021; Bueno de Mesquita et al., 2023; Buonanno et al., 2024). However, UV light may also contribute to indoor air pollution.

Eadie et al. (2022) found that the use of 222 nm light led to a reduction of steady-state pathogen load of up to 98.4% in a 32 m^3 room sized chamber, indicating efficacy even for full sized rooms. This study used a room ventilation rate of 3 air changes per hour, with five kyrpton chloride excimer lamps which only emitted wavelengths below 230 nm. Each lamp had an average irradiance of 0.57 μW cm^{-2} at a height of 1.7 m for a high exposure scenario. Even with only one krypton chloride excimer lamp, the average pathogen percentage reduction was approximately 93.7% for an eight hour exposure dose (Eadie

et al., 2022). Eadie et al. (2022) noted the importance of correctly installing far-UVC lamps, because even with five lamps present, the room sized chamber was not fully irradiated (mostly in between the light fittings) despite the overall high pathogen removal efficacy. This could possibly mean that pathogens could be present in non-radiated areas of the room. This may be an issue in larger rooms or rooms with lower ventilation or air mixing rates.

Some studies have claimed exposure to 222 nm light has a minimal effect on human health (Liang et al., 2023; Truong et al., 2023; Eadie et al., 2021; Sugihara et al., 2023). Buonanno et al. (2020) notes that 222 nm light cannot penetrate the ocular tear layer or the stratum corneum, hence exposure to light at this wavelength does not harm any exposed human tissue. Sugihara et al. (2023) installed two KrCl eximer lamps into an examination room to ascertain the impact of 222 nm light on workers after exposure for one year. The study used six ophthalmologists who worked in the irradiated room for approximately 6.7 hours per week. The irradiation dose of the light was 6.4 mJ cm^{-2}. After a year of work, there were no observed chronic nor acute health effects in the ophthalmologists as a result of 222 nm light irradiation (Sugihara et al., 2023). The study also observed the deactivation of microorganisms in this room, with high levels of efficacy (Sugihara et al., 2023).

There remains some skepticism about whether 222 nm light exposure is safe for humans. Ong et al. (2022) found that compared to 254 nm, exposure of cells to 222 nm light showed a greater degree of damage to DNA. However, the study acknowledged that cells which were illuminated with 222 nm light survived, but cells illuminated with 254 nm light underwent apoptosis (programmed cell death) (Ong et al., 2022). Exposure to 254 nm light is also harmful to humans, damaging exposed tissue and eyes (Zaffina et al., 2012; Buonanno et al., 2020; Trevisan et al., 2006). The overall consensus currently is that far-UVC (222 nm) light is mostly harmless to human health at irradiation levels which are used to efficiently inactivate airborne pathogens and can be used as effective air cleaners (Nardell, 2021). Light at 254 nm is problematic to human health and should be avoided as an air cleaning device if rooms are occupied.

Despite the proven efficacy of the removal of airborne pathogens by 222 and 254 nm light, the implications for indoor air chemistry have been relatively unexplored. Link et al. (2023b) discovered that a single filtered 222 nm wavelength lamp produced a significant amount of ozone. The average ozone generation rate from seven experiments was determined to be 19.4 ±0.3 ppbv hr^{-1} in a 31.5 m^3 stainless steel chamber during a four hour time period. Link et al. (2023b) found ozone concentrations of 53 ppb after the germicidal lamp had been switched on for 4 hours. The baseline ozone concentration was approximately 2 ppb in this study. However, the air change rate used in the Link et al. (2023b) study was very low (average of 0.012 air changes per hour), resulting in a build up of ozone in the stainless steel chamber (Link et al., 2023b). Similarly, Peng et al. (2023a) found that in a 21 m^3 Teflon reaction chamber with a 222 nm lamp, the generation rate of ozone was 22 ppb hr^{-1}. After four hours of the lamps being on, ozone concentrations reached approximately 80 ppb in both studies, this observation is of concern given that longer exposures posed a higher potential risk of harm to the occupants (Weschler, 2006).

The ozone production in these studies followed the photodissociation of oxygen. Molecular oxygen (O_2) absorbs light in the wavelength range between 175 and 242 nm with a quantum yield of one, to yield two oxygen atoms (Reaction 6.1) (both in the ground state ($O(^3P)$), which then react with oxygen molecules to produce O_3 (Reaction 6.2). The species denoted as M, represents a molecule of air which is required in the reaction to soak up excess energy, usually O_2 or N_2 (Link et al., 2023b; Yoshino et al., 1988; Nicolet and Peetersman, 1980; Yoshino et al., 1992).

$$O_2 + h\nu \xrightarrow{175\text{ nm} < \lambda < 242\text{ nm}} 2O(^3P) \tag{6.1}$$

$$O + O_2 + M \longrightarrow O_3 + M \tag{6.2}$$

Consequently, other species can be formed through ozonolysis chemistry following 222 nm light use (Peng et al., 2023b). Barber et al. (2023) found that 222 nm light led to the formation of not only O_3 but also OH radicals. Both oxidants can then react with VOCs

to form secondary organic aerosols (SOA) and oxygenated volatile organic compounds (OVOCs). They found that when 100 ppb of limonene was added to an experimental chamber with 222 nm light irradiation, SOA concentrations were approximately 400 ±80 μg m^{-3} after 30 minutes. In the absence of 222 nm light, new particle formation was not observed and total particle mass was below 1.3 μg m^{-3} (Barber et al., 2023). This indicates that monoterpene cleaning under far-UVC lighting could result in poor indoor air quality. SOA can have impacts on human respiratory systems including lung cell death (Pye et al., 2021).

In a review of 222 nm induced ozone formation, Brenner (2023) concluded that in real-life settings (not in a Teflon chamber), 222 nm light-produced ozone levels are unlikely to exceed 10 ppb and in most cases, will be much less than 5 ppb. Experiments conducted in a hotel room with three 222 nm lamps, showed that the ozone concentration increased by 5.7 ppb over 12 h when the air change rate was 1.4 hr^{-1} (Kalliomäki et al., 2023). In an office with a lower air change rate of 0.44 hr^{-1} and only one 222 nm lamp, the ozone concentration increased by 5.1 ppb (Peng et al., 2023a) over 3 h. These admittedly limited studies appear to show a modest increase in ozone concentration from UVC lighting in 'real-life' microenvironments, possibly owing to surface chemistry. The work developed in Chapter 4 showed that 91-94% of ozone was deposited when entering an indoor environment from outdoors.

Light at 254 nm photolyses ozone, rather than produces it (as with 222 nm). The photolysis of ozone results in the formation of OH radicals. However, Graeffe et al. (2023) found that changes in ozone concentration were small (approximately 2 ppb decrease) in the presence of 254 nm lights. Peng et al. (2023b) modelled the impact of UV irradiation at 254 nm on indoor air chemistry using an oxidation flow reactor (OFR) model (Peng et al., 2015; Peng and Jimenez, 2017, 2020) using the Regional Atmospheric Chemistry Mechanism (RACM) (Stockwell et al., 1997). The modelled room had a volume of 300 m^3 with three different ventilation rates, 0.3, 3.0 and 9.0 air changes per hour to represent low, medium and high ventilation examples (Peng et al., 2023b). Peng et al. (2023b) found that ozone concentrations actually increased marginally upon exposure to 254 nm light

(< 2 ppb increase relative to the baseline values of approximately 3, 18 and 28 ppb for the low, medium and high air change rate scenarios respectively) for all three ventilation rates. The study also found increases in secondary pollutant concentrations including organic nitrates, which increased from 0.3 ppb to over 1 ppb under low ventilation conditions. Other VOC oxidation product concentrations including carbonyls, ketones and organic peroxides all increased by approximately 10% following exposure to 254 nm light under all three ventilation rates (Peng et al., 2023b). This indicates an impact from 254 nm lamps on indoor secondary chemistry (Peng et al., 2023b).

The aim of this chapter is to understand how UVC photolysis can affect the indoor environment. Specifically, it aims to identify which wavelength is the most important in terms of photolysis rates and the production of key indoor species in the lower UV region (200 to 300 nm), and the respective impact on indoor air chemistry. This chapter first describes the development of new indoor photolysis rates in the UVC region in INCHEM-Py. The updated model has then been used to investigate the following specific objectives:

• To quantify formation rates of secondary pollutants (radical chemistry) from UVC lighting.

• To determine which wavelength or wavelength ranges have the biggest impact on indoor air quality.

• To explore how UVC lighting affects indoor air chemistry during cooking and cleaning (both bleach and monoterpene) experiments.

• To discover how UVC lighting impacts secondary pollutant formation in different rooms in a home.

6.2 Methods

6.2.1 Development of the Model

INCHEM-Py originally considered 44 photolysis processes, summing the transmission of light between 300 and 760 nm through windows, with one of seven artificial indoor lights. This chapter develops the photolysis module in INCHEM-Py through the extension of the wavelength range to between 200 to 300 nm. This extension builds on the methodology developed by Wang et al. (2022b). The new wavelength range was split into 10 nm sub-regions, which are named according to the mid-wavelength of each 10 nm range (Table 6.1).

Table 6.1: The ten new wavelength intervals.

Label	Wavelength Interval
UV205	$200 \leq \lambda < 210$ nm
UV215	$210 \leq \lambda < 220$ nm
UV225	$220 \leq \lambda < 230$ nm
UV235	$230 \leq \lambda < 240$ nm
UV245	$240 \leq \lambda < 250$ nm
UV255	$250 \leq \lambda < 260$ nm
UV265	$260 \leq \lambda < 270$ nm
UV275	$270 \leq \lambda < 280$ nm
UV285	$280 \leq \lambda < 290$ nm
UV295	$290 \leq \lambda < 300$ nm

The absorption of light from molecular oxygen in the wavelength range of 175 to 242 nm will cause photodissociation forming two ground state oxygen atoms (Reaction 6.1) (Yoshino et al., 1988, 1992; Nicolet and Peetersman, 1980), as discussed in Section 6.1. The wavelength range we are focussing on to implement into the model is the Herzberg continuum range (200 - 242 nm). The new photodissociation reaction is referred to as J9.

Equation 6.3 details how the photolysis rate coefficient is calculated for each individual species and for a specific wavelength interval, in this case it is the UV205 wavelength range.

$$j_{UV205} = h_{UV205} \times I_{UV205} \tag{6.3}$$

In Equation 6.3, j_{UV205} is the photolysis coefficient (in s^{-1}). h_{UV205} is a constant which is the product of the quantum yield (φ) (dimensionless) and the absorption cross-section (σ) in cm^2 in that particular wavelength range. I_{UV205} represents the spherically integrated photon flux (photons cm^{-2} s^{-1}) (Wang et al., 2022b). This process is repeated for all of the wavelength intervals in the 200-300 nm range.

The absorption cross-sections and quantum yields (for experiments conducted at 298 K where possible) for wavelengths between 200 and 300 nm were obtained from the relevant literature (Burkholder et al., 2017; Master Chemical Mechanism, 2024; IUPAC, 2024). The spherically integrated photon flux values were calculated using irradiance values from Eadie et al. (2022). The lamp used was a KrCl excimer lamp, with measurements of irradiance made at 20 cm from the source. The calculation to convert the irradiance to the photon flux is given in Equation 6.4:

$$I = \frac{R}{E} \tag{6.4}$$

where:

$$E = \frac{hc}{\lambda} \tag{6.5}$$

R is the irradiance (μW cm^{-2}), E is the energy of the photon (J), h is the Planck's constant (6.626×10^{-34} J Hz^{-1}), c is the speed of light (2.997×10^8 m s^{-1}) and λ is the wavelength (m). These photon fluxes were averaged for the designated 10 nm intervals, and are given in Table 6.2.

The photolysis coefficients in each interval were then calculated using Equation 6.3 and are given in Tables 6.3 and 6.4 for each 10 nm wavelength region between 200-300 nm. The photolysis values included in Tables 6.3 and 6.4 are for species that absorb light in the specified regions. The respective reactions for each j value are given in Chapter 3 in Table 3.7.

Table 6.2: The averaged spherically integrated photon flux values (photons cm^{-2} s^{-1}) for each 10 nm interval in the wavelength range between 200 and 300 nm, based on Eadie et al. (2022).

Wavelength Interval (nm)	Photon Flux
UV205	1.7×10^{11}
UV215	2.6×10^{12}
UV225	1.1×10^{13}
UV235	8.2×10^{12}
UV245	6.6×10^{12}
UV255	5.5×10^{12}
UV265	4.7×10^{12}
UV275	4.1×10^{12}
UV285	3.7×10^{12}
UV295	3.3×10^{12}

Table 6.3: The photolysis rate coefficients (j values) in s^{-1} for five wavelength ranges in the far-UVC region at a distance of 20 cm from the light source. The blank values indicate no absorption occurs.

J Value	UV205	UV215	UV225	UV235	UV245
J1	6.1×10^{-8}	4.8×10^{-6}	6.8×10^{-5}	4.8×10^{-6}	3.0×10^{-8}
J2	6.7×10^{-9}	5.4×10^{-7}	7.9×10^{-6}	5.4×10^{-7}	3.3×10^{-9}
J3	7.5×10^{-8}	1.7×10^{-6}	6.4×10^{-6}	1.4×10^{-7}	3.8×10^{-10}
J4	5.8×10^{-8}	2.3×10^{-6}	1.2×10^{-5}	1.9×10^{-7}	2.0×10^{-10}
J7	3.6×10^{-7}	9.8×10^{-6}	3.6×10^{-5}	6.1×10^{-7}	1.2×10^{-9}
J8	6.7×10^{-7}	3.2×10^{-6}	3.1×10^{-6}	3.9×10^{-8}	7.6×10^{-11}
J9	1.2×10^{-12}	2.8×10^{-11}	9.5×10^{-11}	1.4×10^{-12}	1.8×10^{-15}
J11	-	-	1.3×10^{-9}	9.5×10^{-11}	1.5×10^{-12}
J12	-	-	3.5×10^{-9}	2.6×10^{-10}	3.1×10^{-12}
J13	2.8×10^{-11}	7.4×10^{-10}	6.5×10^{-9}	6.4×10^{-10}	6.9×10^{-12}
J14	7.1×10^{-11}	2.9×10^{-9}	2.4×10^{-8}	2.0×10^{-9}	2.2×10^{-11}
J15	8.8×10^{-12}	6.5×10^{-10}	5.3×10^{-9}	3.8×10^{-10}	4.2×10^{-12}
J16	4.2×10^{-12}	3.1×10^{-10}	2.5×10^{-9}	1.8×10^{-10}	2.0×10^{-12}
J17	2.8×10^{-10}	2.7×10^{-9}	8.8×10^{-9}	5.0×10^{-10}	5.4×10^{-12}

continued on next page

J Value	UV205	UV215	UV225	UV235	UV245
J21	-	9.8×10^{-9}	1.0×10^{-7}	7.2×10^{-9}	6.0×10^{-11}
J22	4.7×10^{-10}	3.2×10^{-9}	3.1×10^{-8}	2.2×10^{-9}	1.9×10^{-11}
J34	-	-	3.4×10^{-7}	1.4×10^{-8}	7.3×10^{-11}
J35	1.2×10^{-8}	1.6×10^{-7}	3.1×10^{-7}	1.1×10^{-8}	7.0×10^{-11}
J41	-	1.3×10^{-6}	3.7×10^{-6}	7.2×10^{-8}	1.8×10^{-10}
J51	-	-	-	-	1.7×10^{-10}
J52	1.6×10^{-6}	1.5×10^{-5}	1.8×10^{-5}	1.5×10^{-7}	2.2×10^{-10}
J53	1.8×10^{-6}	1.8×10^{-5}	2.1×10^{-5}	1.8×10^{-7}	2.5×10^{-10}
J54	1.8×10^{-6}	1.9×10^{-5}	2.5×10^{-5}	2.2×10^{-7}	3.0×10^{-10}
J55	1.9×10^{-6}	2.0×10^{-5}	2.3×10^{-5}	2.0×10^{-7}	2.7×10^{-10}
J56	-	-	-	-	6.9×10^{-10}
J57	-	-	-	-	6.9×10^{-10}
J71	5.3×10^{-7}	1.7×10^{-5}	8.2×10^{-5}	1.6×10^{-6}	4.1×10^{-9}
J72	2.9×10^{-7}	9.8×10^{-6}	4.9×10^{-5}	8.9×10^{-7}	1.8×10^{-9}
J73	1.9×10^{-7}	6.5×10^{-6}	3.3×10^{-5}	6.0×10^{-7}	1.2×10^{-9}
J74	1.0×10^{-8}	3.5×10^{-7}	3.5×10^{-6}	1.6×10^{-7}	6.5×10^{-10}

Table 6.4: The photolysis rate coefficients (j values) in s^{-1} for five wavelength ranges in the near-UVC region at a distance of 20 cm from the light source. The blank values indicate no absorption occurs.

J Value	UV255	UV265	UV275	UV285	UV295
J1	8.2×10^{-8}	1.3×10^{-8}	1.8×10^{-8}	1.9×10^{-8}	5.7×10^{-9}
J2	9.1×10^{-9}	1.5×10^{-9}	2.0×10^{-9}	2.1×10^{-9}	6.3×10^{-10}
J3	6.0×10^{-10}	7.3×10^{-11}	9.3×10^{-11}	1.3×10^{-10}	8.9×10^{-11}
J4	1.0×10^{-10}	2.9×10^{-11}	1.1×10^{-10}	4.4×10^{-10}	8.1×10^{-10}
J7	1.2×10^{-9}	1.0×10^{-10}	9.3×10^{-11}	-	-

continued on next page

J Value	UV255	UV265	UV275	UV285	UV295
J8	1.5×10^{-10}	2.8×10^{-11}	4.6×10^{-11}	7.0×10^{-11}	4.2×10^{-11}
J11	9.8×10^{-12}	4.7×10^{-12}	2.4×10^{-11}	1.1×10^{-10}	1.8×10^{-10}
J12	1.5×10^{-11}	5.9×10^{-12}	1.8×10^{-11}	5.0×10^{-11}	6.9×10^{-11}
J13	3.7×10^{-11}	1.5×10^{-11}	6.2×10^{-11}	2.0×10^{-10}	1.9×10^{-10}
J14	1.2×10^{-10}	4.1×10^{-11}	1.2×10^{-10}	3.6×10^{-10}	4.6×10^{-10}
J15	2.5×10^{-11}	9.1×10^{-12}	2.9×10^{-11}	8.6×10^{-11}	1.0×10^{-10}
J16	1.2×10^{-11}	4.3×10^{-12}	1.4×10^{-11}	4.1×10^{-11}	4.9×10^{-11}
J17	3.2×10^{-11}	1.3×10^{-11}	4.2×10^{-11}	2.1×10^{-10}	4.5×10^{-10}
J18	7.4×10^{-13}	2.2×10^{-13}	1.0×10^{-12}	5.2×10^{-12}	1.1×10^{-11}
J19	7.4×10^{-13}	2.2×10^{-13}	1.0×10^{-12}	5.2×10^{-12}	1.1×10^{-11}
J20	7.4×10^{-13}	2.2×10^{-13}	1.0×10^{-12}	5.2×10^{-12}	1.1×10^{-11}
J21	2.5×10^{-10}	6.7×10^{-11}	1.5×10^{-10}	3.3×10^{-10}	2.9×10^{-10}
J22	8.4×10^{-11}	2.5×10^{-11}	6.0×10^{-11}	1.4×10^{-10}	1.2×10^{-10}
J23	7.1×10^{-12}	1.4×10^{-12}	3.2×10^{-12}	1.4×10^{-11}	1.0×10^{-11}
J24	7.1×10^{-12}	1.4×10^{-12}	3.2×10^{-12}	1.4×10^{-11}	1.0×10^{-11}
J31	6.4×10^{-11}	1.4×10^{-11}	2.7×10^{-11}	4.8×10^{-11}	3.2×10^{-11}
J32	1.7×10^{-11}	6.7×10^{-12}	2.7×10^{-11}	1.0×10^{-10}	1.5×10^{-10}
J33	6.7×10^{-13}	3.4×10^{-13}	1.8×10^{-12}	1.0×10^{-11}	2.5×10^{-11}
J34	2.2×10^{-10}	5.3×10^{-11}	1.3×10^{-10}	3.5×10^{-10}	3.9×10^{-10}
J35	2.3×10^{-10}	5.3×10^{-11}	1.2×10^{-10}	2.3×10^{-10}	1.8×10^{-10}
J41	2.9×10^{-10}	3.6×10^{-11}	4.9×10^{-11}	7.1×10^{-11}	5.2×10^{-11}
J51	2.8×10^{-10}	4.5×10^{-11}	6.9×10^{-11}	1.0×10^{-10}	6.0×10^{-11}
J52	3.4×10^{-10}	5.8×10^{-11}	9.1×10^{-11}	1.4×10^{-10}	8.7×10^{-11}
J53	3.7×10^{-10}	5.9×10^{-11}	9.4×10^{-11}	1.5×10^{-10}	9.5×10^{-11}
J54	4.1×10^{-10}	6.9×10^{-11}	1.1×10^{-10}	1.8×10^{-10}	1.2×10^{-10}
J55	4.0×10^{-10}	6.3×10^{-11}	1.0×10^{-10}	1.6×10^{-10}	9.7×10^{-11}
J56	9.1×10^{-10}	1.1×10^{-10}	2.0×10^{-10}	4.2×10^{-10}	4.2×10^{-10}

continued on next page

J Value	UV255	UV265	UV275	UV285	UV295
J57	9.1×10^{-10}	1.1×10^{-10}	2.0×10^{-10}	4.2×10^{-10}	4.2×10^{-10}
J70	-	3.1×10^{-12}	2.6×10^{-11}	1.9×10^{-10}	5.2×10^{-10}
J71	6.8×10^{-9}	8.2×10^{-10}	9.8×10^{-10}	1.5×10^{-9}	1.4×10^{-9}
J72	2.4×10^{-9}	2.8×10^{-10}	3.4×10^{-10}	4.5×10^{-10}	2.7×10^{-10}
J73	1.6×10^{-9}	1.9×10^{-10}	2.3×10^{-10}	3.0×10^{-10}	1.8×10^{-10}
J74	1.2×10^{-9}	1.4×10^{-10}	1.7×10^{-10}	3.4×10^{-10}	4.7×10^{-10}
J75	-	-	1.2×10^{-9}	5.3×10^{-9}	1.2×10^{-8}

6.2.2 Model Simulations and Assumptions

The model simulations use the photon flux data in Table 6.2, investigating the chemistry at 20 cm from a single UVC light source. The new wavelength ranges were implemented into INCHEM-Py to understand how different UVC wavelength ranges affect indoor radical concentrations. The ten different wavelength ranges between 200 and 300 nm were considered individually to understand how they affect indoor gas-phase chemistry, given 222 nm and 254 nm have traditionally been the only wavelengths considered. A series of model runs were simulated in a kitchen for each individual 10 nm wavelength interval with no attenuated outdoor lighting, to understand the chemistry initiated in each region. A kitchen was used to provide a comparison for later simulations when occupants were assumed to cook or clean. Office simulations were also carried out to provide a more realistic investigation of the chemistry initiated by UVC lighting in a work-type environment.

6.2.2.1 Baseline and New Light Additions

The model was parameterised to replicate a kitchen in a typical house located in suburban London, UK. The latitude was set to 51.45 °N. The temperature, relative humidity and air change rate was set to 19.9 °C (Ministry of Housing & Communities & Local Government (UK Government), 2019), 53.8% (Ministry of Housing & Communities & Local Government (UK Government), 2019) and 0.5 hr^{-1} (Nazaroff, 2021). The simulation date was

set to 21st June 2023. The baseline run was conducted in the dark (no indoor or outdoor light) to act as a comparison. The outdoor concentrations used for these simulations are given in Tables 3.4 and 3.5 in Chapter 3.

The simulated kitchen had a total surface area of 63.3 m^2 and a volume of 25.0 m^3, giving a total surface area-to-volume ratio of 2.53 m^{-1}. The surface area-to-volume ratio for each material is given in Table 4.4, and there was assumed to be one adult present in the room. Primary surface emissions have also been included in these simulations as described in Chapter 5, Section 5.2.1. Unless stated, the simulations utilise the same parameters as described in this section.

6.2.2.2 UVC Light Simulations

Using the parameters detailed in the baseline run (Section 6.2.2.1), the new 10 nm wavelength intervals were simulated one at a time. Each UVC wavelength range was 'switched on' at 7am and off at 7pm. No other lighting was present. This pattern was repeated for each of the wavelength ranges (from Table 6.1). The results from these simulations are discussed in Section 6.3.1.

6.2.2.3 Cooking and Cleaning Simulations

The emission rates for cooking were taken from the lunch time cooking activity and those for bleach cleaning from the cleaning event both described in Chapter 5 (Section 5.2.3, Table 5.3). A simulation using a monoterpene-based cleaning product has also been explored, using emission rates from Harding-Smith et al. (2024). The simulations utilise the same parameters as described in Section 6.2.2.1, but focus only on the UV225 wavelength interval, which encompasses far-UVC cleaning devices using 222 nm light. Attenuated outdoor light has been added for these simulations with the glass type as 'glass C' (Blocquet et al., 2018). Simulations are described in Table 6.5.

Table 6.5: The simulation conditions for analysis of cooking and cleaning under the UV225 wavelength interval.

Parameter	Cook	BL Clean	MT Clean	Cook then BL Clean	Cook then MT Clean
Wavelength Interval	UV225	UV225	UV225	UV225	UV225
UV Source On	7am	7am	7am	7am	7am
UV Source Off	7pm	7pm	7pm	7pm	7pm
Outdoor Light	Yes	Yes	Yes	Yes	Yes
Glass Type	Glass C	Glass C	Glass C	Glass C	Glass C
Cooking (Time of Day)	13:00-13:30	No	No	13:00-13:30	13:00-13:30
Bleach Cleaning (Time of Day)	No	13:00-13:30	No	14:00-14:30	No
Monoterpene Cleaning (Time of Day)	No	No	13:00-13:30	No	14:00-14:30

6.2.2.4 Occupied Office Simulations

A densely occupied office scenario was examined to determine the effect of the UV225 wavelength interval on indoor air chemistry. The office was assumed to include ten people and a source of the the UV225 wavelength light alongside standard halogen lighting. A further simulation was run as a comparison with halogen lighting only. The simulations represent a real-life scenario, where a 222 nm air cleaner could be deployed. Attenuated outdoor light has been added for these simulations with the use of 'low emissivity' glass (Wang et al., 2022b). The parameters are set up as detailed in Table 6.6. Unless otherwise stated, the simulations utilise the same parameters as described in Section 6.2.2.1.

Table 6.6: The simulation conditions for the densely occupied office analysis.

Parameter	Office with UV225 Source	Office without UV225 Source
Light Type	Halogen	Halogen
Outdoor Light	Yes	Yes
Glass Type	Low Emissivity	Low Emissivity
Lights On	9am	9am
Lights Off	5pm	5pm
Wavelength Interval	UV225	None
Adults	10	10

The volume of the office is 35 m^3, and the surface area-to-volume ratios are given in Table 4.5, apart from skin which is 0.0057 cm^{-1} for 10 adults. The surface area-to-volume ratio of the office is 0.041 cm^{-1}. Primary surface emissions have also been calculated and included in these simulations for an office, using the methodology described in Chapter 5, Section 5.2.1.

6.3 Results and Discussion

6.3.1 The Impact of UVC Wavelength Ranges on Indoor Radical Concentrations

To understand the impact of the new UV wavelength ranges, the diurnal indoor concentrations of key indoor species are shown in Figure 6.1. Incandescent light was used as a comparison (Wang et al., 2022b). The lights were switched on at 7 am and off at 7 pm with no internal activities (cooking or cleaning), and no attenuated outdoor light, as described in Section 6.2.2.2. This is to ascertain the impact the new UV wavelength ranges have on indoor chemistry, without interference from external lighting. The average concentrations of these key indoor species whilst the lights are on are given in Table 6.7. A scenario where the lights were switched off is also included for comparison.

Table 6.7: The average indoor concentration for a range of key species whilst the lights are on (7am to 7pm) for a selection of different lighting conditions. The units are molecule cm^{-3} for the concentration of OH, ppt for the concentrations of HO_2, RO_2 and organic NO_3 and ppb for the other species.

	Concentration									
Wavelength Range	**OH**	**O_3**	**HO_2**	**RO_2**	**NO**	**NO_2**	**HONO**	**HCHO**	**PANs**	**Organic NO_3**
Dark	$4.6x10^4$	2.6	1.4	2.5	0.3	0.9	0.07	7.2	0.5	8.1
Incand	$4.8x10^4$	2.6	1.5	2.5	0.3	0.9	0.07	7.2	0.5	8.4
UV205	$4.3x10^4$	2.9	1.4	2.5	0.3	0.9	0.07	7.2	0.5	7.5
UV215	$3.0x10^4$	10.2	1.8	4.4	0.1	0.9	0.07	7.8	0.5	4.9
UV225	$1.7x10^5$	28.9	4.7	26.9	0.03	0.7	0.05	9.3	0.9	13.7
UV235	$4.5x10^4$	2.9	1.5	2.6	0.3	0.9	0.07	7.3	0.5	7.7
UV245	$4.6x10^4$	2.5	1.4	2.5	0.3	0.9	0.07	7.2	0.5	8.1
UV255	$4.6x10^4$	2.5	1.4	2.5	0.3	0.9	0.07	7.2	0.5	8.1
UV265	$4.6x10^4$	2.5	1.4	2.5	0.3	0.9	0.07	7.2	0.5	8.1
UV275	$4.6x10^4$	2.5	1.4	2.5	0.3	0.9	0.07	7.2	0.5	8.1
UV285	$4.6x10^4$	2.5	1.4	2.5	0.3	0.9	0.07	7.2	0.5	8.1
UV295	$4.6x10^4$	2.5	1.4	2.5	0.3	0.9	0.07	7.2	0.5	8.1

The UV225 wavelength range has the most significant impact on key indoor concentrations, producing the greatest perturbation. When the light was switched on, the ozone concentration increased from 1.0 ppb to 27.2 ppb (at 7:45 am) in 45 minutes, which is more than the ozone generation rate found by Link et al. (2023b) and Peng et al. (2023a)

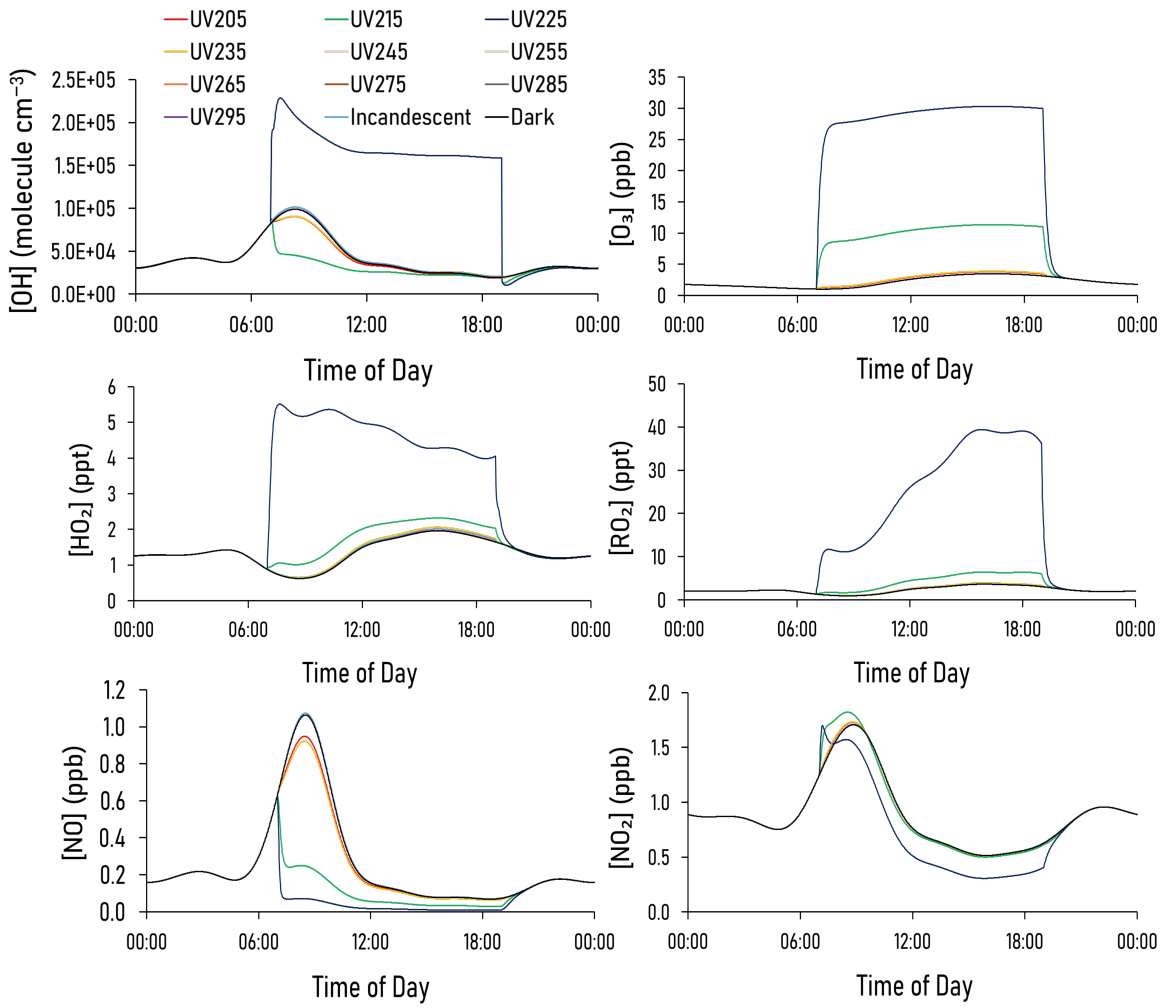

Figure 6.1: The indoor concentrations of key indoor species with photolysis at different wavelengths.

at 222 nm. After the initial increase, the ozone concentration rose gradually throughout the day, reaching a maximum concentration of 30.3 ppb at 4:18 pm before returning to a background concentration (2.6 ppb) at 8:35 pm, one hour and 35 minutes after the light had been switched off. UV215 showed a similar trend in ozone concentration to the UV225 wavelength range, but the ozone concentration only reached a maximum of 11.3 ppb also at 4:18 pm. The only other discernible ozone increases were for UV205 and UV235, which increased ozone concentrations by 0.3 and 0.4 ppb within an hour (8am) respectively.

The main cause of ozone generation from these wavelength ranges is due to the new photolysis reaction J9 (Reaction 6.1). The production of ground state oxygen atoms ($O(^3P)$)

results in a reaction with molecular nitrogen and oxygen (Reactions 6.6 and 6.7 respectively). These reactions drive the formation of ozone indoors under the addition of far-UVC wavelength ranges. The rate of reaction at 7:45 am under the UV225 wavelength range for Reactions 6.6 and 6.7 are 32.9 ppt s^{-1} and 9.3 ppt s^{-1} respectively.

$$O(^3P) + N_2 \longrightarrow O_3 \tag{6.6}$$

$$O(^3P) + O_2 \longrightarrow O_3 \tag{6.7}$$

The wavelength ranges UV245, UV255, UV265, UV275, UV285 and UV295 had a lower average ozone concentration during the day (2.5 ppb) than if incandescent lighting was present or if there was no artificial lighting at all (2.6 ppb).

Indoor OH concentrations increased from 8.2 x 10^4 molecule cm^{-3} (at 7 am) to a daily high concentration of 2.3 x 10^5 molecule cm^{-3} (a 180% increase) in 30 minutes (7:30 am) in the UV225 region. This sharp increase in OH concentration is caused by the photolysis of ozone to form excited state oxygen atoms (described in Reaction 1.1 in Chapter 1, Section 1.3), which react with water (Reaction 6.8) to produce two OH radicals. Reaction 6.8 has a rate of 0.13 ppt s^{-1} for the highest diurnal OH concentration at 7:30 am.

$$O(^1D) + H_2O \longrightarrow OH + OH \tag{6.8}$$

Upon exposure to the UV215 wavelength range, the average OH concentration was lower than for the other wavelength ranges tested. The OH concentration decreased from 8.2 x 10^4 molecule cm^{-3} to 5.1 x 10^4 molecule cm^{-3} in 20 minutes (7:20 am). The average OH concentration during the day in UV215 is 3.0 x 10^4 which is the lowest for the simulated wavelength ranges.

There is a balance between ozone and OH reaction rates. Figures 6.2 and 6.3 shows the diurnal formation and loss rates for OH for the UV215 and UV225 wavelength ranges.

Figure 6.3 shows a sharp increase in the formation rate of OH at 7 am, which heavily outweighs the loss rate. This results in an instant increase in the OH concentration (Figure 6.1). As the HO_2 reacting with NO reaction becomes less important (around 7:30 am), the OH concentration will start to decrease. For the UV215, at 7 am, the loss rates outweigh the formation rates, which results in a decrease of OH (Figure 6.2).

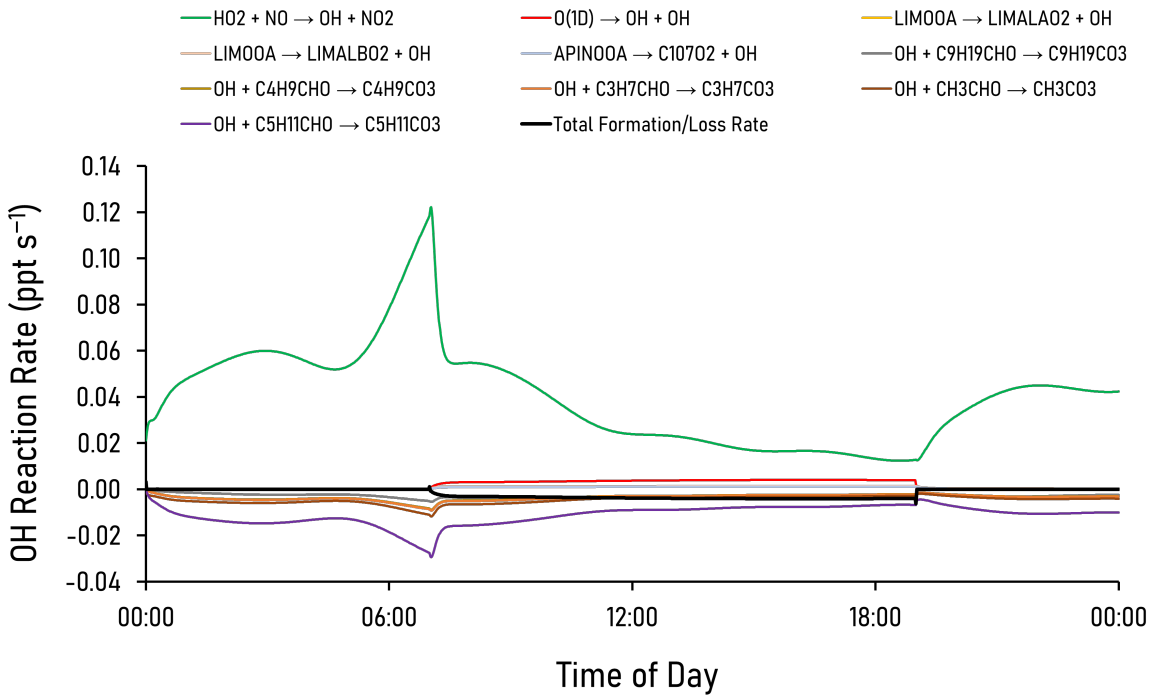

Figure 6.2: The diurnal OH reaction rate (ppt s^{-1}) with the UV215 wavelength range. A positive reaction rate represents a formation of OH. A negative reaction rate representation a loss of OH. The top five formation and loss reactions are represented in the legend (given as MCM names). The total formation/loss rate is also represented (black line).

The total ozone formation rate at 7:05 am for UV215 is 13.8 ppt s^{-1}, which is lower than the total ozone formation rate for UV225 (43.2 ppt s^{-1}) at this time period. The total loss rates for ozone at this time is 6.6 ppt s^{-1} and 18.3 ppt s^{-1} for UV215 and UV225 respectively. O_3 loss is dominated by surface deposition. This results in an increase of ozone in both time periods, but the UV225 scenario elevates ozone to a higher concentration. The most important formation reactions of ozone at this time interval for UV215 and UV225 are Reactions 6.6 and 6.7.

Due to the elevated concentrations of ozone caused by the UV225 wavelength range, av-

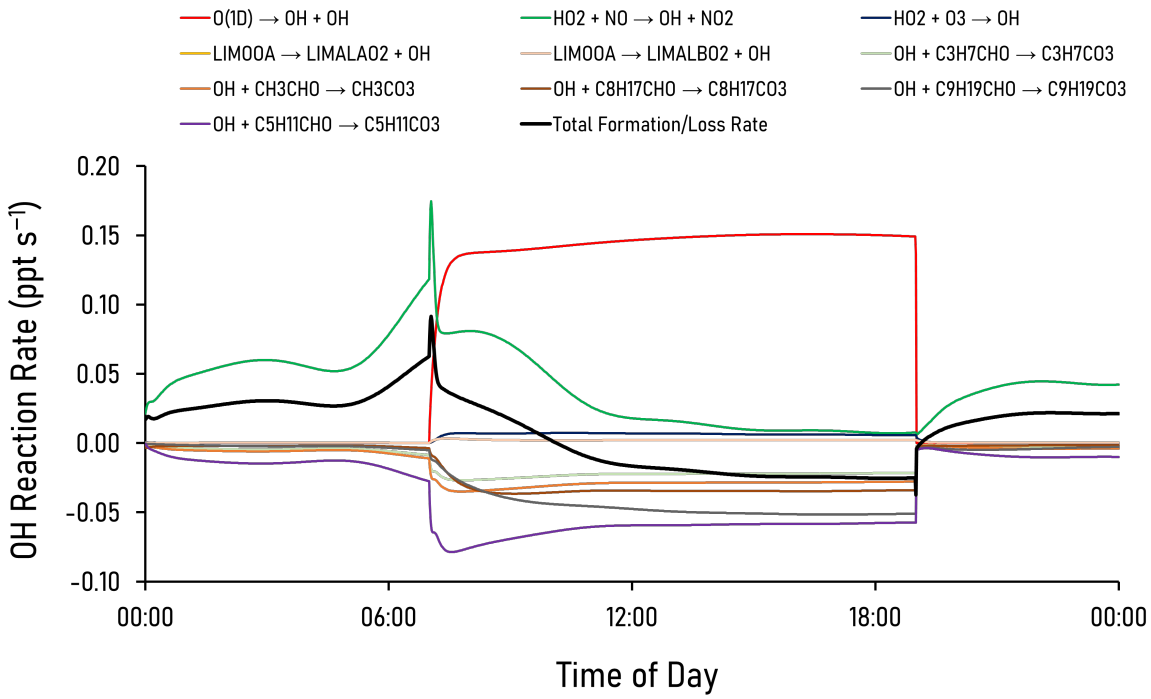

Figure 6.3: The diurnal OH reaction rate (ppt s^{-1}) with the UV225 wavelength range. A positive reaction rate represents a formation of OH. A negative reaction rate representation a loss of OH. The top five formation and loss reactions are represented in the legend (given as MCM names). The total formation/loss rate is also represented (black line).

erage HO_2 (4.7 ppt) and RO_2 (26.9 ppt) concentrations are approximately 3 and 11 times higher respectively than if incandescent lighting is used (1.5 and 2.5 ppt respectively). After the UV225 light was switched on, the HO_2 concentration increased from 0.88 ppt to 5.5 ppt in 39 minutes (7:39 am). This was its highest concentration throughout the day, before it started to gradually decrease until the lights were switched off at 7 pm, returning to an background concentration of 1.5 ppt at 7.51 pm.

RO_2 concentrations behave similarly to HO_2, with an initial increase from 1.4 ppt to 11.7 ppt at 7:41 am. The RO_2 concentration then gradually increased throughout the day to a maximum concentration of 39.4 ppt at 3.48 pm compared to HO_2, which peaks early and slowly decreases. The RO_2 concentration returns to baseline levels (2.3 ppt) 90 minutes after the lights have been switched off. HO_2 and RO_2 concentrations for the UV215 wavelength range also increased, with average concentrations during the day of 1.8 and 4.4 ppt respectively. The other wavelength ranges did not alter the HO_2 and RO_2 concentrations significantly (< 1% change).

NO concentrations showed the opposite trend to ozone, given the two species readily react. The UV215 and UV225 wavelength ranges caused a decrease in NO concentration. This is due to the reaction of NO with HO_2, which can form OH and NO_2. The average diurnal concentrations were 0.1 and 0.03 ppb respectively compared to the other wavelength ranges which had indoor concentrations of 0.3 ppb. The lighting conditions had little effect on average diurnal NO_2 concentrations. The only wavelength range which had a concentration decrease of NO_2 from the baseline was UV225 (decrease of 0.2 ppb relative to a baseline value of 0.9 ppb).

For the UV225 wavelength range, other key indoor species including formaldehyde, peroxyacetylnitrates (PANs) and organic NO_3 had higher average diurnal indoor concentrations (9.3 ppb, 0.9 ppb and 13.7 ppt) respectively than the other lighting scenarios. The concentration of PAN for the other wavelength ranges was 0.5 ppb. The average organic nitrate concentration was lowest for the UV215 wavelength range (4.9 ppt) due to the lower OH concentration. The UV215 wavelength range scenario also led to the second highest concentration of formaldehyde (7.8 ppb).

OH reactivity and production increased sharply upon exposure to the UV225 wavelength range, as shown in Figure 6.4. OH production increased by approximately 3 times from 3.1 x 10^6 molecule cm^{-3} s^{-1} (at 7 am) to 9.8 x 10^6 molecule cm^{-3} s^{-1} at 8:02 am, driven by production from ozone. The OH production rate slowly decreased throughout the day and returned to baseline levels (1.1 x 10^6 molecule cm^{-3} s^{-1}) 111 minutes after lighting had been switched off. The reactivity of OH increased steadily throughout the day. OH reactivity is defined by the sum of OH reactant concentrations multiplied by their respective rate coefficients with OH (Yang et al., 2016; Shaw et al., 2023). Over the course of the 12 hours when the lights were on, the OH reactivity rose from 36.0 s^{-1} to 53.5 s^{-1}, with the largest increase between 7 am and 9:25 am (36.0 s^{-1} to 50.1 s^{-1}), dominated by the reaction of straight-chained aldehydes with OH.

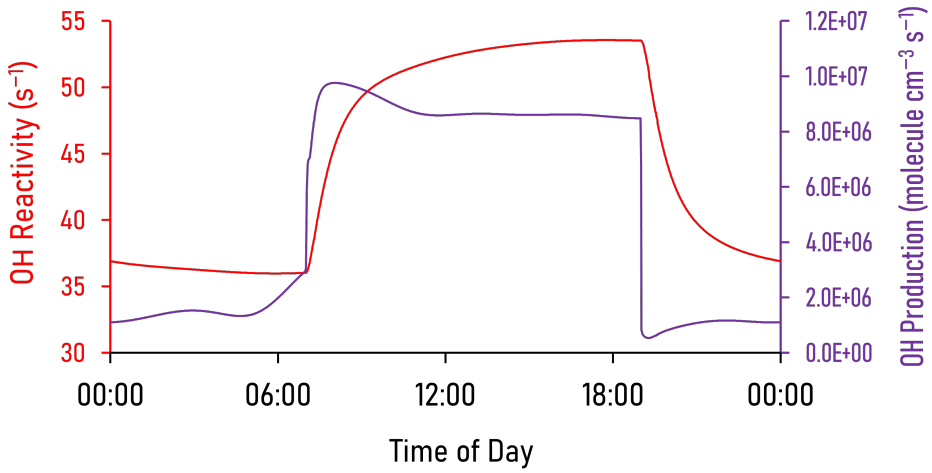

Figure 6.4: The reactivity (s^{-1}) and production (molecule cm^{-3} s^{-1}) of OH during operation of the UV225 light.

Further simulations were conducted to ascertain whether room type affected radical concentrations when exposed to UV215 and UV225 wavelength ranges (Figure 6.5). These simulations followed the same parameterisation as described in Section 6.2.2.2 but included attenuated outdoor lighting with glass C with surface area-to-volumes representative for each room type, as described in Chapter 4 in Tables 4.3, 4.4 and 4.5.

Figure 6.5 shows that the kitchen has a slightly higher maximum OH concentration (5.4 x 10^5 molecule cm^{-3}), than the bedroom (5.3 x 10^5 molecule cm^{-3}) and the office (5.2 x 10^5 molecule cm^{-3}) for the UV225 wavelength range. Similarly, the kitchen had the highest maximum O_3 concentration for both the UV215 and UV225 wavelength ranges (11.8 and 30.6 ppb respectively) in comparison to the bedroom (7.0 and 18.0 ppb respectively) and the office (5.6 and 14.6 ppb respectively). This indicates the surfaces present in the kitchen can lead to higher OH and O_3 concentrations than the other rooms in a home upon exposure to UV225 light, leading to more perturbation of indoor chemistry. The kitchen will now be used to simulate how cooking and cleaning can affect indoor radical concentrations in the presence of the UV225 wavelength range.

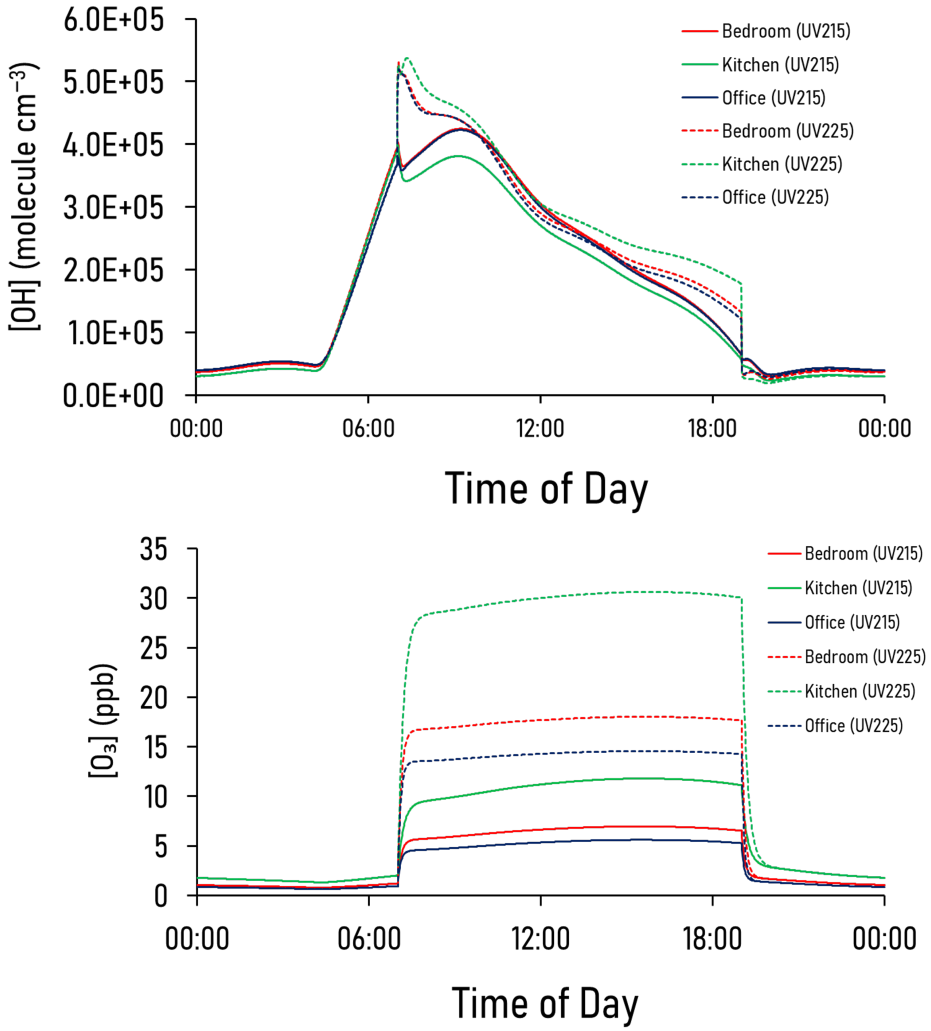

Figure 6.5: The diurnal indoor concentrations of OH and O_3 for the UV215 and UV225 wavelength ranges in a bedroom, kitchen and office, including outdoor attenuated lighting.

6.3.2 Cooking and Cleaning under Far-UVC Lighting

Cooking and cleaning are known to emit indoor pollutants (Davies et al., 2023; Mattila et al., 2020b), but little is known about how these activities interact with far-UVC light. This section describes how cooking and cleaning with far-UVC light (UV225 in the simulations) affect indoor gas-phase concentrations of key species. These simulations have been conducted as described in Section 6.2.2.3. The baseline simulation in this section is a typical kitchen where no cooking or cleaning occurs. Attenuated outdoor lighting is included, using the 'glass C' glass type (Shaw et al., 2023). The concentrations for key indoor species between 12 noon and midnight are provided in Figures 6.6 to 6.11. The

scenarios referred to are described in Table 6.5.

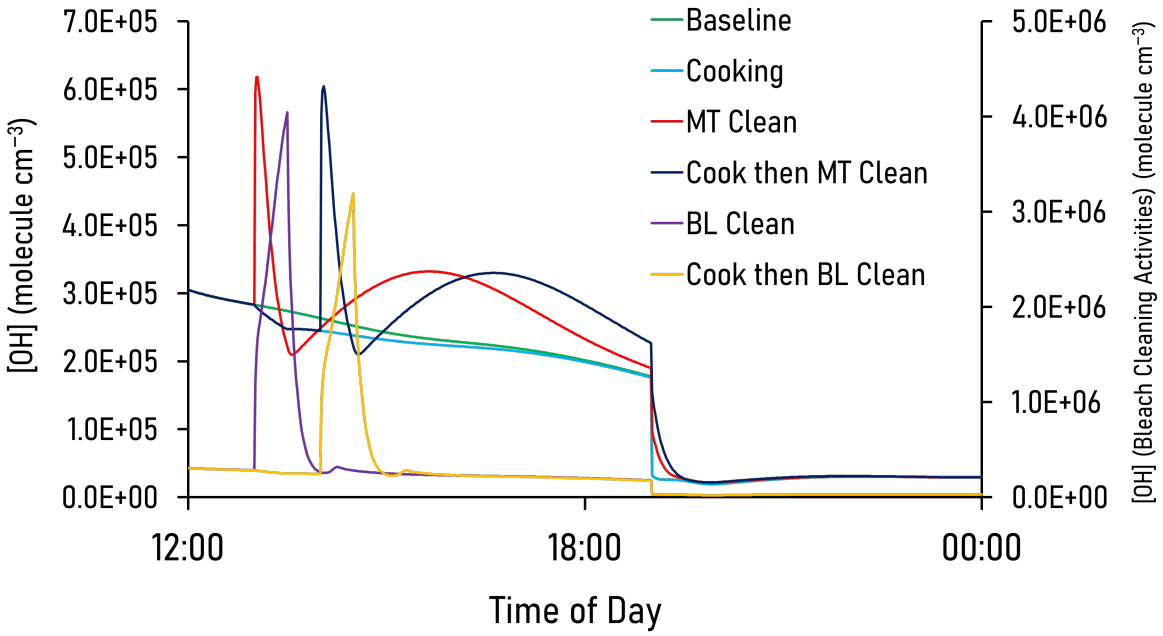

Figure 6.6: The diurnal indoor concentrations of OH during 30-minute periods of cooking, cleaning or both. The 'BL Clean' and 'Cook then BL Clean' concentration profiles are located on the secondary y-axis.

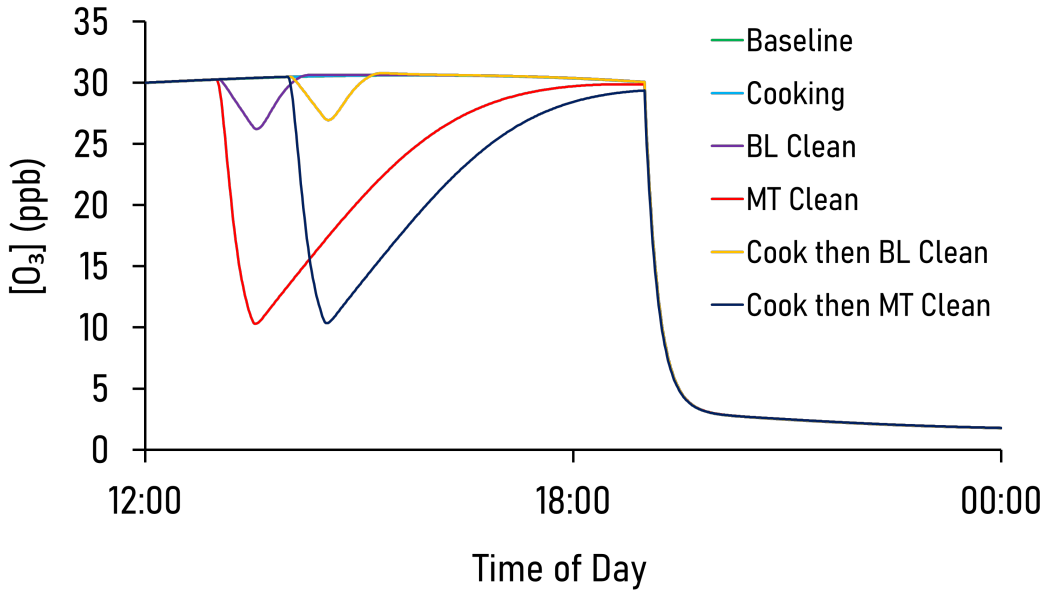

Figure 6.7: The diurnal indoor concentrations of O_3 during 30-minute periods of cooking, cleaning or both.

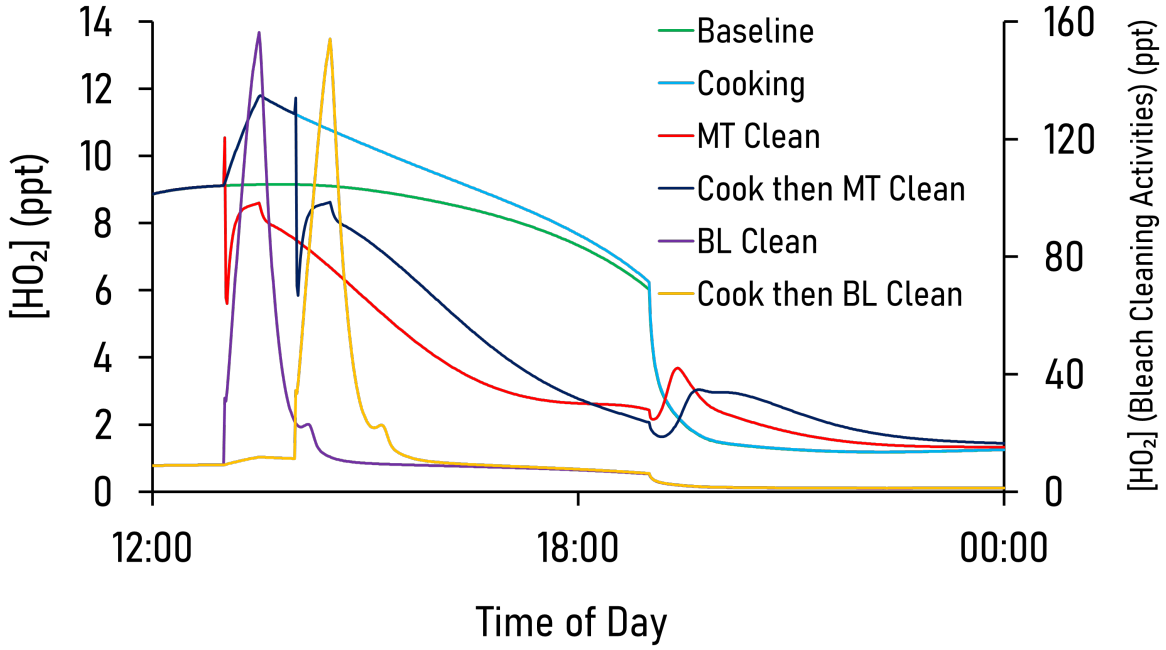

Figure 6.8: The diurnal indoor concentrations of HO_2 during 30-minute periods of cooking, cleaning or both. The 'BL Clean' and 'Cook then BL Clean' concentration profiles are located on the secondary y-axis.

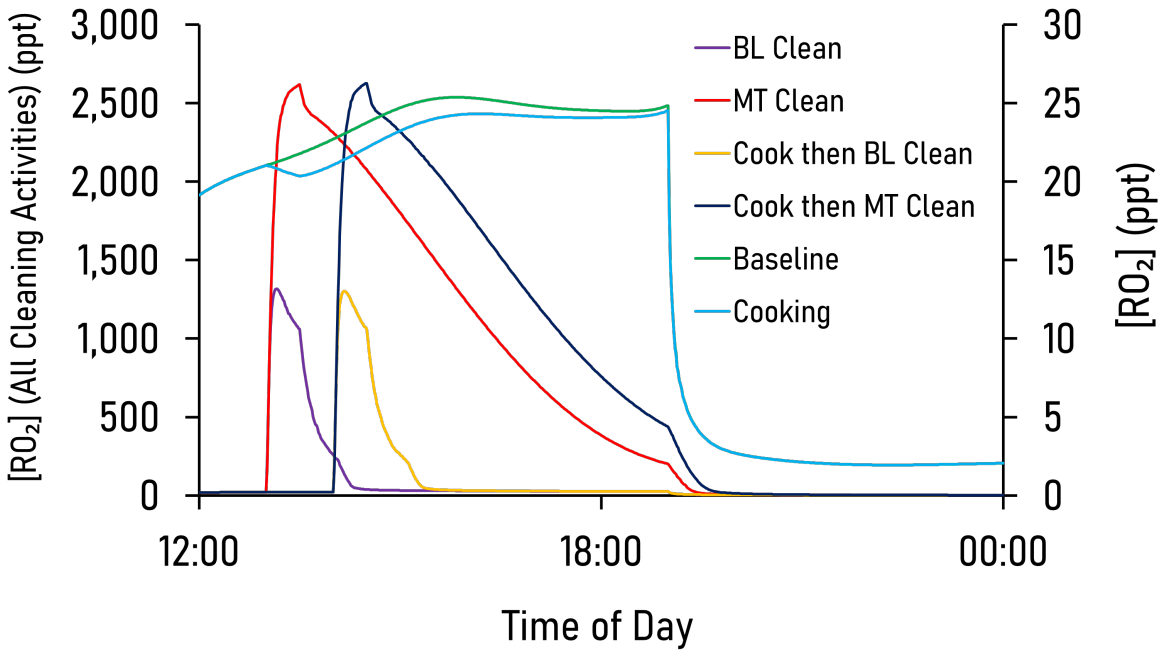

Figure 6.9: The diurnal indoor concentrations of RO_2 during 30-minute periods of cooking, cleaning or both. The 'Baseline' and 'Cooking' then BL Clean concentration profiles are located on the secondary y-axis.

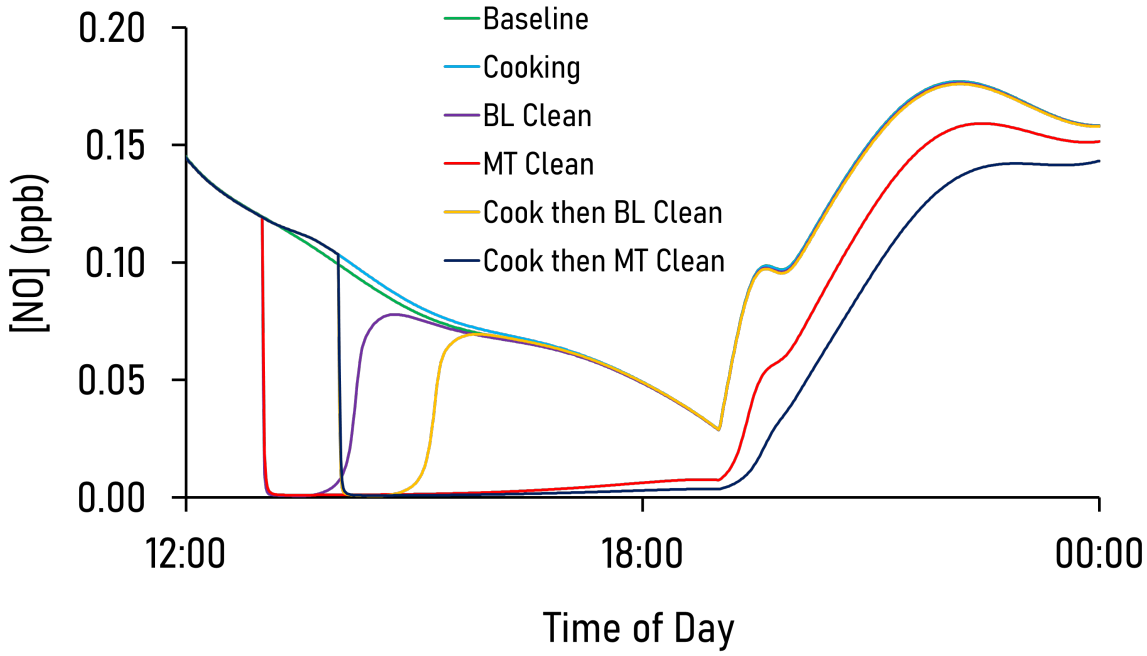

Figure 6.10: The diurnal indoor concentrations of NO during 30-minute periods of cooking, cleaning or both.

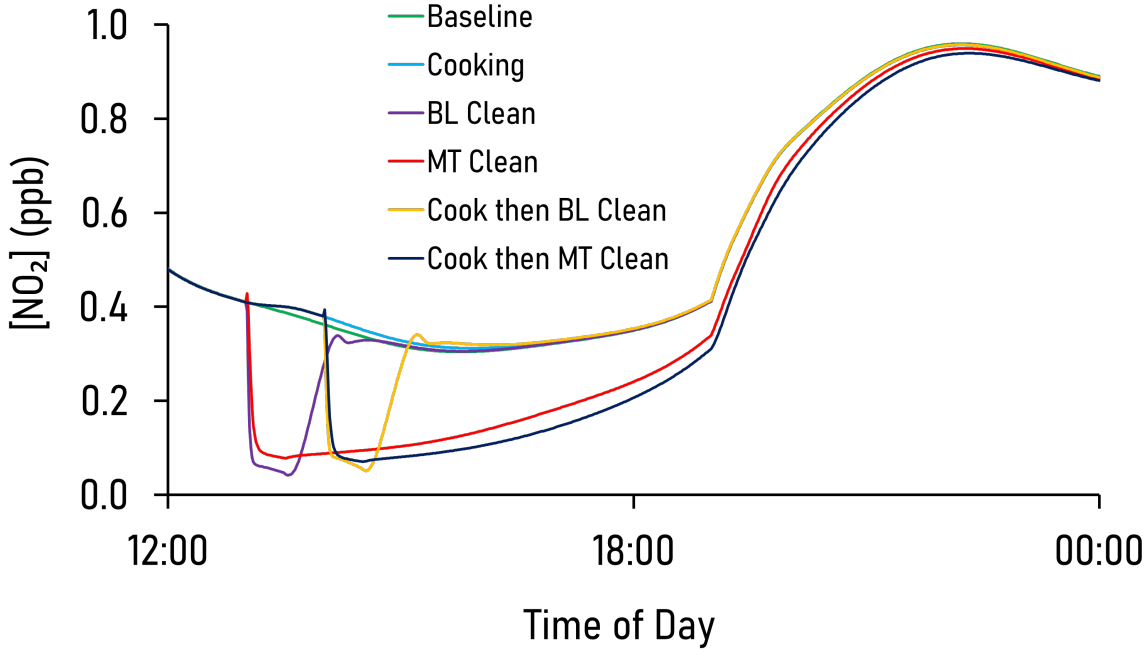

Figure 6.11: The diurnal indoor concentrations of NO_2 during 30-minute periods of cooking, cleaning or both.

Figure 6.6 shows that bleach cleaning has the biggest impact on OH radical concentrations compared to cooking and monoterpene cleaning. Upon initiating bleach cleaning

at 1 pm, the OH concentration increases from 2.8 x 10^5 molecule cm^{-3} to a maximum concentration of 4.0 x 10^6 in 30 minutes (1:30 pm). This sudden increase in the concentration of OH is caused by the photolysis of hypochlorous acid (HOCl) denoted by J74 in Table 3.7 forming chlorine radicals and OH. This reaction has a rate of 3.3 ppt s^{-1}.

The simulation with cooking resulted in a small initial decrease in OH radical concentration (2.5 x 10^5 molecule cm^{-3} at 1:30 pm). Monoterpene cleaning resulted in a sudden OH peak (6.2 x 10^5 molecule cm^{-3} at 1:03 pm). The major formation rate of OH following monoterpene cleaning is described by the formation of secondary pollutants via ozonolysis with limonene (Reaction 6.9) and the subsequent formation of peroxy radicals and OH. The rate of reaction of the formation of OH and the two unique limonene peroxy radicals (Reactions 6.10 and 6.11 respectively) (Carslaw, 2013; Master Chemical Mechanism, 2024), is 1.7 ppt s^{-1} for both reactions.

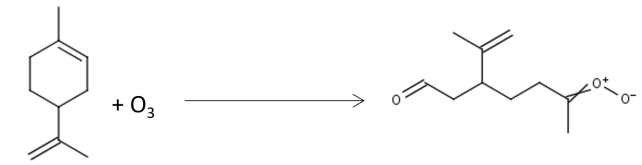

(6.9)

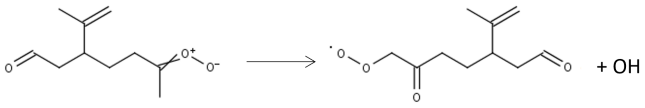

(6.10)

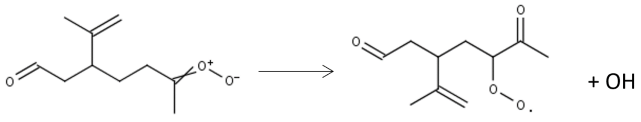

(6.11)

Reaction 6.9 in the simulation with cooking followed by monoterpene cleaning also results in a sudden OH concentration peak at 2:03 pm. The maximum OH concentration in this simulation is 6.0 x 10^5 molecule cm^{-3}, a slightly lower concentration than for isolated monoterpene cleaning, indicating a suppression of OH radicals if cooking occurs before

cleaning. This suppression was also noticed when bleach cleaning followed cooking.

In Figure 6.7, monoterpene cleaning causes a significant decrease in ozone concentration. The UV225 light is on for six hours before the introduction of monoterpenes, so the ozone concentration is 30.3 ppb at the start of indoor activities at 1 pm. However, with monoterpene cleaning, ozone concentration decreases to 10.3 ppb in 33 minutes, given that monoterpenes readily undergo ozonolysis reactions (Reaction 6.9). The rate of reaction of Reaction 6.9 at 1:33 pm is 12.8 ppt s^{-1}. Cooking had little impact on ozone concentration (< 1% change). Bleach cleaning also made ozone concentrations decrease (12.5% decrease in 30 minutes), but quickly returned to baseline levels (34 minutes after cleaning had finished).

Ozone is also depleted by other monoterpenes present in the cleaning mixture including; α-pinene, α-phellandrene, γ-terpinene, terpinolene and Δ3-carene which have rates of reaction with ozone of 1.9, 1.2, 1.1, 0.81, and 0.77 ppt s^{-1} respectively at 1:33 pm. J1 (the photolysis of ozone to form $O(^1D)$ and O_2), is also a source of ozone loss (forming an excited state oxygen atom), with a reaction rate of 0.70 ppt s^{-1}. Ozone also decreases when monoterpene cleaning is followed by cooking. There is a negligible change in ozone concentration following cooking, indicating it has little impact on ozone concentration in the UV225 wavelength range.

In Figure 6.8, the concentration of the HO_2 radical follows an interesting trend following cooking and cleaning. When cooking starts, the HO_2 concentration increases by 2.7 ppt in 32 minutes. Bleach cleaning causes an increase of 147 ppt of HO_2 over 30 minutes. However, when monoterpene cleaning occurs, the concentration of HO_2 decreases to 5.6 ppt (from 9.1 ppt) in three minutes but swiftly increases to 8.6 ppt by 1:30 pm. This is due to the initial reaction of the monoterpene (primarily limonene) RO_2 radicals with HO_2. HO_2 is then replenished from RO radicals reacting with oxygen.

Bleach cleaning at 1 pm gives rise to the highest HO_2 concentration of the five scenarios (156 ppt at 1:30 pm). HO_2 concentrations for bleach cleaning following cooking are also high at 2:30 pm (154 ppt). This is primarily because of VOCs reacting with chlorine

radicals. The HO_2 concentrations for the cooking, bleach cleaning and cook then bleach clean scenarios steadily decrease throughout the day and return to a baseline level of 1.4 ppt by 8:14 pm, 74 minutes after the lights have been switched off. The HO_2 concentrations in both monoterpene cooking and monoterpene cleaning following cooking scenarios continue to decrease following activity until the lights are switched off at 7 pm. The HO_2 concentrations then increase gradually but do not return to baseline levels until after midnight, indicating a lasting effect on HO_2 radical concentrations from monoterpene cleaning well after the activity has finished and lights have been switched off.

Figure 6.9 shows how RO_2 concentrations during the scenarios involving the monoterpene cleaning reach very high concentrations compared to the other scenarios. Monoterpene cleaning at 1 pm causes RO_2 concentrations to increase to a maximum of 2619 ppt at 1:30 pm. The high RO_2 concentrations are caused by the reaction between ozone and monoterpene species, primarily from limonene oxidation (Reactions 6.9, 6.10 and 6.11). The scenario involving monoterpene cleaning which follows cooking, causes RO_2 concentrations to increase to a maximum of 2627 ppt at 2:30 pm. Bleach cleaning also causes an increase in RO_2 concentrations. Following the initiation of bleach cleaning, the concentration of RO_2 rises to a maximum concentration of 1317 ppt (1:09 pm). Cooking actually decreases the concentration of RO_2 slightly, from 21.0 ppt to 20.4 ppt in 30 minutes. Following this, the RO_2 concentration rises to a maximum concentration of 24.5 ppt at 7:00 pm before returning to baseline levels (7.3 ppt), 10 minutes after the lights have been switched off.

The concentration of NO in all five scenarios is low (< 0.02 ppb) throughout the day due to the high concentrations of ozone (Figure 6.10). NO readily reacts with ozone, and the ozone concentration is consistently replenished by oxygen photolysis. The NO_2 concentration increases initially with monoterpene cleaning (Figure 6.11), but decreases initially for bleach cleaning. Following bleach cleaning, the NO_2 concentration reaches a minimum of 0.04 ppb at 1:32 pm and return to baseline levels (0.33 ppb) at 2:33 pm. However, following monoterpene cleaning, NO_2 concentrations reach a minimum of 0.08 ppb at 1:32 pm and do not reach baseline levels until the next day.

6.3.3 Secondary Pollutant Analysis from UVC Lighting

Photolysis of indoor species has been shown to produce secondary pollutants (Wang et al., 2022b), which can impact human health. As previously seen in Chapter 4, a metric designed by Carslaw and Shaw (2019) can be used to compare how different indoor conditions can affect secondary pollutant concentrations and potential health effects. This metric is denoted as the 'Secondary Product Creation Potential' (SPCP), used in its original form, without the division of an added VOC, and is given in Equation 6.12:

$$SPCP = \Sigma \left(\begin{array}{l} [Total\ Organic\ Nitrates] + [PANs] + [O_3] + \\ [Glyoxal] + [Formaldehyde] + [Acetaldehyde] \end{array} \right) \tag{6.12}$$

Figure 6.12 shows the daily averages of SPCP (in ppb) using the newly added UV wavelength ranges. Figure 6.12 shows that lighting in the UV225 wavelength range dominates secondary pollution creation compared to other lighting types (SPCP of 31.3 ppb). This is primarily due to the high concentrations of ozone produced indoors when exposed to this type of lighting. Ozone was the highest contributor to the SPCP metric with an average concentration of 26.3 ppb (contributing 84%). Acetaldehyde and formaldehyde contributed the second (8%) and third (7%) most to the SPCP value with 2.5 and 2.1 ppb respectively at this wavelength.

The UV215 wavelength range scenario resulted in an increase in SPCP (9.0 ppb on average) when the lights were switched on, 2150% higher than UV205 lighting on average during the day. SPCP also increased slightly for the wavelength ranges of UV205 (0.4 ppb) and UV235 (0.5 ppb). The wavelength ranges of UV255, UV265, UV275, UV285 and UV295 resulted in a slightly negative SPCP concentration following the subtraction of the baseline.

Figure 6.13 show how SPCP varies with indoor cooking and cleaning activities. The baseline (no activities) value has been subtracted from the original SPCP value. The SPCP average (between 12 noon and 5 pm) focuses on the period with impacts from cooking and cleaning.

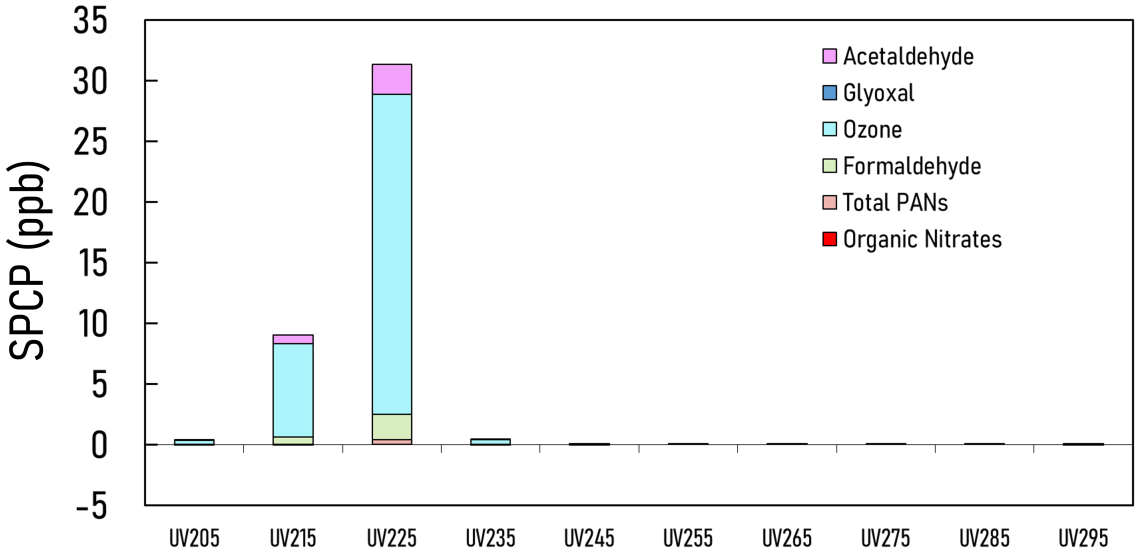

Figure 6.12: The average 'Secondary Product Creation Potential' (ppb) under a selection of different wavelength ranges between 7 am and 7 pm during the time when the lights are on. The baseline value (no lighting) has been subtracted from each of the wavelength ranges

Figure 6.13 shows that monoterpene cleaning following cooking has the highest SPCP value (33.0 ppb) of the six different scenarios. The no activity scenario and cooking had the second highest SPCP values (32.8 ppb). These observations suggest that monoterpene cleaning following cooking under the UV225 wavelength range is the most likely to produce secondary pollutants, however this increase (0.02 ppb) from no activity is minimal. As expected, ozone dominated the total SPCP concentration accounting for 26.8 ppb (86.5 %) in the bleach cleaning scenario. The scenario with the lowest SPCP value was bleach cleaning (31.0 ppb). The bleach cleaning following cooking scenario also had an SPCP value of 31.5 ppb. This indicates that the UV225 wavelength range can produce high concentrations of secondary pollutants. Cooking and cleaning have minimal contribution to secondary pollutant formation if a typical kitchen is exposed to UV225 wavelength.

The secondary chemistry can be scrutinised further by removing the SPCP value with no activity scenario from the other SPCP values (Figure 6.14). Positive (negative) values indicate an overall increase (decrease) in concentration for the activity compared to no activity for a particular pollutant.

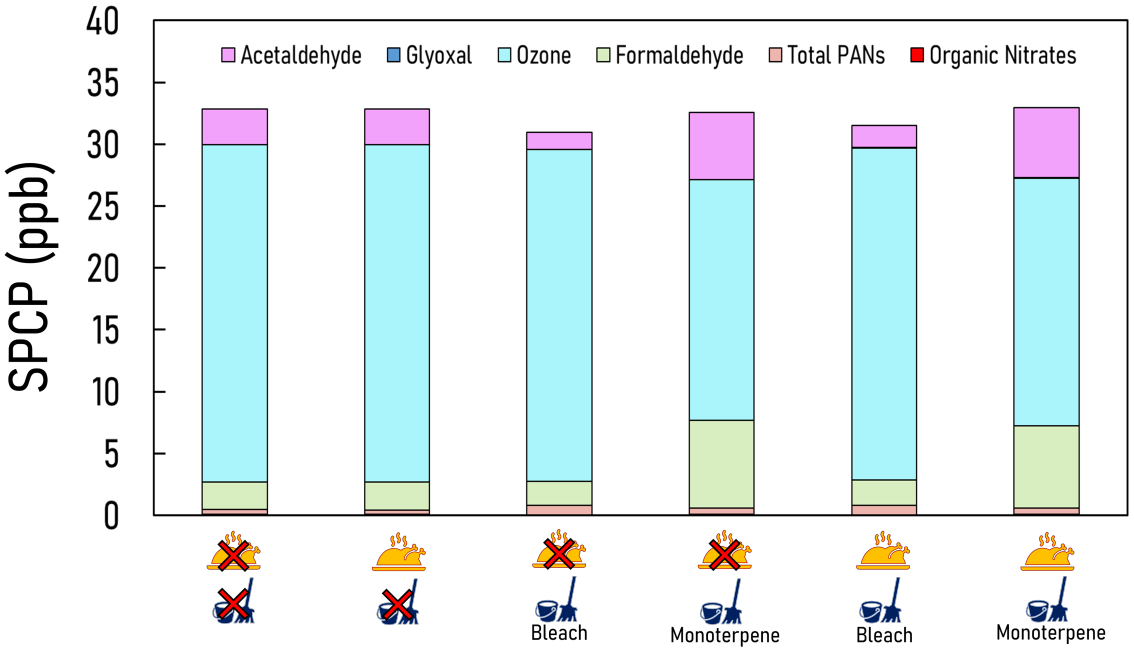

Figure 6.13: The average 'Secondary Product Creation Potential' (ppb) between the hours of 12 noon and 5pm for cooking and cleaning activities under our UV225 wavelength range. The emoticons indicate whether cooking or cleaning took place in that simulations. The baseline (dark) has been subtracted from the original SPCP value.

Figure 6.14 shows that the SPCP for scenarios involving monoterpene cleaning only increases if the increased concentrations of formaldehyde, acetaldehyde, glyoxal, PANs and organic nitrates outweigh ozone loss. For example, for monoterpene cleaning, the concentrations of formaldehyde, acetaldehyde and PANs increase by 7.6 ppb, but this is outweighed by a reduced ozone concentration (by 7.8 ppb). For bleach cleaning, acetaldehyde shows a loss compared to no activity (1.5 ppb), as do organic nitrates (0.01 ppb), formaldehyde (0.27 ppb) and ozone (0.45 ppb). PANs and glyoxal increase (0.3 ppb total), but are heavily outweighed by the loss in concentrations from the other pollutants. Cooking only shows a small decrease in organic nitrate concentration. This, again, shows that the primary source of secondary pollutant formation is from the UV225 wavelength range itself, with cooking and cleaning having little influence.

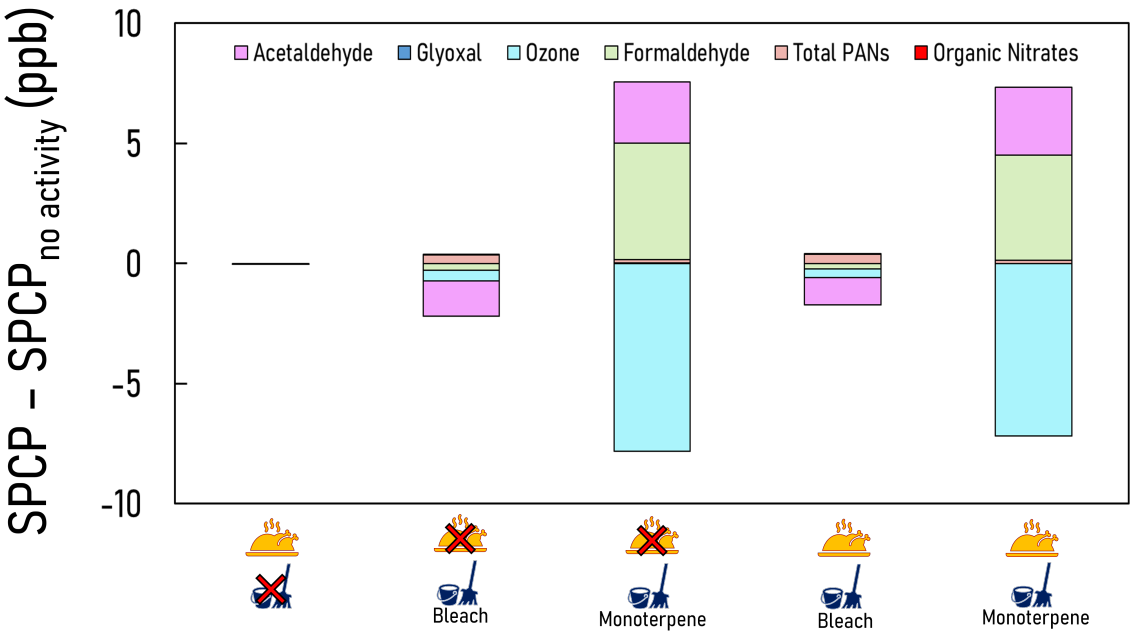

Figure 6.14: The average 'Secondary Product Creation Potential' (ppb) following subtraction of the no activity scenario between the hours of 12 noon and 5pm for cooking and cleaning activities for the UV225 wavelength range. The emoticons indicate whether cooking or cleaning took place in that simulations.

6.3.4 How Does Outdoor Pollution Affect the Impact of Far-UVC Lighting Indoors?

This section compares three different cities, London, Bergen and Milan, which have different outdoor diurnal profiles of O_3 and NO_x, to understand if they have an effect on key indoor species under far-UVC light exposure. These cities represent different concentrations of outdoor pollutants. Bergen has a low level of pollution, London has a medium level and Milan is highly polluted. The simulations assume the same parameters as described in Section 6.2.2.1 except the outdoor pollution profiles change for O_3 and NO_x for the different cities. There is attenuated outdoor light in these simulations, using the 'glass C' glass type (Shaw et al., 2023). For indoor lighting, incandescent and the UV225 wavelength range are simulated individually and compared. Figure 6.15 show the diurnal profiles of O_3 and NO_x for London, Bergen and Milan.

Figure 6.15 demonstrates that the outdoor profile of Milan is heavily polluted, primarily due to bad dispersion and traffic (Terry et al., 2014). These concentrations were measured

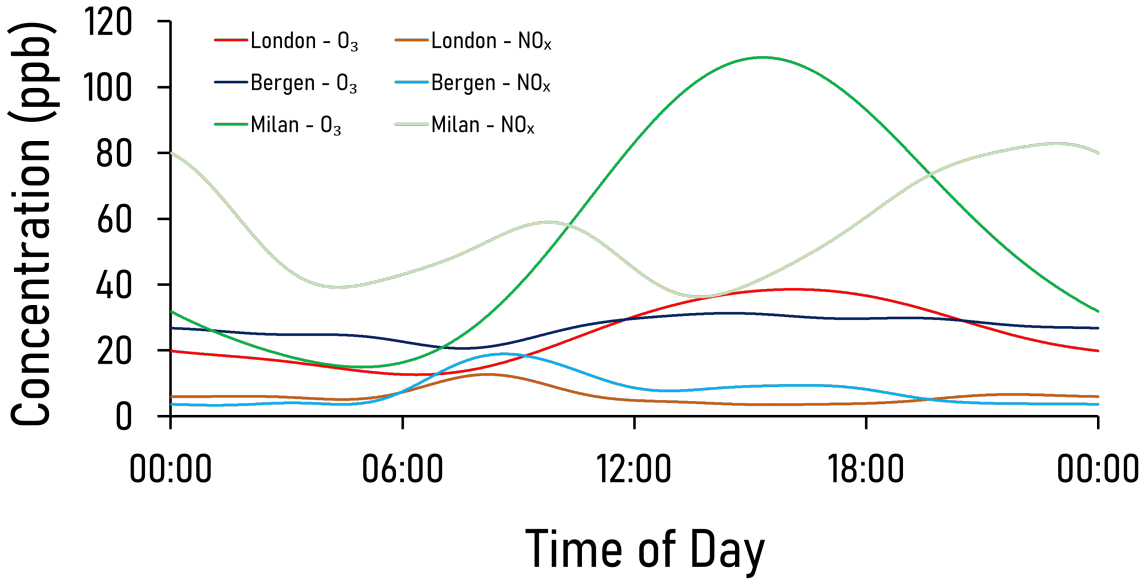

Figure 6.15: The outdoor diurnal concentrations (ppb) of O_3 and NO_x for London, Bergen and Milan.

in the summer of 2003 and represent extremely high levels of pollution (Sangiorgi et al., 2013). Maximum O_3 and NO_x concentrations in Milan reached approximately 109 and 83 ppb respectively, compared to Bergen which has a cleaner profile, with much lower maximum concentrations of O_3 and NO_x of approximately 31 and 19 ppb. The average indoor concentrations of key indoor species with varying outdoor pollution profiles with incandescent light and the UV225 wavelength range are shown in Figures 6.16 to 6.21.

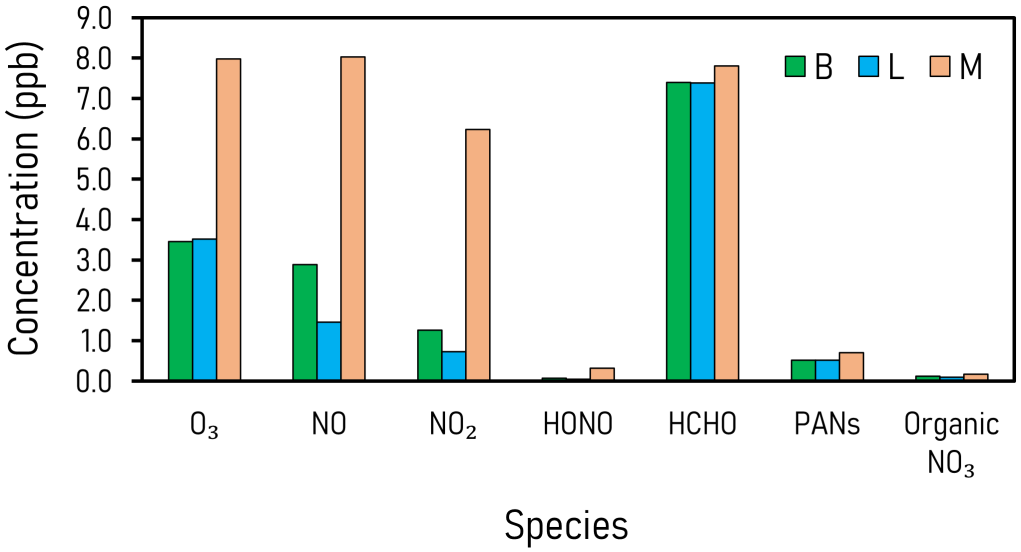

Figure 6.16: The average indoor concentration for O_3, NO, NO_2, HONO, HCHO, PANs and organic NO_3 (all in ppb) whilst the lights are on (7am to 7pm) under incandescent lighting with contrasting outdoor concentrations of O_3 and NO_x defined by measurements taken in different cities. The outdoor concentrations of O_3 and NO_x are diurnally averaged from a seasonal three-month variation, taken from July to September. The cities are Bergen (B), London (L) and Milan (M).

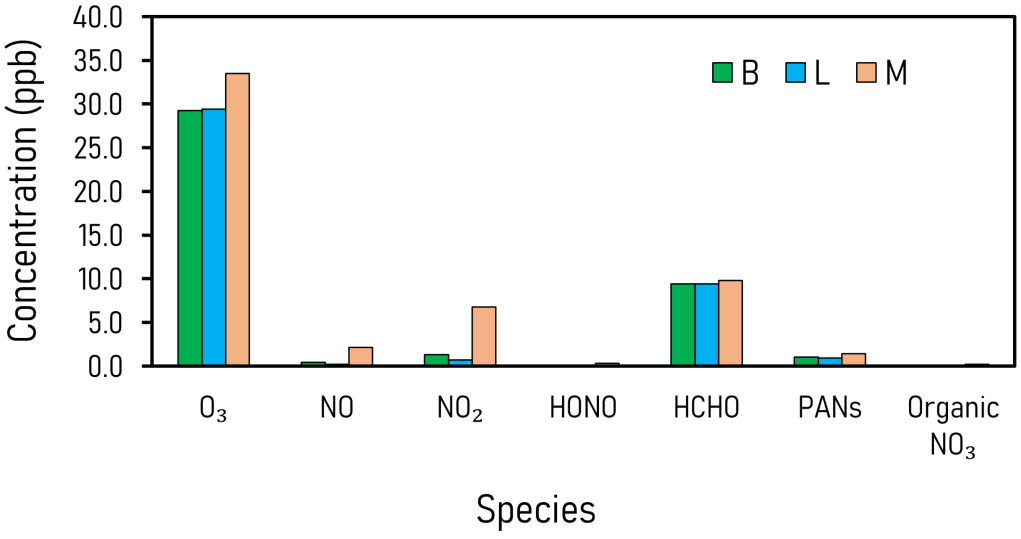

Figure 6.17: The average indoor concentration for O_3, NO, NO_2, HONO, HCHO, PANs and organic NO_3 (all in ppb) whilst the lights are on (7am to 7pm) under the UV225 wavelength range with contrasting outdoor concentrations of O_3 and NO_x defined by measurements taken in different cities. The outdoor concentrations of O_3 and NO_x are diurnally averaged from a seasonal three-month variation, taken from July to September. The cities are Bergen (B), London (L) and Milan (M).

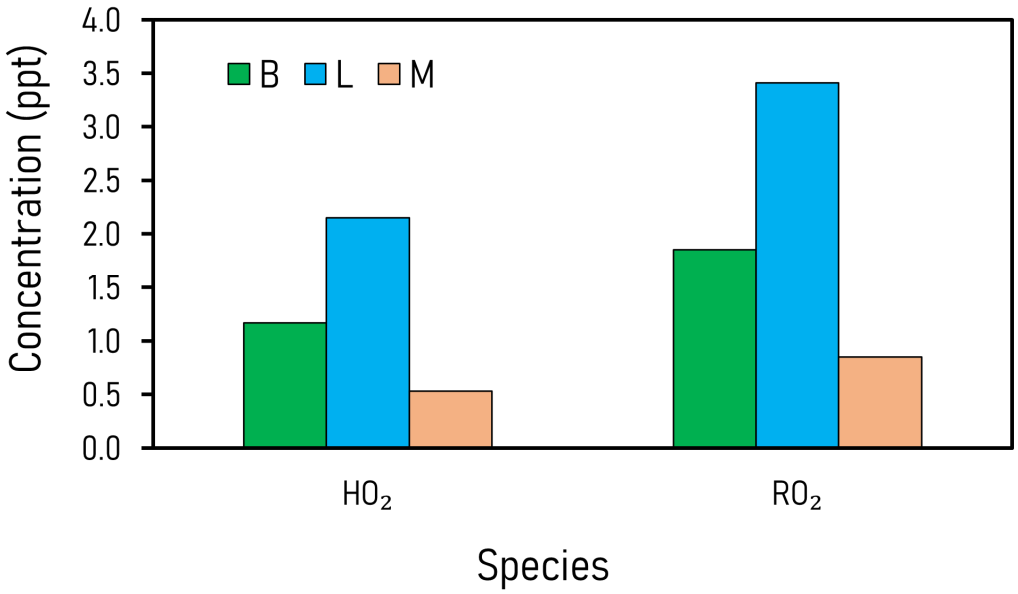

Figure 6.18: The average indoor concentration for HO_2 and RO_2 (all in ppt) whilst the lights are on (7am to 7pm) under incandescent lighting with contrasting outdoor concentrations of O_3 and NO_x defined by measurements taken in different cities. The outdoor concentrations of O_3 and NO_x are diurnally averaged from a seasonal three-month variation, taken from July to September. The cities are Bergen (B), London (L) and Milan (M).

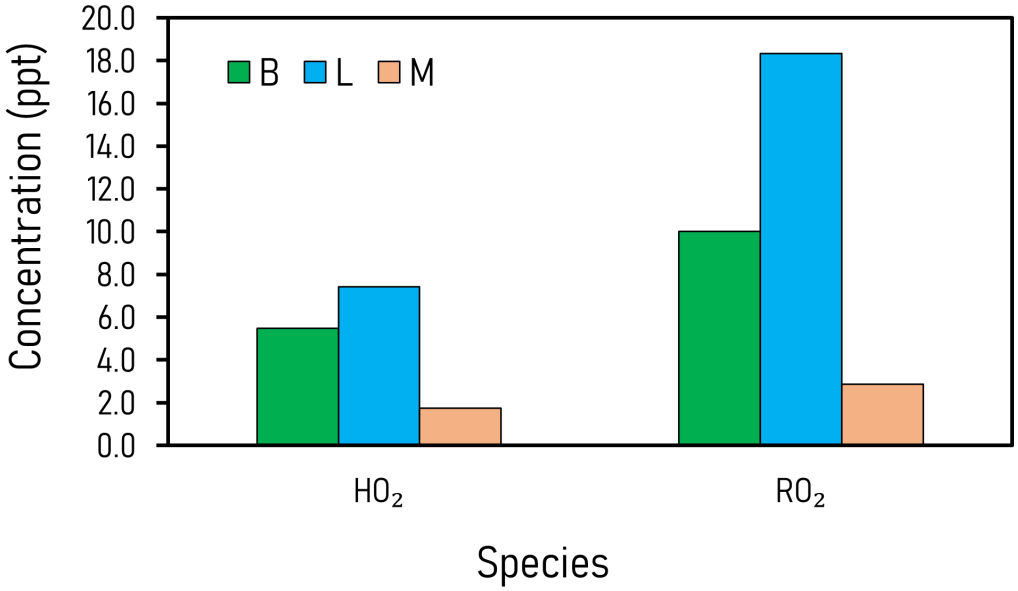

Figure 6.19: The average indoor concentration for HO_2 and RO_2 (all in ppt) whilst the lights are on (7am to 7pm) under the UV225 wavelength range with contrasting outdoor concentrations of O_3 and NO_x defined by measurements taken in different cities. The outdoor concentrations of O_3 and NO_x are diurnally averaged from a seasonal three-month variation, taken from July to September. The cities are Bergen (B), London (L) and Milan (M).

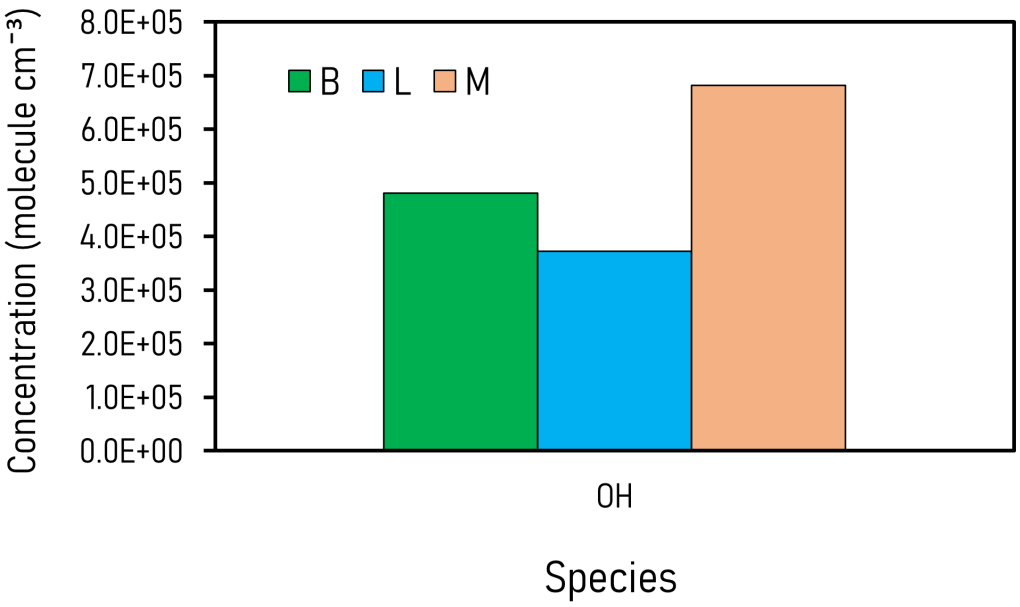

Figure 6.20: The average indoor concentration for OH (in molecule cm^{-3}) whilst the lights are on (7am to 7pm) under incandescent lighting with contrasting outdoor concentrations of O_3 and NO_x defined by measurements taken in different cities. The outdoor concentrations of O_3 and NO_x are diurnally averaged from a seasonal three-month variation, taken from July to September. The cities are Bergen (B), London (L) and Milan (M).

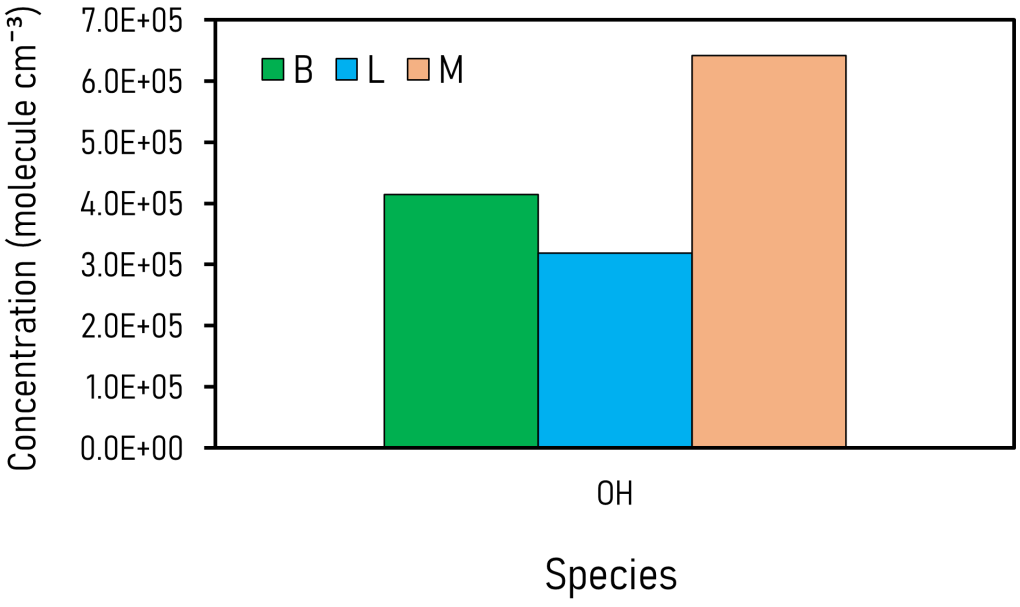

Figure 6.21: The average indoor concentration for OH (in molecule cm^{-3}) whilst the lights are on (7am to 7pm) under the UV225 wavelength range with contrasting outdoor concentrations of O_3 and NO_x defined by measurements taken in different cities. The outdoor concentrations of O_3 and NO_x are diurnally averaged from a seasonal three-month variation, taken from July to September. The cities are Bergen (B), London (L) and Milan (M).

Figures 6.16 to 6.21 demonstrate that outdoor pollution does have an effect on indoor environments exposed to the UV225 wavelength range. The scenario involving the incandescent light in Milan gave rise to the highest indoor OH concentration (6.8 x 10^5 molecule $cm^{-3)}$ (Figure 6.21). This is because the most important reaction in Milan for the formation of OH is HO_2 reacting with NO. The reaction rate for this reaction for incandescent light is 1.5 times higher than the reaction rate with UV225 light, resulting in a higher average OH concentration. This is because although HO_2 concentrations were higher for the UV225 light, the NO concentration was substantially lower due to the high ozone concentrations. The scenario involving the UV225 wavelength range in Milan yields the highest O_3 (33.5 ppb), formaldehyde (9.8 ppb), PANs (1.45 ppb) and organic NO_3 (0.19 ppb) (Figure 6.17) concentrations. The concentrations of O_3, formaldehyde, PANs and organic NO_3 had a percentage increase of approximately 329, 26, 114 and 12% respectively from the scenario in the same city compared with incandescent lighting. HONO concentrations in Milan for both lighting conditions were approximately 8 and 5 times higher than in London and Bergen respectively (Figures 6.16 and 6.17).

The concentrations of HO_2 and RO_2 in Milan with the UV225 wavelength range (1.8 and 2.9 ppt respectively) were lower than in Bergen (5.5 and 10.0 ppt respectively) and London (7.4 and 18.3 ppt respectively) with the same lighting (Figure 6.19). Since heatwaves are supposedly going to become more common due to the impact of climate change, high pollution events will occur more often, leading to high external ozone concentration (Moghani and Archer, 2020). This section has provided an outlook into the future as to how cleaning devices with the UV225 wavelength range can contribute to indoor chemistry with varying levels of outdoor pollution. It is determined that as pollution worsens outdoors, the concentrations of indoor pollutants including ozone, OH and formaldehyde increase. This pollutant increase is exacerbated whilst exposed to the UV225 wavelength range.

6.3.5 The Implications of Far-UVC on Indoor Air Pollution in an Occupied Office

To understand how far-UVC light could affect indoor workplaces, an office which contained 10 adults (each with a skin surface area of 2 m^2 (Fischer et al., 2013; Kruza and Carslaw, 2019)) was simulated. These simulations are detailed in Section 6.2.2.4.

Ozone is a major reactant with human skin oil indoors (Weschler and Nazaroff, 2023). Products released from this reaction include nonanal, decanal, acetone and 4-OPA (4-oxopentanal) (Liu et al., 2021). Since the UV225 wavelength range has been found to produce high concentrations of ozone indoors, it is expected the concentrations of these skin oil-ozone pollutants will also be elevated, particularly since this office is densely packed with occupants compared to the kitchen examples. The concentrations of these secondary pollutants as well as ozone (whilst the office is occupied between the hours of 9am and 5pm) is shown in Figure 6.22 with both lighting scenarios.

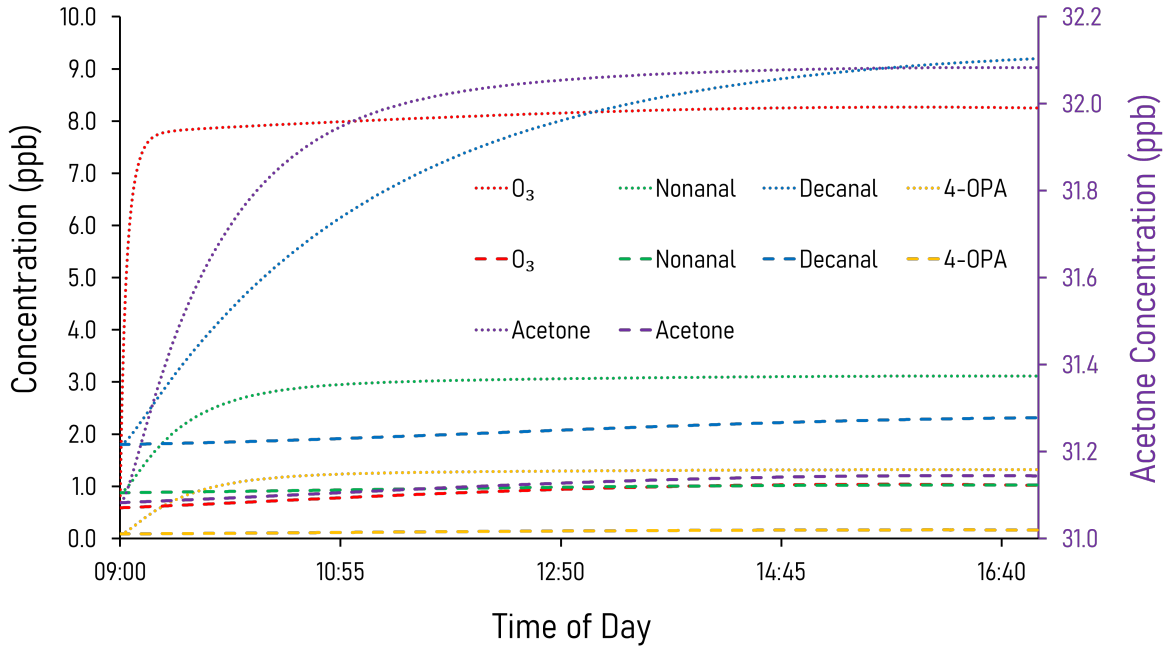

Figure 6.22: The indoor concentration for ozone and a variety of ozone-skin oil oxidation products (all in ppb) in an office occupied by 10 adults. The concentration of acetone is given on the right-hand axis. The concentration of the rest of the species are given on the left-hand axis. The species with a dotted line represent the simulation with UV225 and halogen lighting. The species with a dashed line represent the simulation with halogen lighting only.

Firstly, the addition of the UV225 wavelength range to the halogen light results in an increase in ozone concentration. The average ozone concentration of the halogen lighting simulation was 0.90 ppb, compared to 8.1 ppb for the UV225 and halogen lighting simulation, owing to the new O_2 photolysis reaction (J9). This ozone increase also resulted in an increase in the concentration of skin oil-ozone oxidation products. Maximum nonanal and decanal concentrations reached 3.1 and 9.2 ppb respectively in the UV225 wavelength range with halogen simulation, compared to 1.0 and 2.3 ppb respectively for the halogen lighting only simulation. Concentrations of nonanal and decanal kept gradually rising, throughout the day, and were highest in the afternoon in the UV225/halogen simulation. This is due to the ongoing reactions with the ozone produced from the UV225 wavelength range.

Average 4-OPA concentrations were approximately 12 times higher in the UV225/halogen simulation (1.2 ppb) than the halogen lighting only simulation (0.1 ppb). Acetone concentrations attained a maximum concentration of 32.1 ppb in the UV225/halogen scenario. This was only a small increase (0.1 ppb) in the acetone concentration (31.1 ppb) from the halogen lighting only scenario. The concentrations of some secondary indoor pollutants are also higher in the UV225/halogen scenario. Formaldehyde and PANs have average office concentrations of 5.1 and 0.38 ppb respectively. These are 11 and 27% higher than the concentrations of these pollutants (4.6 ppb and 0.30 ppb respectively) in the halogen only scenario. Organic NO_3 had slightly higher concentrations in the halogen only scenario than the UV225/halogen. Although the secondary pollutant concentrations aren't as extreme in this scenario, it would be safest to proceed with caution if air cleaning devices with the UV225 wavelength range are deployed in densely occupied environments.

6.4 Conclusions

The aim of this chapter was to evaluate photolysis in the UVC region (between 200 and 300 nm) through the construction of new photolysis rates (including the addition of a new photolysis coefficient, J9) to cover this wavelength range, implement them in

INCHEM-Py and explore how UV lighting can affect indoor air chemistry. The results have shown how lighting in the UV region can affect indoor secondary chemistry. The light in the far-UVC range can have a significant impact on indoor gas-phase concentrations of key species, especially ozone, which was found to be 11 times higher than if incandescent lighting was present. The concentrations of OH, HO_2 and RO_2 all increased noticeably upon exposure to this far-UVC light. Lights with a wavelength range of between 200 and 250 nm do affect indoor concentrations, with 220 to 230 nm being the most important. However, lights with a wavelength range of between 250 and 300 nm had little impact on indoor gas-phase concentrations (compared to incandescent lighting).

This chapter also considered the impact cooking and cleaning under far-UVC lighting had on indoor pollutant concentrations. Bleach cleaning caused indoor OH concentrations to increase as a result of the photolysis of HOCl under the UV225 wavelength range. RO_2 concentrations markedly increased upon monoterpene cleaning during far-UVC exposure. Monoterpene cleaning caused a sharp decrease in ozone concentration through ozonolysis reactions with limonene, α-phellandrene, γ-terpinene and other monoterpenoid species. Bleach cleaning and cooking under far-UVC exposure also caused an increase to HO_2 concentrations. However, from the resultant secondary product creation potential analysis, it was determined that the UV225 lamp itself was the cause of the production of secondary products as opposed to the cooking and cleaning. If anything, the household activities decreased secondary pollutant concentrations during exposure to the UV225 wavelength range. This chapter also identified how polluted cities can contribute to indoor air quality and affect indoor pollutant concentrations further when far-UVC lamps are used.

Further experimental studies need to be performed to understand how far-UVC photochemistry affects indoor environmental to further strengthen modelling studies. This includes using different intensity lamps, understanding the transmission of the lights and determining how far the light can move away from its source. One light may also not be particularly efficient in a larger room, where more lights would be potentially required

for increased pathogen reduction efficacy. Despite the apparent evidence that light at 222 nm doesn't cause harm to human health, it is important to still consider how it can and may affect indoor air quality. The results have shown that light at 222 nm can result in high indoor concentrations of ozone which can lead to the creation of secondary pollutants which can be potentially harmful to human health.

This chapter has found that UV225 wavelength range can significantly affect indoor chemistry in comparison to the UV255 wavelength range which showed little impact. It has also shown that, linking back to Chapter 4, surface composition plays an important role in indoor chemistry when exposed to air cleaning devices. In review and in connection with recent health data, the 222 nm lamp affects indoor chemistry but is supposedly safe for human health, however, the 254 nm lamp does little to affect indoor chemistry but can have severe implications on human health upon exposure. It is worth noting the mode that these cleaning devices are used in too, where, different irradiances and number of lamps can increase or decrease exposure. Cleaning with light at 222 nm should preferably be undertaken in an unoccupied room to avoid health complications from the light itself and the resultant chemistry.

Chapter 7

Summary, Conclusions and Proposals for Future Study

7.1 Addressing the Research Gap

Indoor air chemistry is complex. There are numerous sources of indoor air pollution, with many of them playing a key role in the gas-phase chemistry. Identifying which sources are the most important and contribute most to indoor air pollution is challenging. Recently, outdoor atmospheric scientists have started to shift their interest more towards indoor air, since this is where we spend approximately 90% of our lives (Klepeis et al., 2001) and receive most of our exposure to air pollution. Field campaigns including HOMEChem (Farmer et al., 2019), CASA (Farmer et al., 2024) and IMPECCABLE (Davies et al., 2023) have enabled scientists to make more detailed assessments as to how common household activities including cooking and cleaning can affect indoor air pollution in homes (Reidy et al., 2023; Mattila et al., 2020a). These experimental campaigns are critical so that computational models can probe indoor air chemistry and provide deeper insights. With the field of indoor air becoming more prominent (especially since the COVID-19 pandemic), it is important to be able to use computational models to identify impacts of indoor pollution, beyond those that field experiments are able to probe.

This thesis aimed to further develop and evaluate a detailed indoor air model to evaluate

different sources of indoor air pollution. The objectives of the thesis were to determine how surface chemistry, cooking, cleaning and UVC photochemistry contribute to indoor VOC and radical concentrations, and secondary pollutant formation. It also explored how indoor air pollutants released from cooking and cleaning contribute to outdoor air pollution in urban communities through newly developed 'near-field concentrations'.

7.2 Summary of Key Findings

The INdoor CHEmical Model in Python better represents chemical transformations and processes for; surface deposition onto a range of materials and rooms, including the deposition of ozone and hydrogen peroxide (Chapter 4); indoor to outdoor pollutant transfer and the impact on outdoor air quality in an urban community (Chapter 5); and UVC photochemistry from air cleaning devices, including the addition of a new photolysis reaction (Chapter 6).

In Chapter 4, nine materials were added into the model for ozone deposition, and six materials were added for hydrogen peroxide deposition. Tailored surface area-to-volume ratios were developed for a bedroom, a kitchen and an office. The kitchen had the smallest surface area-to-volume ratio whereas the office had the largest. The largest surface area-to-volume ratio in all three rooms was painted surfaces.

The results showed that surfaces which had low deposition velocities had little influence on concentrations of key indoor species. However, skin, soft fabrics and plastic affected modelled concentrations. The OH concentration was highest in an occupied kitchen compared to the other two rooms, because ozone has a higher concentration resulting in less deposition, meaning more OH is made through the resultant chemistry.

Chapter 4 also showed that the highest concentrations of short and long chained aldehydes were found in the kitchen (6.7 ppb), compared to the bedroom (5.8 ppb) and the office (4.8 ppb). These aldehyde emissions were primarily from interactions following ozone deposition, since hydrogen peroxide deposition had little impact.

Chapter 5 analysed the impact of indoor activities, including cooking and cleaning, on outdoor concentrations. The concept of a near-field concentration was introduced, which enabled indoor pollutants to be tracked as they left the building envelope. A ten-house investigation was undertaken to explore the temporal and spatial variability of indoor concentrations in houses with varying lifestyle routines. The ten-house analysis also enabled an investigation into how near-field concentrations can accumulate on a street at different times of the day. Near-field propane and isobutane were good indicators for cooking, whereas, chloroform was a good indicator for bleach cleaning. Along a 140 m street, maximum downwind near-field concentrations of propane increased by 619% at 3 pm: outdoor concentrations were highest adjacent to the houses with the highest air exchange rates. Maximum downwind near-field concentrations of chloroform increased by 754% at 8 am. The emissions released from these houses were scaled up and compared to overall UK VOC emissions. It was found that cooking contributed approximately 0.69% of the total yearly NMVOCs emitted in the UK (5403 tonnes) and cleaning contributed 0.16% (1229 tonnes). The emissions from cooking and cleaning was determined to be 29% of NMVOC emissions released from traffic in the UK.

In Chapter 6, absorption cross sections and quantum yields have been combined with newly determined irradiance fluxes, to determine 45 photolysis rates between the wavelength range of 200 and 300 nm. A new photolysis coefficient, J9, has also been implemented into the model to account for the photodissociation of O_2 (Yoshino et al., 1992) between 200 and 242 nm.

Light with a wavelength between 220 and 230 nm had the most significant effect on key indoor gas-phase species' concentrations. Indoor ozone concentrations rose from 1.0 ppb to 27.2 ppb within 45 minutes of the UV225 light being switched on. This increase in ozone subsequently led to elevated OH, HO_2 and RO_2 concentrations from the resultant chemistry. The increase in ozone was primarily caused by the photolysis of oxygen forming ground state oxygen atoms, leading to the formation of ozone. Light between the wavelengths of between 210 and 220 nm also affected indoor ozone radical concentrations, elevating ozone and OH to a maximum of 11.3 ppb and 8.8 x 10^4 molecule cm^{-3}

respectively. UVC lighting in the wavelength ranges of between 200 to 210 nm and 230 to 240 nm had an observable effect on indoor gas-phase concentrations, but lighting between 240 and 300 nm had little to no effect on these species' concentrations.

7.3 Current and Future Implications of Indoor Air Pollution

Bekö et al. (2020) described potential topics for future indoor air chemistry research, including better understanding of the impacts of chemical transformations, building environments (materials and in-home behaviour), building occupants, microbial activity, particles, source apportionment and modelling (Bekö et al., 2020). These topics will increase in importance as ambient pollution continues to improve with electrification of the vehicle fleet (Grange et al., 2020). Climate change is also expected to increase ambient ozone concentrations even further (Moghani and Archer, 2020), but the impacts on indoor air quality are still unclear.

A new framework, led by a European COST Action Network project, INDAIRPOLLNET, has been created in order to provide instructions and share a blueprint for the future analysis of chemistry in indoor environments, both experimentally and through modelling (Carslaw et al., 2024). The INDAIRPOLLNET network suggested five key future research areas to consider for better understanding indoor air chemistry:

- Reactivity in Indoor Environments
- Mapping of Organic Indoor Constituents
- The Role of Occupancy Indoors
- Indoor Modelling
- Novel Indoor Technologies and Materials

Key sources of reactivity indoors include outdoor air (where ozone and $PM_{2.5}$ ingress indoors), cooking, cleaning and people (Weschler and Carslaw, 2018). This thesis has evaluated each of these sources and provided predicted concentrations of radical species from simulations. As environmental conditions change over time, there needs to be a better understanding of the subsequent impacts on indoor air quality, to facilitate appropriate mitigation policies.

Organic constituents indoors are key to indoor chemistry. Understanding which VOCs derive from different sources is key to limiting exposure. This thesis has begun to differentiate VOCs between sources originating from indoors and outdoors via the inclusion of near-field concentrations. This has been followed up by the calculation of yearly NMVOC emissions from UK households, which can lead into a potential indoor emissions inventory detailing VOCs which originate from various sources (Carslaw et al., 2024). These VOCs from household activities can then be tracked to analyse how they may react and degrade indoors and outdoors.

Current implications for indoor modelling include how we best represent the variety of different factors that affect indoor air pollutant concentrations. For example, air exchange, relative humidity, temperature, photolysis and outdoor concentrations are all key parameters to consider in indoor models (Carslaw et al., 2024). As discussed in Chapter 2, MOCCIE has set the tone for future indoor modelling collaboration and development (Shiraiwa et al., 2019). This thesis has contributed to the addition of more relevant outdoor concentrations, which have been collated from sources globally and implemented into INCHEM-Py. Kinetic data is also required to further reduce uncertainty of indoor air models, particularly for reactions with unknown rate coefficients. We can also learn from outdoor air modelling (Carslaw et al., 2024), which can provide methodology to implement to understand the impact of indoor activities, such as dispersion in the near-field of buildings (McHugh et al., 1997).

Recent technological advancement has led to new electrical devices, furnishings, surfaces and consumer products in our homes (Beel, 2023), all of which can release VOCs (Van Tran et al., 2020). Surfaces and furnishings are a key source of indoor pollution

and reactivity (Ault et al., 2020). Some common indoor materials have been categorically added into INCHEM-Py in this thesis, with a focus on simulating oxidant deposition. This now enables users to simulate chosen surfaces and evaluate which would be best for controlling radical concentrations indoors and determine whether surfaces are sources or sinks of indoor air pollutants (Carslaw et al., 2024). Other novel developments include air cleaning devices and air purifiers. This thesis has analysed potential deployment of these UV air cleaning devices in various indoor settings to ascertain their respective impact on indoor chemistry. It is important that as technology develops, so does our capability to quantify whether it contributes to, or alleviates, indoor air pollution.

7.4 Proposals for Future Study

In a rapidly changing world, computational models need to stay up to date with the latest parameters to ensure that they are fit for purpose and provide relevant information. This thesis has updated INCHEM-Py with three new modules, relevant to increasingly important areas in indoor air chemistry (surfaces, indoor-outdoor exchange and UVC photolysis).

To further this work, experimental work needs to be carried out so that more oxidants could be added to the surface chemistry framework. An example of this could be chlorine dioxide (ClO_2), which is sometimes used as an airborne disinfectant (Wang et al., 2020b). Similarly, to hydrogen peroxide and ozone, chlorine dioxide can deposit onto surfaces and induce gas-phase transformations producing secondary pollutants. Hubbard et al. (2009) found that ozone deposition was much faster than chlorine dioxide deposition onto common household surfaces, however, chlorine dioxide has a faster deposition velocity for a particle board and a ceiling tile. Despite this, there is a lack of literature focusing on chlorine dioxide deposition, and yields of resultant secondary pollutant formation. Other oxidants used for disinfection whose deposition need to be more fully considered include formaldehyde, acetaldehyde and hypochlorous acid (HOCl).

We are also lacking information on the deposition velocities of indoor pollutants. Cur-

rently, deposition velocities are estimated for most indoor species. Surface chemistry is a key element of indoor chemistry, so more research is needed to understand how different species deposit onto, and interact with, selected surfaces and how this deposition, or respective off-gassing, affects indoor air quality.

A requirement for more data from laboratory studies is also needed to further our understanding of indoor chemistry. For example, most of the rate coefficients in the MCM are currently estimated based on a defined protocol (Jenkin et al., 1997) and not laboratory experiments. It is important to be able to categorise rate coefficients for key reactions indoors, including the ozonolysis of terpenes, reactions of VOCs with OH and the reaction of secondary pollutants with oxidants. Defining kinetic data for reactions that drive indoor chemistry is important for models to be able to more accurately predict concentrations of indoor species.

With the recent popularity of air cleaning devices, more experimental studies need to be performed. We need to be able to monitor the concentrations of radicals and VOCs indoors, and especially ozone produced from these devices. With the need for a cleaner, healthier environment becoming more apparent, these devices need to be thoroughly tested in order to be safe for not only indoor air quality but also human health. Understanding how these air cleaners generate pollutants indoors and within different buildings and rooms, is important for computational models to be able to predict how they affect indoor air quality.

In the future, a Monte Carlo analysis could be carried out on the housing analysis from the indoor-outdoor exchange research performed in Chapter 5. An analysis with 1000 houses with varying input parameters could be illustrative, including: if/when people cook or clean during the day, occupancy, air change rates, materials and respective surface area-to-volume ratio, temperature, relative humidity, light typing, whether an air cleaner is used or not, distance between houses and other building parameters (Baeza-Romero et al., 2022). This type of analysis would further determine what impact those parameters may have on 'near-field' concentrations for certain VOCs. It would highlight which species would have particularly high near-field concentrations at certain times of

the day and how these species can affect neighbouring homes or even villages or communities. More in-depth building parameters would also help the Monte Carlo analysis, where surface area-to-volume ratios of rooms and furniture, building materials used in construction and air change rate data would all be beneficial for indoor air models.

The work conducted in Chapter 5 begins to build a framework to understand what happens once these indoor VOCs leave the building envelope. Future extensions of this chapter include development of a housing emissions inventory from a variety of indoor activities. This exercise would allow quantification of concentrations of VOCs at varying distances once they egress from a home (or building), to understand how house pollution at a city-scape level may look.

A few primary VOCs are categorised for their toxicity. For example, acetaldehyde is known to be carcinogenic and is suspected to be a mutagenic (Salthammer, 2023). Acute effects to the human body were noticed after one hour of exposure to 795 ppb of acetaldehyde in Canada (Health Canada, 2017). Despite not reaching these concentrations indoors, there needs to be better links between the predicted concentrations and potential health effects. Combining experimental and computational data can help predict toxicological effects of poor indoor air quality (such as an intense cleaning event). This work with the model could be linked with up-to-date sensor technology, which would identify periods of poor indoor air quality and automatically open a window or switch on a ventilator fan to let the outdoor air replace the poor indoor air.

There is a need for toxicological data on the effects of indoor air pollutants. Secondary pollutants formed from oxidative reactions can potentially affect human health. It is important to be able to characterise these pollutants for their toxicity at relevant exposure levels. Similarly, we know little about the synergistic effects of these products. Toxicological data is also important for ambient pollutants indoors and how they affect different human health. Some components within consumer products have already been identified as endocrine disruptors, including parabens and phthalates (Dodson et al., 2012). The understanding of what forms these pollutants is vital to limiting exposure and living in healthier, cleaner indoor environments. This can also relate to the introduction of

indoor air quality regulations to prevent and limit such exposure.

In summary, this thesis has shown how modelling studies can be used to explore the chemistry of indoor air pollution. The development of the model has enabled novel research into how various types of pollutant sources can affect the concentrations of gas-phase species in the indoor environment. This work will help to build on the importance of indoor air chemistry and help to find ways to improve indoor air quality in the future.

Appendix A

Appendix

A.1 2,5-Dimethylbenzaldehyde Reaction Scheme

The following reactions give the reaction scheme for the degradation of 2,5-dimethylbenzaldehyde (denoted as TM125BCHO). The term on the left represents the rate coefficient (cm^3 $molecule^{-1}$ s^{-1}). The reactants and products of each reaction are given respectively below in Table A.1. All species are given as MCM names as input into the additional model schemes. For those species not located in the MCM, a custom name is given.

Table A.1: The 17 reactions involved in the degradation of 2,5-dimethylbenzaldehyde.

Rate Coefficient	Reactants	Products
J19	TM125BCHO	PXY1O2+HO2+CO
KNO3AL	TM125BCHO+NO3	TM125BCO3+HNO3
2.76 x 10^{-11}	TM125BCHO+OH	TM125BCO3
J18	TM125BCHO	TM125BCO3+HO2
KAPHO2*0.44	TM125BCO3+HO2	PXY1O2+OH
KAPHO2*0.15	TM125BCO3+HO2	TM125BCO2H+O3
1.00 x 10^{-11}*0.30*RO2	TM125BCO3	TM125BCO2H
continued on next page		

Rate Coefficient	**Reactants**	**Products**
KAPHO2*0.41	TM125BCO3+HO2	TM125BCO3H
KAPNO	TM125BCO3+NO	PXY1O2+NO2
KFPAN	TM125BCO3+NO2	TM125BPAN
KRO2NO3*1.74	TM125BCO3+NO3	PXY1O2+NO2
1.00 x 10^{-11}*0.70*RO2	TMB125BCO3	PXY1O2
7.92 x 10^{-13}	TM125BCO2H+OH	PXY1O2
3.86 x 10^{-12}	TM125BCO3H+OH	TM125BCO3
J41	TM125BCO3H	PXY1O2+OH
KBPAN	TM125BPAN	TM125BCO3+NO2
1.06 x 10^{-12}	TM125BPAN+OH	PXY1OOH+CO+NO2

A.2 2-Nonenal Reaction Scheme

The following reactions give the reaction scheme for the degradation of 2-nonenal (denoted as TNON2ENECHO). The term on the left represents the rate coefficient (cm^3 $molecule^{-1}$ s^{-1}). The reactants and products of each reaction are given respectively below in Table A.2. All species are given as MCM names as input into the additional model schemes. For those species not located in the MCM, a custom name is given.

Table A.2: The 138 reactions involved in the degradation of 2-nonenal.

Rate Coefficient	Reactants	Products
J18*1.44	TNON2ENECHO	C6H13CHO+CO+CO+HO2+HO2
0.5*43.5 x 10^{-12}	TNON2ENECHO+OH	C8DBCO3
0.25*43.5 x 10^{-12}	TNON2ENECHO+OH	C6CO2COHCHO
0.25*43.5 x 10^{-12}	TNON2ENECHO+OH	C6COHCO2CHO
2.05 x 10^{-18}*0.5	TNON2ENECHO+O3	C6H13CHO+GLYOOBEX
2.05 x 10^{-18}*0.5	TNON2ENECHO+O3	C7H14OOBEX+GLYOX
6.0 x 10^{-15}*0.65	TNON2ENECHO+NO3	C8DBCO3+HNO3
6.0 x 10^{-15}*0.175	TNON2ENECHO+NO3	C6CO2CNO3CHO
6.0 x 10^{-15}*0.175	TNON2ENECHO+NO3	C6CNO3CO2CHO
KAPHO2*0.15	C8DBCO3+HO2	C8DBCOOH+O3
KAPHO2*0.44	C8DBCO3+HO2	C6H13CHO+HO2+CO+OH
KAPHO2*0.41	C8DBCO3+HO2	C8DBCOHO2
KFPAN	C8DBCO3+NO2	C8DBPAN
KAPNO	C8DBCO3+NO	C6H13CHO+HO2+CO+NO2
KRO2NO3*1.74	C8DBCO3+NO3	C6H13CHO+HO2+CO+NO2
1.00 x 10^{-11}*RO2*0.7	C8DBCO3	C6H13CHO+HO2+CO
1.00 x 10^{-11}*RO2*0.3	C8DBCO3	C8DBCOOH
6.48 x 10^{-11}	C8DBCOOH+OH	C6H13CHO+HO2+CO

continued on next page

Rate Coefficient	Reactants	Products
1.97 x 10^{-11}	C8DBCOHO2+OH	C8DBCO3
J41	C8DBCOHO2	C6H13CHO+HO2+CO+OH
1.65 x 10^{-11}	C8DBPAN+OH	C6H13CHO+CO+CO+NO2
KBPAN	C8DBPAN	C8DBCO3+NO2
KRO2NO*0.957	C6CO2COHCHO+NO	C6CHOCOHCHO+NO2
KRO2NO*0.043	C6CO2COHCHO+NO	C6CNO3COHCHO
KRO2NO3	C6CO2COHCHO+NO3	C6CHOCOHCHO+NO2
KRO2HO2*0.625	C6CO2COHCHO+HO2	C6CHO2COHCHO
8.80 x 10^{-13}*RO2*0.60	C6CO2COHCHO	C6CHOCOHCHO
8.80 x 10^{-13}*RO2*0.20	C6CO2COHCHO	C6COHCOHCHO
8.80 x 10^{-13}*RO2*0.20	C6CO2COHCHO	C6COCOHCHO
KDEC	C6CHOCOHCHO	C6H13CHO+GLYOX+HO2
J41	C6CHO2COHCHO	C6CHOCOHCHO+OH
J17	C6CHO2COHCHO	C6CHOCOHCHO+OH
9.53 x 10^{-11}	C6CHO2COHCHO+OH	C6COCOHCHO+OH
4.55 x 10^{-11}	C6CNO3COHCHO+OH	C6COCOHCHO+NO2
J17	C6COCOHCHO	C6CNO3CHO+HO2+CO
KNO3AL*2.4	C6CNO3CHO+NO3	C6CNO3CO3+HNO3
3.55 x 10^{-12}	C6CNO3CHO+OH	C6CHOCHO+NO2
J56*10	C6CNO3CHO	C6CNO3CO3
KDEC	C6CHOCHO	C6H13CHO+HO2+CO
KAPHO2*0.44	C6CNO3CO3+HO2	C6H13CHO+NO2+OH
KAPHO2*0.15	C6CNO3CO3+HO2	C6CNO3COOH+O3
KAPHO2*0.41	C6CNO3CO3+HO2	C6CNO3CO3H
KAPNO	C6CNO3CO3+NO	C6H13CHO+NO2+NO2
KFPAN	C6CNO3CO3+NO2	C6CNO3CONO3
KRO2NO3*1.74	C6CNO3CO3+NO3	C6H13CHO+NO2

continued on next page

Rate Coefficient	Reactants	Products
1.00 x 10^{-11}*0.7*RO2	C6CNO3CO3	C6H13CHO+NO2+NO2
1.00 x 10^{-11}*0.3*RO2	C6CNO3CO3	C6CNO3COOH
3.14 x 10^{-13}	C6CNO3COOH+OH	C6H13CHO+NO2
3.77 x 10^{-12}	C6CNO3CO3H+OH	C6CNO3CO3
J41	C6CNO3CO3H	C6H13CHO+NO2+OH
KBPAN	C6CNO3CONO3	C6CNO3CO3+NO2
1.43 x 10^{-13}	C6CNO3CONO3+OH	C6H13CHO+CO+NO2+NO2
7.01 x 10^{-11}	C6COHCOHCHO+OH	C6COCOHCHO+HO2
J17	C6COHCOHCHO	C6COHCHO+CO+HO2+HO2
J15	C6COCOHCHO	C6COCHO+CO+HO2+HO2
KNO3AL*4.0	C6COCOHCHO+NO3	C6COCOHCO3+HNO3
2.45 x 10^{-11}	C6COCOHCHO+OH	C6COCOHCO3
KAPHO2*0.56	C6COCOHCO3+HO2	C6COCOHCO3H
KAPHO2*0.44	C6COCOHCO3+HO2	C6COCHO+HO2+OH
KAPNO	C6COCOHCO3+NO	C6COCHO+HO2+NO2
1.00 x 10^{-11}*RO2	C6COCOHCO3	C6COCHO+HO2
KRO2NO3*1.74	C6COCOHCO3+NO3	C6COCHO+HO2+NO2
KFPAN	C6COCOHCO3+NO2	C6COCOHCOCONO3
KFPAN	C6COCOHCOCONO3	C6COCOHCO3+NO2
3.74 x 10^{-12}	C6COCOHCOCONO3+OH	C6COCHO+NO2+CO
J34	C6COCHO	C6H13CO3+HO2+CO
KNO3AL*2.4	C6COCHO+NO3	C6H13CO3+HNO3+CO
1.9 x 10^{-12}*exp(575/temp)	C6COCHO+OH	C6H13CO3+CO
J22	C6COCOHCO3H	C6H13CO3+HCOCO3H+HO2
7.34 x 10^{-12}	C6COCOHCO3H+OH	C6COCOHCO3
J41	C6COCOHCO3H	C6COCHO+HO2+HO
KNO3AL*2.4	C6COHCHO+NO3	C7OHCO3+HNO3

continued on next page

Rate Coefficient	Reactants	Products
J17	C6COHCHO	C6H13CHO+CO+HO2+HO2
1.7×10^{-11}	C6COHCHO+OH	C7OHCO3
KAPHO2*0.44	C7OHCO3+HO2	C6H13CHO+OH+HO2
KAPNO	C7OHCO3+NO	C6H13CHO+NO2+HO2
KRO2NO3*1.74	C7OHCO3+NO3	C6H13CHO+NO2+HO2
1.00×10^{-11}*RO2	C7OHCO3	C6H13CHO+HO2
KFPAN	C7OHCO3+NO2	C7OHCO3NO2
KAPHO2*0.56	C7OHCO3+HO2	C7OHCO2OH
KBPAN	C7OHCO3NO2	C7OHCO3+NO2
2.34×10^{-12}	C7OHCO3NO2+OH	C6H13CHO+CO+NO2
J41	C7OHCO2OH	C6H13CHO+OH+HO2
9.34×10^{-12}	C7OHCO2OH+OH	C7OHCO3
KDEC*0.18	C7H14OOBEX	C7H14OO
KDEC*0.57	C7H14OOBEX	HEXAO2+CO+OH
KDEC*0.125	C7H14OOBEX	NC6H14
KDEC*0.125	C7H14OOBEX	HEXAO2+HO2
6.00×10^{-18}*H2O	C7H14OO	C6H13CHO+H2O2
1.00×10^{-17}*H2O	C7H14OO	C6H13CO2H
7.00×10^{-14}	C7H14OO+SO2	C6H13CHO+SO3
1.00×10^{-15}	C7H14OO+NO2	C6H13CHO+NO3
1.00×10^{-14}	C7H14OO+NO	C6H13CHO+NO2
1.20×10^{-15}	C7H14OO+CO	C6H13CHO
KRO2HO2*0.625	C6CO2CNO3CHO+HO2	C7O2HCCHONO3
8.80×10^{-13}*RO2*0.6	C6CO2CNO3CHO	C7HOCCHONO3
8.80×10^{-13}*RO2*0.2	C6CO2CNO3CHO	C7OCCHONO3
KRO2NO3	C6CO2CNO3CHO+NO3	C7HOCCHONO3+NO2
KRO2NO	C6CO2CNO3CHO+NO	C7HOCCHONO3+NO2

continued on next page

Rate Coefficient	**Reactants**	**Products**
8.80 x 10^{-13}*RO2*0.2	C6CO2CNO3CHO	C7OHCCHONO3
KDEC	C7HOCCHONO3	C6H13CHO+GLYOX+NO2
KNO3AL*4.0	C7OHCCHONO3+NO3	C6CO2CNO3CHO+HNO3
3.45 x 10^{-12}	C7OHCCHONO3+OH	C6CO2CNO3CHO
J17	C7OHCCHONO3	C7HOCCHONO3+OH
J41	C7OHCCHONO3	C7HOCCHONO3+OH
KNO3AL*4.0	C7O2HCCHONO3+NO3	C6CO2CNO3CHO+HNO3
3.45 x 10^{-12}	C7O2HCCHONO3+OH	C6CO2CNO3CHO
J17	C7O2HCCHONO3	C7HOCCHONO3+OH
J41	C7O2HCCHONO3	C7HOCCHONO3+OH
KNO3AL*4.0	C7OCCHONO3+NO3	C6CO2CNO3CHO+HNO3
4.27 x 10^{-12}	C7OCCHONO3+OH	C6CO2CNO3CHO
J34	C7OCCHONO3	C6CO2CNO3CHO+CO+HO2
J55	C7OCCHONO3	C7OCOCHO+NO2
KDEC*0.5	C7OCOCHO	C6H13CO3+GLYOX
KDEC*0.5	C7OCOCHO	C6COCHO+CO+HO2
KRO2HO2*0.625	C6CNO3CO2CHO+HO2	C7NO3CO2HCHO
8.80 x 10^{-13}*RO2*0.2	C6CNO3CO2CHO	C6CNO3COHCHO
8.80 x 10^{-13}*RO2*0.6	C6CNO3CO2CHO	C7NO3COCHO
8.80 x 10^{-13}*RO2*0.2	C6CNO3CO2CHO	C7OCCHONO3
KRO2NO3	C6CNO3CO2CHO+NO3	C7NO3COCHO+NO2
KRO2NO	C6CNO3CO2CHO+NO	C7NO3COCHO+NO2
KDEC	C7NO3COCHO	C6H13CHO+GLYOX+NO2
KNO3AL*4.0	C7NO3CO2HCHO+NO3	C6H13CHO+GLYOX+HNO3+NO2+OH
2.74 x 10^{-11}	C7NO3CO2HCHO+OH	C6CNO3CO2CHO
J17	C7NO3CO2HCHO	C7HOCCHONO3+OH
J41	C7NO3CO2HCHO	C7HOCCHONO3+OH

continued on next page

Rate Coefficient	**Reactants**	**Products**
KRO2HO2*0.625	C6COHCO2CHO+HO2	C7OHCO2HCHO
KRO2NO	C6COHCO2CHO+NO	C7OHCHOCHO+NO2
KRO2NO3	C6COHCO2CHO+NO3	C7OHCHOCHO+NO2
0.2*8.8 x 10^{-13}*RO2	C6COHCO2CHO	C6COHCOHCHO
0.2*8.8 x 10^{-13}*RO2	C6COHCO2CHO	C7OHCOCHO
0.6*8.8 x 10^{-13}*RO2	C6COHCO2CHO	C7OHCHOCHO
J34	C7OHCOCHO	C6COHCO2CHO+CO+HO2
5.29 x 10^{-11}	C6COHCO2CHO+OH	C6COHCO2CHO+CO
KDEC	C7OHCHOCHO	C6COHCHO+CO+HO2
J41	C7OHCO2HCHO	C7OHCHOCHO+OH
J17	C7OHCO2HCHO	C6COHCHO+CO+HO2+OH
6.35 x 10^{-11}	C7OHCO2HCHO+OH	C7OHCOCHO+OH

A.3 Near-Field Species

Table A.3: The near-field species ($C_{i,nf}$) included in INCHEM-Py.

Species		
Formaldehyde	Acetaldehyde	Propanal
3-Methylbutanal	Acrolein	Methacrolein
Crotonaldehyde	Pentanal	Hexanal
Heptanal	Octanal	Nonanal
Decanal	2-Nonenal	Acetone
2-Butanone (MEK)	3-Buten-2-one (MVK)	Cyclohexanone
Benzaldehyde	o-Tolualdehyde	m-Tolualdehyde
p-Tolualdehyde	2,5-Dimethylbenzaldehyde	Benzene
Toluene	p-Xylene	m-Xylene
o-Xylene	Ethylbenzene	Propylbenzene
2-Ethyltoluene	3-Ethyltoluene	4-Ethyltoluene
1,3,5-Trimethylbenzene	1,2,4-Trimethylbenzene	1,2,3-Trimethylbenzene
p-Dichlorobenzene	Styrene	Cumene
Phenol	Ethane	Propane
Butane	Isobutane	2,2-Dimethylbutane
2,3-Dimethylbutane	Pentane	2-Methylpentane
3-Methylpentane	Isopentane	Hexane
2-Methylhexane	3-Methylhexane	Heptane
Octane	Nonane	Decane
Undecane	Dodecane	Cyclohexane
Ethene	Propene	1-Butene
cis-2-Butene	trans-2-Butene	2-Methyl-1-butene
2-Methyl-2-butene	Isoprene	1,3-Butadiene
trans-2-Pentene	cis-2-Pentene	Ethyne

continued on next page

Species		
Methanol	Ethanol	Isopropanol
1-Propanol	1-Butanol	1-Pentanol
1-Hexanol	2-Butoxyethanol	Linalool
Chloroform	Methylchloroform	Dichloromethane
Trichloroethylene	Tetrachloroethylene	1,2-Dichloroethane
Hydrogen Chloride	Chloromethane	α-Pinene
β-Pinene	Limonene	Δ3-Carene
Camphene	Formic Acid	Acetic Acid
Propanoic Acid	Butanoic Acid	Pentanoic Acid
Heptanoic Acid	Hydrogen Peroxide	β-Caryophyllene
Methane (CH_4)	Carbon Monoxide (CO)	Sulfur Dioxide (SO_2)
Nitric Acid (HNO_3)	Peroxyacetyl Nitrates (PAN)	-

List of References

Abbass, O. A., Sailor, D. J., and Gall, E. T. (2017). Effect of fiber material on ozone removal and carbonyl production from carpets. *Atmospheric Environment*, 148:42–48.

Abbatt, J. P. and Wang, C. (2020). The atmospheric chemistry of indoor environments. *Environmental Science: Processes and Impacts*, 22(1):25–48.

Abdullahi, K. L., Delgado-Saborit, J. M., and Harrison, R. M. (2013). Emissions and indoor concentrations of particulate matter and its specific chemical components from cooking: A review. *Atmospheric Environment*, 71:260–294.

Agency for Toxic Substances and Disease Registry (ATSDR) (1997). Toxicological Profile for Chloroform. Technical report, US Department of Health and Human Services.

Ahn, J. H., Szulejko, J. E., Kim, K. H., Kim, Y. H., and Kim, B. W. (2014). Odor and VOC emissions from pan frying of mackerel at three stages: raw, well-done, and charred. *International Journal of Environmental Research and Public Health*, 11(11):11753–11771.

Air Quality Expert Group (2012). Fine Particulate Matter (PM2.5) in the United Kingdom. Technical report, AQEG.

Air Quality Expert Group (2020). Estimation of changes in air pollution emissions, concentrations and exposure during the COVID-19 outbreak in the UK. Technical report, Air Quality Expert Group.

Air Quality Expert Group (2022). Indoor Air Quality. Technical report, Department for Environment, Food and Rural Affairs (UK Government).

Aksenov, A. A., Koelmel, J. P., Lin, E. Z., Melnik, A. V., Vance, M. E., Farmer, D. K., and Godri Pollitt, K. J. (2023). Human Activities Shape Indoor Volatile Chemistry. *Environmental Science & Technology Letters*, 10(11):965–975.

Alapieti, T., Castagnoli, E., Salo, L., Mikkola, R., Pasanen, P., and Salonen, H. (2021). The effects of paints and moisture content on the indoor air emissions from pinewood (Pinus sylvestris) boards. *Indoor Air*, 31(5):1563–1576.

Alford, K. L. and Kumar, N. (2021). Pulmonary Health Effects of Indoor Volatile Organic Compounds—A Meta-Analysis. *International Journal of Environmental Research and Public Health*, 18(4):1578.

Ampollini, L., Katz, E. F., Bourne, S., Tian, Y., Novoselac, A., Goldstein, A. H., Lucic, G., Waring, M. S., and Decarlo, P. F. (2019). Observations and Contributions of Real-Time Indoor Ammonia Concentrations during HOMEChem. *Environmental Science and Technology*, 53(15):8591–8598.

Arata, C., Misztal, P. K., Tian, Y., Lunderberg, D. M., Kristensen, K., Novoselac, A., Vance, M. E., Farmer, D. K., Nazaroff, W. W., and Goldstein, A. H. (2021). Volatile organic compound emissions during HOMEChem. *Indoor Air*, 31(6):2099–2117.

Archangelidi, O., Sathiyajit, S., Consonni, D., Jarvis, D., and De Matteis, S. (2021). Cleaning products and respiratory health outcomes in occupational cleaners: A systematic review and meta-analysis. *Occupational and Environmental Medicine*, 78(8):541–547.

Ault, A. P., Grassian, V. H., Carslaw, N., Collins, D. B., Destaillats, H., Donaldson, D. J., Farmer, D. K., Jimenez, J. L., McNeill, V. F., Morrison, G. C., O'Brien, R. E., Shiraiwa, M., Vance, M. E., Wells, J., and Xiong, W. (2020). Indoor Surface Chemistry: Developing a Molecular Picture of Reactions on Indoor Interfaces. *Chem*, 6(12):3203–3218.

Baeza-Romero, M. T., Dudzinska, M. R., Amouei Torkmahalleh, M., Barros, N., Coggins, A. M., Ruzgar, D. G., Kildsgaard, I., Naseri, M., Rong, L., Saffell, J., Scutaru, A. M., and Staszowska, A. (2022). A review of critical residential buildings parameters and activities when investigating indoor air quality and pollutants. *Indoor Air*, 32(11):e13144.

Bakó-Biró, Z., Wargocki, P., Weschler, C. J., and Fanger, P. O. (2004). Effects of pollution from personal computers on perceived air quality, SBS symptoms and productivity in offices. *Indoor Air*, 14(3):178–187.

Barber, V. P., Goss, M. B., Franco Deloya, L. J., LeMar, L. N., Li, Y., Helstrom, E., Canagaratna, M., Keutsch, F. N., and Kroll, J. H. (2023). Indoor Air Quality Implications of Germicidal 222 nm Light. *Environmental Science and Technology*, 57(42):15990–15998.

Bari, M. A. and Kindzierski, W. B. (2018). Ambient volatile organic compounds (VOCs) in Calgary, Alberta: Sources and screening health risk assessment. *Science of The Total Environment*, 631-632:627–640.

Bari, M. A., Kindzierski, W. B., and Spink, D. (2016). Twelve-year trends in ambient concentrations of volatile organic compounds in a community of the Alberta Oil Sands Region, Canada. *Environment International*, 91:40–50.

Baudic, A., Gros, V., Sauvage, S., Locoge, N., Sanchez, O., Sarda-Estève, R., Kalogridis, C., Petit, J. E., Bonnaire, N., Baisnée, D., Favez, O., Albinet, A., Sciare, J., and Bonsang, B. (2016). Seasonal variability and source apportionment of volatile organic compounds (VOCs) in the Paris megacity (France). *Atmospheric Chemistry and Physics*, 16(18):11961–11989.

Bayati, M., Vu, D. C., Vo, P. H., Rogers, E., Park, J., Ho, T. L., Davis, A. N., Gulseven, Z., Carlo, G., Palermo, F., McElroy, J. A., Nagel, S. C., and Lin, C. (2021). Health risk assessment of volatile organic compounds at daycare facilities. *Indoor Air*, 31(4):977–988.

Beel, G. (2023). *Emissions of volatile organic compounds from household plastics and their controls: An experimental and modelling approach*. PhD thesis, University of York.

Beel, G., Langford, B., Carslaw, N., Shaw, D., and Cowan, N. (2023). Temperature driven variations in VOC emissions from plastic products and their fate indoors: A chamber experiment and modelling study. *Science of The Total Environment*, 881:163497.

Bekö, G., Carslaw, N., Fauser, P., Kauneliene, V., Nehr, S., Phillips, G., Saraga, D., Schoemaecker, C., Wierzbicka, A., and Querol, X. (2020). The past, present, and future of indoor air chemistry. *Indoor Air*, 30(3):373–376.

Bekö, G., Weschler, C. J., Wierzbicka, A., Karottki, D. G., Toftum, J., Loft, S., and Clausen, G. (2013). Ultrafine particles: Exposure and source apportionment in 56 Danish homes. *Environmental Science and Technology*, 47(18):10240–10248.

Beldean-Galea, M. S., Dicu, T., Cucoş, A., Burghele, B.-D., Catalina, T., Botoş, M., Ţenter, A., Szacsvai, K., Lupulescu, A., Pap, I., Dobrei, G., Moldovan, M., Tunyagi, A., Florică, S., Pănescu, V., and Sainz, C. (2020). Evaluation of indoor air pollutants in 100 retrofit residential buildings from Romania during cold season. *Journal of Cleaner Production*, 277:124098.

Bingham, E., Cohrssen, B., and Powell, C. H. (2001). *Patty's Toxicology*, volume 5. Wiley, New York, 5 edition.

Birnbaum, L. S. (2013). State of the Science of Endocrine Disruptors. *Environmental Health Perspectives*, 121(4):1306695.

Bliss, S. (2005). *Best Practices Guide to Residential Construction: Materials, Finishes, and Details*. Wiley, London, United Kingdom.

Blocquet, M., Guo, F., Mendez, M., Ward, M., Coudert, S., Batut, S., Hecquet, C., Blond, N., Fittschen, C., and Schoemaecker, C. (2018). Impact of the spectral and spatial properties of natural light on indoor gas-phase chemistry: Experimental and modeling study. *Indoor Air*, 28(3):426–440.

Bloss, C., Wagner, V., Jenkin, M. E., Volkamer, R., Bloss, W. J., Lee, J. D., Heard, D. E., Wirtz, K., Martin-Reviejo, M., Rea, G., Wenger, J. C., and Pilling, M. J. (2005). Development of a detailed chemical mechanism (MCMv3.1) for the atmospheric oxidation of aromatic hydrocarbons. *Atmospheric Chemistry and Physics*, 5(3):641–664.

Borbon, A., Dominutti, P., Panopoulou, A., Gros, V., Sauvage, S., Farhat, M., Afif, C., Elguindi, N., Fornaro, A., Granier, C., Hopkins, J. R., Liakakou, E., Nogueira, T., Corrêa dos

Santos, T., Salameh, T., Armangaud, A., Piga, D., and Perrussel, O. (2023). Ubiquity of Anthropogenic Terpenoids in Cities Worldwide: Emission Ratios, Emission Quantification and Implications for Urban Atmospheric Chemistry. *Journal of Geophysical Research: Atmospheres*, 128(7):e2022JD037566.

Breen, M. S., Schultz, B. D., Sohn, M. D., Long, T., Langstaff, J., Williams, R., Isaacs, K., Meng, Q. Y., Stallings, C., and Smith, L. (2014). A review of air exchange rate models for air pollution exposure assessments. *Journal of Exposure Science and Environmental Epidemiology*, 24(6):555–563.

Brenner, D. J. (2023). The public-health significance of far-UVC-induced indoor ozone and its associated secondary chemistry. *Photochemistry and Photobiology*, 0:1–5.

Brickus, L. S., Cardoso, J. N., and De Aquino Neto, F. R. (1998). Distributions of indoor and outdoor air pollutants in Rio de Janeiro, Brazil: Implications to indoor air quality in bayside offices. *Environmental Science and Technology*, 32(22):3485–3490.

Brophy, P. and Farmer, D. K. (2015). A switchable reagent ion high resolution time-of-flight chemical ionization mass spectrometer for real-time measurement of gas phase oxidized species: Characterization from the 2013 southern oxidant and aerosol study. *Atmospheric Measurement Techniques*, 8(7):2945–2959.

Bueno de Mesquita, P. J., Sokas, R. K., Rice, M. B., and Nardell, E. A. (2023). Far-UVC: Technology Update with an Untapped Potential to Mitigate Airborne Infections. *Annals of the American Thoracic Society*, 20(12):1700–1702.

Buonanno, G., Giovinco, G., Morawska, L., and Stabile, L. (2015). Lung cancer risk of airborne particles for Italian population. *Environmental Research*, 142:443–451.

Buonanno, M., Kleiman, N. J., Welch, D., Hashmi, R., Shuryak, I., and Brenner, D. J. (2024). 222 nm far-UVC light markedly reduces the level of infectious airborne virus in an occupied room. *Scientific Reports*, 14(1).

Buonanno, M., Welch, D., Shuryak, I., and Brenner, D. J. (2020). Far-UVC light (222nm)

efficiently and safely inactivates airborne human coronaviruses. *Scientific Reports*, 10(1):10285.

Burkholder, J. B., Abbatt, J. P., Barnes, I., Roberts, J. M., Melamed, M. L., Ammann, M., Bertram, A. K., Cappa, C. D., Carlton, A. G., Carpenter, L. J., Crowley, J. N., Dubowski, Y., George, C., Heard, D. E., Herrmann, H., Keutsch, F. N., Kroll, J. H., McNeill, V. F., Ng, N. L., Nizkorodov, S. A., Orlando, J. J., Percival, C. J., Picquet-Varrault, B., Rudich, Y., Seakins, P. W., Surratt, J. D., Tanimoto, H., Thornton, J. A., Tong, Z., Tyndall, G. S., Wahner, A., Weschler, C. J., Wilson, K. R., and Ziemann, P. J. (2017). The Essential Role for Laboratory Studies in Atmospheric Chemistry. *Environmental Science and Technology*, 51(5):2519–2528.

Calderon, L., Maddalena, R., Russell, M., Chen, S., Nolan, J. E. S., Bradman, A., and Harley, K. G. (2022). Air concentrations of volatile organic compounds associated with conventional and "green" cleaning products in real-world and laboratory settings. *Indoor Air*, 32(11):1–10.

Cano-Ruiz, J., Kong, D., Balas, R., and Nazaroff, W. W. (1993). Removal of reactive gases at indoor surfaces: Combining mass transport and surface kinetics. *Atmospheric Environment. Part A. General Topics*, 27(13):2039–2050.

Carslaw, N. (2007). A new detailed chemical model for indoor air pollution. *Atmospheric Environment*, 41(6):1164–1179.

Carslaw, N. (2013). A mechanistic study of limonene oxidation products and pathways following cleaning activities. *Atmospheric Environment*, 80:507–513.

Carslaw, N. (2019). Chemical Reactions in the Indoor Atmosphere. In *Indoor Air Pollution*, number 48, pages 105–126. The Royal Society of Chemistry.

Carslaw, N., Bekö, G., Langer, S., Schoemaecker, C., Mihucz, V. G., Dudzinska, M., Wiesen, P., Nehr, S., Huttunen, K., Querol, X., and Shaw, D. (2024). A new framework for indoor air chemistry measurements: Towards a better understanding of indoor air pollution. *Indoor Environments*, 1(1):100001.

Carslaw, N., Fletcher, L., Heard, D., Ingham, T., and Walker, H. (2017). Significant OH production under surface cleaning and air cleaning conditions: Impact on indoor air quality. *Indoor Air*, 27(6):1091–1100.

Carslaw, N., Mota, T., Jenkin, M. E., Barley, M. H., and McFiggans, G. (2012). A Significant role for nitrate and peroxide groups on indoor secondary organic aerosol. *Environmental Science and Technology*, 46(17):9290–9298.

Carslaw, N. and Shaw, D. (2019). Secondary product creation potential (SPCP): A metric for assessing the potential impact of indoor air pollution on human health. *Environmental Science: Processes and Impacts*, 21(8):1313–1322.

Carslaw, N. and Shaw, D. (2022). Modification of cleaning product formulations could improve indoor air quality. *Indoor Air*, 32(3):1–13.

Carter, T. J., Poppendieck, D. G., Shaw, D., and Carslaw, N. (2023). A Modelling Study of Indoor Air Chemistry: The Surface Interactions of Ozone and Hydrogen Peroxide. *Atmospheric Environment*, 297:119598.

Carter, T. J., Shaw, D. R., Carslaw, D. C., and Carslaw, N. (2024). Indoor cooking and cleaning as a source of outdoor air pollution in urban environments. *Environmental Science: Processes & Impacts*, 26(6):975–990.

CERC (2023). ADMS 6, http://www.cerc.co.uk/environmental-software/ADMS-model.html (Date Accessed: April 2024).

Chen, C., Zhao, Y., and Zhao, B. (2018). Emission Rates of Multiple Air Pollutants Generated from Chinese Residential Cooking. *Environmental Science and Technology*, 52(3):1081–1087.

Chen, J., Møller, K. H., Wennberg, P. O., and Kjaergaard, H. G. (2021). Unimolecular Reactions following Indoor and Outdoor Limonene Ozonolysis. *Journal of Physical Chemistry A*, 125(2):669–680.

Cheng, Y. H., Lin, C. C., and Hsu, S. C. (2015). Comparison of conventional and green building materials in respect of VOC emissions and ozone impact on secondary carbonyl emissions. *Building and Environment*, 87:274–282.

Chin, K., Laguerre, A., Ramasubramanian, P., Pleshakov, D., Stephens, B., and Gall, E. T. (2019). Emerging investigator series: Primary emissions, ozone reactivity, and byproduct emissions from building insulation materials. *Environmental Science: Processes and Impacts*, 21(8):1255–1267.

Clifford, G. M. and Wenger, J. C. (2006). Rate coefficients for the gas-phase reaction of hydroxyl radicals with the dimethylbenzaldehydes. *International Journal of Chemical Kinetics*, 38(9):563–569.

Coleman, B. K., Destaillats, H., Hodgson, A. T., and Nazaroff, W. W. (2008). Ozone consumption and volatile byproduct formation from surface reactions with aircraft cabin materials and clothing fabrics. *Atmospheric Environment*, 42(4):642–654.

Cooper, D. M. and Loxham, M. (2019). Particulate matter and the airway epithelium: the special case of the underground? *European Respiratory Review*, 28(153):190066.

Cox, R. A. and Penkett, S. A. (1972). Effect of relative humidity on the disappearance of ozone and sulphur dioxide in contained systems. *Atmospheric Environment (1967)*, 6(5):365–368.

Cros, C. J., Morrison, G. C., Siegel, J. A., and Corsi, R. L. (2012). Long-term performance of passive materials for removal of ozone from indoor air. *Indoor Air*, 22(1):43–53.

Cummings, B. E., Avery, A. M., DeCarlo, P. F., and Waring, M. S. (2021). Improving Predictions of Indoor Aerosol Concentrations of Outdoor Origin by Considering the Phase Change of Semivolatile Material Driven by Temperature and Mass-Loading Gradients. *Environmental Science and Technology*, 55(13):9000–9011.

Cummings, B. E., Lakey, P. S., Morrison, G. C., Shiraiwa, M., and Waring, M. S. (2024). Composition of indoor organic surface films in residences: simulating the influence

of sources, partitioning, particle deposition, and air exchange. *Environmental Science: Processes and Impacts*, 26(2):305–322.

Cummings, B. E., Li, Y., Decarlo, P. F., Shiraiwa, M., and Waring, M. S. (2020). Indoor aerosol water content and phase state in U.S. residences: Impacts of relative humidity, aerosol mass and composition, and mechanical system operation. *Environmental Science: Processes and Impacts*, 22(10):2031–2057.

Cummings, B. E., Pothier, M. A., Katz, E. F., DeCarlo, P. F., Farmer, D. K., and Waring, M. S. (2023). Model Framework for Predicting Semivolatile Organic Material Emissions Indoors from Organic Aerosol Measurements: Applications to HOMEChem Stir-Frying. *Environmental Science and Technology*, 57(45):17374–17383.

Cummings, B. E., Shiraiwa, M., and Waring, M. S. (2022). Phase state of organic aerosols may limit temperature-driven thermodynamic repartitioning following outdoor-to-indoor transport. *Environmental Science: Processes and Impacts*, 24(10):1678–1696.

Cummings, B. E. and Waring, M. S. (2019). Predicting the importance of oxidative aging on indoor organic aerosol concentrations using the two-dimensional volatility basis set (2D-VBS). *Indoor Air*, 29(4):616–629.

Davies, H. L., O'Leary, C., Dillon, T., Shaw, D. R., Shaw, M., Mehra, A., Phillips, G., and Carslaw, N. (2023). A measurement and modelling investigation of the indoor air chemistry following cooking activities. *Environmental Science: Processes & Impacts*, 25(9):1532–1548.

Davis, A. C. and Francisco, J. S. (2011). Reactivity trends within alkoxy radical reactions responsible for chain branching. *Journal of the American Chemical Society*, 133(45):18208–18219.

DeLuca, N. M., Minucci, J. M., Mullikin, A., Slover, R., and Cohen Hubal, E. A. (2022). Human exposure pathways to poly- and perfluoroalkyl substances (PFAS) from indoor media: A systematic review. *Environment International*, 162.

Department for Environment & Food & Rural Affairs (2023). Emissions of Air Pollutants in the UK - Summary. Technical report, UK Government.

Department of Energy & Climate Change (2013). Energy Follow-Up Survey - Report 9: Domestic appliances, cooking & cooling equipment. Technical report, UK Government.

Destaillats, H., Maddalena, R. L., Singer, B. C., Hodgson, A. T., and McKone, T. E. (2008). Indoor pollutants emitted by office equipment: A review of reported data and information needs. *Atmospheric Environment*, 42(7):1371–1388.

Di, Y., Mo, J., Zhang, Y., and Deng, J. (2017). Ozone deposition velocities on cotton clothing surface determined by the field and laboratory emission cell. *Indoor and Built Environment*, 26(5):631–641.

Dlugokencky, E. (2022). NOAA/GML CH4 Trends, https://gml.noaa.gov/ccgg/trends/ (Date Accessed: March 2022).

Dodson, R. E., Nishioka, M., Standley, L. J., Perovich, L. J., Brody, J. G., and Rudel, R. A. (2012). Endocrine Disruptors and Asthma-Associated Chemicals in Consumer Products. *Environmental Health Perspectives*, 120(7):935–943.

Donahue, N. M., Epstein, S. A., Pandis, S. N., and Robinson, A. L. (2011). A two-dimensional volatility basis set: 1. organic-aerosol mixing thermodynamics. *Atmospheric Chemistry and Physics*, 11(7):3303–3318.

Eadie, E., Barnard, I. M., Ibbotson, S. H., and Wood, K. (2021). Extreme Exposure to Filtered Far-UVC: A Case Study. *Photochemistry and Photobiology*, 97(3):527–531.

Eadie, E., Hiwar, W., Fletcher, L., Tidswell, E., O'Mahoney, P., Buonanno, M., Welch, D., Adamson, C. S., Brenner, D. J., Noakes, C., and Wood, K. (2022). Far-UVC (222 nm) efficiently inactivates an airborne pathogen in a room-sized chamber. *Scientific Reports*, 12(1):4373.

EEA (2018). European Air Quality Portal, https://eeadmz1-cws-wp-air02.azurewebsites.net/, (Date Accessed: December 2021).

Eftekhari, A., Fortenberry, C. F., Williams, B. J., Walker, M. J., Dang, A., Pfaff, A., Ercal, N., and Morrison, G. C. (2021). Continuous measurement of reactive oxygen species inside and outside of a residential house during summer. *Indoor Air*, 31(4):1199–1216.

Emmerson, K. M., Carslaw, N., Carslaw, D. C., Lee, J. D., Mcfiggans, G., Bloss, W. J., Gravestock, T., Heard, D. E., Hopkins, J., Ingham, T., Pilling, M. J., Smith, S. C., Jacob, M., and Monks, P. S. (2007). Free radical modelling studies during the UK TORCH Campaign in Summer 2003. *Atmos. Chem. Phys*, 7:167–181.

EPA (2017). What are the trends in indoor air quality and their effects on human health?, https://www.epa.gov/report-environment/indoor-air-quality (Date Accessed: April 2024).

Fadeyi, M. O., Weschler, C. J., Tham, K. W., Wu, W. Y., and Sultan, Z. M. (2013). Impact of human presence on secondary organic aerosols derived from ozone-initiated chemistry in a simulated office environment. *Environmental Science and Technology*, 47(8):3933–3941.

Fan, H., Frank, E. S., Lakey, P. S., Shiraiwa, M., Tobias, D. J., and Grassian, V. H. (2022). Heterogeneous Interactions between Carvone and Hydroxylated SiO2. *Journal of Physical Chemistry C*, 126(14):6267–6279.

Fang, Y., Riahi, S., McDonald, A. T., Shrestha, M., Tobias, D. J., and Grassian, V. H. (2019). What Is the Driving Force behind the Adsorption of Hydrophobic Molecules on Hydrophilic Surfaces? *Journal of Physical Chemistry Letters*, 10(3):468–473.

Farmer, D. K., Vance, M. E., Abbatt, J. P., Abeleira, A., Alves, M. R., Arata, C., Boedicker, E., Bourne, S., Cardoso-Saldaña, F., Corsi, R., Decarlo, P. F., Goldstein, A. H., Grassian, V. H., Hildebrandt Ruiz, L., Jimenez, J. L., Kahan, T. F., Katz, E. F., Mattila, J. M., Nazaroff, W. W., Novoselac, A., O'Brien, R. E., Or, V. W., Patel, S., Sankhyan, S., Stevens, P. S., Tian, Y., Wade, M., Wang, C., Zhou, S., and Zhou, Y. (2019). Overview of HOMEChem: House Observations of Microbial and Environmental Chemistry. *Environmental Science: Processes and Impacts*, 21(8):1280–1300.

Farmer, D. K., Vance, M. E., Poppendieck, D., Abbatt, J., Alves, M. R., Dannemiller, K. C., Deeleepojananan, C., Ditto, J., Dougherty, B., Farinas, O. R., Goldstein, A. H., Grassian, V. H., Huynh, H., Kim, D., King, J. C., Kroll, J., Li, J., Link, M. F., Mael, L., Mayer, K., Martin, A. B., Morrison, G., O'Brien, R., Pandit, S., Turpin, B. J., Webb, M., Yu, J., and Zimmerman, S. M. (2024). The chemical assessment of surfaces and air (CASA) study: using chemical and physical perturbations in a test house to investigate indoor processes. *Environmental Science: Processes & Impacts*, Advance Article.

Felgueiras, F., Mourão, Z., Moreira, A., and Gabriel, M. F. (2023). Indoor environmental quality in offices and risk of health and productivity complaints at work: A literature review. *Journal of Hazardous Materials Advances*, 10:100314.

Fenske, J. D. and Paulson, S. E. (1999). Human breath emissions of VOCs. *Journal of the Air and Waste Management Association*, 49(5):594–598.

Finlayson-Pitts, B. J. and Pitts Jr, J. N. (1986). *Atmospheric Chemistry: Fundamentals and Experimental Techniques*. John Wiley & Sons, New York.

Finlayson-Pitts, B. J. and Pitts Jr, J. N. (2000). *Chemistry of the Upper and Lower Atmosphere*. Academic Press, San Diego.

Fischer, A., Ljungström, E., and Langer, S. (2013). Ozone removal by occupants in a classroom. *Atmospheric Environment*, 81:11–17.

Frank, E. S., Fan, H., Grassian, V. H., and Tobias, D. J. (2023). Adsorption of 6-MHO on two indoor relevant surface materials: SiO2 and TiO2. *Physical Chemistry Chemical Physics*, 25(5):3930–3941.

Frank, E. S., Fan, H., Shrestha, M., Riahi, S., Tobias, D. J., and Grassian, V. H. (2020). Impact of adsorbed water on the interaction of limonene with hydroxylated SiO2: Implications of π-hydrogen bonding for surfaces in humid environments. *Journal of Physical Chemistry A*, 124(50):10592–10599.

Gaffney, J. S. and Marley, N. A. (2003). Atmospheric Chemistry and Air Pollution. *The Scientific World Journal*, 3:199–234.

Gall, E., Darling, E., Siegel, J. A., Morrison, G. C., and Corsi, R. L. (2013). Evaluation of three common green building materials for ozone removal, and primary and secondary emissions of aldehydes. *Atmospheric Environment*, 77:910–918.

Gallego, E., Roca, F. J., Perales, J. F., Guardino, X., Gadea, E., and Garrote, P. (2016). Impact of formaldehyde and VOCs from waste treatment plants upon the ambient air nearby an urban area (Spain). *Science of The Total Environment*, 568:369–380.

Gallon, V., Le Cann, P., Sanchez, M., Dematteo, C., and Le Bot, B. (2020). Emissions of VOCs, SVOCs, and mold during the construction process: Contribution to indoor air quality and future occupants' exposure. *Indoor Air*, 30(4):691–710.

Gao, T., Andino, J. M., Rivera, C. C., and Márquez, M. F. (2009). Rate constants of the gas-phase reactions of OH radicals with trans -2-hexenal, trans -2-octenal, and trans -2-nonenal. *International Journal of Chemical Kinetics*, 41(7):483–489.

Gaona Colmán, E., Blanco, M. B., Barnes, I., Wiesen, P., and Teruel, M. A. (2017). Mechanism and Product Distribution of the O3-Initiated Degradation of (E)-2-Heptenal, (E)-2-Octenal, and (E)-2-Nonenal. *Journal of Physical Chemistry A*, 121(27):5147–5155.

GBD 2017 Risk Factor Collaborators (2018). Global, regional, and national comparative risk assessment of 84 behavioural, environmental and occupational, and metabolic risks or clusters of risks for 195 countries and territories, 1990-2017: A systematic analysis for the Global Burden of Disease Stu. *The Lancet*, 392(10159):1923–1994.

Gerber, R. B. and Sebek, J. (2009). Dynamics simulations of atmospherically relevant molecular reactions. *International Reviews in Physical Chemistry*, 28(2):207–222.

Gerber, R. B., Varner, M. E., Hammerich, A. D., Riikonen, S., Murdachaew, G., Shemesh, D., and Finlayson-Pitts, B. J. (2015). Computational studies of atmospherically-relevant chemical reactions in water clusters and on liquid water and ice surfaces. *Accounts of Chemical Research*, 48(2):399–406.

Gilbert, N. L., Gauvin, D., Guay, M., Héroux, M.-E., Dupuis, G., Legris, M., Chan, C. C., Dietz, R. N., and Lévesque, B. (2006). Housing characteristics and indoor concentra-

tions of nitrogen dioxide and formaldehyde in Quebec City, Canada. *Environmental Research*, 102(1):1–8.

Gkatzelis, G. I., Coggon, M. M., McDonald, B. C., Peischl, J., Gilman, J. B., Aikin, K. C., Robinson, M. A., Canonaco, F., Prevot, A. S., Trainer, M., and Warneke, C. (2021). Observations Confirm that Volatile Chemical Products Are a Major Source of Petrochemical Emissions in U.S. Cities. *Environmental Science and Technology*, 55(8):4332–4343.

Glojek, K., Močnik, G., Alas, H. D. C., Cuesta-Mosquera, A., Drinovec, L., Gregorič, A., Ogrin, M., Weinhold, K., Ježek, I., Müller, T., Rigler, M., Remškar, M., Van Pinxteren, D., Herrmann, H., Ristorini, M., Merkel, M., Markelj, M., and Wiedensohler, A. (2022). The impact of temperature inversions on black carbon and particle mass concentrations in a mountainous area. *Atmospheric Chemistry and Physics*, 22(8):5577–5601.

Goldstein, A. H., Nazaroff, W. W., Weschler, C. J., and Williams, J. (2021). How Do Indoor Environments Affect Air Pollution Exposure? *Environmental Science and Technology*, 55(1):100–108.

Graeffe, F., Luo, Y., Guo, Y., and Ehn, M. (2023). Unwanted Indoor Air Quality Effects from Using Ultraviolet C Lamps for Disinfection. *Environmental Science and Technology Letters*, 10(2):172–178.

Grand View Research (2023). UV Air Purifier Market Size & Trends, https://www.grandviewresearch.com/industry-analysis/uv-air-purifier-market-report.

Grange, S. K., Grange, S. K., Farren, N. J., Vaughan, A. R., Davison, J., and Carslaw, D. C. (2020). Post-Dieselgate: Evidence of NOxEmission Reductions Using On-Road Remote Sensing. *Environmental Science and Technology Letters*, 7(6):382–387.

Grøntoft, T. (2002). Dry deposition of ozone on building materials. Chamber measurements and modelling of the time-dependent deposition. *Atmospheric Environment*, 36(36-37):5661–5670.

Grøntoft, T. and Raychaudhuri, M. R. (2004). Compilation of tables of surface deposition velocities for O3, NO2 and SO2 to a range of indoor surfaces. *Atmospheric Environment*, 38(4):533–544.

Guenther, A. (1995). A global model of natural volatile organic compound emissions. *Journal of Geophysical Research*, 100(D5):8873–8892.

Güneş, G., Yalçin, N., and Çolaklar, H. (2022). Investigation of indoor air quality in university libraries in terms of gaseous and particulate pollutants in Bartin, Turkey. *Environmental Monitoring and Assessment*, 194(3).

Guo, J., Chai, G., Song, X., Hui, X., Li, Z., Feng, X., and Yang, K. (2023). Long-term exposure to particulate matter on cardiovascular and respiratory diseases in low- and middle-income countries: A systematic review and meta-analysis. *Frontiers in Public Health*, 11:1–13.

Hakola, H., Hellén, H., Tarvainen, V., Bäck, J., Patokoski, J., and Rinne, J. (2009). Annual variations of atmospheric VOC concentrations in a boreal forest. *Boreal Environment Research*, 14(4):722–730.

Harb, P., Locoge, N., and Thevenet, F. (2018). Emissions and treatment of VOCs emitted from wood-based construction materials: Impact on indoor air quality. *Chemical Engineering Journal*, 354:641–652.

Harding-Smith, E., Shaw, D. R., Shaw, M., Dillon, T. J., and Carslaw, N. (2024). Does green mean clean? Volatile organic emissions from regular versus green cleaning products. *Environmental Science: Processes & Impacts*, 26(2):436–450.

Haze, S., Gozu, Y., Nakamura, S., Kohno, Y., Sawano, K., Ohta, H., and Yamazaki, K. (2001). 2-Nonenal Newly Found in Human Body Odor Tends to Increase with Aging. *Journal of Investigative Dermatology*, 116(4):520–524.

He, S. Z., Chen, Z. M., Zhang, X., Zhao, Y., Huang, D. M., Zhao, J. N., Zhu, T., Hu, M., and Zeng, L. M. (2010). Measurement of atmospheric hydrogen peroxide and organic

peroxides in Beijing before and during the 2008 Olympic Games: Chemical and physical factors influencing their concentrations. *Journal of Geophysical Research: Atmospheres*, 115(D17):D17307.

Health Canada (2017). Residential Indoor Air Quality Guideline: Acetaldehyde. Technical report, Government of Canada, Ottawa.

Health Protection Agency (2007). Chloroform Toxicological Overview. Technical report, UK Government.

Hellén, H., Praplan, A. P., Tykkä, T., Ylivinkka, I., Vakkari, V., Bäck, J., Petäjä, T., Kulmala, M., and Hakola, H. (2018). Long-term measurements of volatile organic compounds highlight the importance of sesquiterpenes for the atmospheric chemistry of a boreal forest. *Atmospheric Chemistry and Physics*, 18(19):13839–13863.

Hodgson, A. T., Ming, K. Y., and Singer, B. C. (2004). Quantifying Object and Material Surface Areas in Residences. *Lawrence Berkeley National Laboratory*, pages LBNL–56786.

Hodgson, A. T., Wooley, J. D., and Daisey, J. M. (1993). Emissions of volatile organic compounds from new carpets measured in a large-scale environmental chamber. *Air and Waste*, 43(3):316–324.

Hoyle, G. W. and Svendsen, E. R. (2016). Persistent effects of chlorine inhalation on respiratory health. *Annals of the New York Academy of Sciences*, 1378(1):33–40.

Huang, L., Frank, E. S., Riahi, S., Tobias, D. J., and Grassian, V. H. (2021a). Adsorption of constitutional isomers of cyclic monoterpenes on hydroxylated silica surfaces. *Journal of Chemical Physics*, 154(12).

Huang, L., Frank, E. S., Shrestha, M., Riahi, S., Tobias, D. J., and Grassian, V. H. (2021b). Heterogeneous Interactions of Prevalent Indoor Oxygenated Organic Compounds on Hydroxylated SiO2 Surfaces. *Environmental Science and Technology*, 55(10):6623–6630.

Huang, Y., Yang, Z., and Gao, Z. (2019). Contributions of indoor and outdoor sources to ozone in residential buildings in nanjing. *International Journal of Environmental Research and Public Health*, 16(14).

Hubbard, H., Poppendieck, D., and Corsi, R. L. (2009). Chlorine dioxide reactions with indoor materials during building disinfection: Surface uptake. *Environmental Science and Technology*, 43(5):1329–1335.

IUPAC (2024). Datasheet for Photolysis Reactions, https://iupac.aeris-data.fr/catalogue/#/catalogue/classifications/pho (Date Accessed: March 2024).

Jenkin, M. E. (2004). Modelling the formation and composition of secondary organic aerosol from α- and β-pinene ozonolysis using MCM v3. *Atmospheric Chemistry and Physics*, 4(7):1741–1757.

Jenkin, M. E., Saunders, S. M., and Pilling, M. J. (1997). The tropospheric degradation of volatile organic compounds: A protocol for mechanism development. *Atmospheric Environment*, 31(1):81–104.

Jenkin, M. E., Saunders, S. M., Wagner, V., and Pilling, M. J. (2003). Protocol for the development of the Master Chemical Mechanism, MCM v3 (Part B): tropospheric degradation of aromatic volatile organic compounds. *Atmospheric Chemistry and Physics*, 3:181–193.

Jenkin, M. E., Valorso, R., Aumont, B., Newland, M. J., and Rickard, A. R. (2020). Estimation of rate coefficients for the reactions of O3 with unsaturated organic compounds for use in automated mechanism construction. *Atmospheric Chemistry and Physics*, 20(21):12921–12937.

Jenkin, M. E., Valorso, R., Aumont, B., and Rickard, A. R. (2019). Estimation of rate coefficients and branching ratios for reactions of organic peroxy radicals for use in automated mechanism construction. *Atmospheric Chemistry and Physics*, 19(11):7691–7717.

Jenkin, M. E., Valorso, R., Aumont, B., Rickard, A. R., and Wallington, T. J. (2018). Estimation of rate coefficients and branching ratios for gas-phase reactions of OH with aromatic organic compounds for use in automated mechanism construction. *Atmospheric Chemistry and Physics*, 18(13):9329–9349.

Jenkin, M. E., Wyche, K. P., Evans, C. J., Carr, T., Monks, P. S., Alfarra, M. R., Barley, M. H., McFiggans, G. B., Young, J. C., and Rickard, A. R. (2012). Development and chamber evaluation of the MCM v3.2 degradation scheme for β-caryophyllene. *Atmospheric Chemistry and Physics*, 12(11):5275–5308.

Jenkin, M. E., Young, J. C., and Rickard, A. R. (2015). The MCM v3.3.1 degradation scheme for isoprene. *Atmospheric Chemistry and Physics*, 15(20):11433–11459.

Jimenez, J. L., Canagaratna, M. R., Donahue, N. M., Prevot, A. S. H., Zhang, Q., Kroll, J. H., DeCarlo, P. F., Allan, J. D., Coe, H., Ng, N. L., Aiken, A. C., Docherty, K. S., Ulbrich, I. M., Grieshop, A. P., Robinson, A. L., Duplissy, J., Smith, J. D., Wilson, K. R., Lanz, V. A., Hueglin, C., Sun, Y. L., Tian, J., Laaksonen, A., Raatikainen, T., Rautiainen, J., Vaattovaara, P., Ehn, M., Kulmala, M., Tomlinson, J. M., Collins, D. R., Cubison, M. J., Dunlea, J., Huffman, J. A., Onasch, T. B., Alfarra, M. R., Williams, P. I., Bower, K., Kondo, Y., Schneider, J., Drewnick, F., Borrmann, S., Weimer, S., Demerjian, K., Salcedo, D., Cottrell, L., Griffin, R., Takami, A., Miyoshi, T., Hatakeyama, S., Shimono, A., Sun, J. Y., Zhang, Y. M., Dzepina, K., Kimmel, J. R., Sueper, D., Jayne, J. T., Herndon, S. C., Trimborn, A. M., Williams, L. R., Wood, E. C., Middlebrook, A. M., Kolb, C. E., Baltensperger, U., and Worsnop, D. R. (2009). Evolution of Organic Aerosols in the Atmosphere. *Science*, 326(5959):1525–1529.

Johnson, D., Utembe, S. R., Jenkin, M. E., Derwent, R. G., Hayman, G. D., Alfarra, M. R., Coe, H., and McFiggans, G. (2006). Simulating regional scale secondary organic aerosol formation during the TORCH 2003 campaign in the southern UK. *Atmospheric Chemistry and Physics*, 6(2):403–418.

Juginović, A., Vuković, M., Aranza, I., and Biloš, V. (2021). Health impacts of air pollution exposure from 1990 to 2019 in 43 European countries. *Scientific Reports*, 11(1):22516.

Kahan, T. F., Washenfelder, R. A., Vaida, V., and Brown, S. S. (2012). Cavity-enhanced measurements of hydrogen peroxide absorption cross sections from 353 to 410 nm. *Journal of Physical Chemistry A*, 116(24):5941–5947.

Kalliomäki, P., Sobhani, H., Stratton, P., Coleman, K., Srikakulapu, A., Salawitch, R., Dickerson, R., Zhu, S., Srebric, J., and Milton, D. (2023). Ozone and ultra-fine particle concentrations in a hotel quarantine facility during 222 nm far-UVC air disinfection. *medRxiv preprint 2023092923296366*.

Kang, K., Kim, H., Kim, D. D., Lee, Y. G., and Kim, T. (2019). Characteristics of cooking-generated PM 10 and PM 2.5 in residential buildings with different cooking and ventilation types. *Science of the Total Environment*, 668:56–66.

Karanasiou, A., Minguillón, M. C., Viana, M., Alastuey, A., Putaud, J.-P., Maenhaut, W., Panteliadis, P., Močnik, G., Favez, O., and Kuhlbusch, T. A. J. (2015). Measurement of elemental carbon (EC) and organic carbon (OC) Thermal-optical analysis for the measurement of elemental carbon (EC) and organic carbon (OC) in ambient air a literature review Measurement of elemental carbon (EC) and organic carbon (OC) Measurement of elemental carbon (EC) and organic carbon (OC). *Atmos. Meas. Tech. Discuss*, 8:9649–9712.

Katsoyiannis, A., Leva, P., and Kotzias, D. (2008). VOC and carbonyl emissions from carpets: A comparative study using four types of environmental chambers. *Journal of Hazardous Materials*, 152(2):669–676.

Kerdouci, J., Picquet-Varrault, B., Durand-Jolibois, R., Gaimoz, C., and Doussin, J. F. (2012). An experimental study of the gas-phase reactions of no3 radicals with a series of unsaturated aldehydes: Trans -2-hexenal, trans -2-heptenal, and trans -2-octenal. *Journal of Physical Chemistry A*, 116(41):10135–10142.

Kim, K.-H., Pandey, S. K., Kabir, E., Susaya, J., and Brown, R. J. (2011). The modern paradox of unregulated cooking activities and indoor air quality. *Journal of Hazardous Materials*, 195:1–10.

Kim, S. (2010). Control of formaldehyde and TVOC emission from wood-based flooring composites at various manufacturing processes by surface finishing. *Journal of Hazardous Materials*, 176(1-3):14–19.

Kitagawa, H., Nomura, T., Nazmul, T., Omori, K., Shigemoto, N., Sakaguchi, T., and Ohge, H. (2021). Effectiveness of 222-nm ultraviolet light on disinfecting SARS-CoV-2 surface contamination. *American Journal of Infection Control*, 49(3):299–301.

Klein, F., Baltensperger, U., Prévôt, A. S., and El Haddad, I. (2019). Quantification of the impact of cooking processes on indoor concentrations of volatile organic species and primary and secondary organic aerosols. *Indoor Air*, 29(6):926–942.

Klein, F., Platt, S. M., Farren, N. J., Detournay, A., Bruns, E. A., Bozzetti, C., Daellenbach, K. R., Kilic, D., Kumar, N. K., Pieber, S. M., Slowik, J. G., Temime-Roussel, B., Marchand, N., Hamilton, J. F., Baltensperger, U., Prévôt, A. S., and El Haddad, I. (2016). Characterization of Gas-Phase Organics Using Proton Transfer Reaction Time-of-Flight Mass Spectrometry: Cooking Emissions. *Environmental Science and Technology*, 50(3):1243–1250.

Klenø, J. G., Clausen, P. A., Weschler, C. J., and Wolkoff, P. (2001). Determination of ozone removal rates by selected building products using the FLEC emission cell. *Environmental Science and Technology*, 35(12):2548–2553.

Klepeis, N. E., Nelson, W. C., Ott, W. R., Robinson, J. P., Tsang, A. M., Switzer, P., Behar, J. V., Hern, S. C., and Engelmann, W. H. (2001). The National Human Activity Pattern Survey (NHAPS): A resource for assessing exposure to environmental pollutants. *Journal of Exposure Analysis and Environmental Epidemiology*, 11(3):231–252.

Kruza, M. and Carslaw, N. (2019). How do breath and skin emissions impact indoor air chemistry? *Indoor Air*, 29(3):369–379.

Kruza, M., Lewis, A. C., Morrison, G. C., and Carslaw, N. (2017). Impact of surface ozone interactions on indoor air chemistry: A modeling study. *Indoor Air*, 27(5):1001–1011.

Kruza, M., McFiggans, G., Waring, M. S., Wells, J. R., and Carslaw, N. (2020). Indoor secondary organic aerosols: Towards an improved representation of their formation and composition in models. *Atmospheric Environment*, 240(August):117784.

Kruza, M., Shaw, D., Shaw, J., and Carslaw, N. (2021). Towards improved models for indoor air chemistry: A Monte Carlo simulation study. *Atmospheric Environment*, 262:118625.

Lakey, P. S., Cummings, B. E., Waring, M. S., Morrison, G. C., and Shiraiwa, M. (2023). Effective mass accommodation for partitioning of organic compounds into surface films with different viscosities. *Environmental Science: Processes and Impacts*, 25(9):1464–1478.

Lakey, P. S., Eichler, C. M., Wang, C., Little, J. C., and Shiraiwa, M. (2021). Kinetic multilayer model of film formation, growth, and chemistry (KM-FILM): Boundary layer processes, multi-layer adsorption, bulk diffusion, and heterogeneous reactions. *Indoor Air*, 31(6):2070–2083.

Lakey, P. S., Wisthaler, A., Berkemeier, T., Mikoviny, T., Pöschl, U., and Shiraiwa, M. (2017). Chemical kinetics of multiphase reactions between ozone and human skin lipids: Implications for indoor air quality and health effects. *Indoor Air*, 27(4):816–828.

Lakey, P. S. J., Morrison, G. C., Won, Y., Parry, K. M., von Domaros, M., Tobias, D. J., Rim, D., and Shiraiwa, M. (2019). The impact of clothing on ozone and squalene ozonolysis products in indoor environments. *Communications Chemistry*, 2(1):56.

Lamble, S. P., Corsi, R. L., and Morrison, G. C. (2011). Ozone deposition velocities, reaction probabilities and product yields for green building materials. *Atmospheric Environment*, 45(38):6965–6972.

Lee, K., Xue, J., Geyh, A. S., Özkaynak, H., Leaderer, B. P., Weschler, C. J., and Spengler, J. D. (2002). Nitrous Acid, Nitrogen Dioxide, and Ozone Concentrations in Residential Environments. *Environmental Health Perspectives*, 110(2):145–149.

Lelieveld, J., Evans, J. S., Fnais, M., Giannadaki, D., and Pozzer, A. (2015). The contribution of outdoor air pollution sources to premature mortality on a global scale. *Nature*, 525(7569):367–371.

Leung, D. Y. C. (2015). Outdoor-indoor air pollution in urban environment: challenges and opportunity. *Frontiers in Environmental Science*, 2(Jan):1–7.

Leungsakul, S., Jaoui, M., and Kamens, R. M. (2005). Kinetic mechanism for predicting secondary organic aerosol formation from the reaction of d-limonene with ozone. *Environmental Science and Technology*, 39(24):9583–9594.

Li, M., Karu, E., Brenninkmeijer, C., Fischer, H., Lelieveld, J., and Williams, J. (2018). Tropospheric OH and stratospheric OH and Cl concentrations determined from CH4, CH3Cl, and SF6 measurements. *npj Climate and Atmospheric Science*, 1(1):29.

Li, Y., Cakmak, S., and Zhu, J. (2019). Profiles and monthly variations of selected volatile organic compounds in indoor air in Canadian homes: Results of Canadian national indoor air survey 2012–2013. *Environment International*, 126(February):134–144.

Liang, Z., Cheung, T. Y., Chan, W. L., Lim, C. K., Lai, A. C., Lee, P. K., and Chan, C. K. (2023). Negligible increase in indoor endotoxin activity by 222 nm far-UVC illumination on bioaerosols. *Environmental Science: Atmospheres*, 3(8):1212–1220.

Lilek, J. and Zuend, A. (2022). A predictive viscosity model for aqueous electrolytes and mixed organic-inorganic aerosol phases. *Atmospheric Chemistry and Physics*, 22(5):3203–3233.

Lin, C. C. and Hsu, S. C. (2015). Deposition velocities and impact of physical properties on ozone removal for building materials. *Atmospheric Environment*, 101:194–199.

Lin, C. C., Yu, K. P., Zhao, P., and Whei-May Lee, G. (2009). Evaluation of impact factors on VOC emissions and concentrations from wooden flooring based on chamber tests. *Building and Environment*, 44(3):525–533.

Link, M. F., Li, J., Ditto, J. C., Huynh, H., Yu, J., Zimmerman, S. M., Rediger, K. L., Shore, A., Abbatt, J. P., Garofalo, L. A., Farmer, D. K., and Poppendieck, D. (2023a). Ventilation in

a Residential Building Brings Outdoor NOx Indoors with Limited Implications for VOC Oxidation from NO3 Radicals. *Environmental Science and Technology*, 57(43):16446–16455.

Link, M. F., Shore, A., Hamadani, B. H., and Poppendieck, D. (2023b). Ozone Generation from a Germicidal Ultraviolet Lamp with Peak Emission at 222 nm. *Environmental Science and Technology Letters*, 10(8):675–679.

Liu, C., Zhang, Y., and Weschler, C. J. (2014). The impact of mass transfer limitations on size distributions of particle associated SVOCs in outdoor and indoor environments. *Science of The Total Environment*, 497-498:401–411.

Liu, G., Xiao, M., Zhang, X., Gal, C., Chen, X., Liu, L., Pan, S., Wu, J., Tang, L., and Clements-Croome, D. (2017). A review of air filtration technologies for sustainable and healthy building ventilation. *Sustainable Cities and Society*, 32:375–396.

Liu, L., Wang, X., Chen, J., Xue, L., Wang, W., Wen, L., Li, D., and Chen, T. (2018). Understanding unusually high levels of peroxyacetyl nitrate (PAN) in winter in Urban Jinan, China. *Journal of Environmental Sciences (China)*, 71:249–260.

Liu, Y., Misztal, P. K., Arata, C., Weschler, C. J., Nazaroff, W. W., and Goldstein, A. H. (2021). Observing ozone chemistry in an occupied residence. *Proceedings of the National Academy of Sciences*, 118(6):e2018140118.

Lü, H., Wen, S., Feng, Y., Wang, X., Bi, X., Sheng, G., and Fu, J. (2006). Indoor and outdoor carbonyl compounds and BTEX in the hospitals of Guangzhou, China. *Science of the Total Environment*, 368(2-3):574–584.

Luengas, A., Barona, A., Hort, C., Gallastegui, G., Platel, V., and Elias, A. (2015). A review of indoor air treatment technologies. *Reviews in Environmental Science and Bio/Technology*, 14(3):499–522.

Lunderberg, D. M., Misztal, P. K., Liu, Y., Arata, C., Tian, Y., Kristensen, K., Weber, R. J., Nazaroff, W. W., and Goldstein, A. H. (2021). High-Resolution Exposure Assessment for

Volatile Organic Compounds in Two California Residences. *Environmental Science & Technology*, 55(10):6740–6751.

Malinauskiene, L., Blaziene, A., Chomiciene, A., and Isaksson, M. (2015). Formaldehyde may be found in cosmetic products even when unlabelled. *Open Medicine (Poland)*, 10(1):323–328.

Mandin, C., Trantallidi, M., Cattaneo, A., Canha, N., Mihucz, V. G., Szigeti, T., Mabilia, R., Perreca, E., Spinazzè, A., Fossati, S., De Kluizenaar, Y., Cornelissen, E., Sakellaris, I., Saraga, D., Hänninen, O., De Oliveira Fernandes, E., Ventura, G., Wolkoff, P., Carrer, P., and Bartzis, J. (2017). Assessment of indoor air quality in office buildings across Europe – The OFFICAIR study. *Science of the Total Environment*, 579:169–178.

Manuja, A., Ritchie, J., Buch, K., Wu, Y., Eichler, C. M., Little, J. C., and Marr, L. C. (2019). Total surface area in indoor environments. *Environmental Science: Processes and Impacts*, 21(8):1384–1392.

Martins, V., Moreno, T., Minguillón, M. C., Van Drooge, B. L., Reche, C., Amato, F., De Miguel, E., Capdevila, M., Centelles, S., and Querol, X. (2016). Origin of inorganic and organic components of PM2.5 in subway stations of Barcelona, Spain. *Environmental Pollution*, 208:125–136.

Mason, S. I. and Ceragioli, A. (2011). Paint volatile organic compound emissions and volatile organic compound content comparison study. *12th International Conference on Indoor Air Quality and Climate 2011*, 1(August):396–397.

Master Chemical Mechanism (2024). MCM v3.3.1, https://mcm.york.ac.uk/MCM/browse (Date Accessed: March 2024).

Mata, T. M., Martins, A. A., Calheiros, C. S. C., Villanueva, F., Alonso-Cuevilla, N. P., Gabriel, M. F., and Silva, G. V. (2022). Indoor Air Quality: A Review of Cleaning Technologies. *Environments*, 9(9):118.

Mattila, J. M., Arata, C., Abeleira, A., Zhou, Y., Wang, C., Katz, E. F., Goldstein, A. H., Abbatt, J. P., DeCarlo, P. F., Vance, M. E., and Farmer, D. K. (2022). Contrasting Chemical

Complexity and the Reactive Organic Carbon Budget of Indoor and Outdoor Air. *Environmental Science and Technology*, 56(1):109–118.

Mattila, J. M., Arata, C., Wang, C., Katz, E. F., Abeleira, A., Zhou, Y., Zhou, S., Goldstein, A. H., Abbatt, J. P., Decarlo, P. F., and Farmer, D. K. (2020a). Dark Chemistry during Bleach Cleaning Enhances Oxidation of Organics and Secondary Organic Aerosol Production Indoors. *Environmental Science and Technology Letters*, 7(11):795–801.

Mattila, J. M., Lakey, P. S., Shiraiwa, M., Wang, C., Abbatt, J. P., Arata, C., Goldstein, A. H., Ampollini, L., Katz, E. F., Decarlo, P. F., Zhou, S., Kahan, T. F., Cardoso-Saldaña, F. J., Ruiz, L. H., Abeleira, A., Boedicker, E. K., Vance, M. E., and Farmer, D. K. (2020b). Multiphase Chemistry Controls Inorganic Chlorinated and Nitrogenated Compounds in Indoor Air during Bleach Cleaning. *Environmental Science and Technology*, 54(3):1730–1739.

McDonald, B. C., De Gouw, J. A., Gilman, J. B., Jathar, S. H., Akherati, A., Cappa, C. D., Jimenez, J. L., Lee-Taylor, J., Hayes, P. L., McKeen, S. A., Cui, Y. Y., Kim, S. W., Gentner, D. R., Isaacman-VanWertz, G., Goldstein, A. H., Harley, R. A., Frost, G. J., Roberts, J. M., Ryerson, T. B., and Trainer, M. (2018). Volatile chemical products emerging as largest petrochemical source of urban organic emissions. *Science*, 359(6377):760–764.

McDonnell, G. and Russell, A. D. (1999). Antiseptics and Disinfectants: Activity, Action, and Resistance. *Clinical Microbiology Reviews*, 12(1):147–149.

McHugh, C. A., Carruthers, D. J., and Edmunds, H. A. (1997). ADMS and ADMS-Urban. *International Journal of Environment and Pollution*, 8(3-6):438–440.

Medina-Ramón, M., Zock, J. P., Kogevinas, M., Sunyer, J., Torralba, Y., Borrell, A., Burgos, F., and Antó, J. M. (2005). Asthma, chronic bronchitis, and exposure to irritant agents in occupational domestic cleaning: A nested case-control study. *Occupational and Environmental Medicine*, 62(9):598–606.

Mentese, S. and Bas, B. (2020). A year-round motoring of ambient volatile organic compounds across Dardanelles strait. *Journal of Chemical Metrology*, 14(2):177–189.

Mikuška, P., Křůmal, K., and Večeřa, Z. (2015). Characterization of organic compounds in the PM2.5 aerosols in winter in an industrial urban area. *Atmospheric Environment*, 105:97–108.

Miller, C. N., Dye, J. A., Schladweiler, M. C., Richards, J. H., Ledbetter, A. D., Stewart, E. J., and Kodavanti, U. P. (2018). Acute inhalation of ozone induces DNA methylation of apelin in lungs of Long-Evans rats. *Inhalation Toxicology*, 30(4-5):178–186.

Ministry of Housing & Communities & Local Government (UK Government) (2019). Ventilation and Indoor Air Quality in New Homes. Technical report, Ministry of Housing, Communities and Local Government (United Kingdom).

Missia, D. A., Demetriou, E., Michael, N., Tolis, E. I., and Bartzis, J. G. (2010). Indoor exposure from building materials: A field study. *Atmospheric Environment*, 44(35):4388–4395.

Moghani, M. and Archer, C. L. (2020). The impact of emissions and climate change on future ozone concentrations in the USA. *Air Quality, Atmosphere and Health*, 13(12):1465–1476.

Morgan, M. and Cruickshank, H. (2014). Quantifying the extent of space shortages: English dwellings. *Building Research and Information*, 42(6):710–724.

Morrison, G., Lakey, P. S., Abbatt, J., and Shiraiwa, M. (2019). Indoor boundary layer chemistry modeling. *Indoor Air*, 29(6):956–967.

Morrison, G. C. and Nazaroff, W. W. (2000). The Rate of Ozone Uptake on Carpets: Experimental Studies. *Environmental Science & Technology*, 34(23):4963–4968.

Morrison, G. C. and Nazaroff, W. W. (2002a). Ozone interactions with carpet: Secondary emissions of aldehydes. *Environmental Science and Technology*, 36(10):2185–2192.

Morrison, G. C. and Nazaroff, W. W. (2002b). The rate of ozone uptake on carpet: mathematical modeling. *Atmospheric Environment*, 36(11):1749–1756.

Mueller, F. X., Loeb, L., and Mapes, W. H. (1973). Decomposition Rates of Ozone in Living Areas. *Environmental Science and Technology*, 7(4):342–346.

Murillo, J. H., Roman, S. R., Rojas Marin, J. F., Ramos, A. C., Jimenez, S. B., Gonzalez, B. C., and Baumgardner, D. G. (2013). Chemical characterization and source apportionment of PM10 and PM2.5 in the metropolitan area of Costa Rica, Central America. *Atmospheric Pollution Research*, 4(2):181–190.

Nardell, E. A. (2021). Air Disinfection for Airborne Infection Control with a Focus on COVID-19: Why Germicidal UV is Essential. *Photochemistry and Photobiology*, 97(3):493–497.

Nazaroff, W. W. (2021). Residential air-change rates: A critical review. *Indoor Air*, 31(2):282–313.

Nazaroff, W. W. and Cass, G. R. (1986). Mathematical Modeling of Chemically Reactive Pollutants in Indoor Air. *Environ. Sci. Technol*, 20:924–934.

Nazaroff, W. W. and Cass, G. R. (1989). Mathematical Modeling of Indoor Aerosol Dynamics. *Environmental Science and Technology*, 23(2):157–166.

Nazaroff, W. W. and Weschler, C. J. (2004). Cleaning products and air fresheners: Exposure to primary and secondary air pollutants. *Atmospheric Environment*, 38(18):2841–2865.

Nazaroff, W. W. and Weschler, C. J. (2020). Indoor acids and bases. *Indoor Air*, 30(4):559–644.

Nelin, T. D., Joseph, A. M., Gorr, M. W., and Wold, L. E. (2012). Direct and indirect effects of particulate matter on the cardiovascular system. *Toxicology Letters*, 208(3):293–299.

Nicolas, M., Ramalho, O., and Maupetit, F. (2007). Reactions between ozone and building products: Impact on primary and secondary emissions. *Atmospheric Environment*, 41(15):3129–3138.

Nicolet, M. and Peetersman, W. (1980). Atmospheric absorption in the O2 Schumann-Runge band spectral range and photodissociation rates in the stratosphere and mesosphere. *Planet. Space Sci*, 28:85–103.

Nicolle, J., Desauziers, V., Mocho, P., and Ramalho, O. (2009). Optimization of FLEC®-SPME for field passive sampling of VOCs emitted from solid building materials. *Talanta*, 80(2):730–737.

Nielsen, P. V. (2015). Fifty years of CFD for room air distribution. *Building and Environment*, 91:78–90.

Nørgaard, A. W., Kudal, J. D., Kofoed-Sørensen, V., Koponen, I. K., and Wolkoff, P. (2014). Ozone-initiated VOC and particle emissions from a cleaning agent and an air freshener: Risk assessment of acute airway effects. *Environment International*, 68:209–218.

Nunes, C. R. d. O., Sánchez, B., Gatts, C. E., de Almeida, C. M., and Canela, M. C. (2019). Evaluation of volatile organic compounds coupled to seasonality effects in indoor air from a commercial office in Madrid (Spain) applying chemometric techniques. *Science of The Total Environment*, 650:868–877.

Odabasi, M. (2008). Halogenated volatile organic compounds from the use of chlorine-bleach- containing household products. *Environmental Science and Technology*, 42(5):1445–1451.

Office for National Statistics (2023). Housing in England and Wales 2021 compared with 2011. Technical report, Office for National Statistics.

Ong, Q., Wee, W., Dela Cruz, J., Teo, J. W. R., and Han, W. (2022). 222-Nanometer Far-UVC Exposure Results in DNA Damage and Transcriptional Changes to Mammalian Cells. *International Journal of Molecular Sciences*, 23(16).

Pang, X. and Lewis, A. C. (2011). Carbonyl compounds in gas and particle phases of mainstream cigarette smoke. *Science of the Total Environment*, 409(23):5000–5009.

Pankow, J. F. (1994). An absorption model of the gas/aerosol partitioning involved in the formation of secondary organic aerosol. *Atmospheric Environment*, 28(2):189–193.

Peeples, L. (2020). How air pollution threatens brain health. *Proceedings of the National Academy of Sciences of the United States of America*, 117(25):13856–13860.

Pei, G. and Rim, D. (2021). Quality control of computational fluid dynamics (CFD) model of ozone reaction with human surface: Effects of mesh size and turbulence model. *Building and Environment*, 189.

Pei, G., Xuan, Y., Morrison, G., and Rim, D. (2022). Understanding Ozone Transport and Deposition within Indoor Surface Boundary Layers. *Environmental Science and Technology*, 56(12):7820–7829.

Peng, Z., Day, D. A., Stark, H., Li, R., Lee-Taylor, J., Palm, B. B., Brune, W. H., and Jimenez, J. L. (2015). HOx radical chemistry in oxidation flow reactors with low-pressure mercury lamps systematically examined by modeling. *Atmospheric Measurement Techniques*, 8(11):4863–4890.

Peng, Z., Day, D. A., Symonds, G. A., Jenks, O. J., Stark, H., Handschy, A. V., de Gouw, J. A., and Jimenez, J. L. (2023a). Significant Production of Ozone from Germicidal UV Lights at 222 nm. *Environmental Science and Technology Letters*, 10(8):668–674.

Peng, Z. and Jimenez, J. L. (2017). Modeling of the chemistry in oxidation flow reactors with high initial NO. *Atmospheric Chemistry and Physics*, 17(19):11991–12010.

Peng, Z. and Jimenez, J. L. (2020). Radical chemistry in oxidation flow reactors for atmospheric chemistry research. *Chemical Society Reviews*, 49(9):2570–2616.

Peng, Z., Miller, S. L., and Jimenez, J. L. (2023b). Model Evaluation of Secondary Chemistry due to Disinfection of Indoor Air with Germicidal Ultraviolet Lamps. *Environmental Science and Technology Letters*, 10(1):6–13.

Plaisance, H., Vignau-Laulhere, J., Mocho, P., Sauvat, N., Raulin, K., and Desauziers, V. (2017). Volatile organic compounds concentrations during the construction process in newly-built timber-frame houses: Source identification and emission kinetics. *Environmental Science: Processes and Impacts*, 19(5):696–710.

Polidori, A., Turpin, B., Meng, Q. Y., Lee, J. H., Weisel, C., Morandi, M., Colome, S., Stock, T., Winer, A., Zhang, J., Kwon, J., Alimokhtari, S., Shendell, D., Jones, J., Farrar, C., and Maberti, S. (2006). Fine organic particulate matter dominates indoor-generated PM2.5 in RIOPA homes. *Journal of Exposure Science and Environmental Epidemiology*, 16(4):321–331.

Poppendieck, D., Hubbard, H., and Corsi, R. L. (2021). Hydrogen Peroxide Vapor as an Indoor Disinfectant: Removal to Indoor Materials and Associated Emissions of Organic Compounds. *Environmental Science and Technology Letters*, 8(4):320–325.

Poppendieck, D., Hubbard, H., Ward, M., Weschler, C., and Corsi, R. L. (2007a). Ozone reactions with indoor materials during building disinfection. *Atmospheric Environment*, 41(15):3166–3176.

Poppendieck, D. G., Hubbard, H. F., Weschler, C. J., and Corsi, R. L. (2007b). Formation and emissions of carbonyls during and following gas-phase ozonation of indoor materials. *Atmospheric Environment*, 41(35):7614–7626.

Pothier, M. A., Boedicker, E., Pierce, J. R., Vance, M., and Farmer, D. K. (2022). From the HOMEChem frying pan to the outdoor atmosphere: chemical composition, volatility distributions and fate of cooking aerosol. *Environmental Science: Processes and Impacts*, 25(2):314–325.

Pye, H. O. T., Ward-Caviness, C. K., Murphy, B. N., Appel, K. W., and Seltzer, K. M. (2021). Secondary organic aerosol association with cardiorespiratory disease mortality in the United States. *Nature Communications*, 12(1):7215.

Rafaj, P., Kiesewetter, G., Gül, T., Schöpp, W., Cofala, J., Klimont, Z., Purohit, P., Heyes, C., Amann, M., Borken-Kleefeld, J., and Cozzi, L. (2018). Outlook for clean air in the context of sustainable development goals. *Global Environmental Change*, 53:1–11.

Rai, A. C., Guo, B., Lin, C.-H., Zhang, J., Pei, J., and Chen, Q. (2014). Ozone reaction with clothing and its initiated VOC emissions in an environmental chamber. *Indoor Air*, 24(1):49–58.

Reidy, E., Bottorff, B. P., Rosales, C. M. F., Cardoso-Saldaña, F. J., Arata, C., Zhou, S., Wang, C., Abeleira, A., Hildebrandt Ruiz, L., Goldstein, A. H., Novoselac, A., Kahan, T. F., Abbatt, J. P., Vance, M. E., Farmer, D. K., and Stevens, P. S. (2023). Measurements of Hydroxyl Radical Concentrations during Indoor Cooking Events: Evidence of an Unmeasured Photolytic Source of Radicals. *Environmental Science and Technology*, 57(2):896–908.

Reiss, R., Ryan, P. B., and Koutrakis, P. (1994). Modeling Ozone Deposition onto Indoor Residential Surfaces. *Environmental Science and Technology*, 28(3):504–513.

Remucal, C. K. and Manley, D. (2016). Emerging investigators series: The efficacy of chlorine photolysis as an advanced oxidation process for drinking water treatment. *Environmental Science: Water Research and Technology*, 2(4):565–579.

Rim, D., Gall, E. T., Ananth, S., and Won, Y. (2018). Ozone reaction with human surfaces: Influences of surface reaction probability and indoor air flow condition. *Building and Environment*, 130:40–48.

Rim, D., Gall, E. T., Maddalena, R. L., and Nazaroff, W. W. (2016). Ozone reaction with interior building materials: Influence of diurnal ozone variation, temperature and humidity. *Atmospheric Environment*, 125:15–23.

Ritchie, H. and Roser, M. (2017). Air Pollution, https://ourworldindata.org/air-pollution (Date Accessed: June 2021).

Ritchie, H. and Roser, M. (2019). Outdoor Air Pollution, https://ourworldindata.org/outdoor-air-pollution (Date Accessed: June 2021).

Rosales, C. M. F., Jiang, J., Lahib, A., Bottorff, B. P., Reidy, E. K., Kumar, V., Tasoglou, A., Huber, H., Dusanter, S., Tomas, A., Boor, B. E., and Stevens, P. S. (2022). Chemistry and human exposure implications of secondary organic aerosol production from indoor terpene ozonolysis. *Science Advances*, 8(8):9156.

Rossignol, S., Rio, C., Ustache, A., Fable, S., Nicolle, J., Même, A., D'Anna, B., Nicolas, M., Leoz, E., and Chiappini, L. (2013). The use of a housecleaning product in an indoor

environment leading to oxygenated polar compounds and SOA formation: Gas and particulate phase chemical characterization. *Atmospheric Environment*, 75:196–205.

Ruiz-Jimenez, J., Heiskanen, I., Tanskanen, V., Hartonen, K., and Riekkola, M.-L. (2022). Analysis of indoor air emissions: From building materials to biogenic and anthropogenic activities. *Journal of Chromatography Open*, 2(March):100041.

Sabersky, R. H., Sinema, D. A., and Shair, F. H. (1973). Concentrations, Decay Rates, and Removal of Ozone and Their Relation to Establishing Clean Indoor Air. *Environmental Science and Technology*, 7(4):347–353.

SAGE EMG (2020). Potential application of Air Cleaning devices and personal decontamination to manage transmission of COVID-19. Technical report.

Salthammer, T. (2019). Formaldehyde sources, formaldehyde concentrations and air exchange rates in European housings. *Building and Environment*, 150(October 2018):219–232.

Salthammer, T. (2023). Acetaldehyde in the indoor environment. *Environmental Science: Atmospheres*, 3(3):474–493.

Samara, C., Voutsa, D., Kouras, A., Eleftheriadis, K., Maggos, T., Saraga, D., and Petrakakis, M. (2014). Organic and elemental carbon associated to PM10 and PM2.5 at urban sites of northern Greece. *Environmental Science and Pollution Research*, 21(3):1769–1785.

Sangiorgi, G., Ferrero, L., Ferrini, B. S., Lo Porto, C., Perrone, M. G., Zangrando, R., Gambaro, A., Lazzati, Z., and Bolzacchini, E. (2013). Indoor airborne particle sources and semi-volatile partitioning effect of outdoor fine PM in offices. *Atmospheric Environment*, 65:205–214.

Sankhyan, S., Zabinski, K., O'Brien, R. E., Coyan, S., Patel, S., and Vance, M. E. (2022). Aerosol emissions and their volatility from heating different cooking oils at multiple temperatures. *Environmental Science: Atmospheres*, 2(6):1364–1375.

Sarwar, G. and Corsi, R. (2007). The effects of ozone/limonene reactions on indoor secondary organic aerosols. *Atmospheric Environment*, 41(5):959–973.

Sarwar, G., Corsi, R., Kimura, Y., Allen, D., and Weschler, C. J. (2002). Hydroxyl radicals in indoor environments. *Atmospheric Environment*, 36(24):3973–3988.

Saunders, S. M., Jenkin, M. E., Derwent, R. G., and Pilling, M. J. (2003). Protocol for the development of the Master Chemical Mechanism, MCM v3 (Part A): Tropospheric degradation of non-aromatic volatile organic compounds. *Atmospheric Chemistry and Physics*, 3(1):161–180.

Schauer, J. J., Kleeman, M. J., Cass, G. R., and Simoneit, B. R. (1999). Measurement of emissions from air pollution sources. 1. C1 through C29 organic compounds from meat charbroiling. *Environmental Science and Technology*, 33(10):1566–1577.

Schrank, S. G., Bieling, U., José, H. J., Moreira, R. F., and Schröder, H. F. (2009). Generation of endocrine disruptor compounds during ozone treatment of tannery wastewater confirmed by biological effect analysis and substance specific analysis. *Water Science and Technology*, 59(1):31–38.

Schripp, T., Langer, S., and Salthammer, T. (2012). Interaction of ozone with wooden building products, treated wood samples and exotic wood species. *Atmospheric Environment*, 54:365–372.

Seaman, V. Y., Bennett, D. H., and Cahill, T. M. (2009). Indoor acrolein emission and decay rates resulting from domestic cooking events. *Atmospheric Environment*, 43(39):6199–6204.

Serrano Damha, C., Cummings, B. E., Schervish, M., Shiraiwa, M., Waring, M. S., and Zuend, A. (2024). Capturing the Relative-Humidity-Sensitive Gas–Particle Partitioning of Organic Aerosols in a 2D Volatility Basis Set. *Geophysical Research Letters*, 51(3).

Setokuchi, O. and Sato, M. (2002). Direct dynamics of an alkoxy radical (CH3O, C2H5O, and i-C3H7O) reaction with an oxygen molecule. *Journal of Physical Chemistry A*, 106(35):8124–8132.

Shaw, D. and Carslaw, N. (2021). INCHEM-Py: An open source Python box model for indoor air chemistry. *Journal of Open Source Software*, 6(63):3224.

Shaw, D. R., Carter, T. J., Davies, H. L., Harding-Smith, E., Crocker, E. C., Beel, G., Wang, Z., and Carslaw, N. (2023). INCHEM-Py v1.2: a community box model for indoor air chemistry. *Geoscientific Model Development*, 16(24):7411–7431.

Shen, J. and Gao, Z. (2018). Ozone removal on building material surface: A literature review. *Building and Environment*, 134(March):205–217.

Sheu, R., Fortenberry, C. F., Walker, M. J., Eftekhari, A., Stönner, C., Bakker, A., Peccia, J., Williams, J., Morrison, G. C., Williams, B. J., and Gentner, D. R. (2021). Evaluating Indoor Air Chemical Diversity, Indoor-to-Outdoor Emissions, and Surface Reservoirs Using High-Resolution Mass Spectrometry. *Environmental Science & Technology*, 55(15):10255–10267.

Shin, S. H. and Jo, W. K. (2013). Temporal characteristics of volatile organic compounds in newly-constructed residential buildings: Concentration and source. *Environmental Engineering Research*, 18(3):169–176.

Shinohara, N., Tokumura, M., Kazama, M., Yoshino, H., Ochiai, S., and Mizukoshi, A. (2013). Indoor air quality, air exchange rates, and radioactivity in new built temporary houses following the Great East Japan Earthquake in Minamisoma, Fukushima. *Indoor Air*, 23(4):332–341.

Shiraiwa, M., Carslaw, N., Tobias, D. J., Waring, M. S., Rim, D., Morrison, G., Lakey, P. S., Kruza, M., Von Domaros, M., Cummings, B. E., and Won, Y. (2019). Modelling consortium for chemistry of indoor environments (MOCCIE): Integrating chemical processes from molecular to room scales. *Environmental Science: Processes and Impacts*, 21(8):1240–1254.

Shiraiwa, M., Pfrang, C., Koop, T., and Pöschl, U. (2012). Kinetic multi-layer model of gas-particle interactions in aerosols and clouds (KM-GAP): Linking condensation, evaporation and chemical reactions of organics, oxidants and water. *Atmospheric Chemistry and Physics*, 12(5):2777–2794.

Shiraiwa, M., Pfrang, C., and Pöschl, U. (2010). Kinetic multi-layer model of aerosol surface and bulk chemistry (KM-SUB): the influence of interfacial transport and bulk diffusion on the oxidation of oleic acid by ozone. *Atmospheric Chemistry and Physics*, 10(8):3673–3691.

Shrestha, P. M., Humphrey, J. L., Carlton, E. J., Adgate, J. L., Barton, K. E., Root, E. D., and Miller, S. L. (2019). Impact of Outdoor Air Pollution on Indoor Air Quality in Low-Income Homes during Wildfire Seasons. *International Journal of Environmental Research and Public Health*, 16(19):3535.

Shuai, J., Kim, S., Ryu, H., Park, J., Lee, C. K., Kim, G.-B., Ultra, V. U., and Yang, W. (2018). Health risk assessment of volatile organic compounds exposure near Daegu dyeing industrial complex in South Korea. *BMC Public Health*, 18(1):528.

Siegel, J. A. (2016). Primary and secondary consequences of indoor air cleaners. *Indoor Air*, 26(1):88–96.

Simmons, A. and Colbeck, I. (1990). Resistance of various building materials to ozone deposition. *Environmental Technology (United Kingdom)*, 11(10):973–978.

Simon, V., Uitterhaegen, E., Robillard, A., Ballas, S., Véronèse, T., Vilarem, G., Merah, O., Talou, T., and Evon, P. (2020). VOC and carbonyl compound emissions of a fiberboard resulting from a coriander biorefinery: comparison with two commercial wood-based building materials. *Environmental Science and Pollution Research*, 27(14):16121–16133.

Singer, B. C., Destaillats, H., Hodgson, A. T., and Nazaroff, W. W. (2006). Cleaning products and air fresheners: Emissions and resulting concentrations of glycol ethers and terpenoids. *Indoor Air*, 16(3):179–191.

Sorensen, D. N. and Weschler, C. J. (2002). Modeling-gas phase reactions in indoor environments using computational fluid dynamics. *Atmospheric Environment*, 36:9–18.

Steinemann, A. (2015). Volatile emissions from common consumer products. *Air Quality, Atmosphere and Health*, 8(3):273–281.

Steinemann, A. (2021). The fragranced products phenomenon: air quality and health, science and policy. *Air Quality, Atmosphere & Health*, 14(2):235–243.

Stockwell, W. R., Kirchner, F., Kuhn, M., and Seefeld, S. (1997). A new mechanism for regional atmospheric chemistry modeling. *Journal of Geophysical Research Atmospheres*, 102(22).

Stönner, C., Edtbauer, A., and Williams, J. (2018). Real-world volatile organic compound emission rates from seated adults and children for use in indoor air studies. *Indoor Air*, 28(1):164–172.

Sturaro, A., Rella, R., Parvoli, G., and Ferrara, D. (2010). Long-term phenol, cresols and BTEX monitoring in urban air. *Environmental Monitoring and Assessment*, 164(1-4):93–100.

Sugihara, K., Kaidzu, S., Sasaki, M., Ichioka, S., Takayanagi, Y., Shimizu, H., Sano, I., Hara, K., and Tanito, M. (2023). One-year Ocular Safety Observation of Workers and Estimations of Microorganism Inactivation Efficacy in the Room Irradiated with 222-nm Far Ultraviolet-C Lamps. *Photochemistry and Photobiology*, 99(3):967–974.

Swenberg, J. A., Moeller, B. C., Lu, K., Rager, J. E., Fry, R. C., and Starr, T. B. (2013). Formaldehyde carcinogenicity research: 30 years and counting for mode of action, epidemiology, and cancer risk assessment. *Toxicologic Pathology*, 41(2):181–189.

Szabados, M., Csákó, Z., Kotlík, B., Kazmarová, H., Kozajda, A., Jutraz, A., Kukec, A., Otorepec, P., Dongiovanni, A., Di Maggio, A., Fraire, S., and Szigeti, T. (2021). Indoor air quality and the associated health risk in primary school buildings in Central Europe – The InAirQ study. *Indoor Air*, 31(4):989–1003.

Tamás, G., Weschler, C. J., Bakó-Biró, Z., Wyon, D. P., and Strøm-Tejsen, P. (2006). Factors affecting ozone removal rates in a simulated aircraft cabin environment. *Atmospheric Environment*, 40(32):6122–6133.

Tang, R. and Pfrang, C. (2023). Indoor particulate matter (PM) from cooking in UK students' studio flats and associated intervention strategies: evaluation of cooking meth-

ods, PM concentrations and personal exposures using low-cost sensors. *Environmental Science: Atmospheres*, 3(3):537–551.

Tang, X., Misztal, P. K., Nazaroff, W. W., and Goldstein, A. H. (2016). Volatile organic compound emissions from humans indoors. *Environmental Science and Technology*, 50(23):12686–12694.

Terry, A. C., Carslaw, N., Ashmore, M., Dimitroulopoulou, S., and Carslaw, D. C. (2014). Occupant exposure to indoor air pollutants in modern European offices: An integrated modelling approach. *Atmospheric Environment*, 82:9–16.

Tichenor, B. A. and Mason, M. A. (1988). Organic emissions from consumer products and building materials to the indoor environment. *Journal of the Air Pollution Control Association*, 38(3):264–268.

Tran, T. M., Hoang, A. Q., Le, S. T., Minh, T. B., and Kannan, K. (2019). A review of contamination status, emission sources, and human exposure to volatile methyl siloxanes (VMSs) in indoor environments. *Science of The Total Environment*, 691:584–594.

Trevisan, A., Piovesan, S., Leonardi, A., Bertocco, M., Nicolosi, P., Pelizzo, M. G., and Angelini, A. (2006). Unusual High Exposure to Ultraviolet-C Radiation. *Photochemistry and Photobiology*, 82(4):1077.

Truong, C.-S., Muthukutty, P., Jang, H. K., Kim, Y.-H., Lee, D. H., and Yoo, S. Y. (2023). Filter-Free, Harmless, and Single-Wavelength Far UV-C Germicidal Light for Reducing Airborne Pathogenic Viral Infection. *Viruses*, 15(7):1463.

Turpin, B. J., Saxena, P., and Andrews, E. (2000). Measuring and simulating particulate organics in the atmosphere: Problems and prospects. *Atmospheric Environment*, 34(18):2983–3013.

Tyndall, G., Cox, R., Granier, C., Lesclaux, R., Moortgat, G., Pilling, M., Ravishankara, A., and Wallington, T. (2001). Atmospheric chemistry of small organic peroxy radicals. *Journal of Geophysical Research*, 106:12157–12182.

Uchiyama, S., Tomizawa, T., Tokoro, A., Aoki, M., Hishiki, M., Yamada, T., Tanaka, R., Sakamoto, H., Yoshida, T., Bekki, K., Inaba, Y., Nakagome, H., and Kunugita, N. (2015). Gaseous chemical compounds in indoor and outdoor air of 602 houses throughout Japan in winter and summer. *Environmental Research*, 137:364–372.

Van Tran, V., Park, D., and Lee, Y. C. (2020). Indoor air pollution, related human diseases, and recent trends in the control and improvement of indoor air quality. *International Journal of Environmental Research and Public Health*, 17(8).

Veres, P. R., Faber, P., Drewnick, F., Lelieveld, J., and Williams, J. (2013). Anthropogenic sources of VOC in a football stadium: Assessing human emissions in the atmosphere. *Atmospheric Environment*, 77:1052–1059.

Vichi, F., Mašková, L., Frattoni, M., Imperiali, A., and Smolík, J. (2016). Simultaneous measurement of nitrous acid, nitric acid, and nitrogen dioxide by means of a novel multipollutant diffusive sampler in libraries and archives. *Heritage Science*, 4(1):4.

Von Domaros, M., Lakey, P. S., Shiraiwa, M., and Tobias, D. J. (2020). Multiscale Modeling of Human Skin Oil-Induced Indoor Air Chemistry: Combining Kinetic Models and Molecular Dynamics. *Journal of Physical Chemistry B*, 124(18):3836–3843.

Von Domaros, M., Liu, Y., Butman, J. L., Perlt, E., Geiger, F. M., and Tobias, D. J. (2021). Molecular Orientation at the Squalene/Air Interface from Sum Frequency Generation Spectroscopy and Atomistic Modeling. *Journal of Physical Chemistry B*, 125(15):3932–3941.

Vu, T. V., Stewart, G. B., Kitwiroon, N., Lim, S., Barratt, B., Kelly, F. J., Thompson, R., Smith, R. B., Toledano, M. B., and Beevers, S. D. (2022). Assessing the contributions of outdoor and indoor sources to air quality in London homes of the SCAMP cohort. *Building and Environment*, 222:109359.

Walgraeve, C., Demeestere, K., Dewulf, J., Van Huffel, K., and Van Langenhove, H. (2011). Diffusive sampling of 25 volatile organic compounds in indoor air: Uptake rate deter-

mination and application in Flemish homes for the elderly. *Atmospheric Environment*, 45(32):5828–5836.

Wang, C., Bottorff, B., Reidy, E., Rosales, C. M. F., Collins, D. B., Novoselac, A., Farmer, D. K., Vance, M. E., Stevens, P. S., and Abbatt, J. P. (2020a). Cooking, Bleach Cleaning, and Air Conditioning Strongly Impact Levels of HONO in a House. *Environmental Science and Technology*, 54(21):13488–13497.

Wang, H. and Morrison, G. (2010). Ozone-surface reactions in five homes: Surface reaction probabilities, aldehyde yields, and trends. *Indoor Air*, 20(3):224–234.

Wang, H. and Morrison, G. C. (2006). Ozone-initiated secondary emission rates of aldehydes from indoor surfaces in four homes. *Environmental Science and Technology*, 40(17):5263–5268.

Wang, N., Ernle, L., Bekö, G., Wargocki, P., and Williams, J. (2022a). Emission Rates of Volatile Organic Compounds from Humans. *Environmental Science & Technology*, 56:4838–4848.

Wang, Z., Kowal, S. F., Carslaw, N., and Kahan, T. F. (2020b). Photolysis-driven indoor air chemistry following cleaning of hospital wards. *Indoor Air*, 30(6):1241–1255.

Wang, Z., Shaw, D., Kahan, T., Schoemaecker, C., and Carslaw, N. (2022b). A modeling study of the impact of photolysis on indoor air quality. *Indoor Air*, 32(6):1–10.

Waring, M. S. (2014). Secondary organic aerosol in residences: Predicting its fraction of fine particle mass and determinants of formation strength. *Indoor Air*, 24(4):376–389.

Waring, M. S. and Siegel, J. A. (2011). The effect of an ion generator on indoor air quality in a residential room. *Indoor Air*, 21(4):267–276.

Waring, M. S. and Siegel, J. A. (2013). Indoor Secondary Organic Aerosol Formation Initiated from Reactions between Ozone and Surface-Sorbed d-Limonene. *Environmental Science & Technology*, 47(12):6341–6348.

Waring, M. S. and Wells, J. R. (2015). Volatile organic compound conversion by ozone, hydroxyl radicals, and nitrate radicals in residential indoor air: Magnitudes and impacts of oxidant sources. *Atmospheric Environment*, 106(3):382–391.

Weill, H., George, R., Schwarz, M., and Ziskind, M. (1969). Late evaluation of pulmonary function after acute exposure to chlorine gas. *The American review of respiratory disease*, 99(3):374–9.

Wernis, R. A., Kreisberg, N. M., Weber, R. J., Drozd, G. T., and Goldstein, A. H. (2022). Source apportionment of VOCs, IVOCs and SVOCs by positive matrix factorization in suburban Livermore, California. *Atmospheric Chemistry and Physics*, 22(22):14987–15019.

Weschler, C. J. (2000). Ozone in indoor environments: Concentration and chemistry. *Indoor Air*, 10(4):269–288.

Weschler, C. J. (2006). Ozone's impact on public health: Contributions from indoor exposures to ozone and products of ozone-initiated chemistry. *Environmental Health Perspectives*, 114(10):1489–1496.

Weschler, C. J. (2016). Roles of the human occupant in indoor chemistry. *Indoor Air*, 26(1):6–24.

Weschler, C. J. and Carslaw, N. (2018). Indoor Chemistry. *Environmental Science and Technology*, 52(5):2419–2428.

Weschler, C. J. and Nazaroff, W. W. (2023). Human skin oil: a major ozone reactant indoors. *Environmental Science: Atmospheres*, 3(4):640–661.

Weschler, C. J., Wisthaler, A., Cowlin, S., Tamás, G., Strøm-Tejsen, P., Hodgson, A. T., Destaillats, H., Herrington, J., Zhang, J., and Nazaroff, W. W. (2007). Ozone-initiated chemistry in an occupied simulated aircraft cabin. *Environmental Science and Technology*, 41(17):6177–6184.

Wisthaler, A., Tamás, G., Wyon, D. P., Strøm-Tejsen, P., Space, D., Beauchamp, J., Hansel, A., Märk, T. D., and Weschler, C. J. (2005). Products of ozone-initiated chemistry in a

simulated aircraft environment. *Environmental Science and Technology*, 39(13):4823–4832.

Wisthaler, A. and Weschler, C. J. (2010). Reactions of ozone with human skin lipids: Sources of carbonyls, dicarbonyls, and hydroxycarbonyls in indoor air. *Proceedings of the National Academy of Sciences of the United States of America*, 107(15):6568–6575.

Wolkoff, P. (2020). Indoor air chemistry: Terpene reaction products and airway effects. *International Journal of Hygiene and Environmental Health*, 225:113439.

Wolkoff, P., Clausen, P. A., Wilkins, C. K., and Nielsen, G. D. (2000). Formation of strong airway irritants in terpene/ozone mixtures. *Indoor Air*, 10(2):82–91.

Won, Y., Lakey, P. S., Morrison, G., Shiraiwa, M., and Rim, D. (2020). Spatial distributions of ozonolysis products from human surfaces in ventilated rooms. *Indoor Air*, 30(6):1229–1240.

Won, Y., Waring, M., and Rim, D. (2019). Understanding the Spatial Heterogeneity of Indoor OH and HO2 due to Photolysis of HONO Using Computational Fluid Dynamics Simulation. *Environmental Science and Technology*, 53(24):14470–14478.

Wong, J. P., Carslaw, N., Zhao, R., Zhou, S., and Abbatt, J. P. (2017). Observations and impacts of bleach washing on indoor chlorine chemistry. *Indoor Air*, 27(6):1082–1090.

World Health Organisation (2021a). Air Pollution, https://www.who.int/health-topics/air-pollution (Date Accessed: April 2024).

World Health Organisation (2021b). WHO global air quality guidelines - Particulate matter (PM2.5 and PM10), ozone, nitrogen dioxide, sulfur dioxide and carbon monoxide. Technical report, World Health Organisation (WHO).

World Health Organisation (2023). Household air pollution and health, https://www.who.int/en/news-room/fact-sheets/detail/household-air-pollution-and-health (Date Accessed: April 2024).

Xiong, J., Chen, F., Sun, L., Yu, X., Zhao, J., Hu, Y., and Wang, Y. (2019). Characterization of VOC emissions from composite wood furniture: Parameter determination and simplified model. *Building and Environment*, 161(April):106237.

Xue, L. K., Saunders, S. M., Wang, T., Gao, R., Wang, X. F., Zhang, Q. Z., and Wang, W. X. (2015). Development of a chlorine chemistry module for the Master Chemical Mechanism. *Geoscientific Model Development*, 8(10):3151–3162.

Yang, S., Perret, V., Hager Jörin, C., Niculita-Hirzel, H., Goyette Pernot, J., and Licina, D. (2020). Volatile organic compounds in 169 energy-efficient dwellings in Switzerland. *Indoor Air*, 30(3):481–491.

Yang, Y., Shao, M., Wang, X., Nölscher, A. C., Kessel, S., Guenther, A., and Williams, J. (2016). Towards a quantitative understanding of total OH reactivity: A review. *Atmospheric Environment*, 134:147–161.

Yao, M., Ke, L., Liu, Y., Luo, Z., and Zhao, B. (2020). Measurement of ozone deposition velocity onto human surfaces of Chinese residents and estimation of corresponding production of oxidation products. *Environmental Pollution*, 266:115215.

Ye, W., Wang, H., Chen, Z., and Zhang, X. (2020). Ozone Deposition on Free-Running Indoor Materials and the Corresponding Volatile Organic Compound Emissions: Implications for Ventilation Requirements. *Applied Sciences*, 10(12):4146.

Yeoman, A. M., Shaw, M., and Lewis, A. C. (2021). Estimating person-to-person variability in VOC emissions from personal care products used during showering. *Indoor Air*, 31(4):1281–1291.

Yoshino, K., Cheung, A.-C., Esmond, J., Parkinson, W., Freeman, D., Guberman, S., Jenouvrier, A., Coquart, B., and Merienne, M. (1988). Improved absorption cross-sections of oxygen in the wavelength region 205–240 nm of the Herzberg continuum. *Planetary and Space Science*, 36(12):1469–1475.

Yoshino, K., Esmond, J., Cheung, A.-C., Freeman, D., and Parkinson, W. (1992). High resolution absorption cross sections in the transmission window region of the Schumann-

Runge bands and Herzberg continuum of O2. *Planetary and Space Science*, 40(2-3):185–192.

Young, C. J., Zhou, S., Siegel, J. A., and Kahan, T. F. (2019). Illuminating the dark side of indoor oxidants. *Environmental Science: Processes and Impacts*, 21(8):1229–1239.

Yrieix, C., Dulaurent, A., Laffargue, C., Maupetit, F., Pacary, T., and Uhde, E. (2010). Characterization of VOC and formaldehyde emissions from a wood based panel: Results from an inter-laboratory comparison. *Chemosphere*, 79(4):414–419.

Zaffina, S., Camisa, V., Lembo, M., Vinci, M. R., Tucci, M. G., Borra, M., Napolitano, A., and Cannatà, V. (2012). Accidental Exposure to UV Radiation Produced by Germicidal Lamp: Case Report and Risk Assessment. *Photochemistry and Photobiology*, 88(4):1001–1004.

Zhang, D. C., Liu, J. J., Jia, L. Z., Wang, P., and Han, X. (2019). Speciation of VOCs in the cooking fumes from five edible oils and their corresponding health risk assessments. *Atmospheric Environment*, 211:6–17.

Zhong, Y., Wang, X., and Cheng, S. (2020). Characteristics and Source Apportionment of PM2.5 and O3 during Winter of 2013 and 2018 in Beijing. *Atmosphere*, 11(12):1324.

Zhou, S. and Kahan, T. F. (2022). Spatiotemporal characterization of irradiance and photolysis rate constants of indoor gas-phase species in the UTest house during HOMEChem. *Indoor Air*, 32(1):1–11.

Zhou, S., Liu, Z., Wang, Z., Young, C. J., Vandenboer, T. C., Guo, B. B., Zhang, J., Carslaw, N., and Kahan, T. F. (2020). Hydrogen Peroxide Emission and Fate Indoors during Nonbleach Cleaning: A Chamber and Modeling Study. *Environmental Science and Technology*, 54(24):15643–15651.

Zhou, S., Yeung, L. W., Forbes, M. W., Mabury, S., and Abbatt, J. P. (2017). Epoxide formation from heterogeneous oxidation of benzo[: A] pyrene with gas-phase ozone and indoor air. *Environmental Science: Processes and Impacts*, 19(10):1292–1299.

Zhou, Z., Lakey, P. S., Von Domaros, M., Wise, N., Tobias, D. J., Shiraiwa, M., and Abbatt, J. P. (2022). Multiphase Ozonolysis of Oleic Acid-Based Lipids: Quantitation of Major Products and Kinetic Multilayer Modeling. *Environmental Science and Technology*, 56(12):7716–7728.

Zhu, J., Wong, S. L., and Cakmak, S. (2013). Nationally representative levels of selected volatile organic compounds in canadian residential indoor air: Population-based survey. *Environmental Science and Technology*, 47(23):13276–13283.